भौमिक एवं ग्रहीय पर्यावरण के उर्जा विज्ञान, गतिकी, एवं रसायन शास्त्र की वैज्ञानिक समझ, तथा समाज पर इनकी विवक्षा

Scientific understanding of the energetics, dynamics and chemistry of the terrestrial and planetary environments and implications to the society

वैज्ञानिक उपलब्धियाँ SCIENTIFIC ACCOMPLISHMENTS

2022-2023

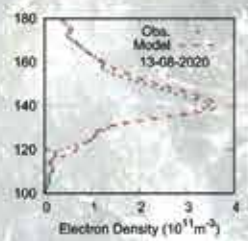

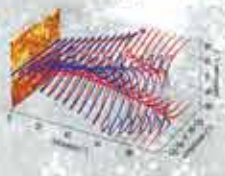

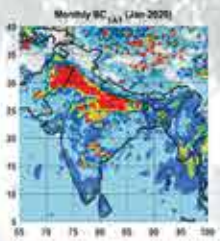

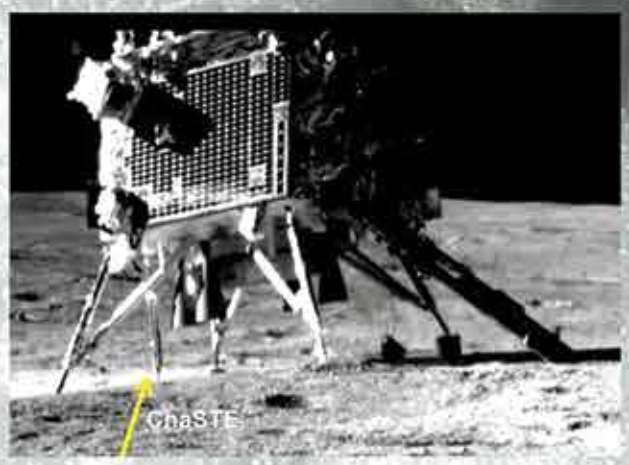

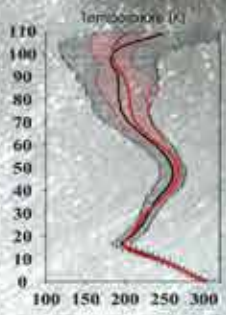

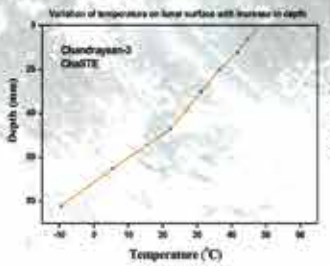

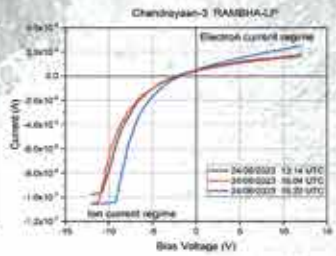

अंतरिक्ष भौतिकी प्रयोगशाला
विक्रम साराभाई अंतरिक्ष केंद्र
तिरुवनन्तपुरम

SPACE PHYSICS LABORATORY
Vikram Sarabhai Space Centre
Thiruvananthapuram

MSLP ATRF NAM ADB ITMP PSB ATD PCC ADM

Scientific Advisory Committee of SPL

Chairman

Dr. T. K. Alex, Hon. Distinguished Professor, ISRO HQ

Alternate Chairman

Dr. S. Unnikrishnan Nair, Director, IIST

Members

Prof. A. P. Dimri, Director, IIG
Sri. Shantanu Bhatawdekar, Scientific Secretary, ISRO HQ
Dr. Raj Kumar, Satish Dhawan Professor, SAC
Dr. A K Patra, Director, NARL
Director, NCESS, Thiruvananthapuram
Mrs. Athula Devi S., Deputy Director, AVN, VSSC
Dr. Tirtha Pratim Das, Director, SPO, ISRO HQ
Prof. K. Mohan Kumar, Emeritus Professor, CUSAT
Prof. Animesh Maitra, Calcutta University
Prof. S. K. Satheesh, Chairman, DCCC, IISc, Bangalore
Prof. R. Sridharan, Former Director, SPL (Emeritus Scientist, PRL)
Prof. P. Balarama Rao, Former Director, NARL
Prof. A. Jayaraman, Former Director, NARL
Dr. S. Seetha, Former Director, SSPO, ISRO HQ

Member Secretary

Dr. K. Rajeev, Director, SPL

Editorial Team

Dr. C. Vineeth, Dr. Mukunda M. Gogoi, Dr. S. Suresh Babu

अंतरिक्ष भौतिकी प्रयोगशाला

SPL

Space Physics Laboratory

वैज्ञानिक उपलब्धियाँ
Scientific Accomplishments
2022-2023

विक्रम साराभाई अंतरिक्ष केंद्र
Vikram Sarabhai Space Centre

भारतीय अंतरिक्ष अनुसंधान संगठन
Indian Space Research Organisation


GOVERNMENT OF INDIA
DEPARTMENT OF SPACE
VIKRAM SARABHAI SPACE CENTRE

भारत सरकार
अंतरिक्ष विभाग
विक्रम साराभाई अंतरिक्ष केंद्र
तिरुवनंतपुरम - 695 022, भारत
दूरभाष : 0471-2565567/2704412
फैक्स : 0471-2704105
ईमेल : director@vssc.gov.in

डॉ उण्णिकृष्णन नायर एस
Dr Unnikrishnan Nair S
विशिष्ट वैज्ञानिक व
Distinguished Scientist &
निदेशक/Director

Government of India
Department of Space
Vikram Sarabhai Space Centre
Thiruvananthapuram - 695 022, India
Phone : +91-471-2565567/2704412
Fax : +91-471-2704105
Email : director@vssc.gov.in

FOREWORD

November 3, 2023

The Space Physics Laboratory (SPL) at VSSC conducts research and development in the domains of atmospheric, space and planetary sciences using space-borne and ground-based experimental techniques and theoretical modelling. It supports ISRO's science plans with clearly defined scientific programmes. SPL is engaged in the conceptualisation and design of space-borne payloads and ground-based experimental systems for scientific investigations, and their realisation with strong support from the other entities of VSSC. SPL has been operating a network of ground-based observatories and conducting field experiments, in collaboration with universities and national institutions, for investigating aerosols, boundary layer, atmospheric dynamics and ionospheric characteristics in a national canvas.

SPL has accomplished significant progress during 2022-23. The ChaSTE and RAMBHA-LP payloads on-board Chandrayaan-3, conceptualised and developed by SPL in collaboration with other entities of VSSC, were deployed and operated successfully and provided the first observations on lunar regolith characteristics and near-surface plasma content at the south pole of moon. The Plasma Analyser Package for Aditya (PAPA) payload, jointly developed by SPL and Avionics entity of VSSC, was integrated with the Aditya-L1 spacecraft, which is currently enroute to the L1 point.

It gives me immense pleasure to report that SPL has brought out several major scientific findings based on experiments and modelling during the reporting period and published seventy research papers in reputed high-impact journals. The doctoral research programme leading to Ph.D degree through ISRO Research Fellowship scheme and post-doctoral research under ISRO's Research Associate scheme and other national schemes such as INSPIRE fellowship, Ramanujan fellowship, national post-doctoral fellowship and DST women fellowship are progressing well at SPL, contributing to the human resource development in space research. Four researchers were awarded Ph.D degree during the reporting period.

The Scientific Advisory Committee (SAC) comprising of eminent scientists critically review the research and development activities and future plans of SPL every year. The insightful discussions and guidance from SAC will help SPL to further focus its activities to the needs of the country, in line with the 'Vision 2047' and absorbing the essence of space sector reforms.

Best wishes to SPL for more fruitful and productive years ahead.

(Unnikrishnan Nair S)

SCIENTIFIC DISCIPLINES AND ACTIVITIES

From the Director

Greetings from SPL!

I am very happy to present the report on the major research activities and scientific accomplishments of SPL during July 2022 to June 2023 and to update the developments that occurred afterwards, especially with regard to the observations made with RAMBHA-LP and ChaSTE payloads on-board Chandrayaan-3.

The Chandrayaan-3 lander, which made precise landing at the intended location (69.3°S, 32.3°E) in the South Polar region of moon on 23 August 2023, carried the Langmuir Probe (RAMBHA-LP) and Chandra's Surface Thermophysical Experiment (ChaSTE) payloads developed by the SPL-led teams. Both ChaSTE and RAMBHA-LP were deployed and successfully operated from 24 August to 02 September 2023, and made the first in-situ measurements of the thermal properties of the lunar regolith and plasma content near the lunar surface. Several entities of VSSC (MVIT, AVN, PCM, STR, SR, MME, AERO, SPRE and CMSE) and review committees made significant contributions to the development and operation of these payloads. Physical Research Laboratory (PRL), Ahmedabad also contributed to the development and operation of ChaSTE.

As planned, the ChaSTE probe was telecommanded to release from its stowed position, deployed, and slowly inserted into the lunar regolith in steps of 2.5 mm till its tip reached 140 mm deep (including 40 mm nose cone). The surface touchdown of the sensors and further penetration were unambiguously detectable from the variations of sensor temperature and penetration motor current. The penetrated ChaSTE probe was clearly seen in the photographs taken by the Rover. The temperature profile of the regolith up to 96 mm depth and its variations at 1 second intervals during the lunar day were observed using ten PT1000 temperature sensors. Heating experiments were conducted at two different depths to determine thermal conductivity of the regolith. The observations revealed large vertical temperature gradients and poor soil thermal conductivity, which have several scientific and practical implications.

The RAMBHA-LP was deployed along the axis perpendicular to the lander such that the distance between the probe centre and the hinge at the lander body is 117 cm. The deployed position of the probe was further ascertained from the photographs taken by the lander. After deployment, the variations of current as a function of bias voltage, which was swept between -12 V to +12 V in steps of 0.1 V, were measured continuously throughout the lunar day to derive the plasma density variations with a sweep cadence of about 15 seconds. The observations were made when moon was within and outside the geomagnetic tail. The estimated electron density was typically a few hundred million electrons per cubic meter, and is comparable to the daytime electron densities derived from DFRS/Chandrayaan-2 observations at the lowest possible altitude (~2 km) and that calculated using the lunar photochemical model near the surface.

The flight model of the Plasma Analyser Package for Aditya (PAPA) payload onboard Aditya-L1 satellite has been developed, tested and delivered to URSC on 04 November 2022. PAPA is a joint development of SPL and AVN, with the support of other entities of VSSC. The payload was integrated with the spacecraft and all tests were successfully completed. The PAPA-FM and Proto-FM were calibrated at the High Vacuum Space Simulation Facility of SPL using standard ion and electron sources. PAPA QLD software has been installed at ISSDC and the team is preparing for the payload operations before the L1 orbit insertion.

During the reporting period, SPL has made significant progress in the scientific activities and new developments and has published 70 papers in peer-reviewed journals, with an average impact factor of 4.0. Five Technology Development Programmes (TDPs) are nearing completion. Four researchers were awarded Ph.D degree. Some of the major scientific accomplishments during the reporting period are highlighted below.

Surface layer characteristics over the tropical coastal station, Goa, were estimated and empirical relations connecting normalised wind and temperature variations with stability parameter were derived based on the micrometeorological observations (ISRO GBP-NOBLE Project). As part of the marine atmospheric boundary layer (ABL) characterisation over the Indian Ocean, the vertical structure and diurnal development of ABL over the tiny island Mahé, Seychelles (4.68°S, 55.53°E) in the western equatorial Indian Ocean have been investigated based on the

radiosonde observations, which showed significant diurnal variation with a daytime mean of 855±300 m and a nighttime mean of 165±85 m. The Palghat Gap Exit Jet during the summer monsoon season was investigated based on 30 years of reanalysis data, which showed that the high speed wind zonally extend for ~300 km over the Indian peninsula and is driven by the surface pressure variations at the north Bay of Bengal. Deep convective clouds derived from multi-year observations using SAPHIR/Megha-Tropiques have been used to characterise the meridional width of the ITCZ and their seasonal variations over the tropics.

The terrestrial biospheric CO_2 fluxes over India during 2011-2020 period have been estimated using the Vegetation Photosynthesis and Respiration Model (VPRM). The VPRM for the Indian region was configured using high-resolution data from Resourcesat-1 and Land Use-Land Cover data from IRS-P6 AWiFS. The estimates indicate that the average Net Ecosystem Exchange over the Indian region during 2011-2020 is -0.16 ± 0.02 PgC yr^{-1}. Large eddy simulations have been made for studying the coastal boundary layer characteristics and compared with Reynolds Averaged Navier-Stokes (RANS) simulations. An empirical model atmosphere from the surface to 110 km over the low latitude Indian region has been developed based on multi-decade observations from radiosonde, rocket-, and satellite-based measurements.

Multispectral - multidirectional observations using CAI-2 imager onboard GOSAT-2 satellite were used to retrieve black carbon (BC). These were validated with the near-surface BC mass concentration measured at the ISRO GBP-ARFINET observatories, and subsequently extended for elucidating the global distribution of BC. The polarization-resolved altitude profiles of backscatter coefficient observed from CALIPSO have been used to assess the mineral dust aerosols, their deposition rate and impact over the Himalayas, which indicate that dry deposition of dust aerosols on aged snow would reduce the albedo up to 2.7%. Chemical aging of biomass burning emissions transported over the northwestern Indo-Gangetic Plain (IGP) and its impact on BC light-absorption enhancement have been examined using simultaneous measurements of single particle refractory BC and near-real-time mass spectrometry measurements of non-refractory submicron aerosols at the IGP outflow site, Bhubaneswar. This study revealed that the BC particles were thickly coated, with mean relative coating thickness of 1.32 ± 0.14. Detailed studies on the chemical composition of aerosols, primarily focussed on the so far least explored organic aerosols (OA), have been carried out over distinct geographical regions in India and nearby oceanic region. Over the tropical coastal environments, OA are found to have a substantial mass fraction (67–85%) in the non-refractory mass loading during all seasons. Oxalic acid was found to be a dominant component of the dicarboxylic acids at the coastal regions (Thumba, Kochi), Western Ghats (Ponmudi) and semi-arid station (Ballari) in the peninsular India. Chemical properties of the continental outflow to the northern Indian Ocean (ICARB-2018 experiment) showed loss of organic aerosols due to ageing during long-range transport. The short-term increase in OC, OC/EC ratio, OM and OM/sulfate ratio during ultrafine particle bursts over the equatorial Indian Ocean indicate the possibility of prominent sources of marine organic compounds. A comprehensive study on aerosols over south Asia revealed that oxidation and ageing of long-range transported primary organic aerosols emitted from biomass burning serve as an important source of the water-soluble organic aerosols in this region.

Multi-year C-band polarimetric Doppler Weather Radar observations at Thumba were used to investigate the structure and evolution of organized precipitation bands during the Indian summer monsoon, which provided evidence for the upstream blocking mechanism for the formation of organized precipitation bands. Climate model simulations by IITM-Earth System Model were used to identify the long term changes in Hadley cell under different radiative forcing scenarios. The vertical distribution of ozone in the troposphere over the Arabian Sea and the Indian Ocean during winter (ICARB-2018 experiment) showed that the transport of polluted air mass from the Indian sub-continent cause an ozone-rich plume around 1-3 km altitude over the Indian Ocean. The changes in the intensity of Brewer-Dobson Circulation (BDC) during sudden stratospheric warming (SSW) and its impact on the tropical thermal structure and ozone distribution revealed abrupt decrease in BDC strength during major SSWs. Multi-year balloon-borne cryogenic frost-point hygrometer observations along with MLS satellite observations showed that the Indian sector is one of the major entry points of water vapour into the lower stratosphere. Two decades of temperature (SABER) and wind (TIDI) measurements onboard TIMED satellite showed that the vertical structure of zonal winds and meridional temperature gradient regulate the vertical propagation of quasi-2-day waves (QTDW) in the MLT region. The SABER observations showed a long-term decreasing trend of ~0.5 to 2.5 K per decade in the middle atmospheric temperature in the 50°S to 50°N latitude range and a corresponding increasing trend of ~4.5% per decade in CO_2. Short-term variabilities of diurnal tidal characteristics in the MLT region over Thumba observed using a decade of meteor wind radar measurements showed distinct events of anomalous tidal weakening that arise from the non-linear interaction between tides and QTDW.

First observations of the nocturnal thermospheric neutral wind and temperature over the geomagnetic equatorial region, Thumba (8.5°N, 77°E, 0.5° dip latitude) made using Fabry-Perot Interferometer (FPI) showed highest thermospheric temperature during post-sunset period in all seasons. Response of the thermospheric O^1D 630.0 nm dayglow emission to the variability associated with equatorial Counter Electrojet (CEJ) events were investigated based on the observations from scanning dayglow photometer, ionosonde and magnetometer over Thumba. Simulations using the in-house developed quasi 2-dimensional ionospheric model showed that the modified plasma fountain during the CEJ can alter the plasma density at the emission centroid, thus revealing a strong dynamical coupling between the E and F-region

at the dip equator. The electron density and ion drift velocity/neutral wind profiles derived from the observations using ENWi and LP payloads onboard the RH300 rocket flight (SOUREX experiment) revealed the presence of well structured electron density profile. These observations reveal the role of gravity wave induced winds in producing ion convergence over the geomagnetic equatorial region during post-sunset period. The effect of space weather events on the ionosphere-magnetosphere system over the Indian region were investigated based on TEC, HF radar and satellite observations during multiple events.

The characteristic features of different layers in the Venus ionosphere during the deep solar minimum were investigated using radio occultation (RO) experiment conducted by Akatsuki spacecraft, with radio signals tracked at IDSN-India, UDSC-Japan, and DLR-Germany, which revealed a distinct influence of the low solar activity on the V1 and V2 layer peak electron densities. The Akatsuki RO experiment in Venus ionosphere and simulations using the in-house developed 1-D photochemical model for Venus revealed that O_2^+ ions dominate when the V1 layer appears as a slope change below the V2 layer. The RO experiments conducted by Venus Express and Akatsuki indicate the vital role of gravity waves in shaping the V0 layer.

Model simulations were carried out to investigate the electrostatic solitary waves (ESWs) in the Venusian ionosphere impinged by the solar wind in a homogeneous, collisionless and magnetized multi-component plasma consisting of Venusian H^+ and O^+ ions, Maxwellian Venusian electrons and streaming solar wind protons and suprathermal electrons. The simulations could explain the observed features of ESWs in the Venus ionosphere. The two-stream instability generation in the lunar ionosphere has been examined by considering it as a small perturbation in plasma number density that leads to the bunching of electrons and the resulting electric field growing with time. The impact of the stealth CME on the topside Martian ionosphere was investigated using observations made by MAVEN and Mars Express missions; energization of both heavy and lighter ions during the event at ionospheric altitudes of Mars suggest deeper penetration of solar wind causing considerable acceleration and heating of the ionospheric plasma leading to enhancement in atmospheric loss. The 'Peak Filter Algorithm' was developed to determine and calibrate the mass shift in CHACE-2 observations onboard Chandrayaan-2, verify the spectrum quality and generate suitable flags in the output file.

The TDP activities have progressed well during the reporting period. Atmosphere Technology Division of SPL played a pivotal role in the design and development of various payloads and ground-based experiment systems. SPL took up a TDP to develop a suitable thermal sensor package for in-situ measurements of middle atmospheric temperature (up to ~60 km onboard RH200 rocket). The sensor is a small bead thermistor of 0.3 mm diameter coated with aluminium with lead wires of 0.03 mm diameter and was designed to have quick response time and minimise the effects of shortwave and longwave radiation. The design and development of this Rocketsonde system and its calibration (at 1 bar), response at 0.1 hpa level, and error analysis have been completed, in collaboration with other entities of VSSC (MME, PCM, AVN, and ESAE). The Rocketsonde has battery power supply and telemetry and is planned for high altitude balloon test at TIFR Hyderabad. The optics, control electronics and sun tracking system for the laboratory model of the Solar Occultation Experiment payload were realized and the ground-level testing of the system is being carried out. The system has to be augmented with more agile sun sensors and tracking system, which is being pursued. As part of TDP, a Standalone Sun Tracking Radiometer has been developed and its field testing is progressing, with the support of a design and fabrication team (SPL, ESAE and MME). A geomagnetically induced current (GIC) monitor has been designed, developed and tested in the laboratory (SPL and AVN). It can be used to measure the GIC - generated by a geomagnetic storm - that can potentially flow through power grids. The development of the Atomic Oxygen Sensor is progressing.

A new deep learning technique has been developed and validated for the retrieval of atmospheric temperature and humidity profiles from ground-based Microwave Radiometer observations. A multi-layered microwave radiative transfer model has been developed and used to simulate the microwave emission from the lunar subsurface at L and S bands. Methodology and software were developed for the 3D orbital simulations of occultation-viewing geometry for Solar Occultation Experiments in Venus atmosphere. This incorporates planetary motions and orbital propagation and was validated using the observations from SPICAV/SOIR and orbital parameters of Venus Express. A new method that enhances the frequency residual estimates in a one-way downlink single frequency RO experiment was developed and extensive error analysis has been carried out. This was validated using Akatsuki radio signals and the method used in Cassini RO data analysis. Subsequently, it has been used extensively to derive Venus ionospheric profiles of electron density. Development of the methodology and software, employing band radiation transfer that incorporate multiple scattering, absorption and surface reflectance, for the retrieval of aerosol optical depth from the visible and near infrared spectral radiances measured by Ocean Colour Monitor - 3 (OCM-3) onboard EOS-06 has progressed well.

The Payload Operation Centre (POC) at SPL serves as the nodal point connecting the payloads, mission, and ISSDC teams. CHACE-2 data is regularly received and processed at POC. Total of 836 data products from CHACE-2 were released during the reporting period, through the PRADAN portal. The POC has been also used for ChaSTE and RAMBHA-LP operations and is ready to meet the requirements of PAPA

and MAG payloads onboard Aditya-L1. As a member of the Inter-Centre Weather Forecast Expert Team of ISRO, SPL provides short-range weather predictions for all launch vehicle missions from Sriharikota.

Extensive discussions were held at SPL for preparing the "Vision 2047" and identifying the future scientific and technical developments to be taken up. Two major science problems to be addressed jointly by multiple divisions were identified: (i) Development of high-resolution radiation transfer models and inversion techniques for retrieval of the altitude profiles of atmospheric trace constituents in earth and planetary bodies based on high resolution limb, nadir and occultation measurements. These will have further applications in the retrieval of other atmospheric parameters. (ii) Development of models for predicting space weather events (including AI/ML techniques) and their impact on earth's ionosphere-magnetosphere system. SPL will also take up developments of inversion techniques for spaceborne lidar and radar. As part of the long-term plans, the spaceborne sensors to be developed for in-situ measurements of atmospheric parameters and plasma environment onboard future lander and orbiter missions to Moon, Mars, Venus and other planets were identified. Infrastructure to be developed for the analysis of samples returned from planetary bodies has been identified. Actions are initiated to realise these mid- and long-term goals.

SPL has organised the first scientific conference on "Science from In-situ Measurements of Aditya-L1" during 11-13 April 2023, which was attended by over 155 delegates from different universities and institutions across the country. Along with IIST, SPL has co-hosted the "23rd National conference on Atomic and Molecular Physics" during 20-23 February, 2023.

Dr. K. M. Ambili was awarded the Kerala State Young Scientist Award for the year 2022, instituted by Government of Kerala. Five Research Fellows who completed Ph.D. from SPL were awarded post-doctoral positions at prestigious institutions in USA, Europe and Japan during the reporting period. SPL continues its strong collaboration with several national and international institutions/universities. Senior scientists at SPL are members of the Research Advisory Committees and Academic Council/Board of Studies of leading national institutes/universities (ARIES, IIG, IITM, NARL, CRL-TIFR, Goa University and Rajasthan Central University). SPL has participated in the Indian Arctic Expedition (June-July 2023) based on the acceptance of the proposal for finger printing the sources of organic aerosols at the Arctic. Collaborative research activities were initiated between SPL/VSSC and Tokyo University on satellite-based retrieval of BC aerosols using CAI-2/GOSAT-2. SPL is leading the ISRO-JAXA Collaboration for Akatsuki Radio Science Experiment. Fifteen Research Fellows, Research Associates and scientists from SPL attended international scientific assemblies, conferences, workshops and training held at Greece, USA, Singapore, and Japan. A 5-member science team from the Swedish Institute of Space Physics (IRF), Sweden, led by Dr. Olle Norberg, Director General, IRF and Prof. Stas Barabash, Deputy Director General, IRF, visited SPL during 9-10 November 2022 and discussed on potential collaborations and joint developments in planetary research.

SPL scientists had interacted with students from various schools, colleges and with university researchers. Initial observations from ChaSTE and RAMBHA on-board Chandrayaan-3 were released through ISRO's website and Twitter handle, which evoked enthusiastic response from students, scientists and public. The ChaSTE and LP Twitter messages had multimillion views. Several electronic and print media also gave detailed coverage to these initial results and their impact.

We are thankful to Dr. T.K. Alex (Chairman, SPL-SAC) and members of the Scientific Advisory Committee of SPL (SPL-SAC) who meticulously review our scientific and technical development activities and future plans. The scientific deliberations with SPL-SAC are rejuvenating, and we have made the best efforts to implement the recommendations made by the committee.

All our major scientific and technical goals could be achieved only because of the visionary leadership at VSSC and ISRO. Dr. S. Unnikrishnan Nair, Director, VSSC has meticulously reviewed our research and development activities as well as plans in "Vision 2047" and is a driving force for the development activities. His unfailing support is a key factor in our achievements. We are extremely thankful to Shri. S. Somanath, Chairman, ISRO, for his valuable guidance, constant encouragements and inspiration for the research and development activities at SPL. His review and advices further sharpened our "Vision 2047" plans. We also thank our collaborating centres/institutions within and outside ISRO/DoS for their support.

I thank Team SPL for their scientific contributions towards realizing our objectives and congratulate them for the achievements. Thanks to the Editorial Team - Dr. C. Vineeth, Dr. Mukunda Gogoi, and Dr. S. Suresh Babu – for bringing out this report in its present form.

K. Rajeev
Director, SPL

02 November 2023

प्रकाशन / Publications

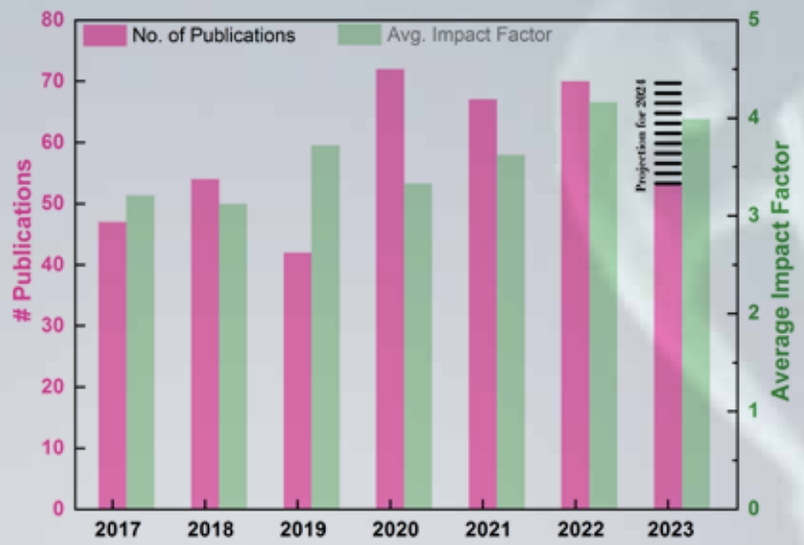

पीएच.डी. से सम्मानित / Ph.D. Awarded

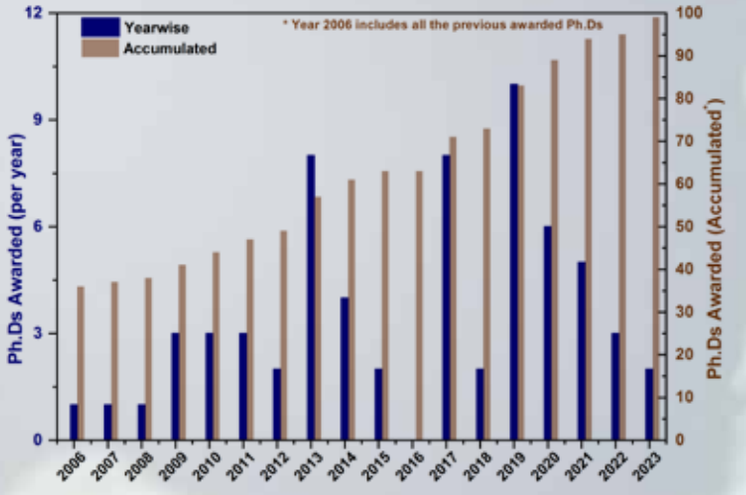

EDWIN DAVIS

- "Investigations on the Diurnal and Intraseasonal Variations of Tropical Coastal Atmospheric Boundary Layer, Forcing Mechanisms and Associated Changes in Tropospheric Water Vapour", University of Kerala, Thiruvananthapuram, September 2022 [Supervisor: Dr. K. Rajeev].

ARUN B. S.

- "Investigation of Atmospheric Aerosols over the Himalayas: Direct and Snow Albedo Forcing", University of Kerala, Thiruvananthapuram, October 2022 [Supervisor: Dr. Mukunda M. Gogoi].

GOVIND G. NAMPOOTHIRI

- "Studies on the Electron Velocity Distributions in the Solar Wind at 1 AU during Solar Transient Events", Cochin University of Science and Technology, Kochi, January 2023 [Supervisor: R. Satheesh Thampi].

USHA K.H.

- "Investigation of climate impacts of aerosols over the Himalayas using Regional Climate Model", University of Kerala, Thiruvananthapuram, June 2023 [Supervisor: Dr. Vijayakumar S. Nair].

सम्मान / Recognitions

AMBILI K. M.

- Kerala State Young Scientist Award, Kerala State Council for Science, Technology and Environment, Government of Kerala, 2022.

ANKUSH BHASKAR T.

- Guest Editor, Frontiers in Astronomy and Space Sciences, 2023.

अकादमिक उत्कृष्टता / Academic Excellence

RICHA NAJA JAIN

- First prize in the URSI-RCRS - Student Paper Competition, URSI-Regional Conference on Radio Science (URSI-RCRS 2022), IIT Indore, December 1-4, 2022.

SRUTHI T. V.

- Honorary mention in Student Paper Competition, URSI-Regional Conference on Radio Science (URSI-RCRS 2022), IIT Indore, December 1-4, 2022.

राष्ट्रीय संस्थानों तथा शिक्षा में योगदान / Contributions to National Institutions and Academia

- Member, COSPAR Council (Indian Representative).
- Fellow, Indian Academy of Sciences.
- Corresponding Member, International Academy of Astronautics.
- Member, Scientific Advisory Committees of;
  Indian Institute of Geomagnetism
  Indian Institute of Tropical Meteorology
  Cosmic Ray Laboratory - TIFR
  National Atmospheric Research Laboratory
  Aryabhatta Research Institute of Observational Sciences.
- Member, Advisory Committees for Atmospheric Radars at University of Calcutta and CUSAT.
- Member, INSA National Committee for Future Earth.
- Member, Academic Council, Central University of Rajasthan.
- Member, Board of Studies, Goa University, Goa.
- Team Lead (India), ISRO-JAXA Collaboration for Akatsuki Radio Science Experiment.
- Associate Editor, Journal of Earth System Sciences.
- Subject Editor (Space and Atmospheric Science, Planetary Science, Remote Sensing), Current Science.

समझौता ज्ञापन / Memorandum of Understanding

- MoU on Cooperation in Space Science Research and Academic activities between SPL-VSSC and Department of Higher Educatin, Institute for Excellence in Higher Education, Bhopal, Madhya Pradesh, June 11, 2023.

अंतर्वस्तु / Contents

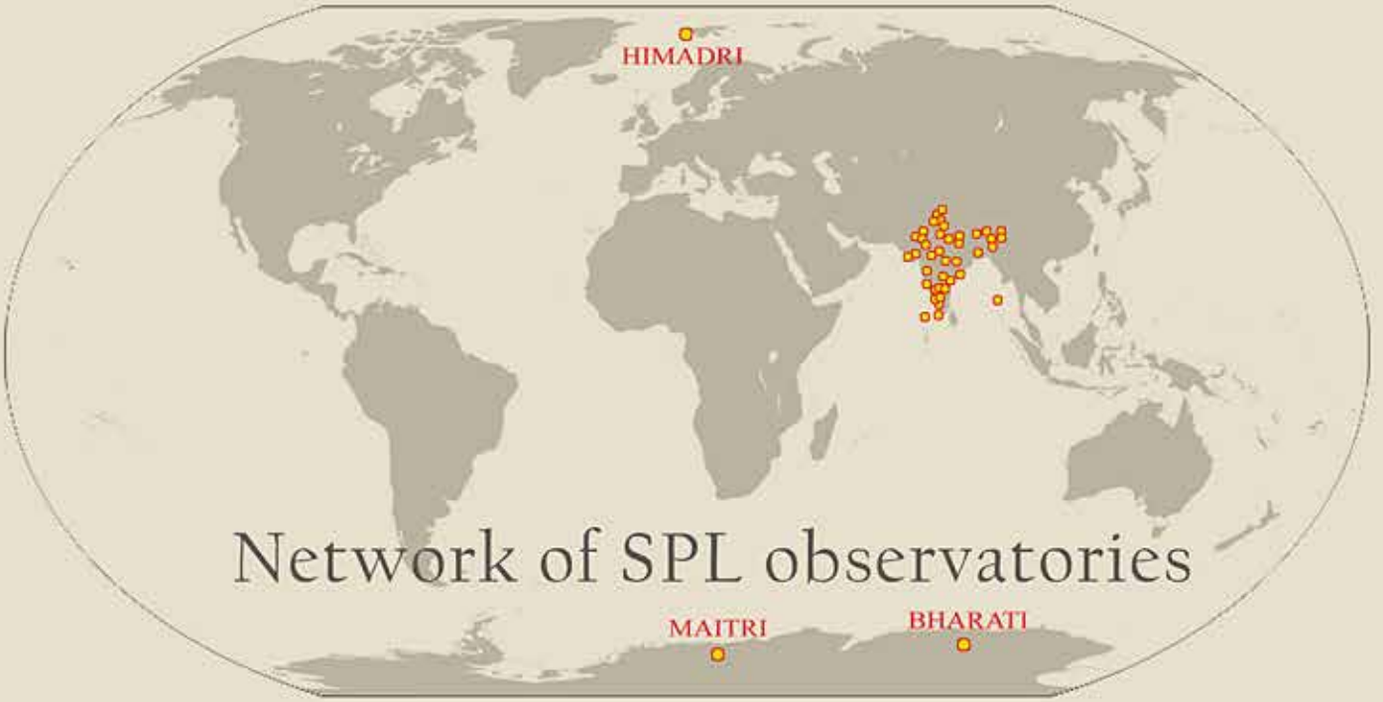

Network of SPL observatories

माइक्रोवेव एवं परिसीमा स्तर भौतिकी
Microwave and Boundary Layer Physics

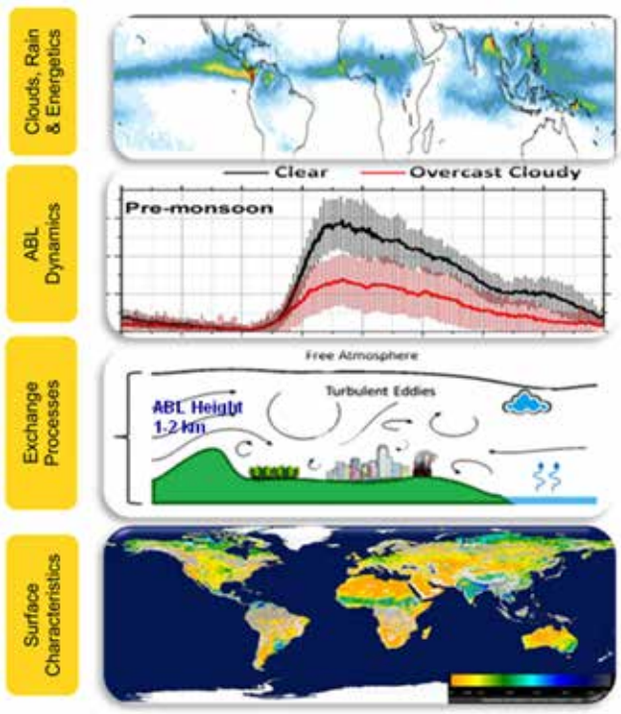

एमबीएलपी शाखा वायुमंडलीय परिसीमा परत (एबीएल) के पृष्ठीय अभिलक्षणों, संरचना एवं गतिकी तथा मुक्त क्षोभमंडल, मेघों, संवहन, अवक्षेपण के साथ इसके युग्मन और पृथ्वी एवं अन्य ग्रहीय पिंडों के माइक्रोवेव सुदूर संवेदन पर ध्यान केंद्रित करती है। इस शाखा के मुख्य लक्ष्य हैं: (i) पृष्ठ-वायु अन्योन्यक्रिया प्रक्रियाओं, एबीएल के दैनिक प्रादुर्भाव व प्रदूषक प्रकीर्णन में एबीएल प्रक्रियाओं की भूमिका सहित सुस्पष्ट भौगोलिक पर्यावरण के बारे में समझ को बढ़ाना (ii) मेघों, अवक्षेपण एवं भू-वायुमंडल प्रणाली की ऊर्जिकी से संबंधित समझ को सुधारना, एवं (iii) ग्रहों के सतहों की अंतरिक्षवाहित तथा भू-आधारित माइक्रोवेव सुदूर संवेदन से पृष्ठीय गुणधर्मों, वायुमंडलीय जल वाष्प, मेघ अभिलक्षणों एवं अवक्षेपण, तथा वायुमंडल के माध्यम से माइक्रोवेव संचरण पर उनके संभाव्य प्रभावों का अध्ययन।

The MBLP branch focuses on the surface characteristics, structure and dynamics of the atmospheric boundary layer (ABL) and its coupling with free-troposphere, clouds, convection, precipitation, and microwave remote sensing of the Earth and other planetary bodies. The main objectives are: (i) to improve the understanding of the ABL processes under distinct geographical environments, including surface-air interaction processes, diurnal evolution of ABL, and the role of ABL processes in pollutant dispersal (ii) improve the understanding on clouds, precipitation and energetics of the Earth-atmosphere system and (iii) space-borne and ground based microwave remote sensing of planetary surface and atmosphere for deriving the surface properties, atmospheric water vapour, cloud characteristics and precipitation, including their potential impact on microwave propagation through the atmosphere.

वैज्ञानिक टीम / Science Team
सत्यमूर्ती वी. / Sathiyamoorthy V.
किरण कुमार एन. वी. पी. / Kiran Kumar N. V. P.
निज़ी मात्यू / Nizy Mathew
संतोष एम. / Santosh M.
रंजू आर. / Renju R.
शैलेन्द्र कुमार / Shailendra Kumar
राजीव के. / Rajeev K.

तकनीकी टीम / Technical Team
दिनकर प्रसाद वज्जा / Dinakar Prasad Vajja
प्रमोद पी. पी. / Pramod P. P.
लाली पी. टी. / Lali P. T.

अनुसंधान सहयोगी / Research Associates
लावण्या एस. / Lavanya S.[@]
एडविन वी. डेविस / Edwin V. Davis[#]

अनुसंधान अध्येता / Research Fellows
सीस्मा सामुवल / Sisma Samuel[&]
अश्वती आर. एस. / Aswathy R. S.
फात्तिमा षिरिन पी. टी. / Fathima Shirin P. T.*
स्वाती बी. / Swathi B.*

@ Relieved in August 2022
 # Relieved in January 2023
& Relieved in March 2023
** Joined in March 2023*

Characterization of Atmospheric Boundary Layer

Structure and Development of the Atmospheric Boundary Layer over a Small Island in the Equatorial Indian Ocean

The island of Mahé, Seychelles (4.68 °S, 55.53 °E) is located in the western equatorial Indian Ocean close to the region responsible for the initiation and eastward propagation of the Madden-Julian oscillation. It is also a part of the Seychelles dome (an oceanic thermal dome) and the Seychelles-Chagos Thermocline Ridge each of which influences the atmosphere at multiple time scales. This small island (area ~150 km^2) can be considered as a large ship permanently anchored at the equatorial Indian Ocean, capable of making long-term atmospheric observations representing its surroundings provided its ABL structure and development are known. This study presents in-situ observations of day-night variability of ABL over Mahé, Seychelles using high vertical resolution radiosonde ascents. The data were collected as part of the DYNAMO field campaign conducted during November 2011 - January 2012. The ABL height (ABLH) was observed to vary in the range of 200-1300 m in the course of a day with a day-time mean of 855 ±300m and a night-time mean of 165±85 m (Fig. 1a). The occurrence of unstable boundary layer is high at 15:30 LT and stable boundary layer is high during 03:30 LT (Fig. 1b). During the unstable boundary layer occurrences, a statistically significant positive (negative) correlation was observed between ABLH and near-surface temperature (near-surface relative humidity) with a correlation coefficient, R = 0.77 (R = -0.45) indicating that a warmer island produces a deeper boundary layer subject to limits imposed by the marine influence (Fig. 1c-d). It also indicates the significant contribution of sensible heat flux to ABLH at the site. The near-surface wind speeds do not correlate with ABLH in the stable, unstable, and neutral regimes. But wind speeds greater than 5 ms^{-1}are observed to be not coincident with highly stable (virtual potential temperature gradient > 8 K km^{-1}) near-surface layer (Fig. 2) indicating that they either disrupt it by mechanical wind shear or advect it out of the island leading to dissipation over the surrounding marine ABL.

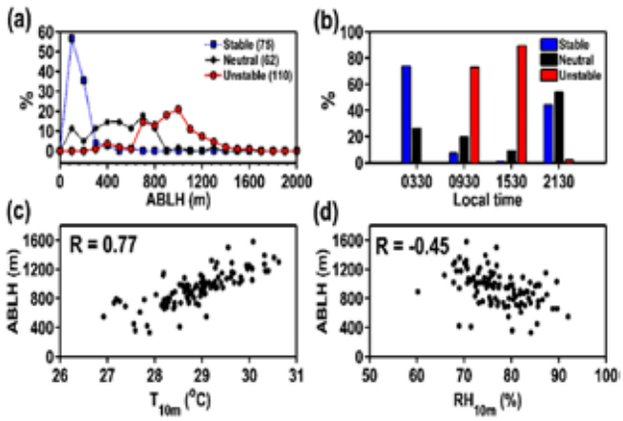

Figure 1: (a) Probability distribution for the occurrences of ABLH for stable, neutral, and unstable regimes of ABL. The histogram is divided into bins of 100 m height (in the vertical) for all the cases. The number of radiosonde ascents in each regime is shown in parenthesis (b) Diurnal evolution of frequency of occurrence of stable, neutral, and unstable boundary layer regimes. Dependence of ABLH to (c) near-surface temperature and (d) near-surface relative humidity [Santosh M, Meteorology and Atmospheric Physics, 2022].

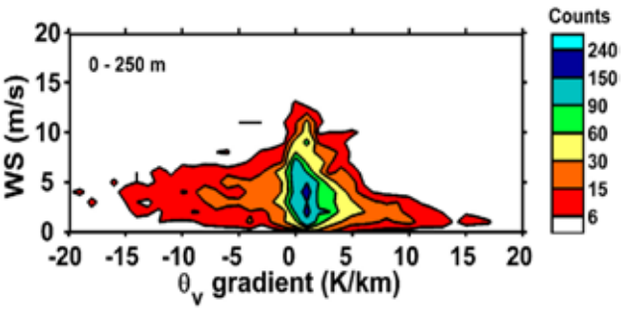

Figure 2: Contour plot of the θ_v gradient and wind speed for the altitude range 0-250 m for all the radiosonde ascents conducted from Mahé island. The total counts are shown in contours. The contour intervals are chosen to highlight the extreme values of the θ_v gradient [Santosh M, Meteorology and Atmospheric Physics, 2022].

Surface Layer Characteristics over the tropical coastal station, Goa (IGBP-NOBLE Project)

Understanding of the atmospheric surface layer (ASL) processes over a region requires knowledge of the turbulence characteristics during different seasons. Such studies attain important implications for modelling the turbulent exchange coefficients in regional scale numerical models and pollutant dispersion studies. The surface layer characteristics over the tropical coastal station, Goa (15.46 °N, 73.83 °E) was explored in this study. The seasonal mean ASL energy and momentum fluxes and turbulence characteristics over Goa were investigated based on the observations from fast-response sonic anemometers mounted at two levels (10-m and 20-m) on a 32-m meteorological tower installed at the University of Goa campus under the IGBP-NOBLE Project during March 2015 - February 2016. The data was subjected to quality checks such as double rotation and tilt corrections to minimize the effect of misalignment of sensors. The sensible heat flux (H) at 10-m attains the maximum seasonal mean value (76 Wm^{-2}) during pre-monsoon season, followed by winter season (61 Wm^{-2}), post-monsoon season (51 Wm^{-2}) and minimum (11 Wm^{-2}) during summer monsoon season (Fig.3). Seasonal mean values of H at 20-m height lie within 15% of the values obtained at 10-m height. Seasonal mean value of turbulent kinetic energy (e) is high during the summer monsoon season (≈0.76±0.33 m^{2}s^{-2} at 10-m height) due to strong monsoon winds. Variation of momentum flux (τ) exhibits a typical diurnal cycle in phase with e during all the seasons. The highest seasonal mean τ at 10-m is observed during the summer monsoon season (≈0.17±0.09 Nm^{-2}) and lowest during post-monsoon season (≈0.07±0.03

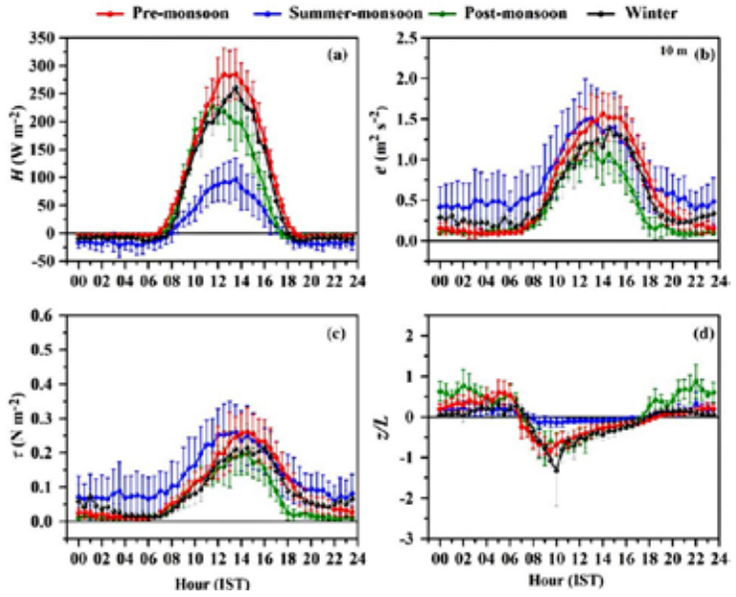

Figure 3: Seasonal mean diurnal variations of [a] sensible heat flux (H), [b] turbulent kinetic energy (e), [c] momentum flux (τ), and [d] stability parameter (z/L) observed at 10-m height during winter, pre-monsoon, summer-monsoon and post-monsoon seasons. The vertical bars indicate standard deviations [Salim, S. N. et al., Meteorology and Atmospheric Physics,2023].

Nm^{-2}). The observed diurnal variation of stability parameter (z/L) at 10-m height showed a systematic unstable and stable conditions during day-time and nocturnal periods respectively.

Figure 4 shows the variation of normalized standard deviations of along wind (σ_u/u_*), cross wind (σ_v/u_*), and vertical wind (σ_w/u_*) components as a function of z/L at 10-m and 20-m heights for stable and unstable conditions. Results show that $\sigma_{i=u,v,w}/u_*$, follow the '1/3' power law in the free convection limit and approach constant value of about 1.2 in neutral stratifications thereby conforming to the Monin-Obukhov similarity theory. The mean values of $\sigma_u/u_* > \sigma_v/u_* > \sigma_w/u_*$ in the neutral regime agree well with other locations. The present results confirm that the surface turbulence characteristics observed over Goa follow similarity relations. Present results also show that turbulence statistics are independent of season. Additionally, the normalized temperature variances (σ_T/T_*) follow $(z/L)^{-1/3}$

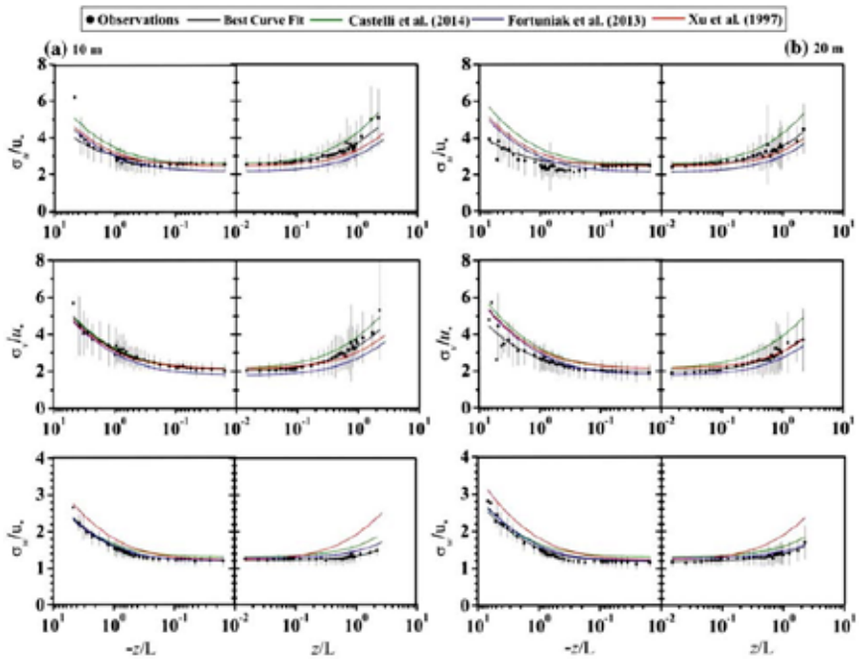

Figure 4: Variation of normalized standard deviation of wind velocities as a function of z/L for unstable (z/L < 0) and stable (z/L > 0) conditions over Goa at 10-m height (left panel) and 20-m height (right panel). The vertical bars indicate standard deviations. The black solid curve represents curve fitted using present observations; green, blue and red curves represent the function curves of Trini Castelli et al. (2014), Fortuniak et al. (2013) and Xu et al. (1997) respectively [Salim, S. N. et al., Meteorology and Atmospheric Physics,2023].

during unstable conditions and approach a constant value in stable limit.

Characteristics of Strong Boundary Layer Winds on the Exit Region of the Palghat Gap during the Indian Summer Monsoon Season

Palghat gap (~76.5°E; 10.75°N) is a narrow gap in the Western Ghats mountain chain of south India. Strong westerly winds flow from its exit during the Indian summer monsoon season (June to September, JJAS). Climatological three-dimensional structure of these exit winds is presented using thirty years (1983-2012) 'Indian Monsoon Data Assimilation and Analysis' regional reanalysis data (Fig.5). These exit winds initially accelerate, attain their maximum speed around 77.5°E and slow down thereafter. This wind flow is prominently seen between the surface and ~ 700 hPa in the vertical, ~ 77°E and ~ 80°E in the zonal and ~ 10.5°N and 11.5°N in the meridional directions. We refer these strong winds as the Palghat Gap Exit Jet (PGEJ). Core of the PGEJ is found ~ 950 hPa with its axis passing along ~ 10.8°N. Direction of the PGEJ is steady throughout JJAS.

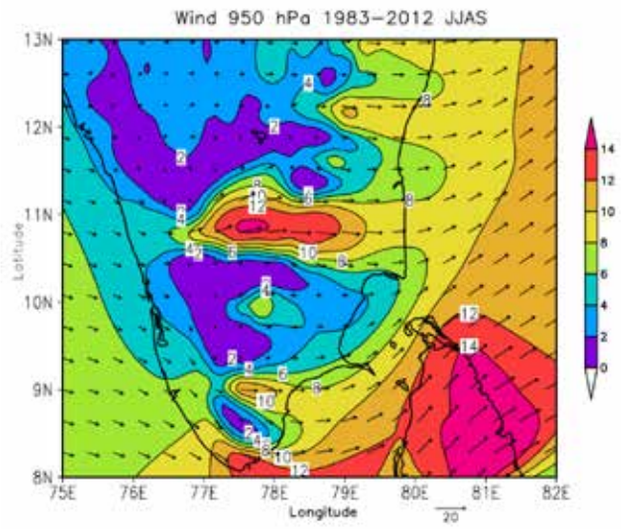

Figure 5: Thirty years (1983-2012) climatology of 950 hPa wind speed (ms^{-1}) at 00:00 UTC averaged during the summer monsoon season of JJAS for the south peninsular India [in contours as well as in shades].Climatological seasonal mean wind vectors are also overlaid [Sathiyamoorthy et al., Climate Dynamics,2023].

To understand the possible reasons behind the formation of PGEJ, detailed analysis using four years (2009-2012) of reanalysis data is carried out. The spatial correlation analysis suggests that the strength of the PGEJ is inversely correlated to the mean sea level pressure variations over the monsoon trough region and weakly positively correlated to the pressure variations in the entrance region of the Palghat gap (Fig. 6). PGEJ fluctuates from diurnal to intraseasonal (30-60 days) time scales. On diurnal scale, strength and zonal extent of the PGEJ are stronger and wider respectively around mid-night whereas weaker and shorter respectively around noon. Also, PGEJ is shallow during night but relatively deeper during day. On intraseasonal time scale, PGEJ is stronger (weaker) than its seasonal mean strength during active (break) monsoon phase. Besides, PGEJ becomes stronger when synoptic scale monsoon low-pressure systems pass over the northwest Bay of Bengal and adjoining monsoon trough region. Occurrence of PGEJ only during JJAS with characteristic variabilities of the Indian summer monsoon and its close association with

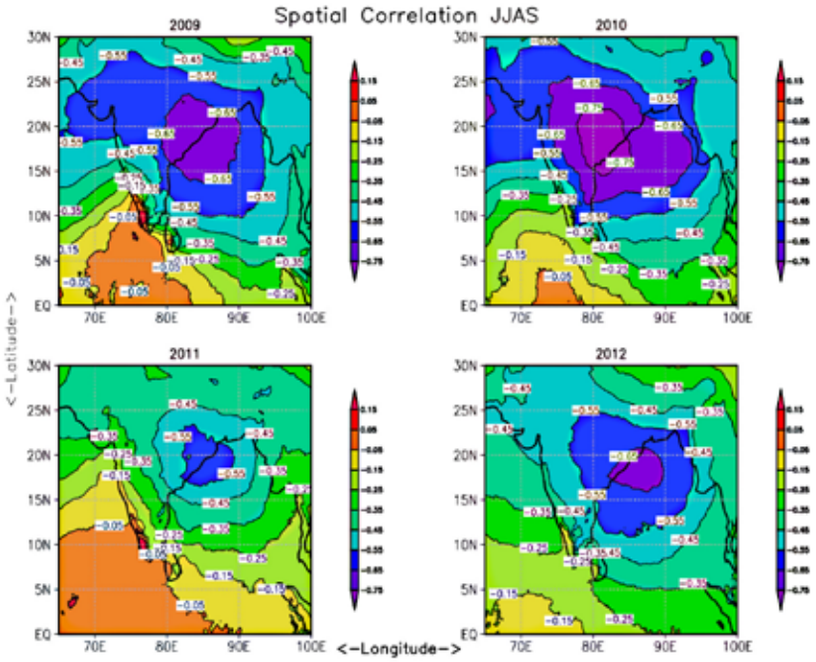

Figure 6: Horizontal distribution of temporal correlation between daily 950 hPa zonal wind at 00:00 UTC averaged over the box bound by 77.5°E-78.5°E and 10.6°N-11.0°N (exit region of the Palghat gap) and daily mean sea level pressure over the study region during 01 June to 30 September for 2009 to 2012 [Sathiyamoorthy et al., Climate Dynamics,2023].

monsoon trough collectively suggest that it is an integral part of the Indian summer monsoon low-level /circulation.

Clouds, Precipitation and Energetics of the Earth-Atmosphere System

Vertical Characteristics of Precipitating Cloud systems during Different Phases of their Life Cycle over Tropical Oceanic Regions using Satellite-based Radar Data

An index-based approach is applied to investigate the climatological characteristics of precipitating cloud systems (PCSs) during different phases of their evolution over different tropical oceanic regions [Bay of Bengal, West Equatorial Indian Ocean, East Equatorial Indian Ocean, Maritime Continent, North Pacific Ocean, Central Pacific Ocean and Atlantic Ocean] using Precipitation Radar (PR) onboard Tropical Rainfall Measuring Mission (TRMM) satellite. Connecting pixels having radar reflectivity (Z_e) ≥ 17dBZ are defined as PCS. A cloud system consists of four phases namely, initial, intensifying, mature and dissipating phases. An index (ratio of maturity level, ML) is defined based of normalized cloud liquid water (NCLW) to identify different phases onthe cloud systems:

ML = Maximum NCLW (4-6 km) /Maximum NCLW (1-3 km)

ML values corresponding to the four PCS phases are as follows: (a) Initial phase (ML1: ML ≤ 0.5, (b) Intensifying phase (ML2: 0.5 < ML ≤ 0.75), (c) Mature phase (ML3: 0.75 < ML < 1.0 and (d) Dissipating phase (ML4: ML ≥1.0).

Figure 7 reveals that average vertical profiles of Z_e show higher reflectivity values near the surface during the initial phase and peak reflectivity near the freezing level during dissipating phase. The peak in Z_e during different phases of evolution depends on the balance between growth and removal of hydrometeors. Large difference in radar reflectivity is found between different regions (a) below the freezing level and (b) during initial and dissipating phases. Fewer regional differences are seen in Z_e values above 8 km as TRMM could not detect the ice. The climatology of cloud vertical structures remained almost similar over all the tropical oceanic regions considered for the study. The convective to stratiform ratio decreases as the cloud system mature and is minimum during the decaying stage. From the analysis it is clear that the maturity indexing approach is able to discriminate the PCSs into different phases of evolution well.

Characteristics of cloud properties over South America and the Andes Mountains observed using CloudSat and Reanalysis data

CloudSat profiles of attenuation corrected radar reflectivity (Z_e) and cloud mask data were used to investigate the cloud properties over South America (SA) during Austral Summer monsoon season (December to March). Deep convective core (DCC), deep & intense convective systems (DCSs & ICSs) and cloud clusters (CCs) are defined based on Z_e and cloud mask values. Fig. 8 shows that horizontal

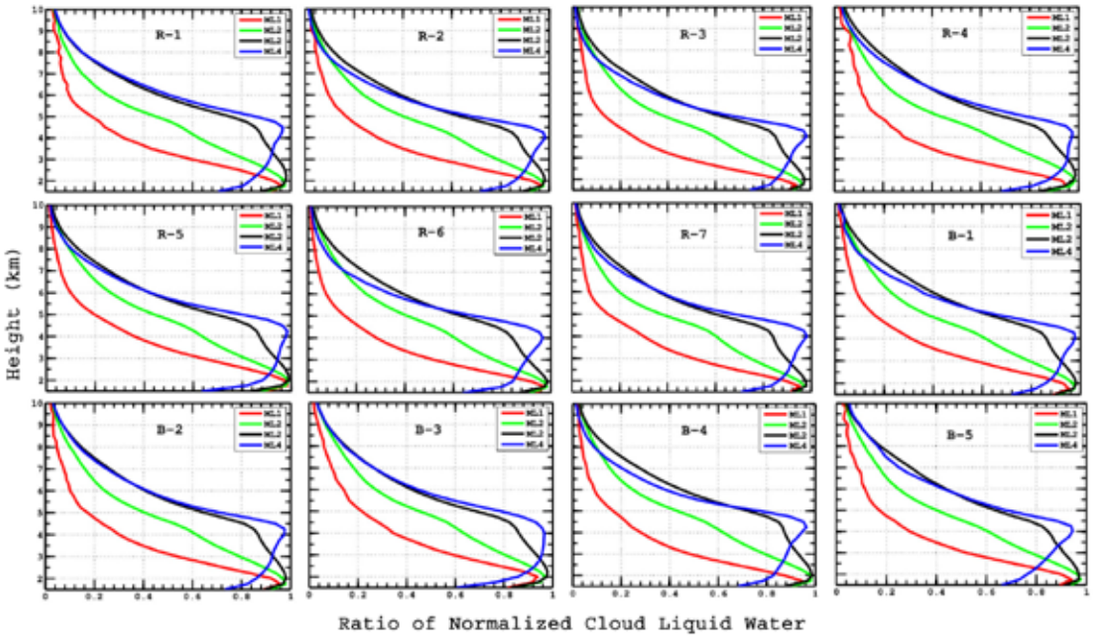

Figure 7: Areal evolution of the fraction of precipitation area for PCSs during different ratio of maturity levels. The different regions considered for the analysis are: Bay of Bengal (R-1), West Equatorial Indian Ocean (R-2), East Equatorial Indian Ocean (R-3), Maritime Continent (R-4), North Pacific Ocean (R-5), Central Pacific Ocean (R-6), Atlantic Ocean (R-7). West Equatorial Indian Ocean (B-1), East Equatorial Indian Ocean (B-2), Maritime Continent (B-3), Central Pacific Ocean (B-4), Atlantic Ocean (B-5). Regions R-1 to R-7 are selected during June to September months whereas regions B-1 to B-5 are selected during December to March months [Shailendra Kumar and S. Srivastava, J. Applied and Nat. Sci., 2022].

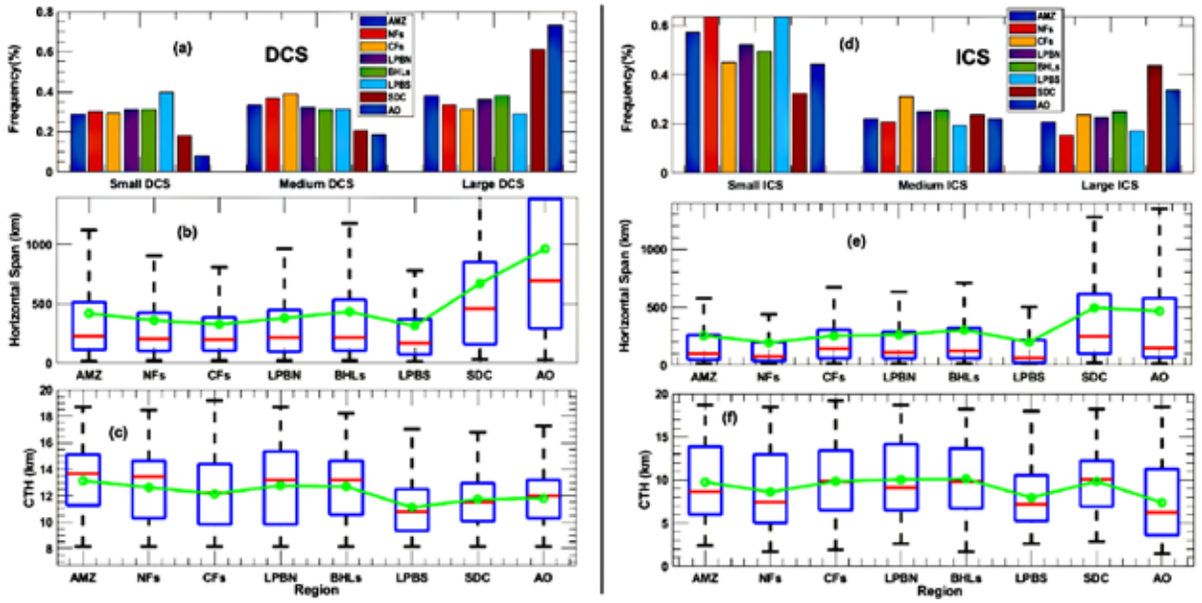

Figure 8: (a) Normalized occurrence frequencies (%) of deep convective systems (DCSs) at different horizontal spans in the eight regions [AMZ: Amazon, NFs: North Foothills, CFs: Central Foothills, LPBN: La Plata Basin North, BHLs: Brazilian Highlands, LPBS: La Plata Basin south, SDC: Sierra de Cordoba, AO: Atlantic Ocean]. For each region, bars represent (left to right) small (120 km), medium (120-320 km) and large (>320 km) convective systems. (b) Box-plot of the width of the deep convective systems (DCSs) observed over the selected areas. In each box-plot the red line is showing the median horizontal span of the DCSs, whereas green dots are showing the average horizontal span of the DCSs. (c) Box-plot of Cloud Top Height (CTH) for DCS over the selected regions. (d), (e) and (f) are same as (a), (b) and (c), but for ICSs [Shailendra Kumar et al., Int. J. Rem. Sensing, 2023].

span of DCSs and ICSs are higher over Sierra de Cordoba and the Atlantic Ocean compared to other South American areas. South La Plata basin (Atlantic Ocean) has the highest (lowest) frequency of small DCSs. DCSs and ICSs show the opposite characteristics as all the selected areas (Amazon, North Foothills, Central Foothills, La Plata Basin North, Brazilian Highlands, La Plata Basin south, Sierra de Cordoba and Atlantic Ocean) have a higher fraction of large (small) sized DCSs (ICSs). It is important to observe that the regional differences are larger in height based convective systems (DCSs) compared to intensity (Z_e) based ICSs. Cloud clusters develop more in horizontal than in vertical direction over the high latitudes and vice versa over lower latitudes. Horizontal span of cloud clusters increases from north to south over South America and adjoining oceans for all the longitude belts but at the same time their cloud top height decreases.

The eastern flank of Andes has higher frequency of cloud systems compared to western flank. Deep convection over the Sierra de Cordoba and South La Plata Basin is characterized by precipitation-size particles whereas over north La Plata Basin is dominated mostly by cloud-size particles. The characteristics of cloud clusters are influenced by the orography and moisture flow pattern at the east and west sides of the Andes. Easterly moisture loaded flow transports moisture from the Amazon which converges near the Andes and their lifting by upslope flow causes higher rainfall rate. Rising wind along the north-east slope of the Andes condensate quickly and precipitate locally, producing higher Z_e.

Microwave studies

Characterization of the Inter Tropical Convergence Zone Using SAPHIR/Megha-Tropiques Satellite Brightness Temperature Data

Conventionally, parameters such as low outgoing longwave radiation (OLR), high precipitation and strong surface wind convergence are used to identify and characterize the Inter Tropical Convergence Zone (ITCZ). These parameters suffer from some inherent issues while identifying the ITCZ. A new method based on the identification of deep convective cloud cores (DCCCs), derived from brightness temperature (TB) data of the water vapour absorption channels of Sondeur Atmosphérique du Profil d'Humidité Intertropicale par Radiométrie (SAPHIR), onboard Megha-Tropiques (MT) satellite is proposed in this work to identify the ITCZ. Using this new method, ITCZ is identified over the global tropics using eight years (2011-2018) of SAPHIR data and studied its characteristics (Fig. 9). In this method, deep convective cloud cores where large upscale growth of the cloud occurs alone are identified, excluding the cirrus anvils associated with them. The spatial pattern of ITCZ derived using the occurrence frequency of DCCC is in good agreement with the surface wind convergence over the global oceans derived from satellite scatterometer observations.

This new method identifies the ITCZ well and performs better over (a) anvil and cirrus dominated areas where OLR based methods face difficulties, (b) coastal and continental areas where satellite scatterometer data are unavailable to

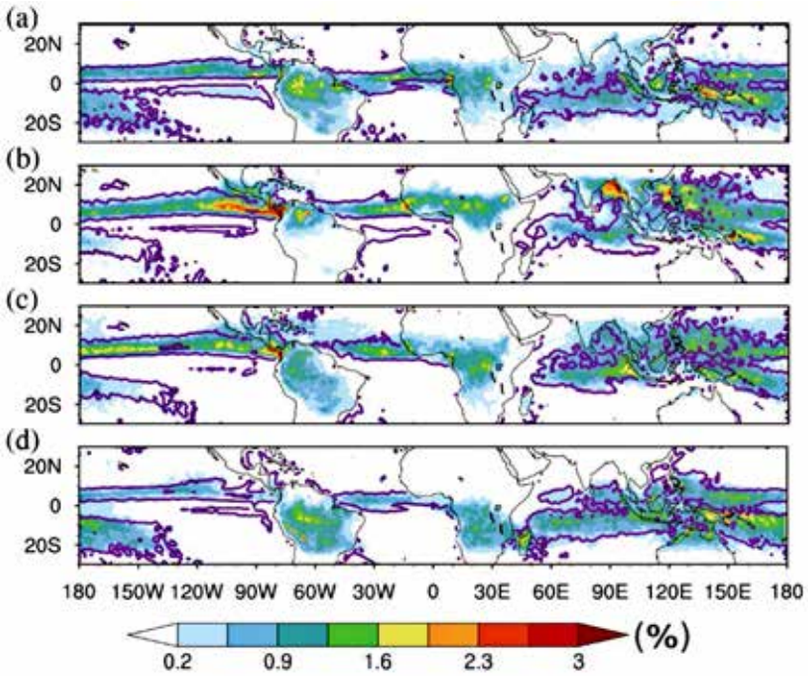

Figure 9 (a-d) : Seasonal mean distribution of occurrence frequency of DCCCs in percentage (shades) during (a) March to May (MAM), (b) June to August (JJA), (c) September to November (SON) and (d) December to February (DJF) seasons estimated using SAPHIR data of 2011-2018 showing the spatio-temporal distribution of the ITCZ.The contours overlaid show the boundary of surface wind convergence threshold (-0.1x10^{-5} s^{-1}) obtained from ASCAT scatterometer wind data over global oceans [Samuel, S. et al., Climate Dynamics, 2023].

estimate surface convergence and (c) windward side of orographic regions where rainfall based methods fail. The global mean position of the ITCZ is north of the equator, with maximum northward migration up to 24°N during June-August months over the Asian summer monsoon region and maximum southward migration up to 20°S during December-February months over the Indian and the Pacific Oceans. The ITCZ has a broad structure over the West Pacific Ocean and Indian Ocean regions, extending from 10° N to 10°S latitudes, and has a narrow band structure over the Central Pacific Ocean, East Pacific Ocean and the Atlantic Ocean. Over the Atlantic and West Pacific Oceans, the ITCZ has a reduced strength during ElNĩno periods compared to normal years.

Retrieval of atmospheric temperature and humidity profiles from ground-based Microwave Radiometer using deep learning technique

Ground-based multi-frequency Microwave Radiometer Profiler (MRP) provides valuable information of the altitudinal distribution of atmospheric humidity and temperature in the troposphere (up to ~10 km) with high temporal resolution (~1 minute) under all-weather conditions. These are vital inputs for the characterization of atmospheric boundary layer, convective cloud systems, local weather and for studying atmospheric dynamics. One such MRP was installed and in operation at Space Physics

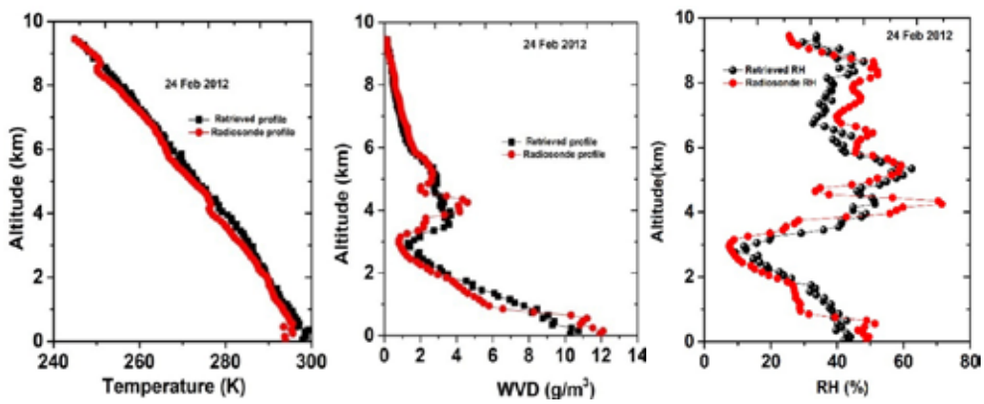

Figure 10: Comparison between retrieved (black line) and radiosonde (red line) temperature profiles (left panel), WVD profiles (middle panel) and RH profiles (right panel) over Thiruvananthapuram for 24 February 2012 [Renju, R. et al., Journal of Atmospheric and Solar Terrestrial Physics, 2023].

Laboratory, Thiruvananthapuram from 2010 and it provided continuous data for about seven years. This instrument measures brightness temperatures (T_B) at Ka- and V-bands. A trained back-propagation neural network technique based on the radiosonde data of more than a decade was used to derive the atmospheric humidity and temperature profiles. A new retrieval technique based on deep learning approach - batch normalization and neural network (BNN) has been developed to retrieve temperature and water vapour density (WVD) profiles from T_B values for clear sky conditions. This retrieval technique, faster in computation, consists of two hidden layers. The rectified linear unit is used as the activation function as it overcomes the problems of saturation and vanishing gradients. Using the forward radiative transfer model, T_B values are simulated using collocated radiosonde measurements and compared them with the T_B values observed by MRP. Bias correction is done before retrieving the atmospheric profiles from the observed T_B values. Comparison of retrieved temperature (K) profile, WVD (g/m^3) profile and relative humidity (RH (%)) profile against the radiosonde measurements is shown for 24 February 2012 in Fig. 10. Validation of retrieved profiles using new technique with radiosonde observations suggests a good retrieval capability with a root mean square error of 1.8 K for temperature, < $2g/m^3$ for WVD and ~14% for relative humidity.

Simulation analysis of Microwave Emission from Lunar subsurface for SAR Radiometric Mode Dual Frequency (L & S bands) observations onboard Chandrayaan-2

Dual Frequency Synthetic Aperture Radar (DFSAR) onboard Chandrayaan-2 has the provision for experimental radiometric mode of operation. A multi-layered microwave radiative transfer model coupled with a thermal model has been used to account for the microwave thermal emission or the brightness temperature (T_B) from the lunar subsurface at 1.25 GHz and 2.5 GHz frequencies. Simulated vertical temperature profiles for every four-hour interval using thermal model at different depths (0-50 cm) at the lunar equator over a lunation period are shown in Fig. 11. This figure shows that the lunar surface temperature varies over a large range of 95 K - 385 K during the lunation period at the equator. The impacts of solar forcing in day-time and radiative cooling in night-time are prominent up to ~ 30 cm depth.

As the dielectric property of the lunar regolith is the primary deciding factor of microwave penetration into the lunar surface, the dielectric model which considers both frequency and metallic content is used in this study. In Fig. 12, T_B simulated by the model are compared with the observed T_Bs of Chang'E-2/Microwave Radiometer (MRM) at 3 GHz. The diurnal variationof simulated T_B at 1.25 GHz is small (~3 K) with a mean value of ~250K while that at 2.5 GHz is >7-8 K with a mean value of ~ 245 K. Fig.13 shows the polarization difference (T_{BV} -T_{BH}) at different frequencies for varying depths of regolith. The frequency variations of polarization difference in different regolith layer thickness indicate that the lower frequencies with deeper penetration are sensitive to the dielectric fluctuations at deeper depths. Hence lower frequency (longer wavelength) radiometric probing of DFSAR could be useful for studying the sub-surface inhomogeneity caused by water ice, minerals and rocky layers.

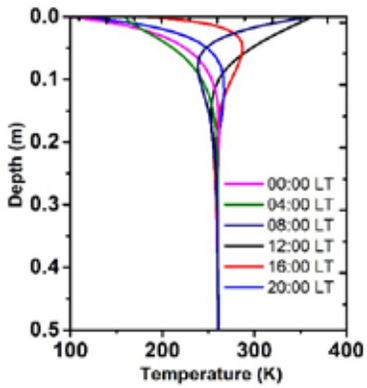

Figure 11: Simulated temperature profiles (K) for every four hour using thermal model at different depths over a lunation period at the lunar equator [Renju, R. and C. Suresh Raju, Advances in Space Research, 2023].

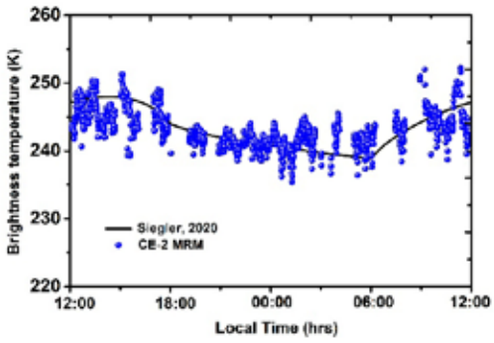

Figure 12: Diurnal variation of simulated brightness temperature at 3 GHz (solid line) and the observations (circles) from observational data at 3 GHz over the lunar equator [Renju, R. and C. Suresh Raju, Advances in Space Research, 2023].

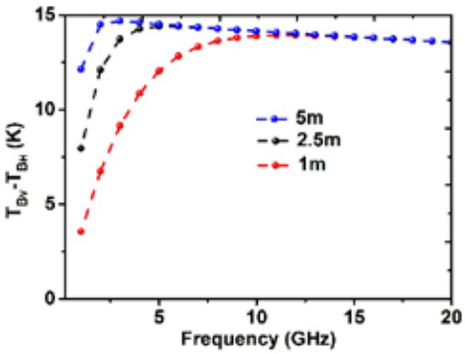

Figure 13:The amplitude of T_B difference between V and H polarizationsof different microwave frequencies (1-20 GHz) with an observation angle of 40°for varying depths of the regolith at lunar noon [Renju, R. and C. Suresh Raju, Advances in Space Research, 2023].

Payload Development

Chandra's Surface Thermophysical Experiment (ChaSTE) Payload Development for Chandrayaan-3 Lander

ChaSTE payload is designed to investigate the thermophysical properties of the lunar regolith over the polar region. The Flight Model of ChaSTE payload has been developed, qualified and delivered to the project (Fig. 14). The following Integrated Spacecraft Tests (IST) have been completed.

(a) Disassembled mode IST

(b) Assembled mode IST

(c) Pre-thermovacuum IST

(d) IST during thermovacuum cycling in the following conditions:

  (i) Cold soak

  (ii) Hot soak

  (iii) Short cold soak

  (iv) Short hot soak

(e) Post Thermovacuum IST

Figure14: Chandrayaan-3 spacecraft with ChaSTE payload.

During the retraction of the probe after Post Thermovacuum IST, a crack was observed on the probe. A new probe with sensors and heater and the fore-end assembly mechanism were developed, qualified for the flight and replaced with the probe with crack. Test and evaluation of ChaSTE Quick Look Display (QLD) software were completed.

Performance of ChaSTE/Chandrayaan-3 payload

Chandrayaan-3 was launched from SDSC, Sriharikota on 14 July 2023 by LVM3 rocket. The ChaSTE payload was switched ON in the earth bound orbit on 30 July 2023 and in the lunar orbit on 12 August 2023. Chandrayaan-3 successfully soft-landed on the moon on 23 August 2023.

ChaSTE was released from its stowed configuration on 24 August 2023. Subsequently the deployment motor was powered ON and ChaSTE was deployed. The thermal probe was inserted in to the lunar regolith step by step up to 140 mm by powering the penetration motor.

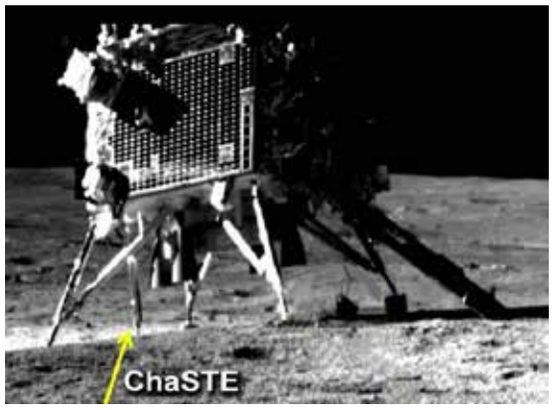

Figure 15: The photo of Chandrayaan-3 lander taken by the rover camera. ChaSTE is seen in the inserted configuration.

The photo of lander captured by the rover is shown in Fig. 15. It shows the ChaSTE in fully penetrated condition. Thermal conductivity experiments were conducted by powering ON the heater. To facilitate Lander Hop-on experiment, the thermal probe was retracted from lunar regolith. On successful completion of the Hop-on experiment, the probe was inserted again into the regolith. All activities were conducted by the tele-command through ChaSTE electronics. The BDH data were dumped in regular intervals. All operations on ChaSTE have been conducted successfully and the performance of ChaSTE was normal.

Scientific Outcome of ChaSTE Operation

Temperature profile of lunar regolith from the lunar surface to the depth of 10 cm was measured by the ten PT1000 temperature sensors mounted on ChaSTE, for the first time over the south polar region. The temperature data were acquired during different solar illumination conditions. Thermal conductivity of lunar regolith was estimated by heating the lunar soil. Fig. 16 shows and example of the temperature variations of the lunar surface/near-surface at various depths as recorded during the probe's penetration.

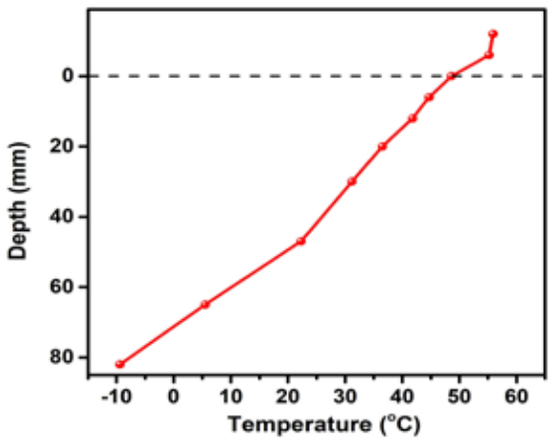

Figure 16: The variation of temperature (C) of lunar surface with depth during the ChaSTE penetration operation.

Laboratory - based experiment and model simulated heat transfer are being carried out to quantify the effect of thermal probe conductivity in modifying the observed variations of the temperature profile.

Ongoing Activities

Commissioning of a new Doppler SODAR at Mahendragiri to study the Atmospheric Boundary Layer Characteristics over the rain-shadow region of the Indian summer monsoon

A new Doppler SODAR system to study the boundary layer characteristics was installed at the SPL observational facility at IPRC, Mahendragiri (Tamil Nadu) situated on the rain shadow part of the Indian summer monsoon region on the eastern side of the Western Ghats in March 2023 (Fig. 17). This new system will be helpful to study the boundary layer characteristics on the rain shadow region and the influence of orography on boundary layer characteristics. This system started to provide data continuously. Initial results showing diurnal variability of wind (horizontal and vertical winds) over Mahendragiri are shown for four days of March 2023 (Fig. 18). Onset of sea-breeze around 10-12 IST and its time evolution are captured well by the SODAR. Quality of the wind data derived from SODAR has been evaluated with the radiosonde data collected at IPRC, Mahendragiri in campaign mode.

Figure 17: Newly installed Doppler SODAR at IPRC, Mahendragiri.

Estimation of Cloud Radiative Forcing of Deep Convective Cloud Cores (DCCC)

SAPHIR and ScaRaB payloads onboard Megha-Tropiquessatellite provide collocated and concurrent observations of convective cores and broadband radiative fluxes on top of the atmosphere, respectively. The vertical extent of the DCCCs is being estimated using collocated and concurrent CloudSat and SAPHIR observations. Diurnal variation in the occurrence frequency of DCCCs and their radiative forcing are being estimated during 2011-2018 using the synergy of SAPHIR and ScaRaB payloads.

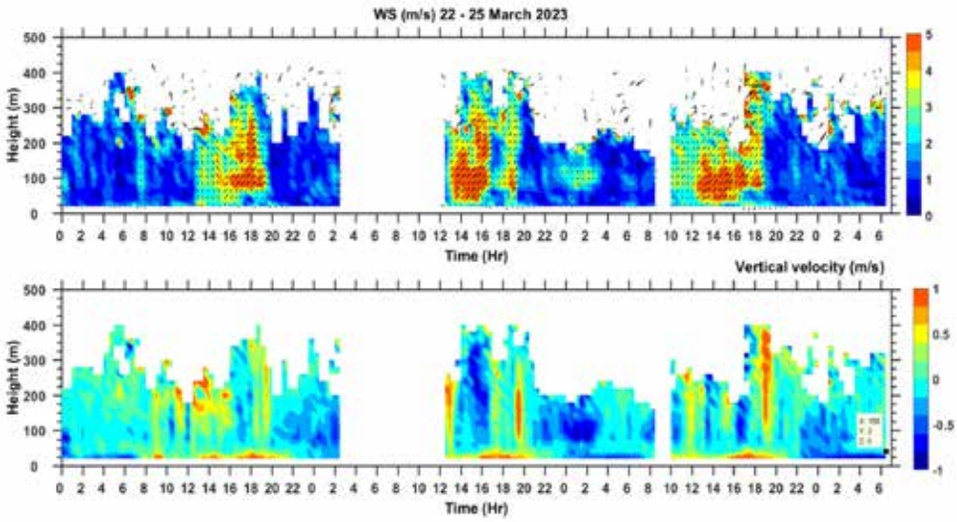

Figure 18: Time evolution of (top) horizontal wind and (bottom) vertical wind in ms^{-1} over Mahendragiri captured by the SODAR during 22-24 March 2023.

Future Projections

- Expansion of NOBLE network to north-west and central Indian regions for further understanding of ABL characteristics over India.
- Eddy covariance measurements of boundary layer energy and momentum fluxes over different geographical regions and quantification of surface energy balance.
- Thermo-physical properties of lunar regolith using ChaSTE/Chandrayaan-3 lander and simulation studies.
- Three dimensional distributions of tropical clouds and precipitation and their impact on atmospheric energetics.
- Altitudinal variation of drop-size distribution over Thumba using in-situ and satellite observations.

Publications in Peer-Reviewed Journals

1. Santosh, M. "Structure and development of the atmospheric boundary layer over a small island (Mahé island, Seychelles) in the equatorial Indian Ocean", Meteorology and Atmospheric Physics, https://doi.org/10.1007/s00703-022-00924-3, 2022.
2. Samuel, S., N. Mathew, and V. Sathiyamoorthy, "Characterization of Intertropical Convergence Zone using SAPHIR/Megha-Tropiques satellite brightness temperature data", Climate Dynamics, http://doi.org/10.1007/s00382-022-06549-x, 2022.
3. Shailendra Kumar and S. Srivastava "Vertical characteristics of precipitating cloud systems during different phases of life cycle of cloud systems using satellite-based radar over tropical oceanic areas", Journal of Applied and Natural Science, http://doi.org/10.31018/jans.v14i4.3691, 2022.
4. Salim, S. N., A. Adhikari, A. A. Shaikh, H. B. Menon, N. V. P. Kiran Kumar, and K. Rajeev, "Aerosol-boundary layer dynamics and its effect on aerosol radiative forcing and atmospheric heating rate in the Indian Ocean sector of Southern Ocean", Science of the Total Environment, https://dx.doi.org/10.1016/j.scitotenv.2022.159770, 2022.
5. Sathiyamoorthy, V., Swathi, B. and S. Samuel, "Characteristics of the strong winds on the exit region of the Palghat gap during the Indian summer monsoon season". Climate Dynamics, https://doi.org/10.1007/s00382-023-06915-3, 2-23,2023.
6. Renju, R. and C. Suresh Raju, "Simulation analysis of microwave emission from lunar subsurface for SAR radiometric mode dual frequency (L/S Bands) observations onboard Chandrayaan-2", Advances in Space Research, https://doi.org/10.1016/j.asr.2023.06.040, 2023.
7. Renju, R., C. Suresh Raju, R. Swathi, V. G. Milan, "Retrieval of atmospheric temperature and humidity profiles over a tropical coastal station from ground-based Microwave Radiometer using deep learning technique", Journal of Atmospheric and Solar Terrestrial Physics, https//doi.org/10.1016/j.jastp.2023.106094, 2023.
8. Salim, S. N., A. Adhikari, H. B. Menon, N. V. P. Kiran Kumar and K. Rajeev, "Thermodynamic characteristics of Marine Atmospheric Boundary Layer across Frontal Regions of the Indian Ocean Sector of Southern Ocean up to Prydz Bay region of Antarctica (24°S to 67°S) based on three field campaigns", Atmospheric Research, https://doi.org/10.1016/j.atmosres.2023.106678, 2023.
9. Salim, S. N., H. B. Menon, N. V. P. Kiran Kumar and K. Rajeev, "Study of micrometeorological characteristics of the atmospheric surface layer over a tropical coastal station in Goa", Meteorology and Atmospheric Physics, https://doi.org/10.1007/s00703-022-00940-3, 2023.
10. Shailendra Kumar, J. L. Flores, Aldo S. Moya-Álvarez, D. M. Castro and Y. Silva, "Characteristics of cloud properties over South America and over Andes observed using CloudSat and reanalysis data", International Journal of Remote Sensing, https://doi.org/10.1080/01431161.2023.2193301, 2023.

Presentations in Symposium/Conferences/Workshops

International

1. Aswathy, R. S., and K. Rajeev, 'Three-dimensional structure and variability of double-ITCZ and the associated cloud heating rates over tropical oceans: decadal observations using CloudSat and CALIPSO', COSPAR 2022, 16-24 July 2022, Athens, Greece.
2. Aswathy, R. S., and K. Rajeev, 'Characteristics of Double-ITCZ over tropical Oceans: Decade of observations using CloudSat and CALIPSO' TropMet-2022, 29 November to 1 December 2022, IISER Bhopal.
3. Aswathy, R. S., and K. Rajeev, 'Vertical Structure of Atmospheric Energetics due to Clouds Associated with Walker Cells: Estimations Using a Decade of CloudSat and CALIPSO Observations' URSI-RCRS, 1-4 December 2022, IIT Indore.
4. Edwin V. Davis and K. Rajeev, 'Observed Relations among the Hydrological Cycle Components Over a Tropical Region', COSPAR 2022, 16-24 July 2022, Athens, Greece.
5. Mathew, N, S. Samuel and V. Sathiyamoorthy, 'New Insights in to the Tropical Deep Convective Clouds, Water cycle and Radiation Balance from 8-years of Megha-Tropiques SAPHIR and ScaRaB Data', URSI-RCRS, 1-4 December 2022, IIT Indore.

6. Samuel, S., N. Mathew and V. Sathiyamoorthy, 'Association of Deep Convective Cloud Cores with Sea Surface Temperature over the Tropical Oceans', COSPAR 2022, 16-24 July 2022, Athens, Greece.
7. Samuel, S., N. Mathew and V. Sathiyamoorthy, 'Characterization of ITCZ using deep convective cloud cores derived using the water vapour absorption channels around 183.31 GHz onboard SAPHIR/Megha-Tropiques', URSI-RCRS, 1-4 December 2022, IIT Indore.

Invited Talks

K. Rajeev

1. "Space Science Research with Small Satellites In India", Representing ISRO in 'Space Agency Leaders Roundtable on Space Science with Small Satellites', 5th COSPAR Symposium, Nanyang Technological University (NTU), Singapore, 17 April 2023.
2. "Advances in Space Science and Technology", Antariksh Vigyan Karyashala for students, Indian Institute of Space Science and Technology, 17 July 2022.
3. "Introduction to Space Science", Department of Physics, University of Kerala, Trivandrum, 30 July 2022.
4. "Earth's Atmosphere & Space", National Astronomy Challenge for School Students, Thiruvananthapuram, 16 August 2022.
5. "Tropical Clouds and Radiative Impact", Advances in the Science of Earth: Relevance to the Society, SRT Marathwada University, 22 November 2022.
6. "Challenging Problems in Space Science", Seminar for Research Fellows, IIST, 5 April 2023.

Kiran Kumar N. V. P.

1. "Atmospheric surface layer characteristics at different geographical locations over Indian region", National Workshop on Boundary Layer Exchange Processes and Climate Change (NoBLExClim) 2023, SRM Institute of Science and Technology, Chennai, 24 March 2023.

Renju R

1. "Convective studies using Microwave Radiometer Profiler", National Symposium on Convective storms: Thunderstorms and Lightning Physics, National Centre for Earth Science Studies, Thiruvananthapuram, 23 March 2023.
2. "Planetary atmosphere and surface studies using Microwave remote sensing", National Seminar on Materials, Astrophysics, Plasma Physics and Space Physics, Mar Thoma College, Chungathara, Kerala, 22-24 February 2023.

Sathiyamoorthy V.

1. "Indian Satellites for weather monitoring", National Symposium on Convective storms: Thunderstorms and Lightning Physics, National Centre for Earth Science Studies, Thiruvananthapuram, 23 March 2023.
2. 'Importance of Climate Knowledge: Examples from the past & Requirements for the Present' World Meteorological Day celebrations, Indian Meteorological Society (Cochin Chapter) and Advanced Centre for Atmospheric Radar Research, Cochin University of Science and Technology, Cochin, 24 March 2023.

Training Programmes

1. Fathima P T, National Workshop on 'Boundary Layer Exchange Processes and Climate Change (NoBLExClim) - 2023', SRM Institute of Science and Technology, Chennai,23-24 March 2023.
2. Renju R, 'Hindi Workshop for Scientists and Engineers of the Technical area of VSSC', VSSC, Thiruvananthapuram, 31 March 2023.
3. Renju R, 'NISAR Science Workshop', Space Applications Centre, Ahmedabad, 20-21 March 2023.
4. Shailendra Kumar, Training on 'Dynamic data Assimilation' National Atmospheric Research Laboratory, Tirupati, India. 27 February - 3 March 2023.
5. Shailendra Kumar, 'NISAR Science Workshop', Space Applications Centre, Ahmedabad, 20-21 March 2023.
6. Swathi B, National Symposium on 'Convective storms: Thunderstorms and Lightning Physics', National Centre for Earth Science Studies, Thiruvananthapuram, 23 March 2023.

ऐरोसॉल, ट्रेस गैस तथा रेडिएटिव फोर्सिंग
Aerosols Trace gases and Radiative Forcing

एसपीएल की 'ऐरोसॉल, ट्रेस गैस एवं विकिरणी प्रभाव (एटीआरएफ)' शाखा का ध्येय ऐरोसॉलों और ट्रेस गैसों के भौतिक/रासायनिक गुणधर्मों की वैज्ञानिक समझ विकसित करना है, जिसमें ऐसी प्रक्रियाएं शामिल हैं जो जलवायु परिवर्तनों का कारण बनने वाले उनके त्रिविमीय वायुमंडलीय वितरण और विकिरण के साथ संबंधों को नियंत्रित करती हैं। इस शाखा के प्राथमिक लक्ष्य हैं (i) अंतरिक्ष-वाहित और भू-आधारित प्रेक्षणों के संयोजन से भारतीय उपमहाद्वीप, निकटवर्ती महासागरों के साथ-साथ हिमालय एवं ध्रुवीय वातावरणों के ऊपर स्थित ऐरोसॉल और ट्रेस गैसों के दिगीय एवं समयानुसार विभेदित आंकड़ों के संग्रह का विकास, (ii) ऐरोसॉल और ट्रेस गैसों के जलवायु प्रभावों से संबन्धित विशिष्ट वैज्ञानिक समस्याओं का अध्ययन करनेवाले विषयगत बहु-मंचीय (जहाज, वायुयान और उच्च तुंगतावाला गुब्बारा) क्षेत्र परीक्षणों का आयोजन (iii) पृथ्वी एवं ग्रहीय वायुमंडलों में ऐरोसॉलों और ट्रेस गैसों के सुदूर संवेदन के लिए पुनःप्राप्ति कलन-विधियों और अंतरिक्ष-वाहित संवेदकों का विकास (iv) संभावित जलवायु प्रभाव के मूल्यांकन हेतु क्षेत्रीय जलवायु प्रतिमानों के साथ ऐरोसॉल और ट्रेस गैस के आंकड़ों को समावेशित करना।

Aerosols, Trace gases and Radiative Forcing (ATRF) branch of SPL aims at scientific understanding of the physical/chemical properties of aerosols and trace gases, involving processes that control their three-dimensional atmospheric distribution and interaction with radiation leading to climate changes. The primary objectives are (i) development of spatially and temporally resolved aerosol and trace gas database over the Indian subcontinent, adjoining oceans as well as the Himalayan and Polar environments by combining the space-borne and ground-based observations, (ii) conducting thematic multi-platform (ship, aircraft and high altitude balloon) field experiments addressing specific problems pertinent to the climate impact of aerosols and trace gases, (iii) development of retrieval algorithms and space-borne sensors for the remote sensing of aerosols and trace gases in earth and planetary atmospheres and (iv) assimilation of the aerosol and trace gas data with regional climate models for the assessment of potential climate impact.

वैज्ञानिक टीम / Science Team
सुरेश बाबू एस. / Suresh Babu S.
विजयकुमार एस. नायर / Vijayakumar S. Nair
प्रशांत हेग्डे / Prashant Hegde
मुकुंदा एम. गोगोई / Mukunda M. Gogoi
शोभन कुमार कोंपल्ली / Sobhan Kumar Kompalli
प्रिजित एस. एस. / Prijith S. S.
रेवती एस. अजयकुमार / Revathy S. Ajayakumar
सुरेश कुमार रेड्डी बी. / Suresh Kumar Reddy B.

तकनीकी टीम / Technical Team
अजीषकुमार पी. एस. / Ajeeshkumar P. S.
संतोष कुमार पांण्डे / Santosh Kumar Pandey

अनुसंधान सहयोगी, ईन्स्पयर/रामानुजन फेलो और एनपीडीएफ / Research Associates, INSPIRE/Ramanujan Fellows & NPDF
धनन्जय कुमार / Dhananjay Kumar
रम्या सी. बी. / Ramya C. B.
सौम्यज्योति जाना / Soumyajyoti Jana
आर्या वी. बी. / Arya V. B.
लिमा सी. बी. / Lima C. B.
अखिला आर. एस. / Akhila R. S.

अनुसंधान अध्येता / Research Fellows
अजित टी. सी. / Ajith T. C.*
अनस इब्नु बशीर / Anas Ibnu Basheer
अतुल ए. के. / Athul A. K.
नितिन बाबू / Nithin Babu
पार्वती आनंद / Parvathy Anand
शिब शंकर गौडा / Shiba Shankar Gouda

* *Relived in March 2023*

Satellite Remote Sensing of Aerosols

Satellite (GOSAT-2 CAI-2) retrieval and surface (ARFINET) observations of Aerosol Black Carbon over India

Light-absorbing Black Carbon (BC) aerosols strongly affect the Earth's radiation budget and climate. Concerted efforts have been made to elucidate the radiative properties of BC originating from the incomplete combustion of bio-fuel or fossil-fuel sources. Although nearly accurate estimation of BC can be made using in-situ approach (uncertainty in BC measurements < 5-10 %), most studies confined to in-situ measurements (ground-based or air-borne) lack sufficient spatial coverage. In this regard, retrieval of BC from satellite-based radiation measurements, synchronized with the ground-based point measurements, is a novel method for quantifying and classifying the real BC environment across distinct geographic regions worldwide.

In the present study, the satellite-based retrievals of BC are made from the Cloud and Aerosol-Imager-2 (CAI-2) observations on-board the Greenhouse gases Observing Satellite-2 (GOSAT-2). CAI-2 is a push-broom imaging sensor that records backscattered radiances at 7-wavelengths / 10-spectral bands in the ultraviolet (UV: 339, 377 nm), visible (VIS: 441, 546, 672 nm) and near-infrared (NIR: 865, 1630 nm) equipped in forward (bands: 339, 441, 672, 865 and 1630 nm) and backward (bands: 377, 546, 672, 865 and 1630 nm) looking directions (± 20°).

The retrieval technique of BC from CAI-2 measurements is based on the estimation of volume mixing ratio of BC in fine-mode particles. The Multi-Wavelength and -Pixel Method (MWPM) can simultaneously retrieve fine-mode and coarse-mode AOD, soot volume fraction in fine-mode aerosols, and surface reflectance over heterogeneous surfaces at multiple wavelengths and pixels. To evaluate and validate the spatiotemporal distribution of BC from satellite retrieval, near-surface BC mass concentrations measured across the Aerosol Radiative Forcing over India NETwork (ARFINET) of aerosol observatories are used (Fig. 1). Then the findings are extended to elucidate the global BC features.

Regional distributions of BC from satellite retrieval (GOSAT-2 CAI-2) and surface measurements (ARFINET) during three distinct periods of December, January, and February (DJF), March, April, and May (MAM), and June, July and August (JJA) (Fig. 2) showed good agreement between the two datasets over the Indian region. Especially during winter and pre-monsoon months, the satellite retrieval clearly identifies the regional hotspots of BC over India. Inter-comparison of satellite retrieved BC with surface measurements revealed the absolute difference between the two data sets as < 2 μg m^{-3} over 60 % of the observations in this study. Associations between the two datasets having absolute difference < 2 μg m^{-3} are highest in MAM (R ~ 0.76), followed by DJF (R ~ 0.73), and JJA (R ~ 0.61).

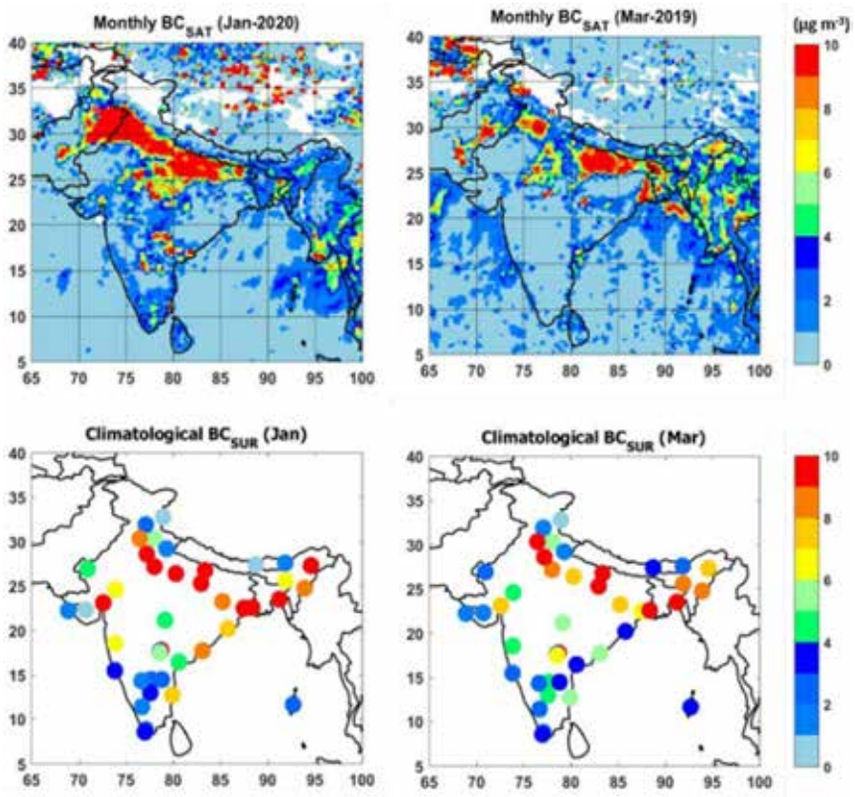

Figure 1. Regional distribution of monthly average BC over the Indian region from satellite (top panel) and surface measurements (bottom panel) during January and March. [Gogoi et al., Atmos. Chem. Phys, 2023].

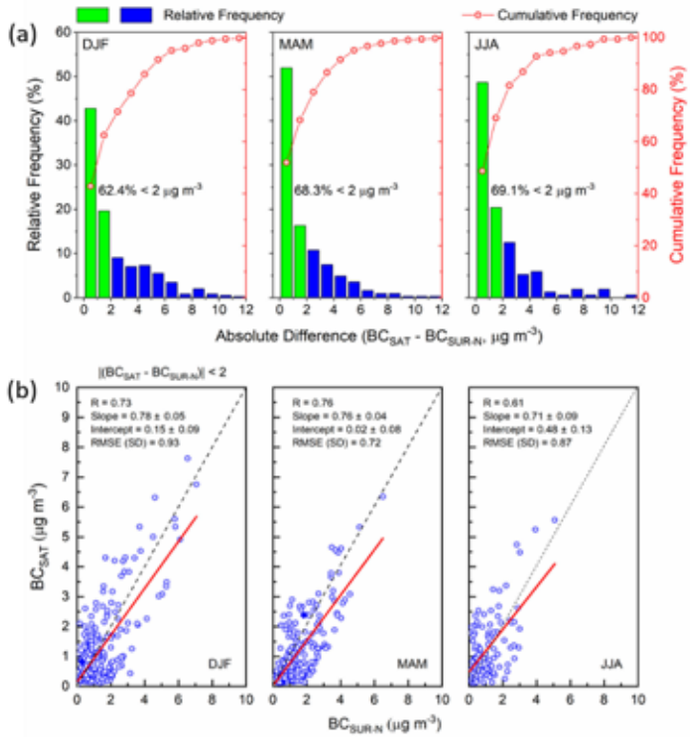

Figure 2: (a) Frequency counts (in percentage) of the absolute difference in BC (in μg m^{-3}) between simultaneous satellite (BC_{SAT}, averaged over 1°× 1° area around each of the ARFINET sites) and normalized surface BC (BC_{SUR-N}) concentrations, (b) Association between simultaneous satellite and normalized surface BC concentrations. The solid red line is the linear fit. The grey dashed line is the one-to-one line of BC_{SAT} and BC_{SUR-N} [Gogoi et al., Atmos. Chem. Phys, 2023].

Mineral dust aerosols over the Himalayas from polarization-resolved satellite LIDAR observations

The Himalayan region is consistently under the influence of long-range transport of dust aerosols from the arid areas of West Asia and the Thar Desert. Studies based on aerosol chemical analyses have shown the profound presence of mineral dust aerosols in the snow and the atmosphere of the Himalayas. Several studies have indicated the transport of mineral dust to the Himalayan region, but using passive observations of spectral aerosol optical depth supplemented with back trajectory analysis. However, passive remote sensing of aerosols over the cryosphere faces significant challenges due to enhanced radiance received from the highly reflective snow surface. Cloud-Aerosol Lidar with Orthogonal Polarization (CALIOP) on-board Cloud-Aerosol Lidar Infrared Pathfinder Observations (CALIPSO) satellite measures back-scattered radiation from each layer of the atmosphere without being influenced by surface reflection, which makes it a very useful tool when assessing aerosol over highly reflective snow surfaces.

In this study, polarization-resolved observations of CALIOP during 2006 - 2018 are used to assess the mineral dust aerosols over the Himalayas. The extinction coefficient due to dust aerosols is retrieved using observations of the depolarization ratio, which gives the relative contribution of dust aerosols in the scattering volume. Dust extinction coefficients show significant regional and seasonal variation over the Himalayas (Fig. 3). High dust loading is observed during the pre-monsoon season (March-May), whereas dust loading is low during the summer monsoon season (June - September). This is due to the reduced dust transport associated with the weak westerlies that prevailed over the Himalayas. Regionally, the mid-Himalayas is characterized by the highest dust extinction coefficient with a 10-fold increase as the season changes from winter (December-February) to pre-monsoon (March-May). Polluted dust (dust combined with anthropogenic aerosols) contributes to 64 to 74 % of total aerosols over the Himalayas. Dry deposition causes a substantial amount of dust aerosols (1 - 31 mg m^{-2} day^{-1}) to be deposited over the Himalayas (Fig. 4), reducing the albedo by 0.3 % on fresh snow and up to 2.7 % on aged snow, causing a radiative forcing of 0.38 to 23.7 Wm^{-2} at the top of the atmosphere.

Aerosol Microphysical Properties

Black carbon light-absorption enhancement due to aging of biomass burning emissions in the Indo-Gangetic Plain outflow

Recent studies worldwide have demonstrated that coating on atmospheric black carbon (BC) aerosol enhances its absorption potential. However, studies quantifying the light-absorption enhancement of BC are extremely limited over the Indian region. The northwestern Indo-Gangetic Plain (IGP) region witnesses annual episodes of substantial crop-residue burning during the post-monsoon season

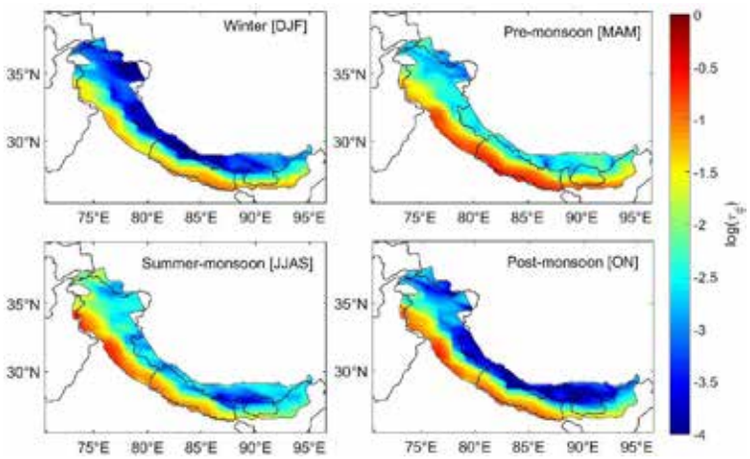

Figure 3: Spatial distribution of average dust optical depth (τ_d) in logarithmic scale over the Himalayas during the winter season (DJF), pre-monsoon season (MAM), summer-monsoon season (JJAS) and post-monsoon season (ON) [Lakshmi et al., Atmos. Env., 2023].

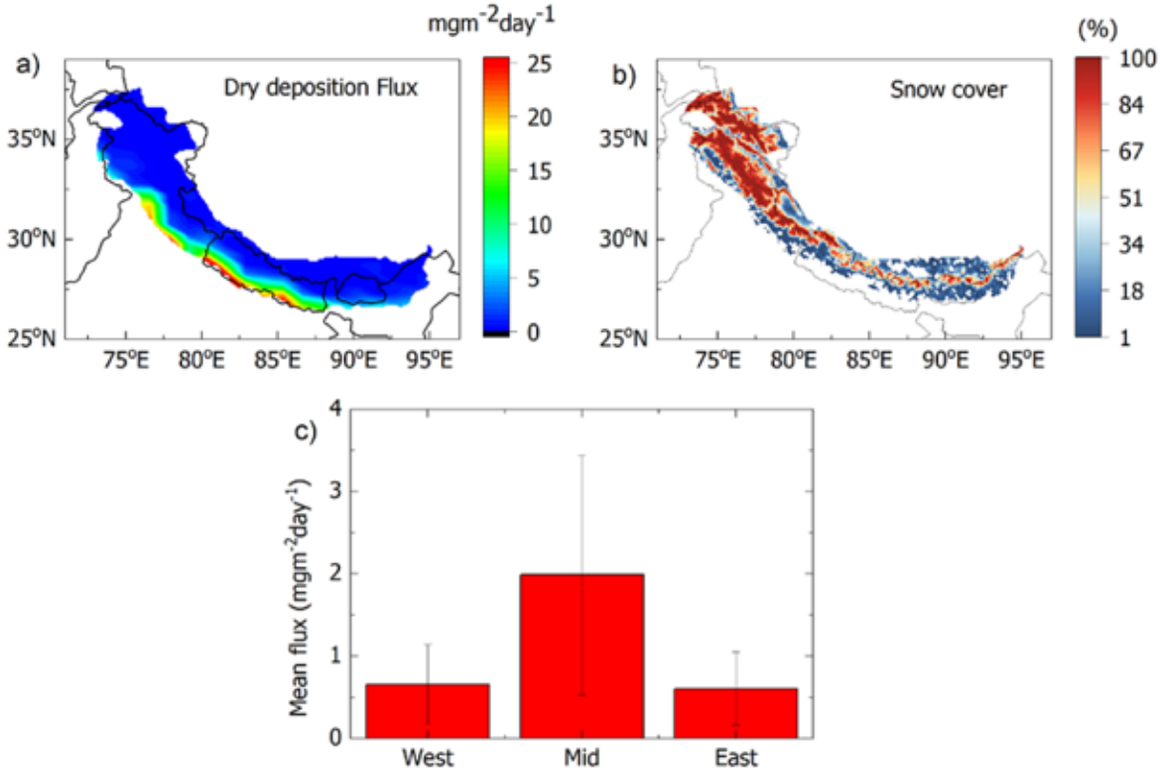

Figure 4. (a) Spatial variation of dry-deposition dust mass flux over the Himalayas during the pre-monsoon (March-May) of 2006 to 2018 (b) spatial distribution of snow cover fraction during the pre-monsoon of 2006 to 2018 and (c) Average dry-deposition mass flux over the snow-covered regions [Lakshmi et al., Atmos. Env., 2023].

(PoMS). Chemical aging of these biomass burning (BB) emissions occurs during its long-range transport across the IGP by the weak westerlies, and such atmospheric processing affects aerosol characteristics over downwind locations. This study examines the impact of atmospheric aging of BB emissions on BC light-absorption enhancement (E_{abs} = $b_{abs,coat}/b_{abs,BC}$, where $b_{abs,coat}$ and $b_{abs,BC}$ are the absorption coefficients for coated and uncoated BC) using simultaneous measurements of single particle refractory BC and near-real-time mass spectrometry measurements of non-refractory submicron aerosols (NR-$PM_{1.0}$) from an IGP outflow site, Bhubaneswar during the PoMS 2016. The results highlighted that the BC particles were thickly coated, having relative coating thickness (RCT) in the range of 1.3-1.8 (mean RCT ~ 1.32 ± 0.14). Further, the bulk mixing ratio of coating mass over rBC mass ($M_{R,bulk}$) was in the range of 0.32- 7.0 (mean ~1.21 ± 0.69). Concurrent NR-$PM_{1.0}$ measurements revealed that organic aerosols (OA) were dominant. The positive matrix factorization analysis of organics mass spectra suggested that a large fraction (64%) of OA was secondary in which dominant contribution (36%) is from more-oxidized oxygenated OA (MO-OOA highlighting the extent of aging). Overall, secondary aerosols, which are potential coating

species on BC, accounted for the dominant fraction (82%) of NR-$PM_{1.0}$ mass loading.

Figure 5 (a & b) depicts the evolution of coatings on BC as a function of aging of OA, shown as the relationship between (a) f_{44} versus f_{43}; (b) f_{44} versus f_{60}. Here the f_{44} (f_{43} and f_{60}) (tracer signals) represent the fraction of signal at *m/z* 44 (43 and 60) to total signal in the organics mass spectra. As implied from the f_{44} vs. f_{43} plot along with concurrent values of RCT on BC, highly oxidized OA are potential contributors to enhanced BC coatings (~30-70 %). The evolution of BB emissions (from the f_{44} vs. f_{60} plot) indicated the presence of a considerable amount of aged-BBOA (which originates from the transformation of primary and semi-volatile BBOA to a highly oxygenated OA during aging) and contribution of resultant BB oxidation products to thicker coatings on BC. Further, Mie core-shell theory calculations were used to assess the changes in BC light absorption characteristics (Fig. 5c-d) due to the coatings. It revealed that thick coatings on BC led to significant light-absorption enhancement (1.14-1.94) at 550 nm. Further, E_{abs} (and MAC) depicted sensitivity to BC microphysical properties (core size and RCT). E_{abs} increased linearly with RCT at lower coatings and then tended to a threshold value at higher coatings. For thicker coatings, E_{abs} increased ≥1.8. The E_{abs} depicted a better association with highly oxidized secondary OA (SOA) than sulfate suggesting an SOA-dominant regime. The present findings highlight the impact of aging BB emissions to the regional radiative implications.

Formation pathways of organic aerosols in a tropical coastal atmosphere

Organic Aerosols (OA), with hundreds to thousands of internal components, account for a substantial mass fraction of submicron aerosols (20-90%). OA over different regions/seasons and/or even within a day evolve significantly in terms of their oxidation state, volatility and hygroscopicity. OA can be classified into primary OA (directly emitted) and secondary OA (formed via gas-to-particle conversion of volatile organic compounds and/or due to the aging of Primary OA). The first step involved in the formation of SOA is the oxidation of VOCs in the photochemical/aqueous phases forming SOA with different oxidation degree, therefore, distinct atmospheric impacts. Over the Indian region, the studies exploring OA formation and evolution are rather sparse. In this context, multiyear (2017-2021) measurements of submicron aerosol chemical composition from a tropical coastal location, Thumba were examined.

The results indicated organic aerosols as the major

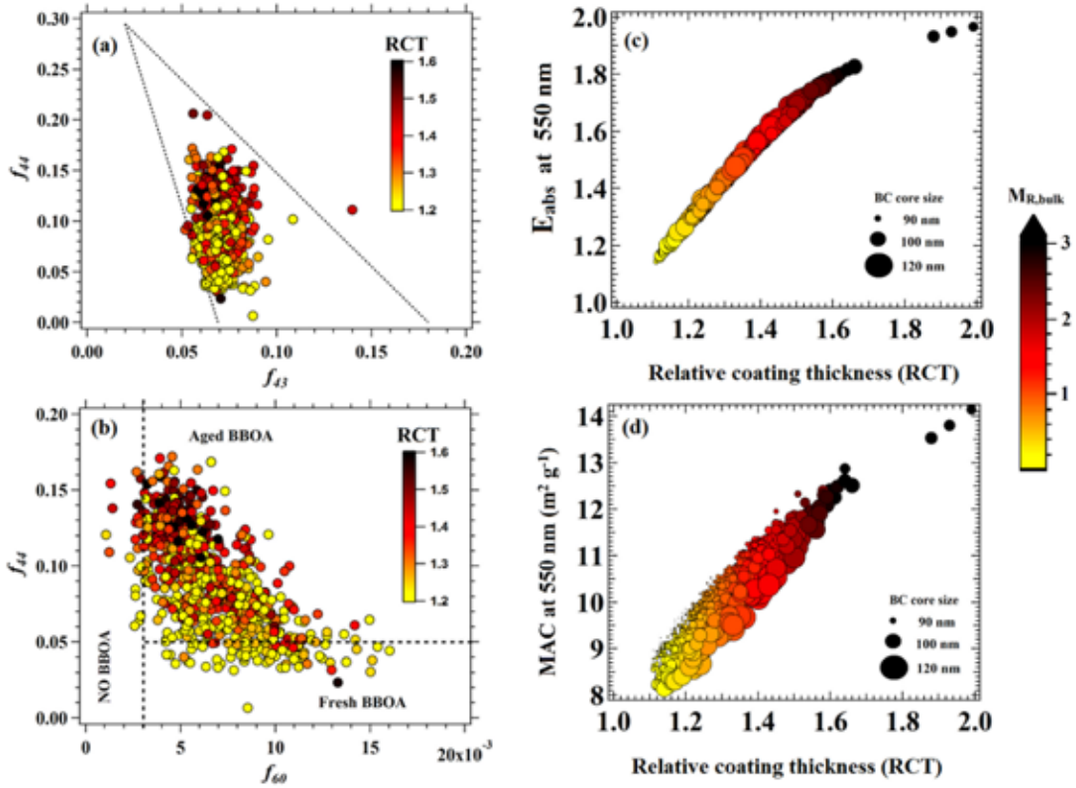

Figure 5: Evolution of coating on BC as a function of aging of organic aerosols shown as the relationship between (a) f_{44} versus f_{43}; (b) f_{44} versus f_{60}. The color scale indicates the magnitude of RCT on BC particles. The background f_{60} level of 0.3% of organic aerosols is indicated by the vertical dashed line in the figure panel (b), and the horizontal dashed line indicates the background f_{44} level. (c-d) Association between RCT on BC and absorption enhancement (E_{abs}) and mass absorption cross-section (MAC) of BC at 550 nm. The size of the points indicate BC core size and the color of the points is scaled by $M_{R,bulk}$ [Kompalli et al., Atmos. Res. 2023].

component (67-85%) in the NR-$PM_{1.0}$ mass loading during all seasons. Positive matrix factorization analysis on the OA mass spectra yielded two factors resolving Hydrocarbon-like organic aerosols (HOA) and Oxygenated organic aerosols (OOA), with the major contribution (>50%) coming from OOA during all the seasons. The mass fractions of different species during the present study are shown in Fig. 6a. A typical example of diurnal pattern of different species (during the premonsoon season) is shown in Fig. 6b. Diurnally, the mass concentrations of HOA, ammonium, and nitrate exhibited a typical two peaks (typical fumigation and nocturnal peaks) and a daytime trough pattern associated with the local atmospheric boundary layer dynamics. In contrast, sulfate showed daytime enhancement. Though OOA also depicted a diurnal pattern with a daytime-enhancement, the time of occurrence of its peak and subsequent reduction are dissimilar to sulfate.

Further, the daytime photochemical formation efficiency of OOA was examined using the conserved photochemical tracer - odd oxygen (O_3+NO_2) (Figs. 6c and 6d). The OOA showed a good correlation (R>0.5) with odd oxygen during all the seasons with varying formation efficiencies highlighting the varying strength of photochemistry. This is further reaffirmed by the positive correlation between the dayime OOA and odd oxygen (R~0.65 during the premonsoon season (PMS); Fig. 6d). A positive association between the oxygen-to-carbon ratio (O:C), which is a measure of the oxidation degree of OA, and odd oxygen (ΔO:C ~ 0.11 to 0.35 with Δodd oxygen = 60 µg m^{-3} for different seasons) further highlighted the role of photochemistry and enahced OA oxidation degree due to photochemistry. Subsequently, the role of aqueous-phase formation of OA is examined using aerosol inorganic liquid water content (AILWC), estimated using the Extended-Aerosol Inorganic Model and then total aerosol liquid water content (ALWC) from the real-time NR-$PM_{1.0}$ measurements. A strong diurnal pattern for ALWC was seen during all the seasons (example pattern for PMS

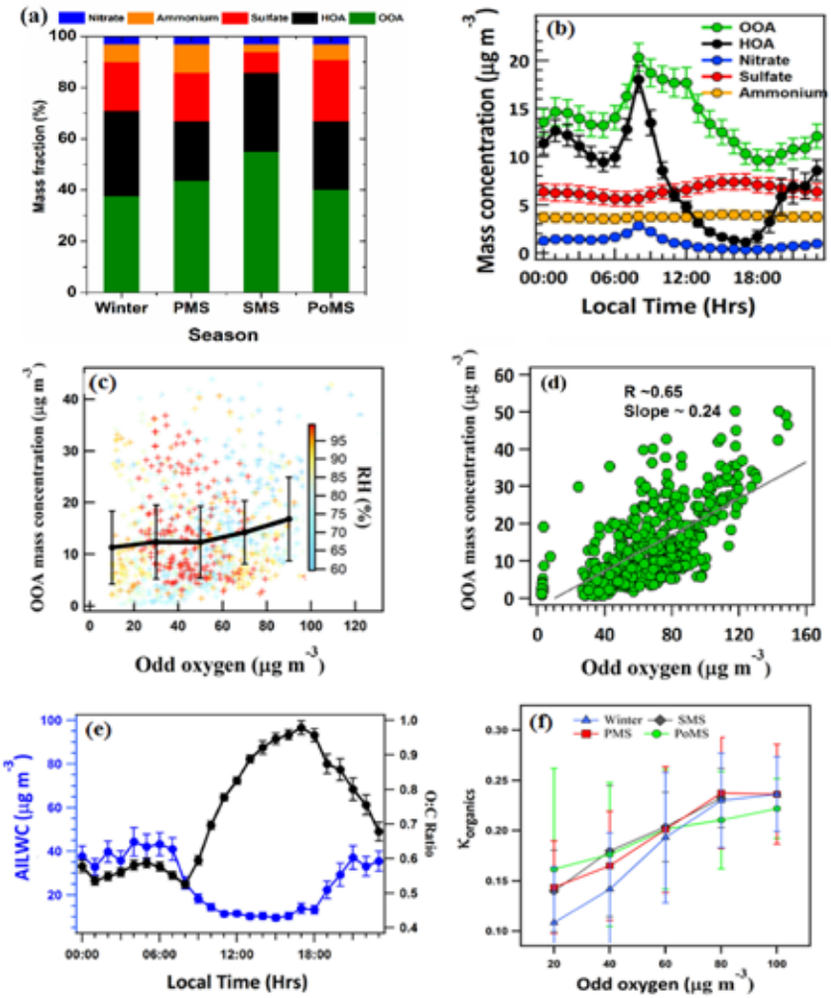

Figure 6: (a) Mean mass fractions of NR-$PM_{1.0}$ species during different seasons: winter, pre-monsoon (PMS), summer monsoon , and post-monsoon; (b) Diurnal variation of average mass concentrations for organic and inorganic species during the PMS; (c) OOA mass concentration versus odd oxygen during the PMS scaled with RH; (d) Correlation between daytime OOA and odd oxygen for the PMS; (e) Diurnal variation of aerosol liquid water content and the O:C ratio of OA during the PMS; (f) Dependence of OA hygroscopicity ($\kappa_{organics}$) on photochemical processing. [Ajith et al., Atmos. Environ. 2023].

is shown in Fig. 6e) with varying amplitudes, indicating the combined impact of varying aerosol composition and ambient RH.

Combining this information with source apportionment of OA, it was found that less oxidized/less-hygroscopic OA were prevalent during the nighttime, resulting in lower aqueous-phase OA processing. During all the seasons, the hygroscopicity of organics ($\kappa_{organics}$) (Fig. 6f) reached as high as > 0.22, and was mainly driven by photochemical processing rather than aqueous-phase chemistry.

South Asian outflow characteristics

Observational evidence for ultrafine organics over the open ocean

Chemical properties of the continental outflow over to the northern Indian Ocean are investigated using shipborne measurements carried out as a part of the Integrated Campaign for Aerosols, gases and Radiation Budget (ICARB-2018) experiment during winter 2018. The short-term increase in OC, the OC/EC ratio, OM and the OM/sulfate ratio during ultrafine particle bursts (17, 24, 29, and 30 January 2018) over the equatorial Indian Ocean indicates the possibility of prominent sources of marine organic compounds. During these event days, the OC mass concentration showed high values for 2 to 3 hours in the early morning (07:00-10:00) and evening (15:00-17:00) hours, whereas simultaneous measurements of EC did not show variations similar to that of OC during these events. Since EC is widely used as a proxy for anthropogenic and biomass burning sources and is co-emitted with OC during combustion, the possibilities of local anthropogenic sources including ship exhaust, or a change in the air mass pattern were ruled out. The diurnal variation of the OC/EC ratio and geometric mean diameter (GMD) estimated from the aerosol number size distribution measurements for the event days are shown in Fig. 7. It should be noted that these short-term events could be averaged out in the conventional offline analysis using filter-based sampling. The source of these ultrafine organics in the equatorial Indian Ocean is an open question, which needs dedicated field experiments to ascertain the possibility of secondary formation or the primary emission of ultrafine organics from the ocean surface layer.

Evaporative decrease of organic aerosols

During ICARB-2018, the organic carbon (OC) and elemental carbon (EC) showed high values (OC = 4.8 ± 2.1 μg m^{-3} and EC = 2.0 ± 0.6 μg m^{-3}) over the northern Indian Ocean and relatively lower values (OC = 1.20 ± 0.50 μg m^{-3} and EC = 0.82 ± 0.53 μg m^{-3}) over the equatorial Indian Ocean. The relative contribution of organic matter (OM) to the sub-micron mass loading also decreased from southeastern Arabian Sea (40%) to the equatorial Indian Ocean (23%). The magnitude of this latitudinal decrease was relatively higher for OC and OM compared to EC and sulfate. The latitudinal gradient of the OC/EC ratio and its association with GMD is shown in Fig. 8. These observations indicate the possible loss of organic aerosols, which might be due to ageing during long-range transport. The organics-rich outflow from South Asia is transformed into a sulfate-dominated outflow over the northern Indian Ocean. Compilation of the earlier measurements over South Asia shows that, the mean OM/sulfate ratio (~4) and OC/EC ratio (6) over the Indian landmass are significantly higher than that over the northern Indian Ocean (0.6 & 2.8). Since EC and sulphate do not have prominent sources over the ocean, the systematic decrease observed in the OC/EC ratio and OM/sulphate is attributed to the depletion of organics during long-range transport. Organics has significant loss

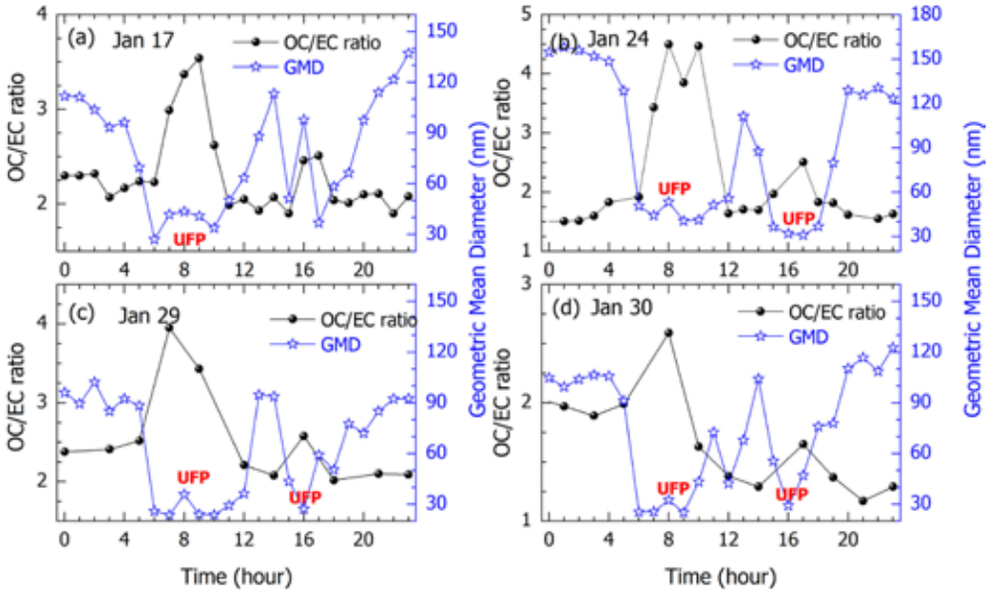

Figure 7: Diurnal variation of the OC/EC ratio and geometric mean diameter (GMD) during the ultrafine particle (UFP) event days: (a) 17 January, (b) 24 January, (c) 29 January and (d) 30 January 2018.[Nair et al., Environ. Sci: Atmos. 2022]

processes initiated by oxidization (heterogeneous and aqueous phases) and photolysis followed by fragmentation and evaporation. These processes reduce the lifetime of organic aerosols to shorter scales and thus decrease the efficiency of their transport to longer distances.

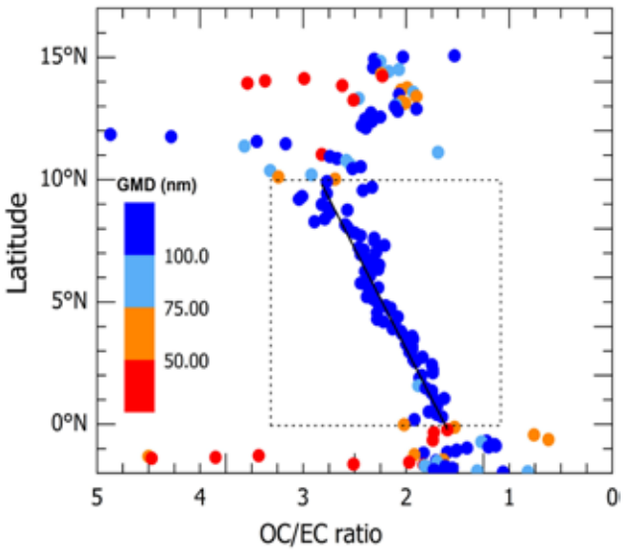

Figure 8: Latitudinal variation of the OC/EC ratio over the Indian Ocean during ICARB-2018. Colour of the scatter indicates the geometric mean diameter (GMD) of the aerosol number size distribution [Nair et al., Environ. Sci: Atmos. 2022]

Water-soluble organic aerosols over South Asia - seasonal changes and source characteristics

Water soluble organic carbon (WSOC) is a ubiquitous component of organic aerosols present in the Earth's atmosphere. This work presents a comprehensive study on the spatial variation and temporal evolution of water-soluble organic aerosols over south Asia combining our extensive observation with the database reported in literature. Variability in the characteristics of WSOC over different sectors over south Asia based on the average concentrations and ratios (OC/EC, WSOC/SOC and WSOC/OC) during different seasons were extensively analysed. The spatial variability of WSOC for distinct sectors over South Asia during winter period is shown in Fig. 9. The three different ratios are used to delineate different source processes; OC/EC for source identification, WSOC/OC for long-range atmospheric transport (ageing) and WSOC/SOC to understand the primary and secondary contribution of WSOC. Considering the entire south Asian region during winter, pre-monsoon and post-monsoon all the reported locations were found to have WSOC/SOC greater than unity. Similarly, during monsoon season, both Himalaya and IGP sectors have shown the similar trend. Over these locations, wide range of water-soluble compounds released by biomass burning contributes directly to the WSOC fraction or undergo further atmospheric processing, such as oxidation or aging, leading to the formation of additional WSOC. WSOC/OC (organic carbon) ratio and the correlation between the WSOC and secondary organic carbon (SOC) are used for assessing the importance of secondary sources.

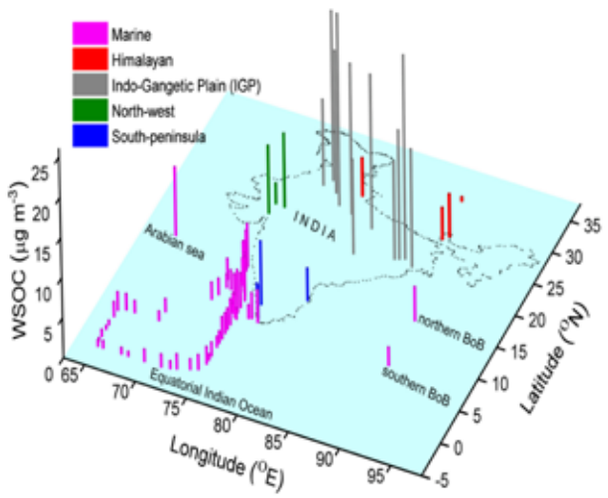

Figure 9. Spatial variability of WSOC for distinct sectors over South Asia during winter period [Ramya et al., Sci. Tot. Environ. 2023].

The present investigation based on the extensive analysis of the data set reported over South Asia, revealed that, the primary OC that have undergone substantial chemical processing as a result of long-range transport have a significant influence on WSOC formation over south Asia, especially in IGP outflow regions such as southern peninsular and adjacent marine regions. Overall, oxidation and ageing of primary organic aerosols emitted from biomass burning was found to serve as an important source of WSOC over South Asia.

Aerosol Chemistry

Molecular fingerprints of water-soluble organic aerosols at a tropical hill station in the Western Ghats of India

Water-soluble organics form a substantial portion of organic aerosols in the atmosphere. They have grown a momentous attention because of their effect on aerosol hygroscopic growth and the activation of cloud condensation nuclei (CCN) in the atmosphere. On the basis of the recent studies made over the Western Ghats, there is a need to investigate into the molecular-level characterization of organic aerosols. Aerosols ($PM_{1.1}$) collected during January-March 2020 and February-April 2021 at Ponmudi (8.8 °N and 77.1 °E), in the Western Ghats (960 m a.s.l.), were analyzed to assess the molecular fingerprints of water-soluble organic aerosols using the gas chromatography technique.

The trajectories revealed that the air masses derived from land and ocean had an impact on aerosol characteristics at Ponmudi (Fig. 10). It is observed that the aerosol characteristics at Ponmudi are inflenced by mixed airmasses from continental and oceanic regions as well as from Bay of Bengal and Arabian Sea. The impact of both the air masses on the molecular fingerprints of water-soluble organics as well as their origins and formation mechanisms were explored in $PM_{1.1}$ over the Western Ghats.

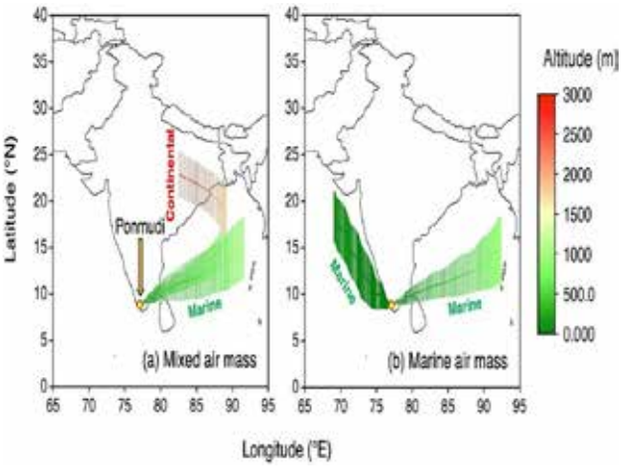

Figure 10. Backward trajectories of air masses over the Ponmudi site for the observation period. The altitude of the air mass is indicated by the color scale [Deshmukh et al., Earth and Space Science, 2023].

Water-soluble organics presented the high levels of third generation oxidation products in aerosols at Ponmudi (Fig. 11). This indicates that they are the product of photochemical reactions in the atmosphere. Interestingly, oxalic acid is detected as the dominant compound followed by terephthalic acid in mixed air mass sample and malonic acid in marine air mass sample. These diverse molecular signature in different air mass aerosols indicate their diverse origins over the Western Ghats. High oxalic acid abundance in marine air mass sample compared to that in mixed air mass sample implies more oxalic acid production in marine air mass aerosol by photochemical oxidation over the Western Ghats. The predominance of oxalic acid in aerosols is indicative of the fact that it is possibly the final compound of photochemical reaction of anthropogenic and biogenic precursors in the atmosphere. Another noticeable feature over the Western Ghats is that water-soluble organics had a stronger impact from anthropogenic sources in mixed air mass aerosols, whereas they were strongly affected by biogenic sources in marine air mass aerosols. Since there is a strong continental outflow in the mixed air mass case, they are derived primarily from anthropogenic sources and secondarily from the oxidation of anthropogenic precursors during the atmospheric transport. They were attributed to atmospheric photo-oxidation of biogenic precursors such as oleic acid and isoprene in marine air mass aerosols due to the strong oceanic outflow from the oceanic regions. Results suggest that water-soluble organic aerosols over the Western Ghats is photochemically more processed in marine air mass sample than that in mixed air mass sample. They substantially contribute to WSOC not only in mixed air mass aerosols but also in aerosols affected by the marine air masses. It is worth noting that the high oxalic acid abundances in aerosols affected by distinct air masses could impact the aerosol hygroscopic and CCN properties over the Western Ghats.

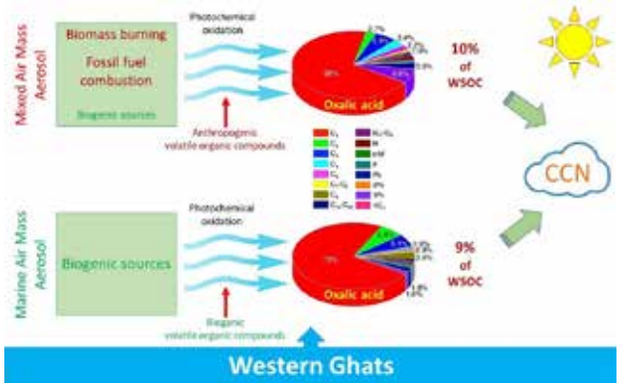

Figure 11. Water-soluble organic compounds and their contribution on water-soluble organic carbon (WSOC) in $PM_{1.1}$ at a tropical hill station in the Western Ghats [Deshmukh et al., Earth and Space Science, 2023].

Molecular composition and light-absorbing properties of organic aerosols over the west coast of tropical India

Due to the high humidity and intense solar radiation, tropical coastal environments may offer a unique feature for studying the photo-oxidation of diverse organic aerosols and their climatic implications. Here the sources and formation processes of diacids and related compounds, brown carbon (BrC), and other chemical species in $PM_{1.1}$ collected on a campaign mode under different air masses at a coastal urban location (CUSAT, Kochi) on the west coast of tropical India are examined. Low molecular weight dicarboxylic acids in $PM_{1.1}$ were determined using Gas Chromatography (GC) technique, while light absorption spectra were recorded for these filtrated water and methanol solutions using a UV/VIS spectrometer in the range of 200-800 nm.

The HYSPLIT five-day air mass back trajectories revealed that the sampling site experiences unique air masses emanating from various areas of the Indian subcontinent and its nearby maritime region during the sampling period. Non-sea-salt sulfate ($nss\text{-}SO_4^{2-}$) predominated in the northeast (NE) and northwest (NW) air masses, whereas organic carbon (OC) predominated in the southwest (SW) and mixed (SE + NW) air masses. WSOC/OC ratios were greater in mixed air masses, followed by NE or NW air masses, and lower in SW air masses.

The molecular distribution of dicarboxylic acids in all air masses was characterised by the predominance of oxalic acid (C_2), followed by adipic (C_6) or terephthalic (tPh) and phthalic (Ph) acids (Fig. 12). Total diacids-C were responsible for 5.03±1.01% of total carbon (TC). The concentration of total diacid was found to have strong linear correlations with OC, EC, and $nss\text{-}K^+$. Except for the NW air mass period, C_2 diacid concentrations and ratios (C_2/total diacids, $C_2/\omega C_2$, C_2/Gly) exhibited a significant linear connection with $nss\text{-}SO_4^{2-}$. By combining all these results together with Pearson correlation coefficient

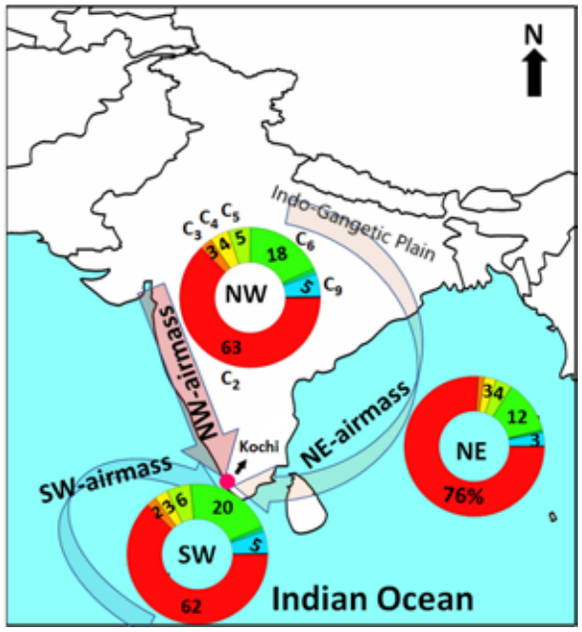

Figure 12. The geographical location of the sampling site (Kochi, indicated as a solid red circle). Doughnut charts indicate the relative abundance of various major dicarboxylic acids under different air masses [Boreddy et al., Science of the Total Environment, 2022].

analysis, we emphasise that organic aerosols over the study region were largely produced by secondary oxidation reactions of precursor compounds derived from biomass burning and combustion-related emissions in an aqueous-phase medium. This scenario, however, did not hold true for the NW air mass, where organic aerosols are thought to be related to photochemical oxidations, as demonstrated by the linear association found between total diacids and air temperature.

The mass absorption coefficient of BrC ($b_{abs\text{-}BrC\text{-}365nm}$) was found to be highly linked with nss-K^+, showing that biomass-burning emissions are significant sources of BrC. During the whole sampling period, the absorption angstrom exponent (AAE) values of water (methanol) extracts ranged from 3.20 to 3.83 (3.05-4.55), showing a significant contribution of BrC chromophores to light absorption over the region (Fig. 13). In water and methanol extracts, BrC absorbs 10.6 ± 6.4% and 22.4 ± 5.75% of solar radiation, respectively, indicating that BrC is a significant aerosol climate-forcing agent over the west coast of tropical India. The findings of this study can help in increasing knowledge of the regional climate effects of carbonaceous aerosols, particularly organic carbon aerosols over the west coast of tropical India, and should be considered in future modeling studies.

Sulfate-associated liquid water amplifies the formation of secondary organic aerosols over peninsular India during winter

Aerosol liquid water (ALW) can act as an aqueous-phase medium for a variety of chemical processes, increasing the

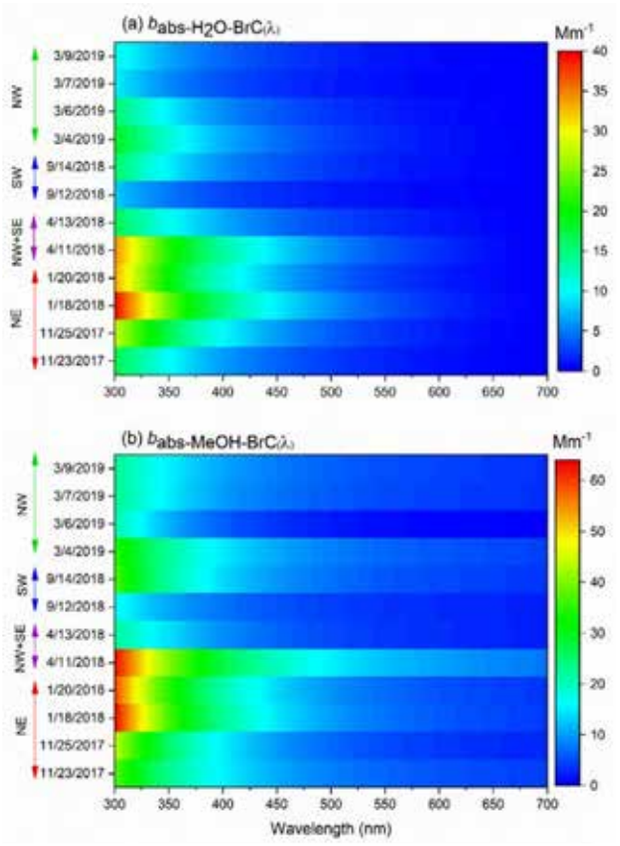

Figure 13. Spectral variation of BrC in (a) water and (b) methanol extracts of $PM_{1.1}$ at Kochi from the west coast of tropical India. It was observed that, BrC chromophores started absorbing light around the mid visible region (around 500 nm) and increased rapidly toward shorter wavelengths, which was typical of BrC chromophores absorption characteristics [Boreddy et al., Sci.Tot. Environ., 2022].

formation of secondary aerosols in a humid environment. During the winter of 2016, we collected total suspended particle samples from a semiarid site (Ballari: 15.15 °N, 76.93 °E; 495 m.a.s.l.) in tropical peninsular India. Using a water extraction of aerosol, homologous series of dicarboxylic acids (C_2-C_{12}), oxoacids (C_2-C_9), pyruvic acid (Pyr), and glyoxal (Gly) were identified and analysed using capillary gas chromatography (GC). The most abundant organic acid was oxalic acid (C_2), followed by succinic (C_4), malonic (C_3), azelaic (C_9), glyoxylic (ωC_2), or phthalic (Ph) acids. Total diacids-C made up 1.7-5.8% of the water-soluble organic carbon (WSOC) and 0.6-3.6% of the total carbon (TC). The linear relationship between C_2 diacid and SO_4^{2-} gives critical information regarding the in-cloud or aqueous-phase production processes of C_2 in the ambient environment. In this study, the relationship between C_2 diacid and SO_4^{2-} is shown in Fig. 14. The results clearly show that there is a strong linear relationship between these two compounds, indicating that the formation of C_2 diacid is strongly connected with SO_4^{2-}, which is mainly formed through aqueous-phase reactions in the atmosphere.

We computed aerosol liquid water using the ISORROPIA-II model to further support aqueous-phase formation of

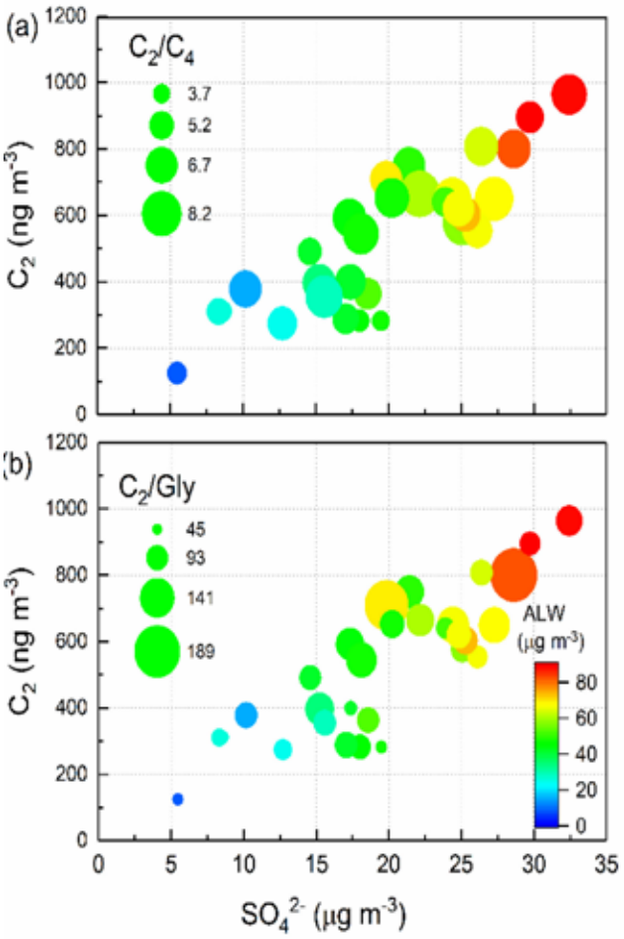

Figure 14. Scatter plot between the concentration of SO_4^{2-} and C_2 diacid as a function of (a) C_2/C_4 and (b) C_2/Gly mass ratio. The estimated aerosol liquid water (ALW) is superimposed on each data point and shown as a color scale to understand the aqueous-phase processes. The enhancement in mass ratios are indicated by the size of circles (large size implies a higher ratio) [Boreddy et al., Sci. Tot.Environ., 2023].

C_2 diacid. It is also clear from Fig. 14 that C_2 diacid has a strong linear connection with ALW. As a result, the strong linear connections among C_2 diacid, SO_4^{2-} and ALW show that secondary organic aerosols are formed in the aqueous phase in wintertime aerosols at the Ballari location. It is also well known that the precursor compounds of C_2 diacid are primarily associated with either photochemical breakdown of its higher homologous (>C_2) or oxidation products of dicarbonyls (C_2 and Pyr acids) and are most likely produced from unsaturated FAs (formation pathway: unsaturated FAs → C_4→ C_3→ C_2) and HCs (formation pathway: α-dicarbonyls→ oxoacids → C_2). In this context, we looked at two typical mass ratios, C_2/C_4 and C_2/Gly, which reflect the two major pathways of C_2 diacid that may result from the degradation and oxidation of unsaturated FAs and aromatic HCs in the environment, respectively. The correlations of these C_2/C_4 and C_2/Gly mass ratios with SO_4^{2-} and C_2 diacid mass concentrations are illustrated in Figs. 14a and 14b, respectively. Both ratios were shown to be strongly linked with C_2 diacid, SO_4^{2-}, and ALW. This inference shows that the atmospheric oxidation of both unsaturated FAs and aromatic HCs, followed by aqueous-phase transformation, is the primary cause of C_2 generation over the sampling site.

These findings will be useful in better understanding the generation mechanisms of secondary organic aerosols (SOA), particularly under aqueous-phase atmospheric conditions throughout the winter. Furthermore, understanding the function of ALW in aqueous-phase SOA production mediated by sulphate (anthropogenic pollutants) and the chemical pathways involved is crucial for accurate SOA prediction. As a result, future climate and air quality estimates should take these findings into account, at least over tropical peninsular India.

Ongoing Activities

Retrieval of Aerosol Optical Depth from EOS-06 OCM3 and Oceansat-2 OCM2

Retrieval of aerosol parameters from satellite observations at finer spatial resolutions is of paramount importance, in assessment of aerosol impacts and monitoring of air quality. Ocean Color Monitor-3 (OCM-3) onboard EOS-06 and Ocean Color Monitor 2 (OCM-2) onboard Oceansat-2 provide radiance measurements in the visible and near infrared bands at a spatial resolution of 360 m at nadir. Algorithms have been developed for the retrieval of aerosols parameters over the oceanic regions from EOS-06 OCM-3 and Oceansat-2 OCM-2. These algorithms incorporate multiple scattering, atmospheric gas absorption and surface reflectance in the radiative transfer computations for the retrieval. Using these algorithms, pixel level aerosol optical depth at 555 nm, has been retrieved from the radiance measurements by EOS-06 OCM-3 and Oceansat-2 OCM-2. The algorithms are based on look up table approach, in which pre-computed TOA reflectance using radiative transfer computations at different wavelength bands are matched with satellite measured reflectance at corresponding channels to obtain the best agreement in spectral variation of reflectance. In order to perform the retrieval, look up tables are generated by computing TOA reflectance corresponding to three wavelength bands of OCM-3 (555 nm, 620 nm and 780 nm) and OCM-2 (555 nm, 620 nm and 740 nm). In order to perform aerosol retrievals over clear sky pixels of OCM2 and OCM3 level 2 radiance measurements, a cloud screening module has been developed for the detection of cloud pixels. Identification of cloud pixels has been carried out by performing three tests; (i) spatial coherence test using reflectance at 555 nm, (ii) reflectance threshold test using the measurement at 490 nm and (iii) ratio of reflectance at 490 nm and 620 nm to distinguish heavy dust loading conditions, which can provide comparable spatial inhomogeneity as that of clouds. Fig. 15 shows retrieved AOD at 555 nm on April 01, 2023 from EOS-06 OCM-3.

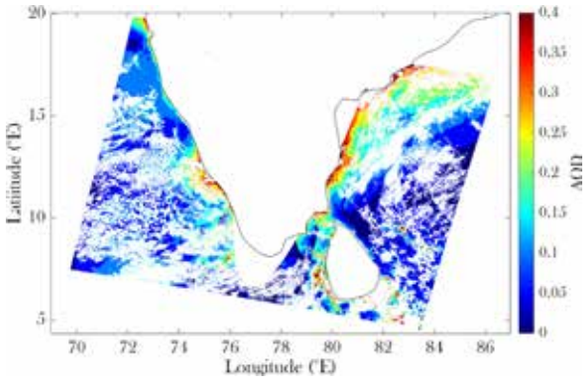

Figure 15: Aerosol Optical Depth at 555 nm on April 01, 2023, retrieved using the radiance measurements from EOS-06 OCM-3.

Quantification of the impacts of aerosol-induced cooling and meteorological feedback on Heat waves over South Asia through regional climate modeling

As the global temperature rises towards higher values, the increase in intensity, duration, and frequency of extremely hot days is of no surprise. The recent trend in global mean temperature is expected to increase the frequency, duration, and intensity of heat waves and heat stress all around the world, especially over the Indian subcontinent. To investigate the plausible mechanisms and implications of meteorological feedback of aerosol forcing on heat stress over South Asia, simulation studies are initiated using a regional climate model (RegCM4) coupled with aerosols.

Assessments of the effect aerosol-induced snow darkening on the elevation-dependent warming observed over the Himalayan Tibetan region

Temperature trends over the high-altitude mountains depict an increase with elevation during recent years. These stratified warming trends observed over the Himalayan-Tibetan regions are higher than the mean warming trends observed over low-elevation regions of South and East Asia, which is attributed to several factors including snow albedo feedback, clouds and water vapour feedback. In this study, the effects of deposition of absorbing aerosols like black carbon and dust on snow albedo and its implications for elevation-dependent warming is being investigated.

Development of Standalone Sun Tracking Radiometer (SSTR)

The Standalone Sun Tracking Radiometer (SSTR) is a fully automatic radiometer, which tracks the Sun and measures direct solar flux at nine wavelengths. It is an active sun-tracking instrument, which uses a solar position estimation algorithm, coupled with sun sensor alignment for precise sun tracking. Its major features are (i) active sun-tracking, (ii) Lightweight, compact and standalone system, (iii) Sensitive optics unit and (iv) Modular design of the sub-systems. The system is aimed at tracking the sun in two steps: firstly, using GPS/ Navic based solar positioning for initial assessment and precise sun pointing with a sun sensor having a narrow FOV. SSTR is a compact and lightweight instrument and will replace the existing passive tracking radiometers operational in ARFI network stations under ISRO-GBP.

Figure 16: 3D model of Standalone Sun Tracking Radiometer.

Future Projections

- Development of high altitude balloon payload for the aerosol characterisation in UTLS.
- Altitude distribution of aerosol chemistry, onboard aircraft.
- Isotope analysis of terrestrial and extra-terrestrial samples for climate research as well as for addressing outstanding questions in solar system science.
- Development of inversion techniques for satellite based retrieval of trace/greenhouse gases.
- Development of light weight instruments for the measurement of aerosol size distribution/extinction coefficient at visible wavelength in Earth and Planetary atmospheres at various atmospheric pressure levels/altitudes.

Publications in Peer-Reviewed Journals

1. Godhani, N., Joshi, H. P.,Jana, S.,Gogoi, M. M, Babu, S.S., "Columnar aerosol optical depth, water vapor andozone over a semi-arid urban location of western India: Potential sources and direct radiative effects", Advances inSpace Research, https://doi.org/10.1016/j.asr.2022.07.046, 2022.
2. Nair, V.S., Babu, S.S, Kompalli, S.K., Jayachandran,V., Ajith T.C., Gogoi, M. M., "Chemical characterizationof aerosols in the South Asian outflow over the Northern Indian Ocean: Latitudinal gradients and ultrafine particleevents", Environmental Science: Atmospheres, https://doi.org/10.1039/d2ea00130f, 2022.
3. Boreddy, S. K. R., Hegde, P.,Arun, B. S., Aswini, A. R., Babu, S. S., "Molecular composition and light-absorbing properties of organic aerosols from west-coast of tropical India", Science of the Total Environment,845,157163, https://doi.org/10.1016/j.scitotenv.2022.157163, 2022.
4. Maitra, A., Rakshit, G., Jana, S.,"Three-Parameter Rain Drop Size Distributions from GPM Dual-Frequency Precipitation Radar Measurements: Techniques and Validation with Ground-Based Observations", IEEE Transactions on Geoscience and Remote Sensing, 60, 1-11,https://doi.org/10.1109/TGRS.2022.3227622, 2022.
5. Gogoi, M. M., Babu, S.S., Imasu, R., Hashimoto, M., "Satellite (GOSAT-2 CAI-2) retrieval and surface(ARFINET) observations of Aerosol Black Carbon over India", Atmospheric Chemistry and Physics, https://doi.org/10.5194/acp-2022-555, 2023.
6. Ramya, C.B., Aswini, A.R., Hegde, P., Boreddy, S.K., Babu, S.S., "Water-soluble organic aerosols over SouthAsia-Seasonal changes and source characteristics". Science of the Total Environment, 165644, https://doi.org/10.1016/j.scitotenv.2023.165644, 2023.
7. Deshmukh, D. K., Aswini, A. R., Ramya, C. B., Hegde, P.,Babu, S. S., "Anthropogenic and biogenic sources drivethe molecular fingerprints and atmospheric processing of water-soluble organic aerosols at the tropical hill stationin the Western Ghats of India", Earth and Space Science, 10, e2023EA002889, https://doi.org/10.1029/2023EA002889,2023.
8. Kompalli, S.K., Babu, S.S, Ajith T.C., Moorthy, K.K., Satheesh, S.K., Boopathy,R., Das, T., Liu,D., Allan, J.,Coe,H., "Aging of biomass burning emissions in the Indo-Gangetic Plain outflow: Implications for black carbonlight-absorption enhancement", Atmospheric Research, https://doi.org/10.1016/j.atmosres.2023.119881, 2023.
9. Ajith, T.C., Kompalli, S.K., Allan, J., Coe, H., Babu, S.S., "Formation pathways of organic aerosolsover a tropical coastal atmosphere", Atmospheric Environment, 309, 119881, https://doi.org/10.1016/j.atmosenv.2023.119881, 2023.
10. Tamanna, S., Pathak, B., Gogoi, M. M., Ajay, P.,Dahutia, P., "Aniket Chakraborty and Pradip K. Bhuyan,Observations on the decadal variability of aerosol in eastern Himalayan foothills: Evidence of an anthropologicallyinduced positive shift", Atmospheric Environment, 299, 119638, https://doi.org/10.1016/j.atmosenv.2023.119638,2023.
11. Panda, S., Babu, S.S., Sharma, S.K., Mandal, T.K., Das, T., Ramasamy,B., "Role of South Asian outflow onthe oxidative potential of marine aerosols over the Indian Ocean", Science of the Total Environment, https://doi.org/10.1016/j.scitotenv.2023.164105, 2023.
12. Boreddy, S. K. R., Divyavani G., Deshmukh, D. K., Kawamura, K., Narasimhulu, K., Rama Gopal, K., "Sulfateassociatedliquid water amplifies the formation of oxalic acid at a semi-arid tropical location over peninsular Indiaduring winter", Science of the Total Environment, 874, 162365. https://doi.org/10.1016/j.scitotenv.2023.162365,2023.
13. Lakshmi, N.B., Babu, S.S.Nair, V.S., "Mineral dust aerosols over the Himalayas from polarization-resolved satellitelidar observations", Atmospheric Environment, 296, 119584, https://doi.org/10.1016/j.atmosenv.2023.119584,2023.
14. Deshmukh, D.K., Kawamura, K., Kobayashi, M., Gowda, D.,"Changes in the size distributions of oxalic acidand related polar compounds over Northern Japan during spring", Journal of Geophysical Research: Atmospheres,128, e2022JD038461, https://doi.org/10.1029/2022JD038461, 2023.
15. Nirmalkar, J., Raman, R.S.,Deshmukh, D.K, Haque,M.M.,"PM2.5-bound biogenic secondary organic aerosol tracersover a regionally representative site in central India: characteristics and sources", Atmospheric Environment, 294,119516,https://doi.org/10.1016/j.atmosenv.2022.119516,2023.

16. Haque, M.M., Verma, S.K.,Deshmukh, D.K, Kunwar,B., Kawamura,K.,"Seasonal characteristics of biogenicsecondary organic aerosol tracers in a deciduous broadleaf forest in northern Japan", Chemosphere, 311,136785,https://doi.org/10.1016/j.chemosphere.2022.136785, 2023.

17. Jana, S., Chakraborty, R., Maitra, A.,"Lightning Prediction Using Electric Field Measurements Associated withConvective Events at a Tropical Location", Pure and Applied Geophysics, 180 (3), 1173-1184,https://doi.org/10.1007/s00024-023-03241-x, 2023.

Presentation in Symposia/Conferences/Workshops

International

1. Sobhan Kumar Kompalli, Babu, S.S., Ajith, T.C., Satheesh, S. K., Moorthy, K.K., Das, T., Boopathy, R., Liu, D.,Darbyshire, E., Allan, J.D., Brooks, J., Flynn, M.J., Coe, H., "Light-absorption Enhancement of Black Carbon inthe Indo-Gangetic Plain Outflow due to Coatings from the Aged-Biomass Burning Emissions", A36E-04, Session:Light-Absorbing Carbon Aerosol from Observations and Models IV Oral, AGU Fall Meeting, 14 December, 2022.

2. Ajith, T.C., Sobhan Kumar Kompalli, S. Suresh Babu, "Role of aerosol microphysical properties on cloudcondensation nuclei activity over a tropical coastal location" A42C-05, Session: A42C: Atmospheric Aerosols andTheir Interactions with Clouds, Radiation, and Climate III Oral, AGU Fall Meeting, 15 December, 2022.

3. Thejas, K.V., Nair, V.S., Sinha, P.R., "Aerosol-warm cloud interaction over Eastern Indo Ganetic Plain duringwinter" International Conference on Nucleation and Atmospheric Aerosols (ICNAA), Brisbane, Australia (online),26-30 June, 2023.

4. Sebastian, M., Sobhan Kumar Kompalli, Kumar, A., Jose, S., Babu, S. S., Pandithurai, G., Singh, S., K. Hooda,R., K. Soni, V., R. Pierce, J., Vakkari, V., Asmi, E., M. Westervelt, D., Hyvarinen, A.-P., and P. Kanawade, V.,"Observations of particle number size distributions and new particle formation in six Indian locations" , A35J,Session: Aerosols and Air Quality over South and Southeast Asia : Observations, Modelling and Impacts II Poster,AGU Fall Meeting, 14 December, 2022.

5. Mukunda M Gogoi, S. Suresh Babu, Ryoichi Imasu, Makiko Hasimoto, "Satellite (GOSAT-2 CAI-2) and surface (ARFINET) observations of Aerosol Black Carbon over India: Regional and Global Inferences", 18th International Workshop on Greenhouse Gas Measurements from Space (IWGGMS-18), National Institute for Environmental Studies (NIES), Japan, July 12-14, 2022.

6. Mukunda M Gogoi, S. Suresh Babu, Ryoichi Imasu, Makiko Hasimoto, "Satellite (GOSAT-2 CAI-2) retrieval and ground-based (ARFINET) observations of Aerosol Black Carbon over India", COSPAR 2022 - 44th Scientific Assembly, Athens, July 16-24, 2022.

7. Dhananjay K. Deshmukh, Prashant Hegde, B.S. Arun, Mukunda M. Gogoi, and S. Suresh Babu, "Anthropogenic sulfate-driven secondary organic aerosol formation over the eastern Himalayas through aqueous phase photochemical reactions", AS3.1 - Aerosol Chemistry and Physics, European Geoscience Union (EGU) General Assembly, Vienna, Austria, 23-28 April 2023.

National

8. Aswini, A. R. "Size-speciated chemistry of ions, trace metals and carbonaceous aerosols over a hill station inpeninsular India - measurement techniques and source apportionment", Indian Analytical Science Congress IASC-2023, Kochi, March 23-25, 2023.

9. Deshmukh, D.K. "Secondary Organic Aerosol Formation over the Eastern Himalayas: Implications fromAtmospheric Water-Soluble Low-Molecular-Weight Organic Compounds", National Conference on Polar Science2023 (NCPS-2023), Open Science Conference (OSC), National Institute for Polar and Ocean Research (NCPOR),Goa, May 18-19,2023.

10. Hegde, P. "Determination of molecular composition of dicarboxylic acids, oxocarboxylic acids, α-dicarbonyls andfatty acids in atmospheric aerosols using gas chromatograph equipped with flame ionization and mass detector",Indian Analytical Science Congress IASC-2023, Kochi, March 23-25, 2023.

11. Mukunda M Gogoi, Santosh K Pandey, Arun B S, Vijayakumar S Nair, Roseline C Thakur, Jai Prakash Chaubey,Anoop Tiwari, Manoj M R, Sobhan Kumar Kompalli, Aditya Vaishya, Prijith S S, PrashanthHegde, and S SureshBabu, "Decadal variability of aerosol properties over Ny-Ålesund: Results from Indian scientific expeditions tothe Arctic", National Conference on Polar Research (NCPS-2023), National Centre for Polar and Ocean Research,Goa, 18-19 May, 2023.
12. Ramya, C. B., "Molecular level characteristics of water-soluble organic aerosols over the Western Ghats: Biogenicand Anthropogenic contributions." International Symposium on Secondary Aerosol Formation and Growth 2023(NANO-2023), University of Hyderabad, March 13-14, 2023.
13. Thejas, K.V., Nair, V.S., Sinha, P.R., "Study of aerosol interactions with warm clods over Eastern Indo-GangeticPlain during Winter season using satellite data", Kerala Science Congress, Kuttikkanam, Idukki, 12-14 Feb., 2023.
14. Ajeeshkumar, P.S., FAST-2023 National Conference on Landing and Recovery systems for Aerospace vehicles (LaRA), VSSC Trivandrum, 30 June - 01 July 2023.

Invited Talks

S. Suresh Babu

1. "Aerosols and Air Quality over South Asia from Long term observations and Modelling" in the iCACGP/IGACjoint International Atmospheric Chemistry Conference, September 11-15, 2022 (online).
2. "Polar Climate Change: On the Warming of the Freezing Environment", National Conference on Polar Science, Young Polar Scientist Meet, NCPOR, Goa, May 17, 2023.

Vijayakumar S. Nair

1. "Aerosol Variability" at National workshop and Brainstorming Meeting, "Space based Information Support for Climate and Environment Studies: Road to the Future", National Information System for Climate andEnvironment Studies (NICES), NRSC, Antariksh Bhawan, Delhi, July 18-19, 2022.
2. "Aerosol-cryosphere-climate interactions over the Himalayan-Tibetan regions", International Conference on Advances in Science of the Earth: Relevance to the Society, SRTM University, Nanded, November 24, 2022.
3. "Effects of aerosols on hydrological cycle" in the SecoNdary Aerosol FormatioN and GrOwth-2023 (NANO-2023), the University of Hyderabad and the Finnish Meteorological Institute (FINLAND), University of Hyderabad, March 13-14, 2023.

Mukunda M. Gogoi

1. "Satellite (GOSAT-2 CAI-2) retrieval and ground-based (ARFINET) observations of Aerosol Black Carbon overIndia: Regional and Global Implications", Research Institute for Humanity and Nature (RIHN), Kyoto, Japan, September 16, 2023.

Prashant Hegde

1. "Welcome to the fascinating world of Space Science through ISRO", 'JIGYASA' a student-scientist connect programme, National Physical Laboratory (NPL), New Delhi, February 24, 2023.

Prijith S. S.

1. "Earth's Atmosphere: Ozone and Other Constituents", as part of the programmes on International Day for the preservation of the Ozone Layer, Marian College of Arts and Sciences, Thiruvananthapuram, September 16, 2022.

Ramya, C. B.

1. "Air/Atmospheric Pollution Using Ground, Airborne and SatelliteRemote Sensing Techniques.", Invited talk, Department of Earth and Space Sciences, Indian Institute of Space Science and Technology, Thiruvananthapuram, March 17, 2023.

Training/Workshop

Vijayakumar S. Nair

- NISAR Science Workshop-2023, SAC, Ahmedabad, March 20-21, 2023.

Mukunda M. Gogoi

- Workshop on “Forward Sensitivity Method (FSM) for Dynamic Data Assimilation”, National Atmospheric Research Laboratory (NARL), Tirupati, 27 Feb - 02 Mar 2023.
- “EOS-06 Oceansat-03” Science and Applications meeting, Space Application Centre (SAC), Ahmedabad, March 30, 2023.

Prijith S. S.

- EOS-06/Oceansat-3 Science and Applications Meet, Space Applications Centre, Ahmedabad, March 30, 2023.
- TRISHNA Project ISRO-CNES Face to Face Meeting, Space Applications Centre, Ahmedabad, June 21- 23, 2023.

Dhananjay Kumar

- Workshop on Sea-Ice Modelling and Observations (SiMO), National Institute for Polar and Ocean Research (NCPOR), Goa, 16-17 May 2023.

संख्यात्मक वायुमंडल प्रतिरूपण
Numerical Atmosphere Modelling

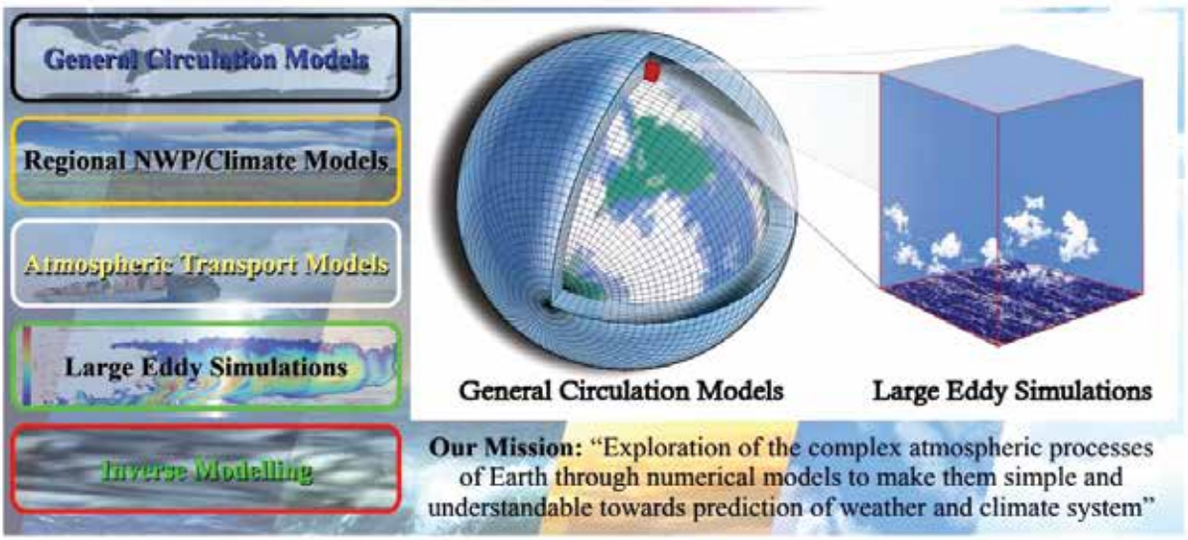

संख्यात्मक वायुमंडल प्रतिरूपण शाखा, सामान्य परिचालन नमूनों, क्षेत्रीय संख्यात्मक मौसम पूर्वानुमान व जलवायु नमूनों, वायुमंडलीय परिवहन नमूनों और बड़े भंवर अनुकरणों सहित वायुमंडलीय नमूनों के एक रेंज के माध्यम से मौसम एवं जलवायु प्रणाली के पूर्वानुमान और विश्लेषण से संबंधित वैज्ञानिक पहलुओं पर ध्यान केंद्रित करती है। यह शाखा प्रेक्षित वायुमंडलीय विचलनों के आधार पर, प्रेक्षित विविध विशेषताओं के लिए उत्तरदायी क्रियाविधियों एवं भौतिक प्रक्रियाओं को समझते हुए और प्रतिलोम प्रतिरूपण का उपयोग करते हुए भारतीय क्षेत्र के ऊपर ग्रीनहाउस गैस अभिवाहों का आकलन करते हुए नमूने संबंधी पूर्वानुमानों में सुधार लाने का लक्ष्य करती है। श्रीहरिकोटा से उड़ान भरनेवाले इसरो के प्रमोचन यान अभियानों का लघु-परास मौसम पूर्वानुमान करने के लिए भी यह शाखा सहयोग प्रदान करती है।

The Numerical Atmosphere Modelling branch focuses on the scientific aspects dealing with the prediction and analysis of the weather and climate system through a range of atmospheric models including the general circulation models, regional numerical weather prediction and climate models, atmospheric transport models, and large eddy simulations. It aims at improving the model predictions based on the observed atmospheric variations, understanding the mechanisms and physical processes responsible for various observed features, and optimizing the estimation of greenhouse gas fluxes over the Indian region using inverse modeling. This branch also supports the short-range weather predictions for ISRO's launch vehicle missions from Sriharikota.

वैज्ञानिक टीम / Science Team
बाला सुब्रहमण्यम डी. / Bala Subrahamanyam D.
सिजिकुमार एस. / Sijikumar S.
उमा के एन. / Uma K. N.

अनुसंधान सहयोगी / Research Associates
नित्या के. / Nithya K.
रोशनी एस. / Roshny S.*
अंजुमोल राजू / Anjumol Raju@

अनुसंधान अध्येता / Research Fellows
बूक्या सामा / Bukya Sama
आदर्श जैन / Adarsh Jain
अक्षय एस. / Akshay S.

** Relieved in August 2022*
@ Relieved in February 2023

Reference Model of Atmosphere for ISRO Launch Vehicle Applications

Model atmosphere from the surface to 110 km over the Indian tropical region developed using in-situ and space-based measurements

Atmospheric model of the altitude variations of temperature, pressure and density are crucial for designing launch vehicles as well as for the scientific research. The models available over the Indian region were developed three decades ago using in-situ observations till 1990, hence a need was felt to update the model. The database for the present study spans 44 years of radiosonde data from IMD Chennai (1975-2018) to cover from 0 to 25 km. For the atmospheric profiles from 25 to 100 km, M-100 Rocket (1971-1991) and Sounding of the Atmosphere by Broadband Radiometry (SABER) satellite measurements of temperature (2002-2018) are used. These individual altitude profiles of temperature, pressure and density obtained from radiosonde, M-100 and SABER for the whole period are shown in Figs.1(a-c), respectively. It shows the quality-controlled profiles with 3σ for M-100 rocket and SABER and 4.5σ for radiosonde as Inter Quartile Range methodology is used for radiosonde data to obtain quality-controlled profiles. SABER data is gridded over Thumba and in order to combine with M-100 rocket, the monthly mean temperature profiles are compared between SABER and M-100. The comparison between the two shown in Fig. 2 agrees well, and the difference is observed to be less than ±6K. The monthly mean of radiosonde and combined monthly mean of M-100 and SABER is used to generate the monthly mean and ±3σ from surface to 110 km. A comparison made between the reference atmosphere generated by the present study and that generated by Sasi and Sengupta 1986 (hereafter, referred as SS86) is shown in Figs. 3(a-c) for temperature, pressure and density, respectively. The dispersion observed in SS86 is less compared to the present observations. In the altitude region between 15 and 40 km, the 3σ deviation in the temperature is about 15 K in the present model, and it is about 5 K in SS86. The deviation is about 18 to 20 K from 40 to 60 km, and between 70 and 80 km, it is 30 to 40 K. The deviation with respect to SS86 is 10 K. The corresponding pressure and density deviation is also observed to be more in the present model compared to SS86. The variation of the present model in pressure and density is 10 to 20% higher compared to SS86. Long-term trend in the temperature is estimated as it is vital in understanding the cooling and warming at different regions of the atmospheres. The monthly mean temperature is mainly influenced by annual, semi-annual, quasi biennial oscillation, El-Nino southern oscillation and the 11-year solar cycle. Hence, it is necessary

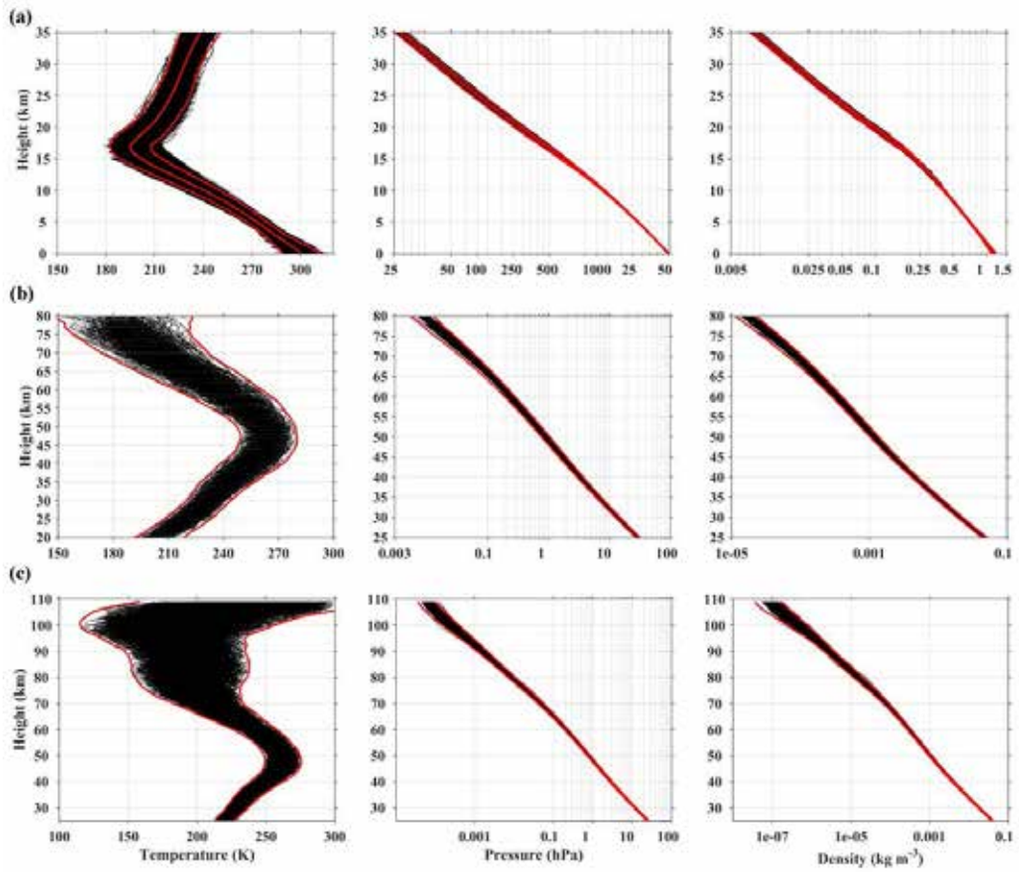

Figure 1: Individual altitude profiles of temperature, pressure and density measured from (a) radiosonde, (b) M-100 rocket and (c) SABER. Red line in each panel indicates ±3σ where σ is the standard deviation [Uma et al., Earth and Space Science, 2023].

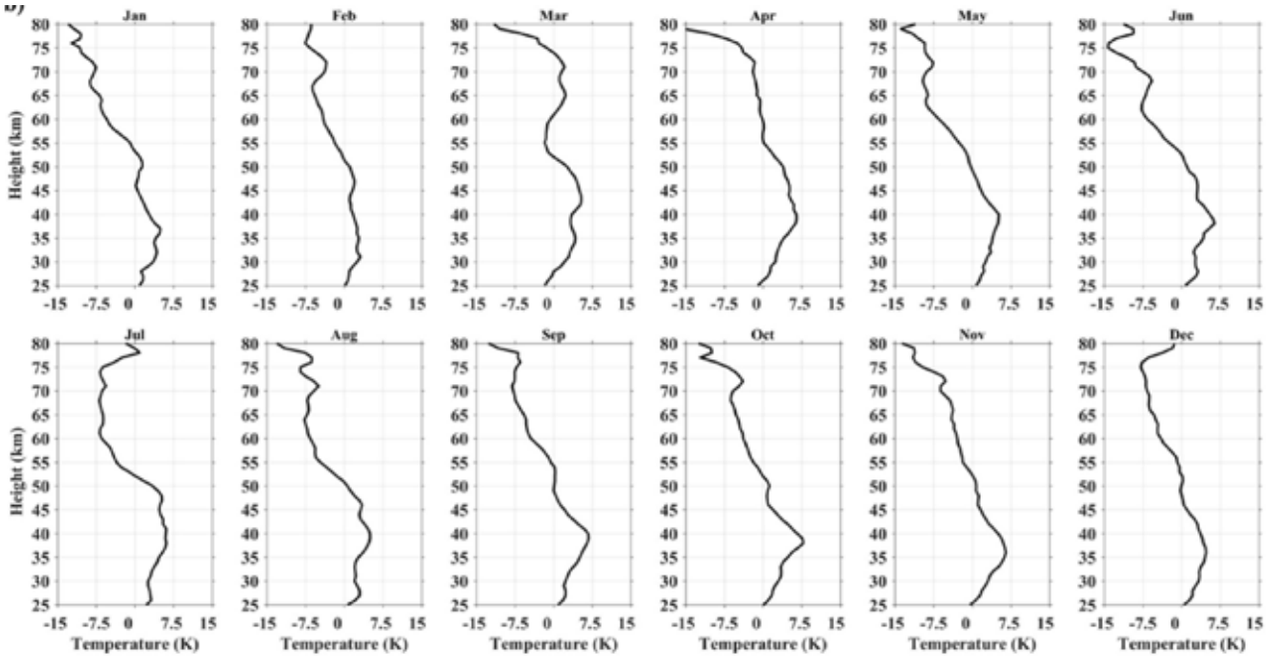

Figure 2: Difference in monthly mean temperature between M-100 and SABER over Thumba [Uma et al., Earth and Space Science, 2023].

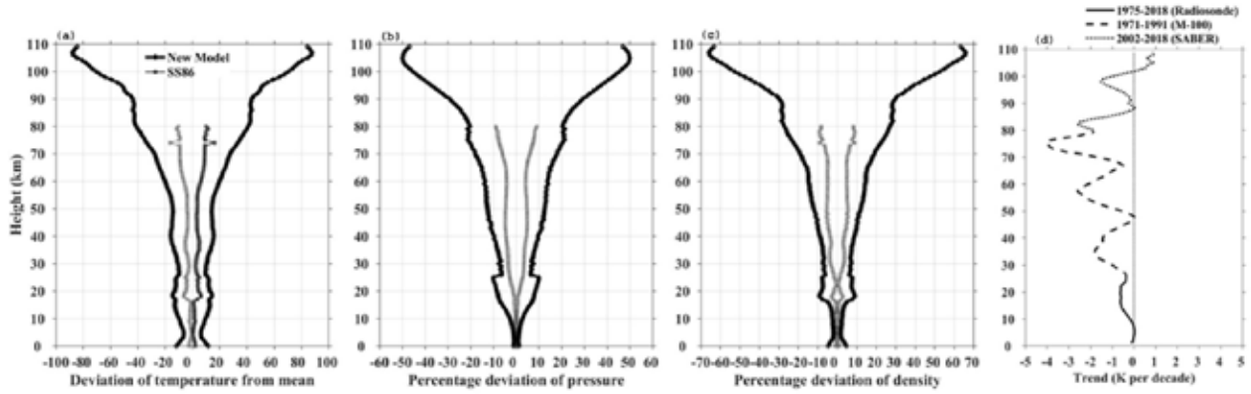

Figure 3: Comparison of present reference atmosphere with SS86 model for (a) 3σ deviation of temperature (b) percentage deviation of pressure and (c) percentage deviation of density. Line with circle indicates the present reference atmosphere and line with square indicates SS86. (d) Vertical variation of long-term trend observed in the temperature with different observations [Uma et al., Earth and Space Science, 2023].

to remove the influence of the above variability and hence a multi-regression analysis is used to remove the above variability in the temperature. The trend in the temperature is shown in Fig. 3d. Warming trend is observed up to an altitude of 8 km. Present analysis shows a cooling trend from 8 km and above except at 50 km, 90 and above 100 km, where a slight warming is observed. The cooling trend is maximum at 35 (~ 2 K/decade), 55 (~ 2.7 K/decade), and 75 km (4 K/decade).

Greenhouse Gas Flux Estimation

Net Ecosystem Exchange over India using Vegetation Photosynthesis and Respiration Model (VPRM) simulations

The terrestrial biospheric CO_2 flux is an inevitable component in the optimisation process of CO_2 flux using inverse modelling. The existing biospheric CO_2 flux data are coarse in resolution, and also the availability of updated data is limited. In this scenario, the present study used a satellite-data derived light-use-efficiency model (the Vegetation Photosynthesis and Respiration Model, VPRM) to compute the biospheric CO_2 fluxes over India. The VPRM for the Indian region was configured by using high-resolution Indian Remote Sensing satellite (Resourcesat-1) Advanced Wide Field Sensor (IRS-P6 AWiFS) derived Land Use-Land Cover (LULC) data, surface reflectance data from MODIS and meteorological parameters from the European Centre for Medium-Range Weather Forecasts (ECMWF) reanalysis ERA5. The model simulation was carried out for a decade (2011-2020) to obtain ecosystem photosynthesis, respiration and net CO_2 exchange. The Net Ecosystem Exchange (NEE) observations from three stations (Kaziranga National Park (KNP), Haldwani (HFS)

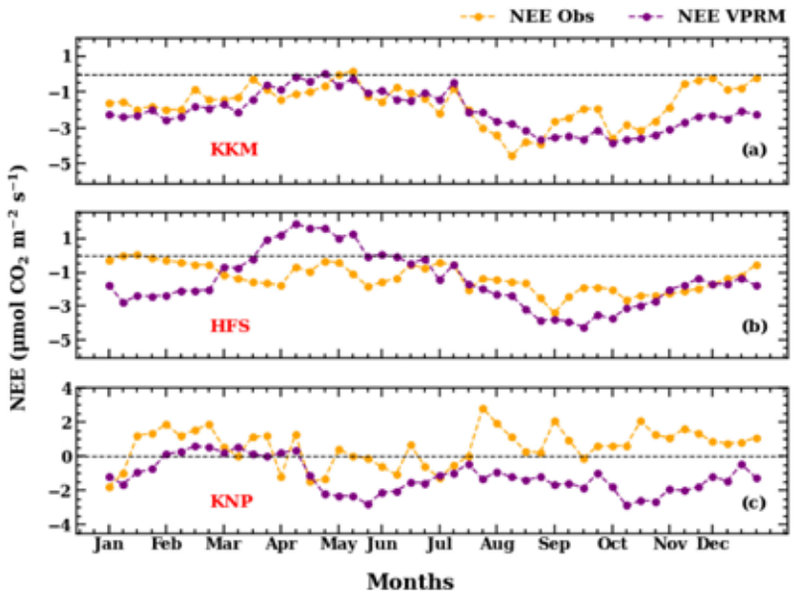

Figure 4: 8-day mean NEE observation (orange) and NEE modelled using VPRM (purple) from three stations: (a) KKM, (b) HFS and (c) KNP during 2016. (Unit: µmol CO_2 m^{-2} s^{-1}) [Raju et. al., Ecological Modelling, 2023].

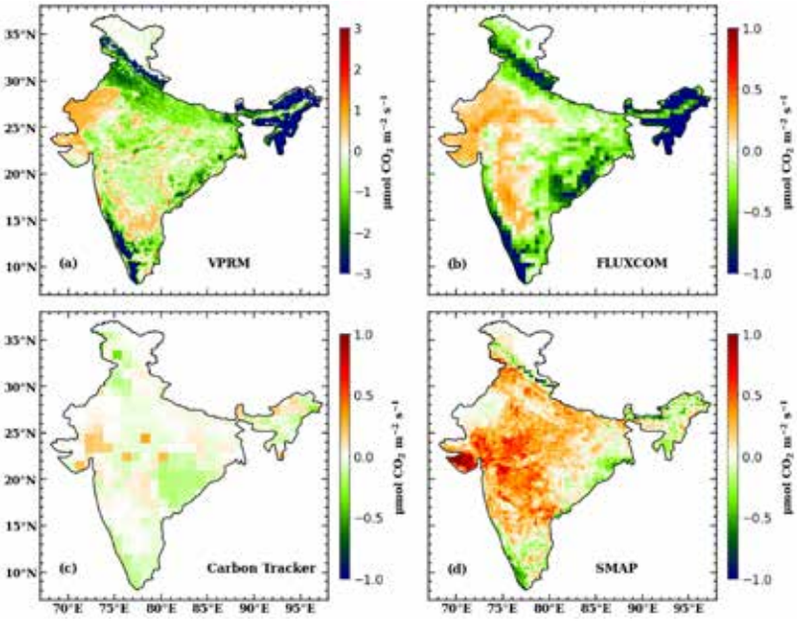

Figure 5: Spatial distribution of the mean NEE from (a) VPRM model, (b) FLUXCOM, (c) Carbon Tracker and (d) SMAP during the period 2016-2018 (Unit: µmol CO_2 m^{-2} s^{-1}) [Raju et. al., Ecological Modelling, 2023].

and Kosi-Katarmal (KKM)) were used to compare the NEE from the model (Fig. 4). Among these stations, the NEE from KKM showed very good agreement with model simulated NEE during most of the year, whereas other stations showed a partial match. Over KKM, the NEE from observation and model showed similar patterns until October, while during November-December, the model indicated higher biospheric uptake of CO_2 compared to the observation. The VPRM could simulate well-matched NEE over HFS from mid-June to December, but the NEE pattern from January to mid-June needs to be better-matched with observations that can be attributed to the difference in the representation of vegetation greenness (Fig. 4b). The VPRM model captured the NEE over KNP fairly well from January to April. After that, the observed NEE is positive till the end of the year, while the model simulated NEE are negative values (Fig. 4c). Overall, the magnitudes of the VPRM simulated NEE aligned with the observations over different vegetated regions in India.

Compared to the other available gridded NEE from Carbon Tracker (CT), FLUXCOM, and Soil Moisture Active Passive (SMAP) Level-4 data, the VPRM model performed reasonably well over the Indian region (Fig. 5). The VPRM captured the spatial pattern and the seasonal features of NEE over the country better than the other

three data. The magnitude of NEE from the VPRM model is relatively high compared to the biospheric CO_2 flux from the CT, FLUXCOM, and SMAP. The fusion of high-resolution LULC and surface reflectance data in VPRM suggested that the average NEE over the Indian region during 2011-2020 is -0.16 ± 0.02 PgC yr^{-1}. Among this, the contribution from Gross Ecosystem Exchange is about -0.47 ± 0.02 PgC yr^{-1}, and Respiration is 0.31 ± 0.01 PgC yr^{-1}. The maximum biospheric CO_2 absorption is during the post-monsoon season, and the minimum is during the pre-monsoon season. The very high spatial resolution and heterogeneity resolved in the NEE data derived in this work offered the first data product of this kind for a variety of NEE analyses over India.

High-Resolution Bayesian Inversion of Carbon Dioxide Flux Over Peninsular India

The Bayesian inversion method is employed to estimate the CO_2 flux over peninsular India during 2017-2020 in combination with a high-resolution Lagrangian particle dispersion model FLEXPART (stands for FLEXiblePARTicle), different prior fluxes and ground-based observations. The prior fluxes include fossil fuel emission from Open-source Data Inventory for Anthropogenic CO_2 (ODIAC), atmosphere-biosphere exchange from the VPRM model, wildfire emission from Global Fire Emissions Database (GFED) and ocean flux from Oceanic Tracer Transport Model (OTTM) model. Observations from three stations located over peninsular India such as Thumba, Gadanki and Pune were used for the inversion. Prominent seasonal variations observed in the CO_2 mixing ratio obtained from all three stations were well reflected in the modelled mixing ratio. The root mean square errors between measured and modelled mixing ratios were 3.4, 4.0 and 6.5 ppm for Thumba, Gadanki and Pune, respectively.

The mean spatial distribution of posterior flux obtained from the Bayesian inversion during 2017-2020 is much closer to the prior fluxes over most of the Indian regions (Fig. 6). The inversion could bring changes mainly over peninsular India as the observation stations are located in this region. The mean flux over peninsular India during 2017-2020 is updated with an additional 3.34 TgC yr^{-1} in the prior flux. During winter, the flux corrections are noticed almost all over the Indian region. The inversion suggests an enhancement in CO_2 emission over most of the peninsular India during the pre-monsoon season. The flux corrections during monsoon season are lesser since the transport is mainly from the southwest oceanic region. The maximum spatial flux corrections are obtained during the post-monsoon season. The seasonal mean area integrated flux corrections over peninsular India are 4.68, 6.53, -2.28 and 4.41 $TgCyr^{-1}$ during winter, pre-monsoon, monsoon, and post-monsoon seasons, respectively.

One of the limitations of the present study is that we used only three station observations to constrain the fluxes over peninsular India. More observations from different locations may better estimate posterior fluxes. Another important point to mention is that we considered prior flux uncertainties are uncorrelated. Therefore the off-diagonal elements of the prior error covariance matrix are zero. The assumption of uncorrelated prior uncertainty is a common method for simplifying the matrix inversions. However, this assumption adds a small source of error in the posterior flux estimation, which is not precisely quantified in this work. By incorporating satellite observations and ground observations, and considering correlation in the flux uncertainties, future studies may bring better estimates of CO_2 fluxes over the Indian region.

Large Eddy Simulations for Atmospheric Boundary Layer (ABL) Studies: A New Initiative

An Assessment of the RANS and LES model simulations of the coastal ABL heights for contrasting sky conditions

In this study, the behaviour of a Reynolds Averaged Navier-Stokes (RANS) and a Large Eddy Simulations (LES) model in the simulation of the diurnally

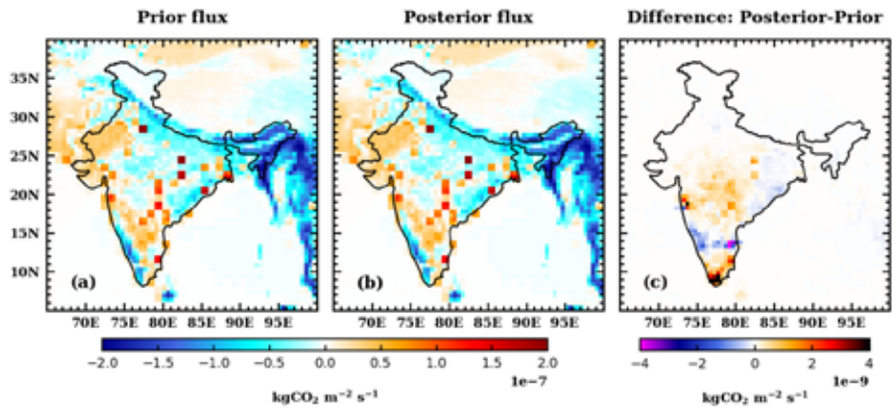

Figure 6: Mean CO_2 (a) prior flux, (b) posterior flux and their difference for 2017-2020 [Sijikumar et al., Atmospheric Environment, 2023].

evolving coastal atmospheric boundary layer (ABL) over Thiruvananthapuram is investigated. The model simulations are carried out for contrasting sky conditions during the passage of a tropical cyclone Ockhi. The Consortium for small-scale modelling (COSMO) model represents the RANS technique, and a mesoscale-to-LES nested configuration of the Parallelized LES Model (PALM) represents the LES technique. The RANS model simulations are carried out at a grid spacing of 2.50 km, whereas the LES experiments are done at 30 m and 100 m grid spacings (hereafter referred to as the LES_{30} and LES_{100}). The main objective of these experiments is to assess the individual model biases of nested LES in conjunction with the RANS model and to find out whether the ABL heights obtained from the LES are considerably different from those obtained in the RANS model simulations.

Figure 7 depicts the time-altitude evolution of virtual potential temperature (θ_v) for clear-sky conditions on 5 December 2017. These profiles indicate the presence of a very shallow stable boundary layer (SBL) between 0530 LT to 0830 LT. This SBL gradually disappears after the sunrise and formation of a shallow mixed layer begins

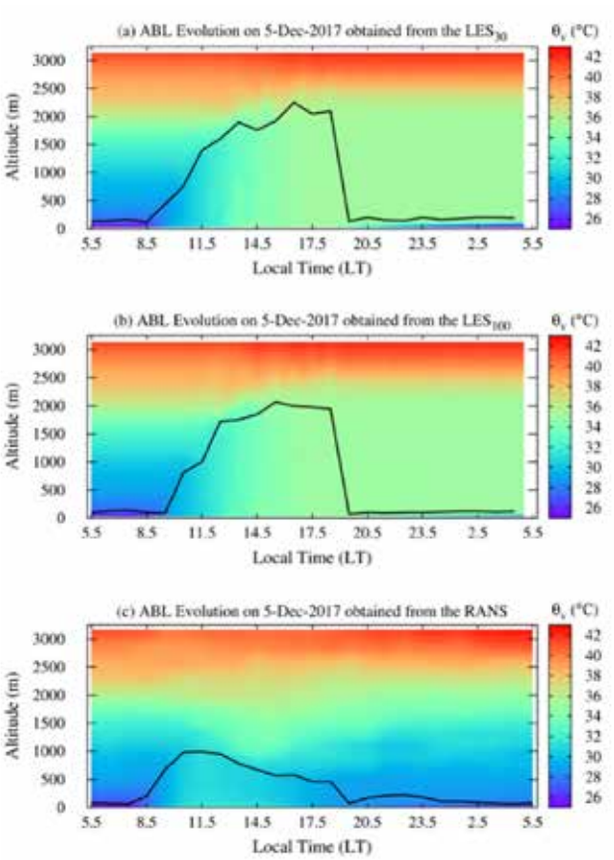

Figure 7: Time-altitude evolution of virtual potential temperature (θv, in °C) for a clear-sky and fair-weather conditions of 5 December 2017 obtained from the (a) RANS, (b) LES_{30} and (c) LES_{100} experiments. The top of the ABL inferred from the individual profiles of θ_v and q is overlaid on the shaded plot as a line curve [Roshny and Subrahamanyam, Journal of Atmospheric Solar Terrestrial Physics, 2022].

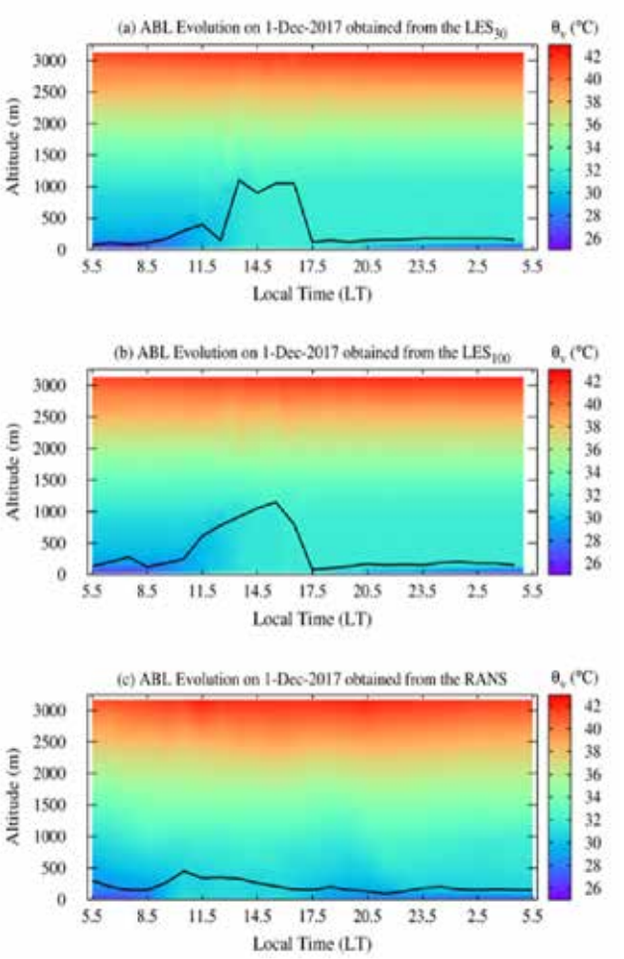

Figure 8: Same as Figure 7, but for the cloudy conditions of 1 December 2017 [Roshny and Subrahamanyam, Journal of Atmospheric Solar Terrestrial Physics, 2022] .

at 0830 LT. After the sunrise, the convection builds up and this mixed layer expands in the daytime and attains a peak during the noon hours. In the RANS experiment, the ABL top attains peak value of about 1000 m between 1030 LT to 1230 LT (Fig. 7a). For clear-sky and fair-weather conditions of 5 December 2017, both the LES experiments indicated a well-developed ABL extending from the surface to an altitude of about 2000 m during 1430 LT to 1530 LT. The ABL heights inferred from the altitude profiles of θ_v showed a gradual rise during the forenoon hours between 0830 LT to 1430 LT and a gradual decrease after 1800 LT for the RANS experiment. The decay of ABL was instantaneous in the LES experiments after 1800 LT. The vertical thickness of ABL simulated by the RANS experiment was significantly lower than that in the LES experiments. The diurnal evolution of ABL for cloudy conditions of 1 December 2017 is shown in Fig. 8. The initial conditions of the atmosphere corresponding to 0530 LT on this day indicated the presence of a very stable boundary layer extending from the surface to an altitude of about 400 m. After the sunrise, the depth of convective mixed layer was confined to well below 500 m at 1130 LT in the RANS experiment. Unlike the growth of ABL on 5

December 2017, the depth of the daytime mixed layer was significantly shallow on 1 December 2017. The presence of a relatively stable layer on the top of the mixed layer (identified through a sharp increase in the magnitudes of θ_v with rising altitudes) restricts the turbulent mixing in the vertical direction within the ABL. From the present investigation, it can be conclusively stated that the depth of a well-developed ABL during the daytime conditions for a clear-sky as well as the cloudy day was deeper in the LES experiments. These features are attributed to the fact that the large eddies responsible for most of the momentum transfer and turbulent mixing are explicitly well-captured in the LES, whereas they are parameterized in the RANS models.

Weather Prediction support to ISRO's Launch Missions

As a member of the Inter-Center Weather Forecast Expert Team of ISRO, SPL extends support to all the PSLV and GSLV missions undertaken from SDSC, Sriharikota by providing short-range weather predictions with the aid of its operational numerical weather prediction model COSMO. During the review period, weather forecasting support was extended to the following missions:

SSLV-D1 (EOS-02, 7 August 2022)

LVM3/M3 (OneWeb India-1, 23 October 2022)

PSLV-C54 (EOS-06, 26 November 2022)

SSLV-D2 (EOS-07, 10 February 2023)

LVM3/M3 (OneWeb India-2 mission, 26 March 2023)

PSLV-C55 (TeLEOS-02, 22 April 2023)

GSLV-F12 (NVS-01, 29 May 2023).

As per the requirements of the Inter-Center Weather Forecast Expert Team, location-specific weather predictions for Sriharikota region with the aid of COSMO model were made available to the Team members on a regular basis.

Future Projections

- Regional estimation of greenhouse emissions over India using satellite observations and atmospheric inverse modelling
- Investigating the characteristics of heavy rainfall events over the west coast of peninsular India during the summer monsoon season
- Representation of subgrid-scale processes in COSMO model during the extreme weather events, such as severe heat waves, heavy precipitation, and tropical cyclones
- Large Eddy Simulations of a solar eclipse event for the investigation of atmospheric boundary layer processes in response to varying solar forcing
- Characterization of tropical cyclone and hailstorms for an assessment on the role of convection

Publications in Peer-Reviewed Journals

1. Raju. A., S.Sijikumar, Pramit Kumar Deb Burman, Vinu Valsala, Yogesh K. Tiwari, Sandipan Mukherjee, Priyanka Lohani, and Kireet Kumar, "Very high-resolution Net Ecosystem Exchange over India using Vegetation Photosynthesis and Respiration Model (VPRM) simulations", Ecological Modelling 481: 110340, 2023. https://doi.org/10.1016/j.ecolmodel.2023.110340.
2. Roshny S., and D. Bala Subrahamanyam, "Do the large-eddy simulations yield deeper atmospheric boundary layers in comparison to the RANS model simulations?", Journal of Atmospheric-Solar Terrestrial Physics, 240: 105954, 2022. https://doi.org/10.1016/j.jastp.2022.105954.
3. Sijikumar S., Anjumol Raju, Vinu Valsala, Yogesh Tiwari, Girach I. A., Chaithanya D. Jain, and M. Venkat Ratnam, "High-Resolution Bayesian Inversion of Carbon Dioxide Flux Over Peninsular India", Atmospheric Environment, 308: 119868, 2023. https://doi.org/10.1016/j.atmosenv.2023.119868
4. Uma, K. N., V. Adimurthy, and R. Ramachandran, "The state-of-the-art model atmosphere from the surface to 110 km over the Indian tropical region for ISRO launching vehicle applications: Developed from in situ and space-based measurements". Earth and Space Science, 10: e2022EA002483, 2023. https://doi.org/10.1029/2022EA002483.
5. Mridula, N., G. Manju, S. Sijikumar, Tarun Kumar Pant, and Raj Kumar Choudhary, "On the significant impact of the 17 March 2015 St. Patrick's Day geomagnetic storm on the Ionosphere over Indian region", Advances in Space Research, 70: 3674 - 3685, 2022. https://doi.org/10.1016/j.asr.2022.08.022.
6. Das, S. S., M. V. Ratnam, M. D. Rao, and K. N. Uma, "Volume imaging of aspect sensitivity in VHF radar backscatters: First results inferred from the Advanced Indian MST radar (AIR)", International Journal of Remote Sensing, 43(12): 4517 - 4540, 2022. https://doi.org/10.1080/01431161.2022.2111667.

7. Sachin Philip Kakkanattu, Sanjay Kumar Mehta, D. Bala Subrahamanyam, V. Rakesh, and Amit P. Kesarkar, "Thermodynamic structure of the atmospheric boundary layer over a coastal station in India for contrasting sky conditions during different seasons", Atmospheric Research 293, 106915, 2023. https://doi.org/10.1016/j.atmosres.2023.106915.

Presentation in Symposium / Conferences / Workshop

1. Bukya Sama, K. N. Uma, and Subrata Kumar Das, "Characteristics of Hail Storms using Doppler Weather Radar and reanalysis over Kolkata", TROPMET-2022, conducted by Indian Institute of Science Education and Research, Bhopal (IISERB), 29 November - 02 December 2022.
2. Bukya Sama, and K. N. Uma, "Diurnal variability of convection over a coastal station Thumba using C- band Doppler Weather Radar (DWR)", URSI - RCRS 2022, Indian Institute of Technology (IIT) Indore, 1 - 4 December 2022.
3. Bukya Sama, K. N. Uma, and Subrata Kumar Das, "Characteristics of Hail Storms using Doppler Weather Radar and reanalysis over Kolkata", AGU Fall meeting, Chicago (In virtual mode), 12 - 16 December 2022.

Invited / Plenary / Lead Talks

1. D. Bala Subrahamanyam, "Journey in the area of atmospheric modelling: face your inhibitions", Department of Physics, Kariyavattom Campus, University of Kerala, 29 July 2022. [INVITED TALK]
2. D. Bala Subrahamanyam, "Diurnal Evolution of the Atmospheric Boundary Layer Heights over a Coastal Station: Amalgamation of the Experimental Observations and Model Simulations", National workshop on Boundary Layer Exchange Processes and Climate Change (NoBLExClim-2023), SRM Institute of Science and Technology, Chennai, 23-24 March 2023. [KEYNOTE ADDRESS]

Chair (Workshop / Conference)

1. D. Bala Subrahamanyam, Session on "Boundary Layer Exchange Processes", National workshop on Boundary Layer Exchange Processes and Climate Change (NoBLExClim-2023), SRM Institute of Science and Technology, Chennai, 23-24 March 2023.

Training Programme

1. Bukya Sama, National Training workshop on fundamentals of Data Assimilation (NTDA -2022) conducted by Indian Institute of Tropical Meteorology (IITM), Pune, 9 - 21 September 2022.

वायुमंडलीय गतिकी शाखा
Atmospheric Dynamics Branch

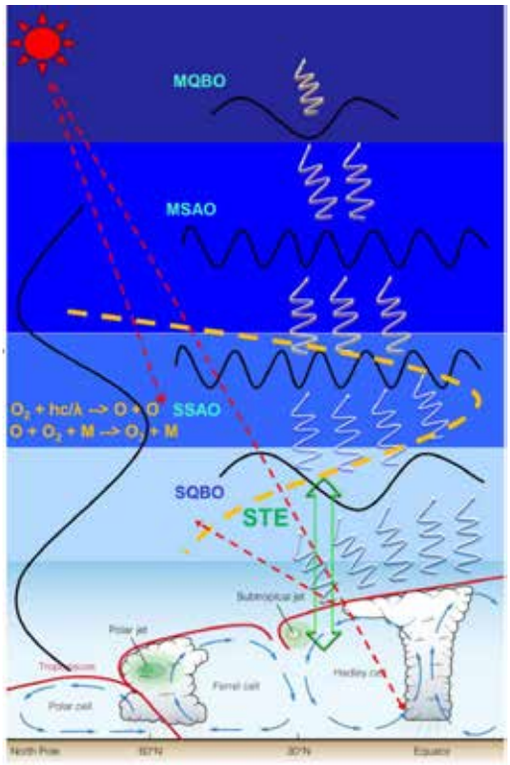

क्षोभमंड़ल से निम्न तापमंड़ल तक ऊर्ध्वाधर युग्मन सहित पृथ्वी के वायुमंड़ल की गति को बदलने के लि ए उत्तरदायी वायुमंड़लीय प्रक्रमणों पर वायुमंडलीयगति की शाखा (एडीबी) अग्रणी अनुसंधान का कार्य कर रही है। इस स्थूल उद्देश्य के साथ अनुसंधान गतिविधि यों का लक्ष्य भू तथा अंतरिक्ष आधारित प्रेक्ष णों का उपयोग करते हुए गुरुत्वीय तरंगों से सौर च्रक तक वायुमंड़लीय तरंगों तथा परिवर्तनी यों के स्पेक्ट्रम का मात्रीकरण करना है। वायुमंड़लीय तरंगों का अभि लक्षणन, उनके स्रोत व क्रियाविधि, संचरण अभि लक्षणन, वायुमंड़ल युग्मन की भूमि का, अल्प व दीर्घकालीन परिवर्तनशीलता तथा वैश्विक नमून में प्रति निधि त्व के आधार पर कि या जाता है। तरंगों और दोलनों पर अध्ययन के अलावा, वायुमंडलीय गतिकी शाखा हवा, तापमान, ओजोन और जल वाष्प के समवर्ती मापनों का उपयोग करते हुए उष्णकटिबंधीय क्षोभमण्डलीय गतिकी और संबंधित समताप मंडल-क्षोभमंडल के बीच होने वाले विनिमय प्रक्रियाओं पर शोध करती है। एडीबी शाखा में बादलों और जलवायु गतिशीलता के क्षेत्र में भी सक्रिय रूप से अध्ययन किया जाता है। हेडली और ब्रेवर-डॉब्सन परिचलन जैसे वृहत पैमाने पर वायुमंडलीय संचार की विशेषता और उनके दीर्घकालिक विकास और जलवायु पर इनके प्रभावों पर जांच जारी है। हाल ही में, शुक्र गृह पर विशेष जोर देने के साथ ग्रहीय वायुमंडलीय गतिशीलता को आगे बढ़ाने के लिए शाखा की गतिविधियों का विस्तार किया गया है।

Atmospheric Dynamics Branch is carrying out the front line research on atmospheric processes responsible for vertical coupling of the Earth's atmosphere, right from the ground to mesosphere-lower thermosphere. With this broad objective, the research activities are aimed at quantifying the atmospheric motion spectra from gravity waves to solar cycle using ground and space based observations and to quantify the various aspects of atmospheric waves such as their source mechanisms, propagation characteristics, role in atmosphere coupling, short and long-term variability and their representation or parameterization in global models. Apart from the studies on waves and oscillations, the branch focuses on the tropical tropopause dynamics and associated stratosphere-troposphere exchange processes making use of simultaneous measurements of wind, temperature, ozone and water vapour. The studies under the realms of cloud and climate dynamics are also actively pursued in the Branch. Large-scale circulations viz., Hadley and Brewer-Dobson Circulations are characterised and their long-term evolution and its impacts on climate are investigated. Recently, the Branch's horizon is extended to pursue Planetary Atmospheric Dynamics with special emphasis on the Venus.

वैज्ञानिक टीम / Science Team
किशोर कुमार के. / Kishore Kumar K.
सिद्धार्थ शंकर दास / Siddarth Shankar Das
सुनिलकुमार एस. वी. / Sunilkumar S. V.
प्रिजित एस. एस. / Prijith S. S.*
जयदेव प्रदीप / Jayadev Pradeep
कौशिक एन. / Koushik N. #
सच्चिन प्रभाकर / Sachin Prabhakar

तकनीकी टीम / Technical Team
मणिकंठन नायर एन. / Manikantan Nair N.
मोहम्मद नज़ीर एम. / Mohammad Nazeer M.
पोन्निसै पेरुमाल जे. / Ponnisai Perumal J.

अनुसंधान अध्येता / Research Fellows
अंजना यू. / Anjana U.
वीनस वी. / Veenus V.
नबारुण पोड्डार / Nabarun Poddar
सनोज एस. एस. / Sanoj S.S.

* *Moved to ATRF in January 2023*
\# *Joined in January 2023*

Mesospheric Dynamics

Investigation on the anomalous weakening of diurnal tides in the mesosphere-lower thermosphere

The present study examines the short-term variabilities in diurnal tidal characteristics, using one decade (2006-2015) of wind measurements in the Mesosphere-Lower Thermosphere (MLT) region over a near equatorial location, Thumba (8.5°N, 77°E). Fig. 1a shows deseasonalized perturbations of monthly mean diurnal tidal amplitude in meridional winds at different altitudes in the MLT region, during the period from February 2006 to December 2015. Two distinct events of anomalous tidal weakening are observed during the years 2010 and 2012. In February 2010, the observed reduction in diurnal tidal amplitude ranges from 16-38 ms^{-1}, as the altitude level increases from 82-98 km as depicted in Fig. 1b. In 2012, a maximum reduction of ~17 ms^{-1} is seen in the month of January at 98 km. However, tidal weakening at lower altitudes, from 82 to 91 km, is observed to be stronger in February, compared to that in January. In February 2012, reduction in tidal amplitude is seen to be as high as ~-16 ms^{-1}, (Fig. 1c).

These events are observed to be coinciding with the occurrence of strong quasi-two-day wave (QTDW). Fig. 2a shows Fourier spectrum of meridional winds at 91 km, during the period from February 2006 to December 2015. The figure shows prominent periodicity of 24 hr throughout the study period, indicating the dominance of diurnal tide. During the periods of anomalous tidal weakening in January - February in 2010 and 2012, occurrence of strong QTDW events can be noticed. Two yellow colour ovals in the figure highlight QTDW amplitudes during the tidal weakening events. In a decade of QTDW observations, depicted in Fig. 2a, their amplitudes are relatively very high during these two episodes. Figs. 2b and 2c show enhanced view of the periodicities during the anomalous events, which emphatically depict time evolution of QTDW activity in the MLT region.

To identify the processes leading to the weakening of the diurnal tides in the MLT region, no-liner wave-wave interactions as well as parametric excitation mechanisms are investigated. The causative mechanisms are found to be different for both the events. While the 2010 event is primarily due to parametric excitation of phase locked two-day waves by diurnal tide, the 2012 event is mainly due to non-linear interaction between tide and QTDW and subsequent generation of secondary waves. These anomalous changes in tidal characteristics would have significant impacts on ionospheric processes. The significance of this study lies in providing observational evidence for the existence of different pathways through which QTDW affects tidal amplitudes over the low-latitude MLT region.

Multi-peak vertical structure of quasi-two-day waves in the MLT region

The QTDW is reported to be the manifestation of westward propagating normal mode of Rossby-gravity wave with zonal wave number 3. Amplitude and vertical structure of QTDW in the MLT region assume importance, because of the role of QTDW in vertical transport of energy and momentum and coupling between lower atmosphere and ionosphere regions. Though QTDW manifests in several

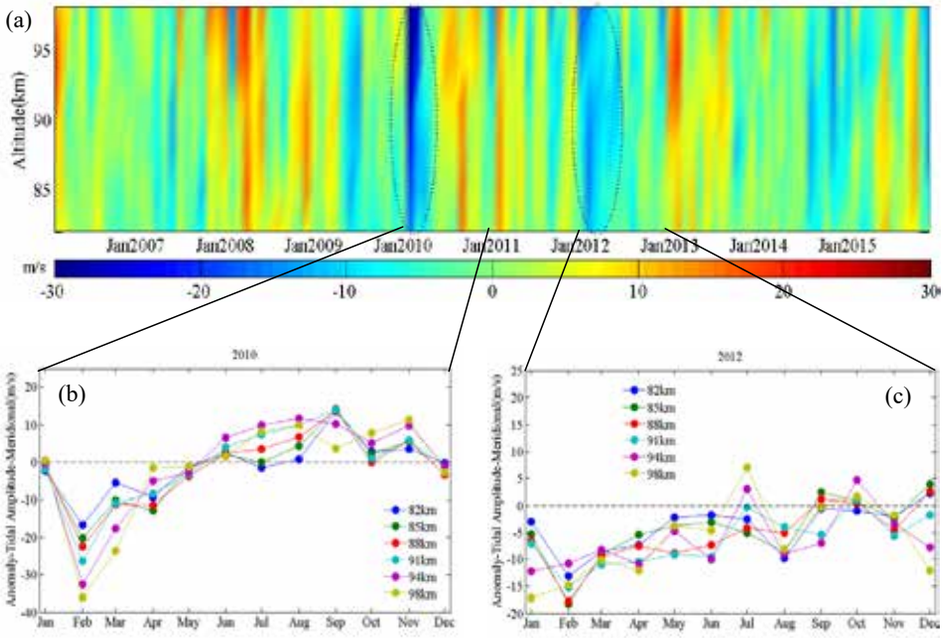

Figure 1.(a) Deseasonalized perturbations of monthly mean diurnal tidal amplitude in meridional winds at different altitudes in the MLT region over Thumba, during the period from February 2006 to December 2015. (b) and (c) show the monthly mean anomaly in the years of 2010 and 2012, respectively [Prijith and Kumar, J. Geophys. Res.: Space Physics, 2023].

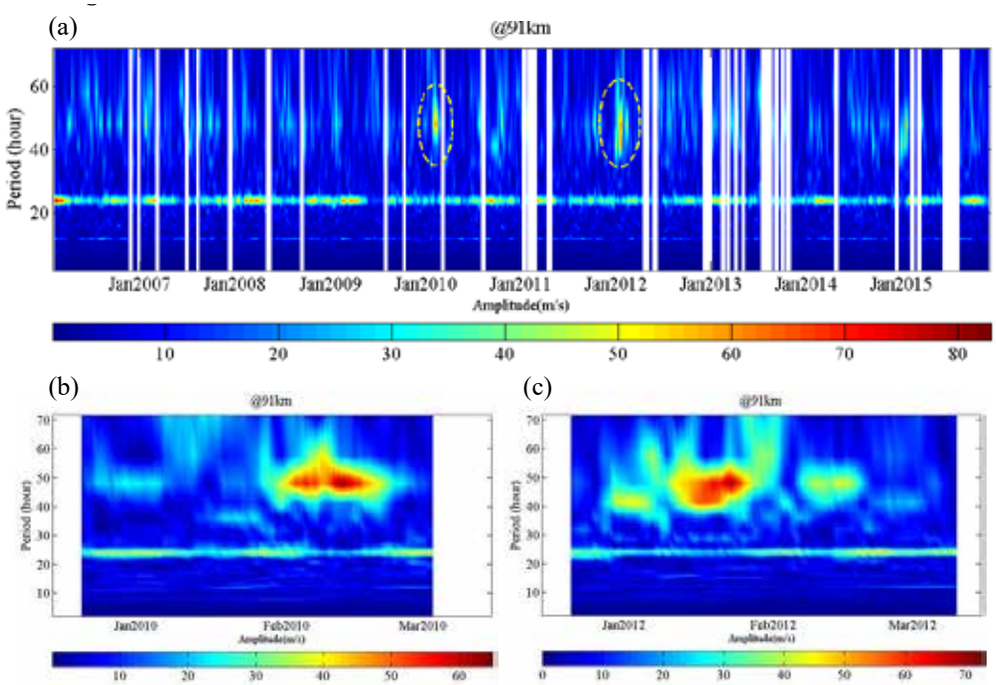

Figure 2. (a) Fourier spectra of meridional winds at 91 km during February 2006 to December 2015. Fourier analysis is carried out by considering a moving window of 12 days. Linear interpolation of wind data is carried out if the gap in hourly data set is for less than 2 days. (b) and (c) are same as (a), but show the spectra during the periods of the anomalous events [Prijith and Kumar, J. Geophys. Res.: Space Physics, 2023].

modes with different wave numbers, in westward and eastward directions, westward propagating mode with wave number 3 (QTDW-W3) in summertime southern hemisphere is the strongest among all of them. The present study examines vertical structure of QTDW-W3 in southern hemisphere in Austral summer and the formation mechanisms. The study has been carried out using kinetic temperature measurements from Sounding of Atmosphere using Broadband Emission Radiometry (SABER) and wind measurements from Timed Doppler Imager (TIDI) onboard the Thermosphere Ionosphere Mesosphere Energetics and Dynamics (TIMED) satellite, for a period of 20 years from 2002 to 2022.

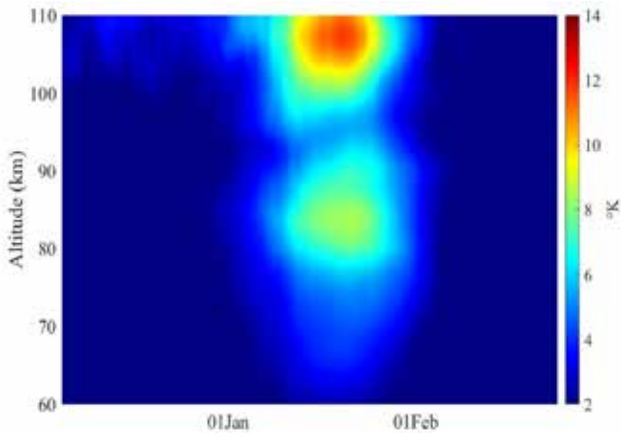

Figure 3: Mean vertical structure of QTDW-W3 over the latitude band between 50 °S - 20 °S in austral summer during the period from 2002-03 to 2021-22 [Prijith and Kumar, Earth, Planet and Space, 2023].

Characteristics of QTDW are extracted by asynoptic spectral analysis, with least square best fitting method. The analysis shows a multi-peak vertical structure of QTDW-W3 in the MLT region of southern hemisphere mid-latitude in austral summer as shown in Fig. 3, which depicts vertical structure of QTDW-W3 in austral summer over the latitude band between 50°S-20°S, averaged for a period of 20 years from 2002-03 to 2021-22. Upper prominent peak is observed at an altitude of 108 km, with QTDW-W3 amplitude 11.24±2.2K, whereas the lower prominent peak is observed at 84 km, with W3 amplitude 8.66±1.1K. Formation mechanism of this double peak vertical structure of QTDW-W3 has been investigated further, by examining the changes in wind and temperature fields at different altitudes in the MLT region. Regions of the upper and lower prominent peaks experience weak eastward/westward winds, which are favourable for the strengthening and vertical growth of QTDW. However, altitude regions between these two peaks experience strong eastward winds, which cause weakening of QTDW-W3. These vertical changes in amplitudes and direction of zonal winds are significantly affected by the meridional temperature gradient and gravity wave filtering in this region. Thus, the vertically alternating structure of zonal winds and meridional temperature gradient provide favourable and unfavourable conditions for the growth and vertical propagation of QTDW-W3 at different altitude levels in the MLT region and hence lead to the formation of a multi-peak vertical structure.

Long-term variabilities in Thermal Structure, CO_2 Concentration and associated Cooling Rates in the Earth's Middle Atmosphere: Observations and Model Simulations

Long-term variations of temperature, CO_2 concentration and associated cooling rates in the middle and upper atmosphere (30-110 km) are investigated using SABER on board TIMED satellite observations during 2002-2021 and Specified Dynamics-Whole Atmosphere Community Climate Model (SD-WACCM) simulations during 2002-2017 over 50 °N-50 °S latitudes.

The trends are estimated by constructing the time series of annual mean temperature from SABER and WACCM and are depicted in Figs. 4a and 4d, respectively. In SABER, the annual mean temperature is showing decreasing trends of the order of ~0.5-2.5 K/decade in all the latitudes and ~2-3 K/decade in the 90-100 km altitudes over mid latitude of Southern and Northern Hemisphere except in the altitude range of ~75-80 km over tropical region where a decreasing trend of ~0.15 K/decade is noted. WACCM simulations also show a significant cooling trend of ~1-1.6 K/decade in the altitude range of 45-100 km. Overall, SABER observed cooling trends are well captured by WACCM except above 100 km. Annual mean relative trend (%/decade) in CO_2 from SABER and WACCM as a function of altitude and latitude is shown in Figs. 4b and 4e, respectively. SABER observations show increasing trends throughout the middle atmosphere with relative trend of 4.5-4.7 %/decade in the altitude 40-90 km altitude (a rate of ~18ppmv/decade in 40-65km altitude region and ~16-15 ppmv/decade in 65-90km altitude). An increasing trend of 5-7 %/decade (7-14 ppmv/decade) is observed above 95 km. The WACCM simulations also show increasing trends throughout the middle atmosphere up to 110 km with relatively weaker trends as compared to SABER observations. Thus WACCM could not capture the magnitude of increasing trends in CO_2 in the middle atmosphere. Figs. 4c and 4f show annual mean trend of CO_2 cooling rate from SABER and WACCM, respectively. It is clear that there exist a large discrepancy between observations and model simulations above 80 km altitude.

From Fig. 4a it can be noted that temperature trends in 75-80 km altitude region over the equator show a decreasing trend with amplitude is less than 0.2 K/day/decade. In order to investigate this feature further, the annual cycle of trends at ~78 km altitude is estimated. Figs. 5a and 5d show the annual cycle of trends in temperature as a function of latitude from SABER and WACCM, respectively. Over the equatorial region (10 °S-10 °N), the decreasing trends are noted with magnitudes of 0.2-0.3 K/decade during all months. However, WACCM shows decreasing trends of 1.3-1.9 K/decade over this region during all the seasons. Figs. 5b and 5e depict annual cycle of trends in CO_2 concentration from observations and model simulations, respectively. The annual cycle in observations shows increasing trends throughout all the latitudes at a rate of 16-18 ppmv/decade whereas model simulations show an increasing trend at the rate of ~3-5 ppmv/decade. The model largely underestimates the CO_2 increasing trends. Similarly, Figs. 5c and 5f shows annual cycle of trends in CO_2 cooling rate from observations and model, respectively. The significance of the present study lies in evaluating the SD-WACCM simulations of long-term variabilities in the thermal structure, CO_2 vmr and associated cooling rates using two decades of observations.

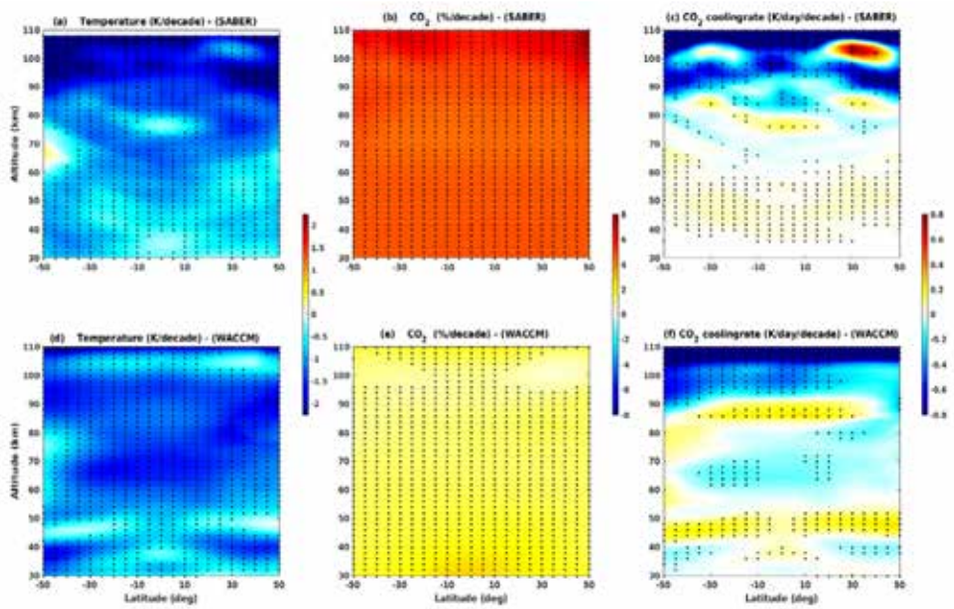

Figure 4. Latitude-altitude section of long-term trends in (a) temperature, (b) CO_2 mixing ratio and (c) CO_2 cooling rate estimated from SABER measurements. Figures (d) - (f) are same as (a)-(c) but estimated from SD-WACCM simulations. The black dots represent the trends with 95% confidence level [Pramitha et al., J. Atmos. Sol. Terres. Phys., 2023].

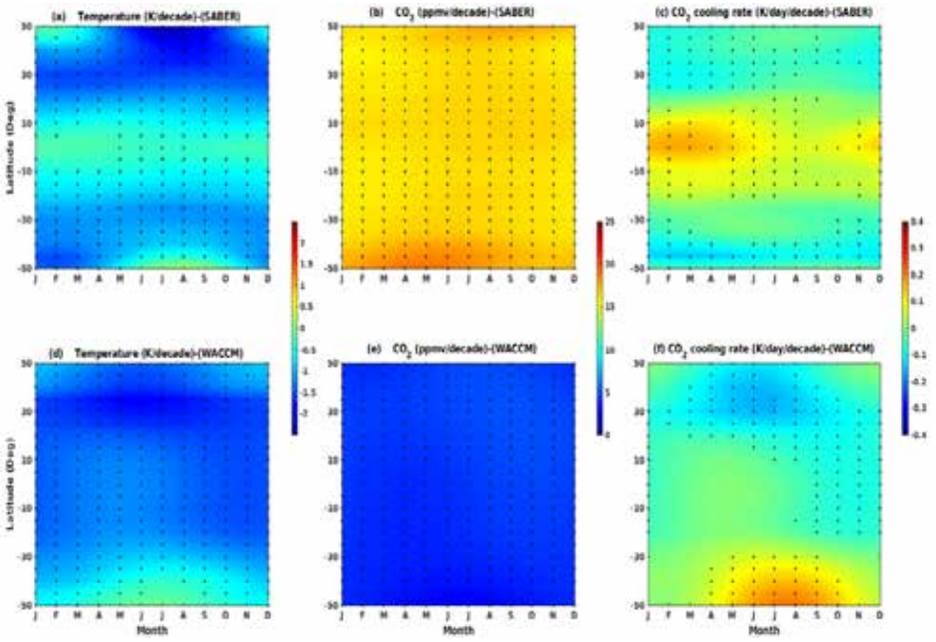

Figure 5. Latitude-month section of long-term trends in (a) temperature, (b) CO_2 mixing ratio and (c) CO_2 cooling rate at 78 km altitude estimated from SABER measurements. Figures (d)-(f) are same as (a)-(c) but estimated from SD-WACCM simulations [Pramitha et al., J. Atmos. Sol. Terres. Phys., 2023].

A Lagrangian Study of Tidal Advection of Mesospheric Water Vapor

Previous studies have demonstrated that the diurnal variability of mesospheric water vapor involves a non-linear interplay between dynamics, photochemistry, and catalytic processes. The inherent difficulty in measurement of winds and water vapor in this region makes the study of mesospheric water vapor complex. We studied the sources of diurnal variability of mesospheric water vapor with the help of the specified dynamics configuration of the Whole Atmosphere Community Climate Model (WACCM) with thermosphere-ionosphere eXtension (SD-WACCM-X) for typical equinox conditions during the solar minimum year 2009. Special emphasis was given to the advective transport by the migrating diurnal tide with wave number 1 (DW1) and its impact on the mean water vapor in the mesosphere. To isolate the contribution from advective and non-advective processes, a Lagrangian parcel trajectory model was employed. Trajectories were launched from a 5◦ × 5◦ × 2.5 km (longitude × latitude × altitude) grid with an integration time step of 15 min. Fig. 6a shows an example trajectory (in the LST frame) for DW1 that was launched at 0◦ longitude, 25◦ N latitude and 75 km altitude on 15 March 2009, 0 hr local time. The air parcel trajectory never returns to its initial position, which implies the net transport induced by the tides. This demonstrates the fact that tides do not just cause simple harmonic oscillation of air parcels but induce a net transport through Stoke's drift. Fig. 6b shows the latitude-height structure of DW1 trajectories for

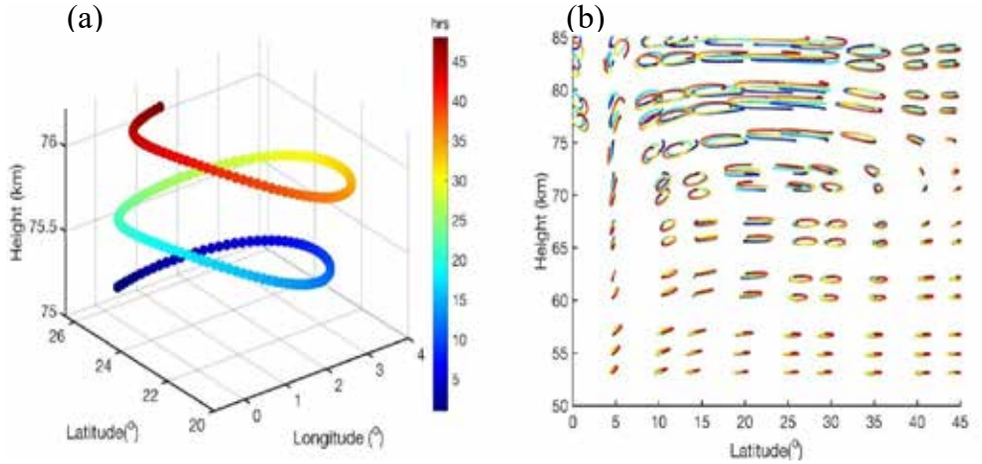

Figure 6. (a) DW1 trajectory for 15 March 2009 launched at 0°E, 25°N, 75 km and 0 hr local time, plotted over 48 hr. (b) Latitude-height section of DW1 trajectories launched every 5° × 2.5 km at 0 hr local time on 15 March 2009. Colour codes in (a) and (b) indicate time evolution from 0 to 48 hr [Koushik et al., J. Geophys. Res. : Atmosphere, 2023].

the same day launched every 5◦ × 2.5 km. The vertical and horizontal parcel displacements depend on the latitude and height. The parcel displacements are nearly vertical in low latitudes where DW1 amplitudes in vertical winds are the strongest. In the upper mesosphere over midlatitudes, the parcel trajectories are nearly horizontal.

After the trajectory analysis, the water vapor mixing ratio along each trajectory is computed to further estimate the tidally advected mixing ratio change (δq). Fig. 7a shows the total advected water vapor for 6 hr local time using the trajectories from Fig. 6b and background water vapor from SD-WACCM-X for 15 March 2009. By artificially setting the horizontal (vertical) tidal winds to zero, one can also calculate the advected water vapor due to vertical (horizontal) tidal advection alone. These quantities are depicted in Figs. 7b and 7c respectively. It can be inferred that the water vapor advection (mainly in the low latitudes) is dominated by vertical tidal advection primarily above 70 km. The horizontal advection is weaker compared to the vertical counterpart above 70 km. Nevertheless, it marginally dominates over the vertical advection below 70 km.

Stratosphere-Troposphere Interactions

Ozone changes due to sudden stratospheric warming-induced variations in Brewer-Dobson Circulation: A composite analysis using observations and chemical-transport model

The changes in the intensity of Brewer-Dobson Circulation (BDC) during sudden stratospheric warming (SSW) and its impact on the tropical thermal structure and ozone distribution was studied using improved reanalysis products, satellite observations, in-situ measurements, and a chemical transport model. BDC undergoes sub-seasonal variations during SSWs. During SSW, the planetary wave activity and changing zonal wind direction in the stratosphere alter the intensity of the circulation. The composite profiles of BDC strength and ozone distributions were generated for major and minor SSW events along with quiet period from 2005 to 2020 using super-epoch analysis. Different BDC metrics, i.e., Eliassen-Palm flux, Residual Mean Meridional Stream Function, residual vertical velocity, and Diabetic heating rate were computed using ERA5 reanalysis products. An enhanced wave driving before the central date was observed from the Eliassen-Palm flux divergence which acts as a proxy for the wave-driven torque (Fig. 8). A strengthened circulation is observed from diabatic heating rate around the central date of SSW. The residual mean meridional stream function showed abrupt decrease after the central date and a decreased latitudinal extent after the peak of SSW. The abrupt decrease in BDC strength was evident in major warming but a gradual change was observed during minor SSWs, which could be attributed to wind reversal in major SSW which is absent in minor SSWs.

The observations from Aura Microwave Limb Sounder, in-situ ozonesonde measurements from India Meteorological Department, and the GEOS-Chem model output were used for analysing the variations in stratospheric temperature and ozone following the changes in BDC. Over the tropical stratosphere a cooling of 2-3 K was observed for major warming (Fig. 9).

The downwelling raised the temperature to 30 K during major warming over the Polar region. The Polar upper stratosphere ozone is depleted by the NOx rich air intrusion from the mesosphere. The ozone mixing ratio shows an increase of ~0.3 ppmv in the tropical upper stratosphere, which is attributed to the reduced reaction rate of nitrogen-cycle in response to the reduction in temperature. The tropical lower stratosphere shows a region of ozone depletion which resulted from the transport by BDC to higher latitudes. For minor SSWs, the anomalies in ozone are much lower in magnitude. The GEOS-Chem model also reproduces the pattern but differ in magnitudes. The patterns in the BDC metrics as well as the ozone and temperature enhancements is reproduced when the ERA5 reanalysis products were used from 1979 to 2020. During the SSW lifespan, the tropopause height was raised by the increased upwelling, causing the tropopause temperature to cool after ~10 days from the central date of SSW. The decrease in temperature affects the freeze-drying mechanism and results in less transport from the troposphere to stratosphere. When the concentration of ozone, which also balances the tropopause temperature, is altered by

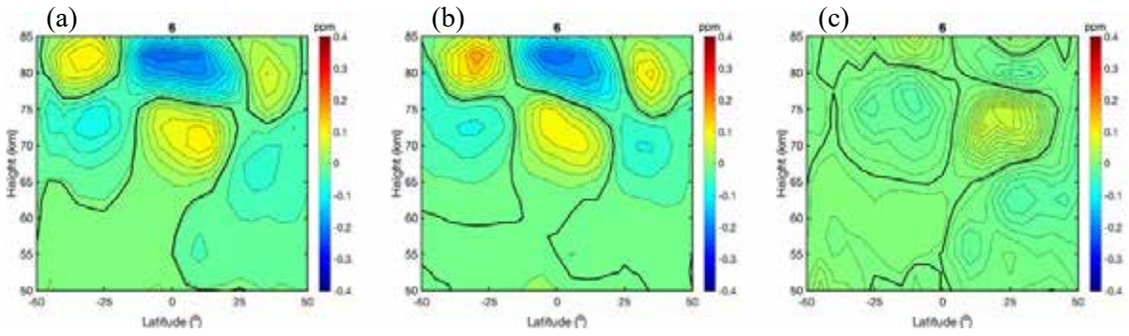

Figure 7. DW1 advected H_2O volume mixing ratio for 6 hr local time on 15 March 2009 for (a) total advection (b) vertical advection alone and (c) horizontal advection alone [Koushik et al J. Geophys. Res.: Atmosphere, 2023].

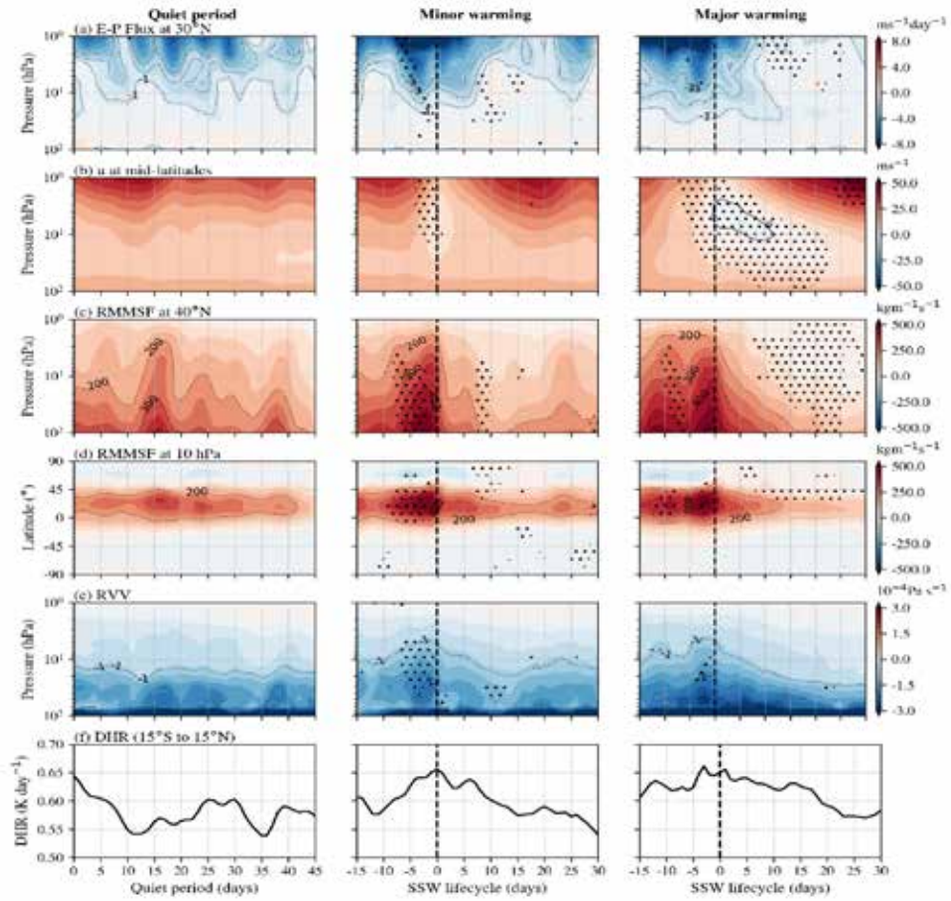

Figure 8.(a) Eliassen-Palm (EP) flux divergence at 30 °N, (b) zonal-mean zonal wind (u) at mid-latitude (averaged between 32.5 °N to 62.5°N), (c), residual mean meridional stream function (RMMSF) at 40°N (d) and its latitudinal distribution at 10 hPa, and (e) residual vertical velocity (averaged between 15.0 °S to 15.0 °N, RVV), (f) diabatic heating rate (DHR) (see text for more details). The vertical dashed line denotes the central date of SSW during minor and major warming events. Statistically significant changes with >90% confidence level is indicated by the black dots [Veenus et al., Geophys. Res., Lett., 2023].

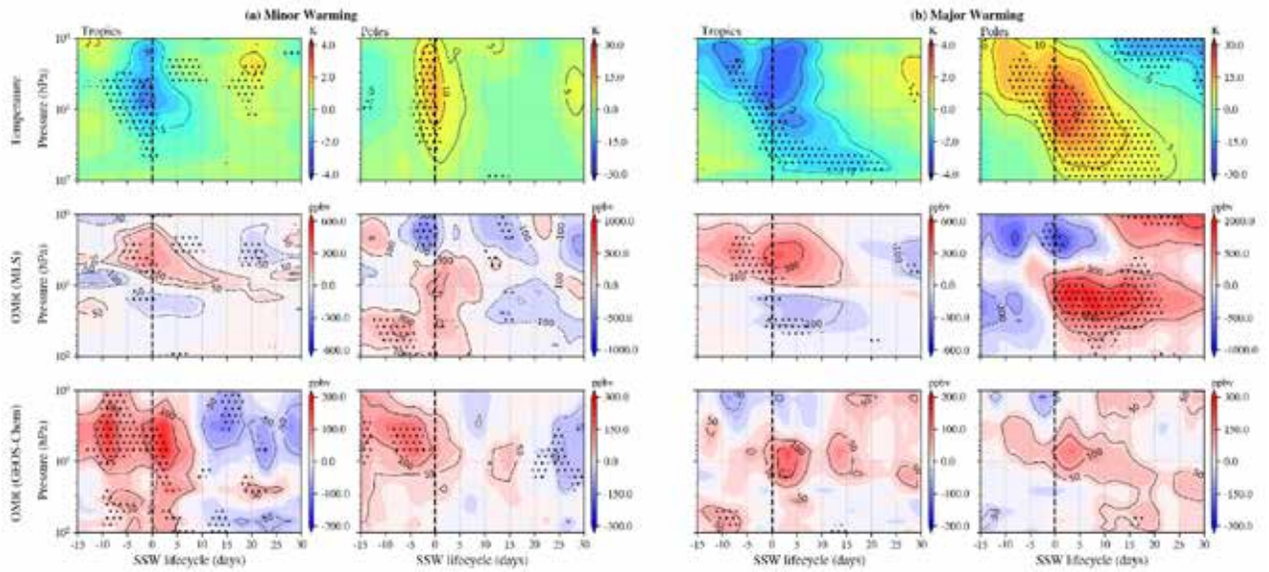

Figure 9.The zonal-mean thermal structure and ozone mixing ratio (OMR) for the (a) minor, and (b) major warmings over tropics (averaged between 12.5°N to 12.5°S) (left), and poles (averaged between 62.5°N to 87.5°N) (right). The temperature and OMR in the top two panels are measured from Aura MLS and the bottom panel shows the OMR from the GEOS-Chem model. The vertical dashed line denotes the central date of SSW. The black dots indicate statistically significant changes with >90% confidence level [Veenus et al., Geophys. Res., Lett., 2023].

SSW-induced changes in BDC, a dry stratosphere is also observed. The changes in stratospheric minor composition have a vital impact on the stratospheric chemistry which finally results in altering the global radiation budget.

Effect of synoptic-scale dynamics on the vertical distribution of tropospheric ozone over the Arabian Sea and the Indian Ocean during the boreal winter of 2018

The influence of synoptic scale dynamics on the vertical distribution of ozone in the troposphere is examined over the Arabian Sea (AS) and the Indian Ocean (IO) during 16 January to 14 February 2018 using ECC ozonesonde-radiosonde observations during ICARB-2018 ship cruise. The vertical distribution of ozone shows distinct characteristics of the prevailing meteorology and dynamics during the leg-1 (fair weather), leg-2 (near to ITCZ) and leg-3 (western disturbance/convectively disturbed) of the ship cruise. Tropospheric ozone exhibits pronounced latitudinal variation with distinct plume-like structures around 1-3 km and 4-5 km altitude regions over the AS and IO during leg-1 period (16-24 January 2018) of the cruise. High ozone values (~60-70 ppbv) are observed above the marine boundary layer (MBL) near to the Indian landmass which decrease to ~20 ppbv at equator (Fig. 10). The ozone-rich plume around 1-3 km is caused by the transport of polluted air masses from Indian sub-continent. Low ozone (< 20 ppbv) and high RH (> 80%) values are observed at the ascending limb of the Hadley circulation and high ozone (> 40 ppbv) low RH (<30 %) are observed at the descending limb. The mid-tropospheric high ozone-low water vapour (HOLW) layer observed around 4-5 km is hypothesised to be associated with the equatorward return flow of the Hadley circulation. On the other hand, tropospheric ozone over the equatorial IO remains nearly at uniform concentrations (about 10-20 ppbv) without any discernible longitude variation during leg-2 period (25-31 January 2018) of the cruise. The ozone distribution in the tropical tropopause layer (~12 km to CPT) shows distinct structures associated with the prevailing synoptic scale dynamics and long-range transport during the respective legs. The ozone rich transition region (~20 ppbv around 15 km to ~100 ppbv at CPT) bound by the double tropopause like structure during leg-1 (over AS and equatorial IO) is maintained by the upper tropospheric inversion (UTI) at the base (~14 km) and the subsidence associated with an anticyclonic system (with its core to the northwest over the Pacific) at the tropopause level. Further, the observed ozone enhancement (> 40 ppbv) above the TTL-base near the ITCZ is attributed to the subsidence of ozone-rich air from higher altitudes associated with the deep convective updrafts of ITCZ. Back trajectory analysis show that long-range transport from biomass burning regions and stratospheric intrusions associated with the western disturbance potentially both contribute to the observed upper tropospheric (around 12-15 km) ozone enhancement of ~50-60 ppbv over AS during leg-3 period (4-9 February 2018) of the cruise.

On the signatures of local and regional dynamics in the distribution of lower stratospheric water vapour over Indian region using balloon-borne and satellite observations

Balloon-borne cryogenic frost-point hygrometer (CFH) observations over two tropical stations Trivandrum (8.53 °N, 76.87 °E) and Hyderabad (17.47 °N, 78.58 °E) [2014-2017] along with Microwave Limb Sounder (MLS) observations [2011-2017] are used to examine the signatures of local and regional dynamics in the distribution of lower stratospheric (LS) water vapour over the Indian region. The annual cycle of lower stratospheric water vapour obtained from CFH observations clearly depicts the tape recorder signal (Fig. 11). This study showed that the tape recorder signal in the lower regime of LS (16-21

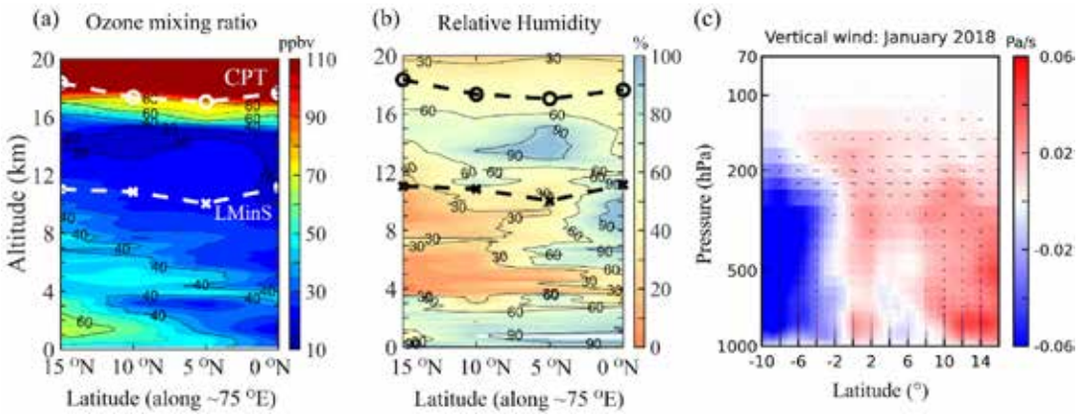

Figure 10. Vertical distribution of ozone mixing ratio and relative humidity from paired ECC ozonesonde and radiosonde measurements during leg-1 period (16th-24th January 2018) of the ship cruise along with the altitude-latitude cross section of mean vertical wind during January 2018 averaged over the longitude band 65-75°E using ERA-interim reanalysis data. The vectors in (c) represent the mean meridional circulation (the meridional wind along x-axis and –100 times vertical wind on the y-axis). The horizontal dashed lines in the sub-plots (a) and (b) represents cold point tropopause (CPT) and convective tropopause (LMinS, the level of minimum stability) heights. Relative humidity above 5 km is calculated with respect to ice [SatheeshChandran et al., J.Geophys. Res.: Atmospheres, 2022].

km) is disturbed by the local /regional dynamics, where as it is mainly controlled by large-scale dynamics (BDC) in the upper regime of LS (21-25 km). The column integrated water vapour in the LS (IWV_{LS}) varies in the range 2.5 to 5 g/m^2 with low values during winter and high values during summer monsoon and post monsoon seasons. About 50-75 % of the IWV_{LS} lies in the lower regime of the LS. The minimum in water vapour, called hygropause, is very near to the cold point tropopause (CPT) in winter and pre-monsoon season and 2-3 km above the CPT in summer-monsoon and post-monsoon season. The CPT temperature shows a negative correlation with the CPT altitude and positive correlation with the water vapour mixing ratio. The minimum in saturation mixing ratio (SMR_{min}) mostly occurs just below the CPT altitude. The values of SMR_{min} are higher than the CPT mixing ratio values indicating that the freeze drying is mainly controlled by the tropopause temperature itself.

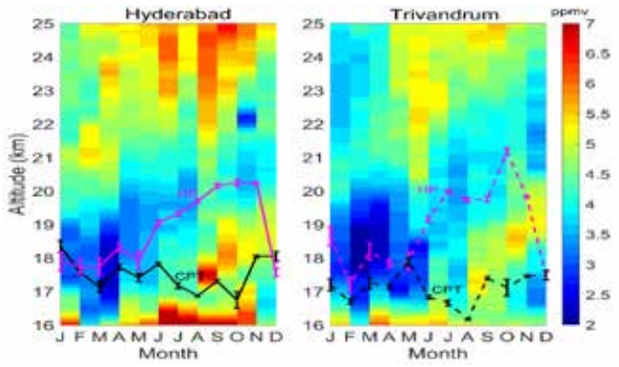

Figure 11. Annual cycle of lower stratospheric water vapour from CFH (in situ) observations during the period 2014-2017 over (a) Hyderabad and (b) Trivandrum. The magenta lines represent the mean annual variation of hygropause and black lines represents mean annual variation of CPT [Emmanuel et al., Clim. Dyn., 2023].

CFH observations shows that amount of water vapour in the lower regime of LS (CPT-21 km) is relatively high over Hyderabad in summer monsoon and winter seasons and over Trivandrum in pre-monsoon and post-monsoon seasons (Fig. 11). The analysis of occurrence of deep convection and temperature histories shows that the potential pathways of air masses reaching at 16 km and 18 km altitudes of the observation sites, Trivandrum and Hyderabad, encounters deep convective outflows with abundance of moisture during summer monsoon season. However, owing to the proximity to deep convective sources over BoB and warmer temperatures experienced along the pathways, more amount of water vapour reaches to the upper troposphere and lower regime of the lower stratosphere over Hyderabad compared to Trivandrum. During the pre-monsoon and post monsoon season, the southern peninsular region experiences deep convection leading to higher amount of water vapour reaching Trivandrum with temperature histories having not much role. In winter, in the absence of deep convection, temperature histories alone determine the amount of water vapour reaching the lower stratosphere over the CFH stations.

The spatial distribution of water vapour from MLS observation indicates that Indian sector is one of the major entry points of water vapour into the lower stratosphere and is closely associated with the prevailing monsoon dynamics and deep convection over this region. The study shows that while the hydration at the tropopause level with water vapour mixing ratio > 6 ppmv is mainly determined by the overshooting/deep convection, monsoon dynamics and horizontal transport, the dehydration effect with values < 3 ppmv could be controlled by large-scale (low) temperature variations and persistence/maintenance of cirrus clouds near the tropopause. The horizontal transport had great role in modulating the lower stratospheric water vapour distribution over the South Asian Region during summer monsoon season.

Aspect sensitivity of VHF radar backscatters in volume scan: First results inferred from the Advanced Indian MST radar (AIR)

With the full azimuthal beam steering capability made available with the upgraded Indian MST radar located at Gadanki known as 'Advance Indian MST Radar (AIR)', it is now possible for full three-dimensional mapping of atmospheric structure in both clear air and extreme weather conditions. In this context, a new experiment was designed and conducted with AIR, and studied the echo power distribution pattern from 1.5 to 21 km as a function of both zenith (0-20°) and azimuth (0-360°) angles. This is the first experiment where the full capability of AIR was utilized to get the three-dimensional mapping of aspect sensitivity.

The experiments were designed by the optimum selection of zenith and azimuth beams, which will have a full volume scan within 5.5 min. Fig. 12a shows the related beam configurations and layout with a range resolution of 150 m. Figs. 12b-12c show the signal-to-noise ratio (SNR) slice maps for two complete volume images at different altitude on 16 April 2018. The radar echoes show isotropic characteristics in the upper troposphere (~17.9 km) and anisotropic structure in the middle troposphere (8-8.9 km). High aspect sensitivity is observed near tropopause and other stratified stable layers (temperature inversion). The presence of stratified stable layers is attributed to the enhanced gradient in potential temperature (Fig. 12d). Fig. 13 shows the scatter plots of aspect sensitivity with (a) wind shear and (b) atmospheric stability for different off-zenith beams above and below 12 km. This shows that a minimum amount of wind shear is required for the observed aspect sensitivity, especially above 12 km. It is also to be noted that the probability of high aspect sensitivity is more when the square of horizontal wind shear is less than 0.25×10^{-3} s^{-2}, and above this wind shear, the target tends to become isotropic, i.e. the received backscattering echoes from zenith and off-zenith remain

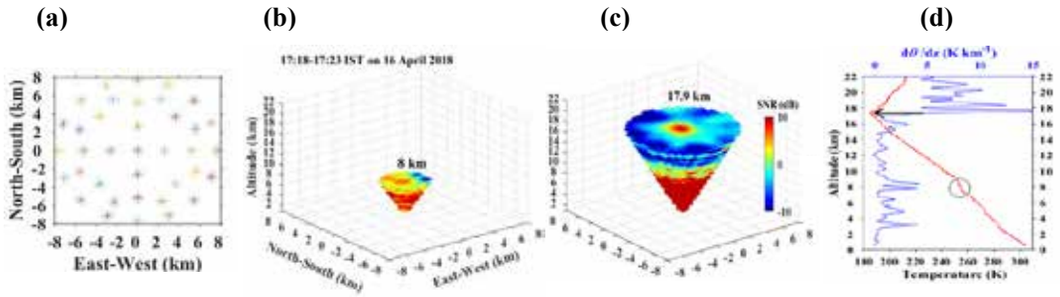

Figure 12.(a) Radar beam configuration, (b)Signal-to-noise ratio (SNR) slice maps of one complete volume, and (c) altitude profiles of temperature and potential temperature gradient [Das et al., International Journal of Remote Sensing, 2022].

equal. The scatters have become isotropic due to turbulent mixing. Aspect sensitivity increases with the enhanced atmospheric stability above 12 km. When the stability parameter is above 0.25 × 10^{-3} s^{-2}, the scatterers become isotropic. Thus, it is concluded that after a certain threshold of enhanced s^2 and N^2, the scatterers become isotropic.

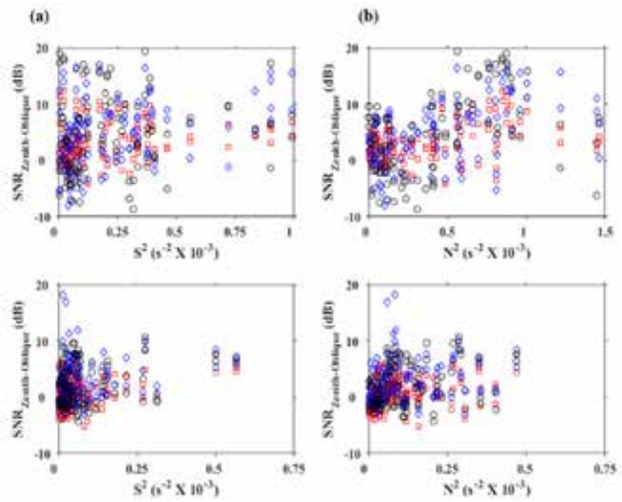

Figure 13. Scatter plots of aspect sensitivity ($SNR_{Zenith-Oblique}$) with (a) wind shear, and (b) atmospheric stability above 12 km (top panels) and below 12 km [bottom panels) (Das et al., International Journal of Remote Sensing, 2022].

The height level where high aspect sensitivity is observed shows more underestimation of winds. Due to the high aspect sensitivity, there may be an underestimate of 5-10% in wind velocity measurements, and it is higher for the low off-zenith beam angle. It is envisaged that the present experiment and results will have an important aspect in designing various experiments with AIR and also in better understanding the dynamical processes taking place in the lower and middle atmosphere.

Climate Dynamics

A Rare Episode of Minor Circulation Embedded in the Northern Hemispheric Zonal Mean Hadley Cell

A rare episode of minor circulation embedded in the Hadley circulation (HC) and processes responsible for its formation was investigated. Using 34 years (1979-2012) of HC climatology derived from reanalysis datasets, a minor circulation centered on ~35 °N and embedded within the northern hemispheric zonal mean HC is observed during July 1993. Fig. 14a shows the zonal mean pressure-latitude section of meridional mass stream function (MSF) for the month of July for the NH latitudes, averaged for the years 1979-2012 estimated from the MERRA reanalysis data. From this figure, it is evident that there is a rising branch of HC over 20 °N and the northern hemispheric HC edge is approximately at 35 °N-40 °N. However, this is not always the case. For instance, Fig. 14b depicts the pressure-latitude section of MSF observed during the month of July 1993. It can be noted from this figure that there exists a minor circulation centered at around 35 °N-40 °N, which is absent in the climatological mean shown in Fig. 14a. There is a narrow region of northward flow at around 40 °N, and another of a southward flow at around 35 °N, which is very evident at the 500 hPa level. The anomalous HC structure is reproduced in the analysis of JRA-55 data also, as shown in Figs. 14c and 14d. Fig.14c depicts the 34-year mean climatology of MSF for the month of July, whereas Fig. 14d depicts the MSF for the July of 1993, both derived from the JRA55 reanalysis dataset.

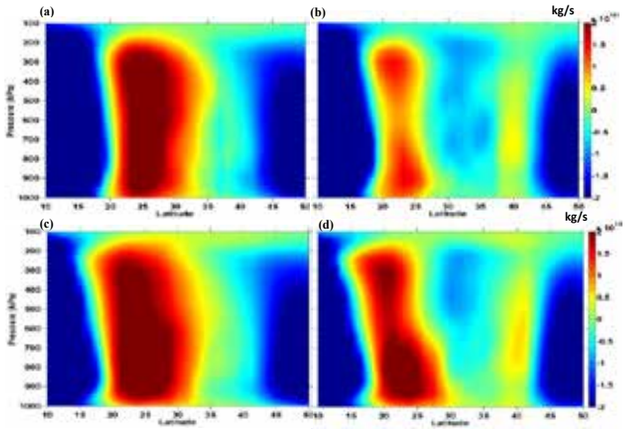

Figure 14. Zonal mean pressure-latitude sections of MSF (a) 34 years mean climatology for the month of July,(b) for July 1993 estimated using MERRA reanalysis. (c) and (d) are same as (a) and (b) respectively but estimated using JRA-55 reanalysis [Anjana et al., J. Atmos. Sol. Terres. Phys., 2023].

Figure 15a shows the 34 years mean pressure-latitude section of vertical velocity during July. The pressure-latitude section of vertical winds during July 1993 is depicted in Fig. 15b. A striking feature of this figure

is the presence of an ascending motion centered on ~35 °N, which is absent in the climatological mean of vertical winds shown in Fig. 15a. From Fig. 15b, it looks as if there are two canters for the HC- one at 20 °N and another at 35 °N. A longitudinally resolved vertical velocity observations centered on 35 °N latitudinal belt revealed that there is an anomalous upwelling over the North American sector possibly associated with "Great Floods of 1993". This analysis thus indicates that the circulation features associated with the Great floods of 1993 during the month of July may be responsible for the observed anomalous features of the HC. The current observation upholds the impact which a prominent localized feature can make on a zonal mean pattern of the HC.

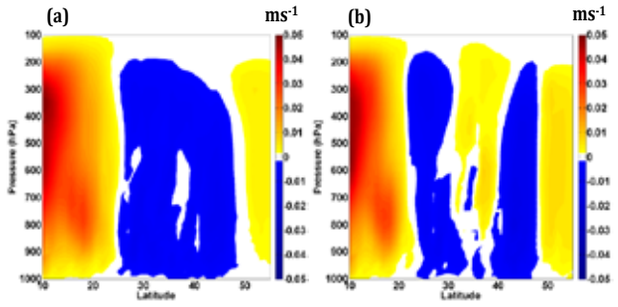

Figure 15. Pressure-latitude section of the vertical winds obtained from MERRA reanalysis averaged for 34 years during the month of July, and (b) for July 1993 [Anjana et al., J. Atmos. Sol. Terres. Phys., 2023].

Hadley Circulation Dynamics in the IITM-Earth System Model Simulations: Evaluation and Future Projections

A study was carried out using climate model simulations from Indian Institute of Tropical Meteorology-Earth System Model (IITM-ESM) archived in the latest Coupled Model Inter-comparison Project 6 (CMIP6) to identify the long term changes and future projections in the width of the ascending and descending branches of the HC, after validating it against the latest generation ERA5 reanalysis. The annual cycle of HC boundaries including its center derived from IITM-ESM model simulations and ERA5 reanalysis are shown in Figure 16. It can be inferred from these figures that the model closely follows the reanalysis during most of the year. However there is considerable difference between the two during certain times of the year, by around 2-5 degrees. The difference between model and reanalysis is pronounced in the annual cycle of northern hemisphere (NH) ascent boundary, where relatively more land regions are present. The most recent CMIP6 models takes into consideration the social and economic dimensions of human development, which changes the emission pathways, thereby leading to certain prescribed radiative forcing levels in 2100. These are known as Shared Socioeconomic Pathways (SSPs). The current study employed IITM-ESM simulations for two high forcing scenarios in CMIP6, viz. SSP370 and SSP585 in order to project the future changes in HC. SSP585 is representative of a technologically advanced society, but at the cost of fossil fuel utilization, which drives the radiative forcing levels to 8.5 W/m^2 by 2100. In SSP370 a society that prioritizes regional rivalry over climate change mitigation policies is represented which pushes the radiative forcing levels to 7W/m^2 by 2100.

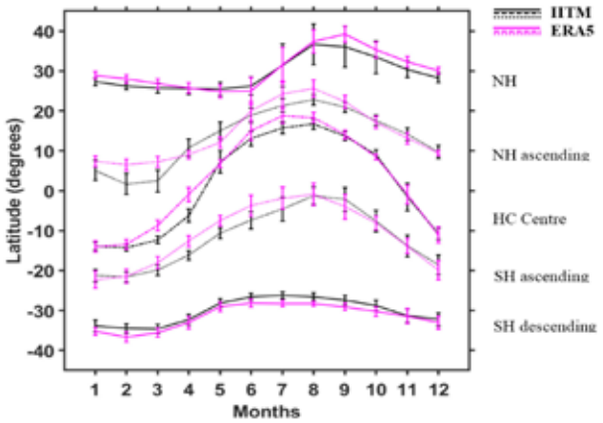

Figure 16. Annual cycle of the HC parameters for 1979-2014 period derived from IITM-ESM and ERA5 datasets. Vertical bars show the interannual variability [Mathew and Kumar, Theo. Appl. Clim., 2023].

The SSP585 forcing scenario shows relatively large expansion of HC edges as compared to SSP370 scenario. In order to bring out the implications of the projected trends in ascending and descending branches of the HC, the changes in precipitation for SSP370 and SSP585 scenario is analysed as shown in Figs. 17a and 17b, respectively. The figure shows annual cycle of precipitation trends (in mm/day/decade) for SSP370 and SSP585 scenario, significant at the 80 % confidence level. The striking feature of this figure is the positive trend in precipitation in the ascending regions and negative trend in the descending region edges in SSP370 scenario. The trends are relatively large and coherent in the SH as compared to NH. Overall it can be inferred from Fig. 17 that the projected trends in precipitation changes for the two future warming scenarios matches well with the trends projected for the width of the HC ascending and descending regions.

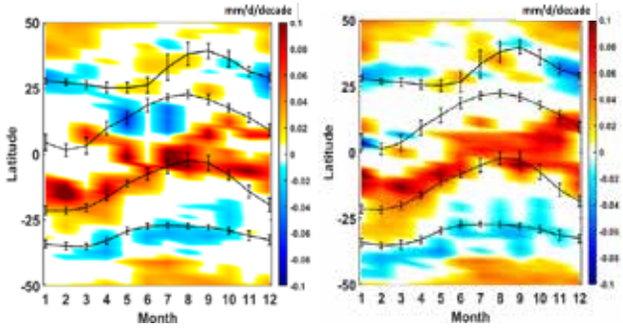

Figure 17. Annual cycle of trends in IITM-ESM zonal mean precipitation for (a) SSP370 scenario and (b) SSP585 scenario. The shaded regions are the precipitation trends significant at 80% confidence level. Solid black lines indicate HC descending region edges and dashed black lines indicate HC ascending region edges [Mathew and Kumar, Theo. Appl. Clim., 2023].

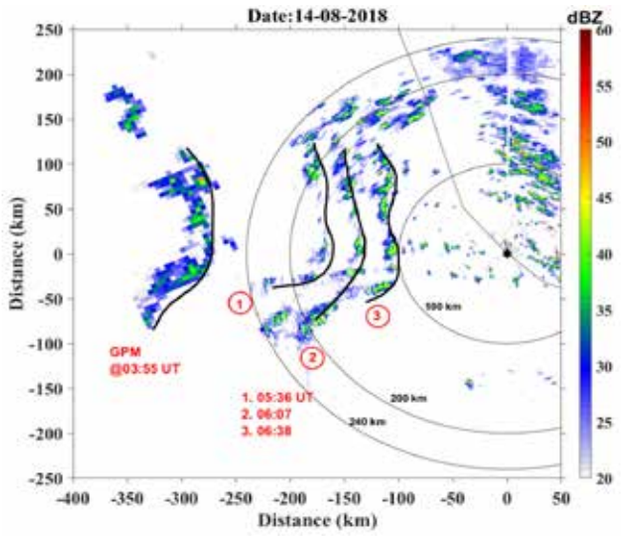

Figure 18. The spatial distribution of radar reflectivity observed by GPM (at 2km height) and C-band DWR at 2° elevation on 14th August 2018. The black star symbol represents the location of DWR [Subrahmanyam and Kumar, Atmos. Res., 2023]

Cloud Dynamics

Structure and Evolution of Organized Precipitation Bands: C-band Doppler Weather Radar Observations over Thumba (8.5 °N, 77 °E)

The C-band polarimetric Doppler Weather Radar (C-DWR) observations are used to investigate the structure and evolution of organized precipitation bands during the Indian summer monsoon (ISM) of 2017-2019 over Thumba, a coastal location in south India. The C-DWR observations show organised high radar reflectivity structures of ~50 dBZ that organised into narrow bands of ~200 km (North-South) in length and 10-20 km (East-West) in width with vertical extent of ~6-8 km. These narrow bands of precipitation structures are observed to be formed over the Arabian Sea and subsequently propagating towards the radar site as shown in Fig. 18. This figure illustrates the observed precipitation bands in the C-DWR observations as well as KU-band radar on board Global Precipitation Monitor (GPM). From this figure, a precipitation band can be noted from GPM observations at 03:55 UT around 350 km west of the radar location. At this time, the band structure is not seen by the DWR, which is out of its range coverage. After ~90 minutes of GPM observations, the banded precipitating system moved towards radar site and its propagation is well captured by the radar as shown in the figure.

Figure 19a-c shows the wind speed at 850 hPa derived from ERA-5 reanalysis dataset on 1 June 2017 at 18UT, 12 August 2018 at 16 UT and 14 September 2019 at 5UT, respectively. From these figures it is evident that there exists a low-level jet with peak wind speed of the order of ~20 m/s over the western Arabian Sea. One can notice the gradual decrease in the wind speed as it approaches the eastern Arabian Sea especially near to the coast. A

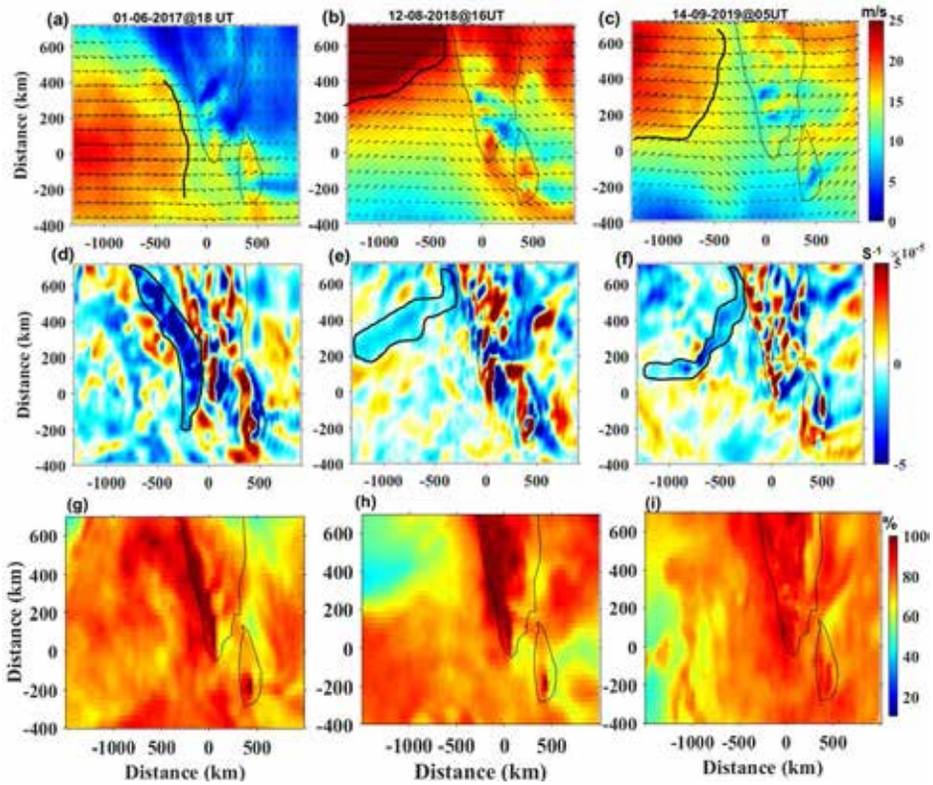

Figure 19. (a-c) Wind speed, (d-f) divergence and (g-i) Relative humidity at 850 hPa on 1 June 2017 at 18 UT, 12 August 2018 at 16 UT and 14 September 2019 at 5UT respectively. Solid black line represents the locations of maximum gradient in wind speed and black contour indicates the convergence (i.e., negative divergence values) [Subrahmanyam and Kumar, Atmos. Res., 2023].

manually drawn black line represents the region of drastic deceleration of the wind. It is known that the low-level jet will be decelerated after interacting with the Western Ghats and a physical process known as upstream blocking takes place at the off-shore. This is the region where convergence of winds can be expected. In order to verify this aspect, the divergence/convergence fields obtained from the ERA-5 are depicted in Figs. 19d-f. It is very interesting to note the elongated structure of convergence field parallel to the Western Ghats on the off-shore. Figs. 19g-i depicts the relative humidity at 850 hPa level derived from ERA-5 reanalysis datasets for three days on which precipitation bands are observed.

The results depicted in Fig. 19 thus provide an evidence for the upstream blocking mechanism for the formation of organized precipitation bands. The observed bands are perpendicular to the low-level jet stream and are carried by the prevailing winds towards the coast.

Characterization of Deep Convective Cells during the Indian summer monsoon using C-band polarimetric Doppler Weather Radar observations over Thumba (8.5 ^{o}N, 77 ^{o}E)

The present study focuses on characterizing deep convective cells (DCC) over a coastal location Thumba during the ISM periods of 2017-2019 using C-DWR measurements in terms of their intensity, vertical extent, top heights and their microphysical properties. A method is devised to identify the DCC from the DWR observed reflectivity cross-sections. Fig. 20 depicts a range height indicator (RHI) of radar reflectivity on 2 June 2017 at 1049 UT. The cross section shown in the inset depicts the horizontal structure of radar reflectivity at 3 degree elevation. The RHI corresponds to the solid black line shown in the inset. The rectangular black box highlights the DCC portion of the convective system, whose echo tops

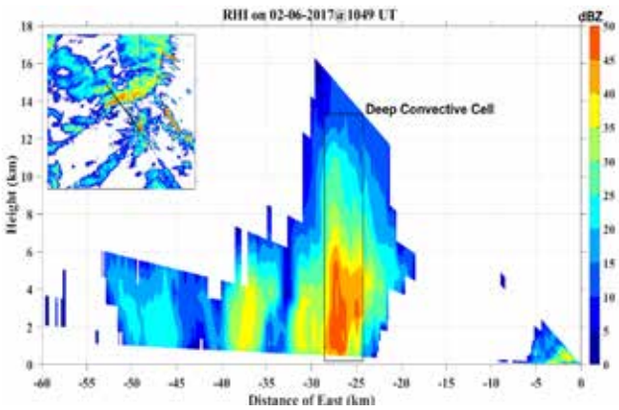

Figure 20. A typical range height indicator of radar reflectivity corresponding to black solid line shown in the inset. The cross section shown in the inset depicts the horizontal structure of radar reflectivity at 3 degree elevation on 2nd June at 1049 UT. The rectangular box shown in the figure highlights the DCC [Subrahmanyam and Kumar, Remote Sensing Applications: Society and Environment, 2023].

are reaching as high as 14 km. The number of occurrence of DCC are investigated during study period. We have followed a widely employed methodology for identifying the DCC profiles from C-DWR observations.

The results showed that the occurrence of reflectivities in the range of 25-35 dBZ dominates below 6 km and the reflectivities in the range of 10-20 dBZ dominates above 6 km. The diurnal evolution of 40 dBZ depth radar echoes in DCC were analysed for June-September months, which showed peaks at preferential timings. The mean diurnal evolution of DCC also been investigated and it is found that these systems peak at three local time intervals viz., 00-05, 13-16 and 19-23 hrs during ISM period as shown in Fig. 21. The present results provide a quantitative assessment of DCC including their diurnal evolution during the Indian summer monsoon season over Thumba using DWR observations.

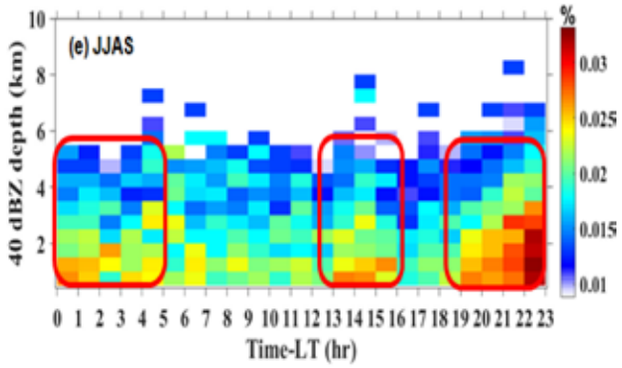

Figure 21. Diurnal evolution of 40 dBZ depth observed by C-band DWR during ISM period over Thumba [Subrahmanyam and Kumar, Remote Sensing Applications: Society and Environment, 2023].

Planetary Atmospheric Dynamics

3D Simulations for Solar Occultation Experiments (SOE) in the Venusian Atmosphere: Effect of Spacecraft Orbital Parameters

Solar occultation is a versatile technique for high-resolution vertical profiling of planetary atmospheres from satellite-borne platforms. Owing to the distinctive observational geometry, the deduction of the spatio-temporal coverage of solar occultation measurements as a function of the spacecraft orbit is non-trivial and involved. In this regard, 3D orbital simulations were implemented to visualize the occultation-viewing geometry for hypothetical Solar Occultation Experiments (SOE) in the Venusian atmosphere. The simulations incorporate planetary motions and orbital propagation, and compute the instantaneous SOE line-of-sight (LoS) tangent point using 3D vector algebra. Extensive validation of the simulations was performed using solar occultation observational points from SPICAV/SOIR and the orbital parameters of Venus Express, confirming excellent agreement. Using the simulations, a first-of-its-kind theoretical analysis was conducted on the effect of

varying different spacecraft orbital elements on the spatio-temporal distribution of solar occultation measurements in the Venusian atmosphere, revealing a highly sensitive dependence. Some of the salient results of this study are presented in Fig. 22.

The simulation show that the spatio-temporal sampling of SOE observations depends on the spacecraft semimajor axis (a), with smaller orbits giving larger number of observational points and longer periods of favourable 'occultation seasons'. The orbital inclination (i) significantly affects the latitudinal extent of observations and the nature of the occultation seasons, with higher inclinations giving widespread latitude coverage. It is observed that polar circular orbits invariably exhibit a distinct region of sparse observations (RSO) over the equatorial region. Varying the eccentricity (e) and argument of periapsis (ω) of the spacecraft orbit results in systematic shifting of the RSO away from the equator towards higher latitudes.

The spatio-temporal spread of individual SOE profiles strongly depends upon the orbital parameters and the solar beta angle, with the spreads being larger for higher beta angles (near the start/end of each occultation season) (Fig. 23). Extensive simulations were specifically performed for 3 different orbital configurations (as proposed for ISRO's Venus Orbiter Mission), viz. (i) 250 km × 66000 km highly elliptical injection orbit; (ii) 300 km circular polar orbit; (iii) 250 km × 600 km elliptical polar orbits. The three configurations result in distinct distributions of SOE observational points and RSOs, revealing the benefit of having multiple orbital phases in a single mission. This study provides valuable inputs for design and optimization of spacecraft orbits for future interplanetary missions for performing SOE measurements, in order to meet the specific science objectives.

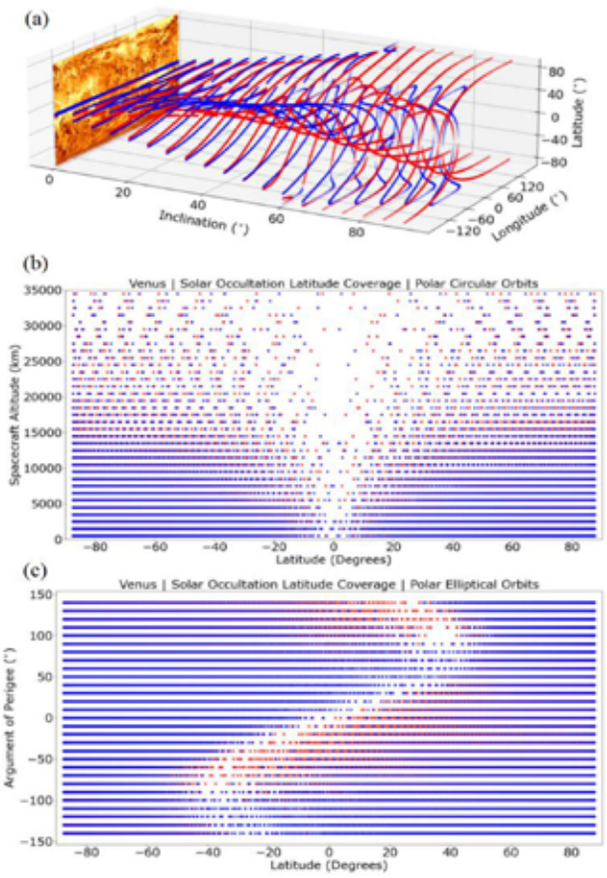

Figure 22. Results of 3D simulations on the effect of spacecraft orbital parameters on SOE measurements in the Venusian atmosphere (simulated for a fixed tangent altitude of 70 km): (a) effect of orbital inclination on the spatial coverage (latitude vs longitude); (b) effect of semimajor axis on latitude coverage; (c) effect of argument of periapsis on latitude coverage. In each plot, the red points correspond to sunrise events and blue points correspond to sunset events [Pradeep and Sunilkumar, Roy. Astro. Soc. Tech. Inst., 2023].

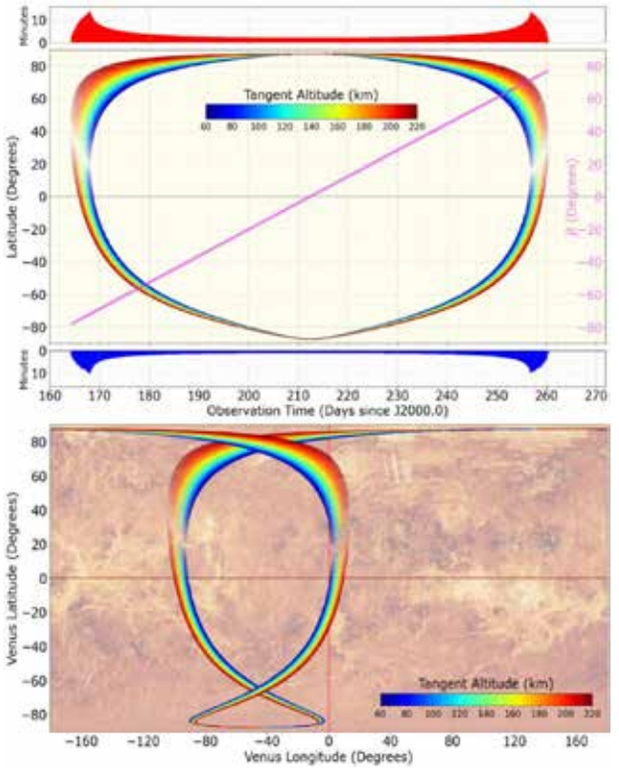

Figure 23. Simulation of SOE profiles spanning tangent altitudes from 60 to 220 km for 1 occultation season, simulated for a 250 km × 600 km elliptical polar orbit around Venus. Top panel shows the latitude-time distribution of the measurements, with x-axis denoting observation time (number of days since J2000.0), and bar plots showing the duration of each occultation event in minutes (red bars indicate sunrise and blue bars indicate sunset events). Solar beta angle (β) values corresponding to the measurements are shown as violet points. Bottom panel shows the latitude-longitude distribution of the simulated SOE measurements[Pradeep and Sunilkumar, Roy. Astro. Soc. Tech. Inst., 2023].

Technical Development Activities

Solar Occultation Experiment (SOE) Payload for Future Earth and Planetary Missions

Design and development of Laboratory Model of Solar Occultation Experiment (SOE) payload has progressed as per the plan, as part of Technology Development

Programme (TDP). The Lab Model consists of Optics Unit (6 co-aligned photometric channels in the 380-1020 nm wavelength range) and a Sun-Tracking Unit (2-axis gimbal mechanism with vacuum-compatible stepper motors), with provisions for incorporating a combination of coarse and fine sun-sensors for accurate sun-pointing (Fig. 24). Preliminary lab test of the instrument was conducted using an Electronics Testing Module, achieving simultaneous gimbal operation and data acquisition from 2 science channels. Initial response of the detectors (linear array and photodiode) was tested using solar simulator. Further activities are currently underway, including integration of electronics cards (front-end, motor drive and processing cards) and in house developed Quadrant Photodiode Sun-Sensor (QPSS) for fine sun-tracking, subsequent to which the instrument will be tested & validated in the lab and ambient conditions.

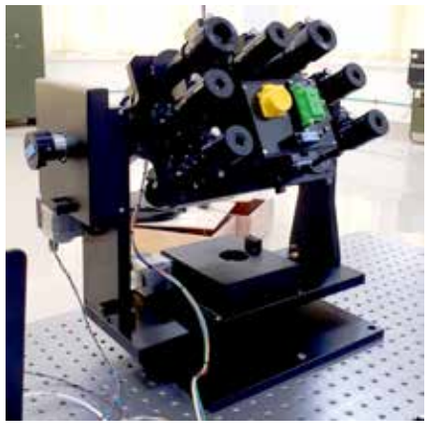

Figure 24. Laboratory Model of SOE payload including optics assembly (6 optical channels), electronics chassis and 2-axis gimbal mechanism with vacuum-compatible stepper motors.

Future Projections

- Completion of the Solar occultation experiment system for planetary atmosphere
- Quantification of Qausi-2 day wave sources
- Development of inversion algorithm to retrieve temperature profiles from radiance measurements at thermal IR
- Development of Line-by-Line Radiation transfer model for Limb Scanning Radiometer Applications
- Imptementation of WACCM model at SPL
- ISO in the Ozone and at Water vapour in the UTLS region
- Characterization of IGW in the UTLS using TTD campaign measurements
- Investigating Tracer-Tracer relations in the UTLS region
- Measurements of turbulence and convection using ST radar Network
- Characterization of Brewer-Dobson Circulation during volcano eruptions
- Marine stratocumulus clouds and their association with Hadley cell expansion
- Multi-frequency radar observations of precipitating clouds
- Design and Development of S-band Profiler
- Investigation of Venusian atmosphere using Venus General Circulation Model: Cyclostrophic Wind balance
- Gravity and planetary waves in Martian Atmosphere

Publications in the peer reviewed journals

1. Anjana, U, S.S. Mathew, and K.K. Kumar (2023), A rare episode of Minor Circulation Embedded in the Northern Hemispheric Zonal Mean Hadley Cell, Journal of Atmospheric and Solar-Terrestrial Physics, Vol.243, 106017, https://doi.org/10.1016/j.jastp.2023.106017
2. Das, S. S., M.V. Ratnam, M. D. Rao, and K.N.Uma (2022), Volume imaging of aspect sensitivity in VHF radar backscatters: First results inferred from the Advanced Indian MST radar (AIR), International Journal of Remote Sensing, 4517-4540, 43 (12), https://doi.org/10.1080/01431161.2022.2111667.
3. Emmanuel. M, S.V. Sunilkumar, P. R. Satheesh Chandran, M. Muhsin (2022), On the Signatures of local/regional dynamics in the distribution of lower stratospheric water vapour over the Indian Peninsula, Climate Dynamics, https://doi.org/10.1007/s00382-023-06749-z.
4. Jayadev Pradeep and S. V. Sunilkumar (2023), Solar Occultation Experiments (SOE) in the Venusian Atmosphere: Effect of Orbital Parameters on the Spatiotemporal Distribution of Measurements, Royal Astronomical Society Techniques and Instruments (RASTI), https://doi.org/10.1093/rasti/rzad019.
5. Koushik, N., J.Oberheide, &N. M. Pedatella (2023). A Lagrangian study of tidal advection of mesospheric water vapor. Journal of Geophysical Research: Atmospheres, 128, e2022JD037943. https://doi.org/10.1029/2022JD037943

6. Mathew, S.S and K.K. Kumar (2023), Hadley Circulation Dynamics in the IITM-Earth System Model Simulations: Evaluation and Future Projections, Theoretical and Applied Climatology, https://doi.org/10.1007/s00704-023-04397-1

7. Pramitha, M., K.K. Kumar, and M.Praveen (2023), Long-term variabilities in Thermal Structure, CO2 Concentration and associated Cooling Rates in the Earth's Middle Atmosphere: Observations and Model Simulations, Journal of Atmospheric and Solar-Terrestrial Physics, Vol. 246, 106070, https://doi.org/10.1016/j.jastp.2023.106070

8. Prijith S.S. and K.K.Kumar, (2023), Investigation on the anomalous weakening of diurnal tides in the mesosphere-lower thermosphere. Journal of Geophysical Research: Space Physics, 128, e2022JA030725, https://doi.org/10.1029/2022JA030725

9. Prijith S.S. and K.K. Kumar, (2023), On the genesis of multi-peak vertical structure of quasi-two-day waves in the mesosphere lower thermosphere. Earth, Planets and Space, doi:10.1186/s40623-023-01875-8 (in press)

10. SatheeshChandran, P. R., S. V. Sunilkumar, M. Muhsin, H. K. Alladi (2022), Effect of synoptic-scale dynamics on the vertical distribution of tropospheric ozone over the Arabian Sea and the Indian Ocean during the boreal winter of 2018, Journal of Geophysical Research: Atmospheres, 127, e2021JD036412, https://doi.org/10.1029/2021JD036412.

11. Subrahmanyam, K. V and K. K. Kumar (2023), Structure and evolution of organized precipitation bands: C-band Doppler weather radar observations over Thumba (8.5 °N, 77 °E). Atmospheric Research, 284,106590, https://doi.org/10.1016/j.atmosres.2022.106590.

12. Subrahmanyam, K. V and K. K. Kumar (2023), Characterization of Deep Convective Cells during the Indian summer monsoon using C-band polarimetric Doppler Weather Radar observations over Thumba (8.50 N, 770 E), Remote Sensing Applications: Society and of Environment, Vol.30, 100956, https://doi.org/10.1002/essoar.10507663.1.

13. Veenus, V., S. S. Das, and L. M. David (2023), Ozone changes due to sudden stratospheric warming-induced variations in the intensity of Brewer-Dobson Circulation: A composite analysis using observations and chemical-transport model, Geophysical Research Letters, 50, e2023GL103353, https://doi.org/10.1029/2023GL103353.

Scientific / Technical Reports

1. Karpechko A., Kremser S., Charlton-Perez A., Ming A., Smith R., Wang S., Tyrrell N., Powell C., Shah K., Bramberger M., Yulan L., Andradas V. M., Bloxam K., Hájková D., Kumar H., Jäger F., Veenus V., Okui H., Kovilakam M., Dai Y., Li G., Kumar V., Millin O., Match A., Loeffel S., Lee S., Kloss C. (2023). Report on the multi-hub 7th SPARC General Assembly, SPARC Newsletter, 60, 17–25.

Presentation in Symposium / Conferences / Workshops

1. Anjana U, S.S. Mathew and K.K.Kumar,"Delineating the Climate Change Signals through Hadley Cell Boundaries-A Study using Radio Occultation Measurements" COSPAR-2022 held at Athens, Greece, 16-24 July 2022

2. Anjana U and K.K Kumar, "An anomalous bite out of the Boreal Winter Tropical tropopause layer over the Eastern Pacific: A study using COSMIC Radio Occultation measurements", URSI - RCRS 2022, IIT (Indore), India, 1 - 4 December 2022

3. Anjana U and K.K. Kumar,"Poleward Shifting of Tropical Cyclone Tracks and their Association with Hadley Cell Expansion", Tropmet-2022, IISER-Bhopal, 29 November-02 December 2022

4. Bhaskar A.,T. K.Pant, S.R. Thampi, J.Pradeep, C.Vineeth and V. K. Yadav, "Twin Cubesat Mission Concept to study Aurora and Particle Precipitation in Northern and Southern Auroral Ovals", 5th COSPAR Symposium, Singapore, 16-21 April 2023.

5. Das, S.S., M. V. Ratnam, M.D. Rao, K. N. Uma, "Understanding the characteristics of stratosphere to troposphere exchange associated with the synoptic scale disturbances using Advanced Indian MST radar", URSI-RCRS 2022 held at Indian Institute of Technology, Indore during 1-4 December 2022.

6. Das, S. S., G. Ramkumar, N. Koushik, D. J. Murphy, I. A. Girach, K. V. Suneeth, K.V. Subrahmanyam, V. K. Soni, V. Kumar, and M. Nazeer, "A new perspective on multi-platform observations of stratospheric intrusion into the troposphere over Bharati (69.41°S, 76.19°E) during ISEA-35", National Conference on Polar Sciences (Open Science conference) held as NCPOR, Goa during 18-19 May 2023.
7. Das, S. S., K. N. Uma, K. V. Suneeth, V. Veenus, "Diurnal variability of lower and middle atmospheric water vapour over the Asian Summer Monsoon region: Results inferred from COSMIC-1 and TIMED-SABER measurements", SPARC General Assembly-2022, 24-28 October 2022.
8. Kumar, K.K and K.V. Subrahmanyam,"Orographical precipitation clouds over the Western Ghats during Indian Summer Monsoon: An overview", IISER-Bhopal, 29 November-02 December, 2022
9. Kumar, K.K., S. V. Sunil Kumar, Jayadev Pradeep, "Theme-based Discussion Meeting on Venusian Atmospheric Science", Science Programme Office (SPO), ISRO HQ, Bengaluru, March 28, 2023 (Online).
10. Prijith, S.S., and K.K. Kumar, "Meteor radar observations of quasi-two-day waves and weakening of diurnal tides in the mesosphere lower thermosphere", at the 2nd Symposium on Meteoroid, Meteor, Meteorites: Messenger from Space, PRL-Ahmedabad (online) Nov 25, 2022
11. Sunilkumar S V, "Tropical Tropopause Dynamics Experiments under GARNETS program: A novel approach to study the thermodynamic and tracer distributions in the troposphere and lower stratosphere over the Indian monsoon region", General Assembly of SPARC (SPARC GA) 2022 via online mode during 24-28 October 2022
12. Veenus, V., S. S. Das, and L. M. David, "Modulation of Brewer-Dobson Circulation's intensity and stratospheric composition by sudden stratospheric warming events", SPARC General Assembly-2022, 24-28 October 2022.
13. Veenus, V., and S. S. Das, "A new perspective on Aura MLS observations of stratospheric ozone distribution associated with Southern Hemisphere sudden stratospheric warming", URSI Regional Conference on Radio Science (URSI-RCRS 2022), held at Indian Institute of Technology, Indore during 1-4 December 2022.
14. Veenus, V., and S. S. Das, "The unprecedented stratospheric water vapor signal and the meridional circulation", 35th Kerala Science Congress at Mar Baselios Christian College of Engineering, Idukki during 10-14 February 2023.
15. Veenus, V., and S. S. Das, "The Tonga volcanic eruption: Implications on the stratospheric circulation and ozone depletion", online Stratospheric Processes and Their Role in Climate (SPARC) "Hunga-Tonga impacts: open science workshop" during 16-17 May 2023 (Online).
16. Veenus, V., S. S. Das, "Impact of Quasi-Biennial Oscillation on Brewer-Dobson Circulation and related ozone and water vapor distributions", QBOi workshop organised by SPARC during 27-31 March 2023 held at the University of Oxford, UK.

Deputations

Anjana U

1. 44th COSPAR Scientific Assembly, Athens, Greece, 16-24 July, 2022

Online meetings / Conferences

1. Anjana U, GNSS Remote Sensing Colloquium, UCAR, Colorado, 5-16, June, 2023 (online)
2. Siddarth Shankar Das, Veenus Venugopal and Anjana U., URSI-RCRS 2022 held at Indian Institute of Technology, Indore during 1-4 December 2022.
3. Siddarth Shankar Das, S. V. Sunilkumar and Veenus Venugopal, 7th SPARC General Assembly-2022, 24-28 October 2022 (Online)
4. Siddarth Shankar Das, National Conference on Polar Sciences (Open Science conference) held as NCPOR, Goa during 18-19 May 2023.
5. K. Kishore Kumar, Anjana U, IISER-Bhopal, 29 November-02 December, 2022
6 . Veenus Venugopal, QBO extratropical teleconnection working group meeting by University of Reading on 15 June 2023 (online).

Invited Talks

K. Kishore Kumar

1. "A Decade of Meteor Radar observations of the low-latitude Mesosphere Lower thermosphere Dynamics", MetMESS-2022, PRL, Ahmedabad, 24-25 November, 2022.
2. "Space-borne Radars for Cloud Research: Hawks in the Sky", Frontier Symposium in Physics 2023 (FS-PHY 2023), IISER-Trivandrum, 24-26 February, 2023.

Siddarth Shankar Das

1. "Atmospheric Dynamics using Wind Profilers", Workshop on Atmospheric Research using Radars held at Indian Institute of Technology, Indore on 1 December 2022.
2. "Understanding the characteristics of stratosphere to troposphere exchange associated with the synoptic scale disturbances using Advanced Indian MST radar", URSI-RCRS 2022 held at Indian Institute of Technology, Indore during 1-4 December 2022.

Training Programmes

Jayadev Pradeep

1. Two Days Training Programme on "Additive Manufacturing in Aerospace", HRDD, VSSC, Thiruvananthapuram, 22-23 February, 2023.

आयनमंडल तापमंडल एवं चुंबकमंडल भौतिकी
Ionosphere Thermosphere Magnetosphere Physics

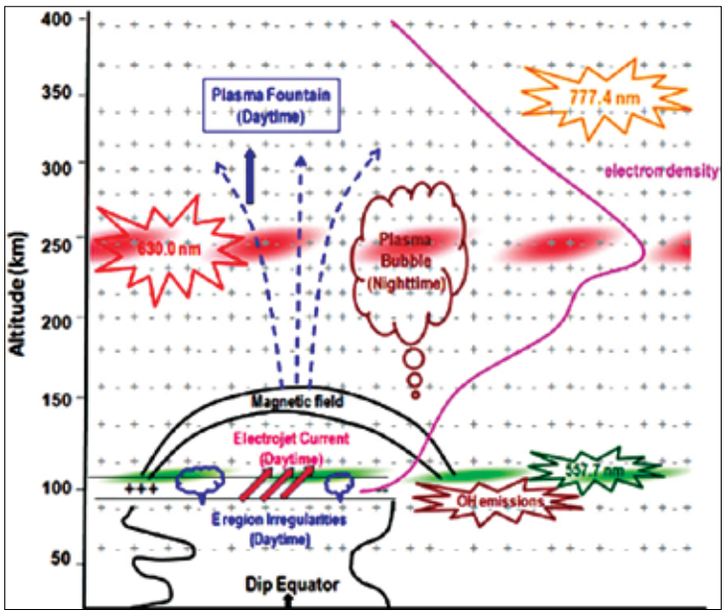

आयनमंडल,तापमंडल एवं चुंबकमंडल भौतिकी (आइटीएमपी) शाखा का लक्ष्य, (क) बदलते अंतरिक्ष मौसम एवं भूचुंबकीय परिस्थितियों तथा इसके अक्षांशीय असमानताओं पर चुंबकमंडल तापमंड़ल आयनमंड़ल प्रणाली की अनुक्रिया का अध्ययन (ख) तापमंड़ल-आयनमंड़ल का उसके नीचे प्रसरित वायुमंड़ल के साथ गतिकीय युग्मन पर अध्ययन (ग) ऊपरि वायुमंड़लीय प्रक्रमों का प्रतिनिधित्व करने के लिए तापमंड़ल-आयनमंड़ल मॉडलों का आंतरिक विकास व उपयोग, और प्रौद्योगिक अनुप्रयोगों के लिए बेहतर इनपुट प्रदान करने हेतु इन अध्ययनों का उपयोग करने पर ध्यान केंद्रित करते हुए, भौमिक ऊपरी वायुमंड़ल की ऊर्जिकी तथा गतिकी की जाँच करना है। आइटीएमपी शाखा का यह प्रयास रहता है कि वह इन अनुसंधान लक्ष्यों को भूमि, रॉकेट तथा अंतरिक्ष आधारित मंचों में प्रयोग हेतु क्षमता रखनेवाले स्वदेशी तौर पर विकसित परीक्षणों के माध्यम से तथा अनुसंधान की व्याप्ति को अन्य सौर प्रणाली पिंड़ों के चुंबकमंड़ल, तापमंड़ल तथा आयनमंड़ल तक भी बढ़ाकर पूरा करे।

Ionosphere Thermosphere Magnetosphere Physics (ITMP) branch aims at investigation of the energetics and dynamics of terrestrial upper atmosphere, with focus on (a) Study of the response of the magnetosphere thermosphere ionosphere system to varying space weather and geomagnetic conditions and it's latitudinal differences, (b) Study of the dynamical coupling thermosphere ionosphere has with the atmosphere below it, (c) In house development and use of thermosphere-ionosphere models to represent the upper atmospheric processes and make use of these studies to provide better input for technological applications. ITMP strives to meet these research objectives through indigenous development of experiments capable of being used on ground, rocket and space based platforms and extending the scope of its research to the magnetospheres, thermospheres, and ionospheres of other solar system bodies as well.

वैज्ञानिक टीम / Science Team
तरुण कुमार पंत / Tarun Kumar Pant
राज कुमार चौधरी / Raj Kumar Choudhary
मंजू जी. / Manju G.
विनीत सी. / Vineeth C.
मो. मोसारफ होस्सैन / Md. Mossarraf Hossain
मृदुला एन. / Mridula N.
संध्या के. नायर / Sandhya K. Nair
अंबीली के. एम. / Ambili K. M.
अजय अनिल पोटदार / Ajay Anil Potdar
आयिषा एम. अश्रफ / Ayisha M. Ashruf

तकनीकी टीम / Technical Team
अनुमोद पी. जी. / Anumod P. G.
मणिकंठन नायर एन / Manikantan Nair N.
मोहम्मद नज़ीर एम Mohammad Nazeer M.
उत्तम एस. पूर्ती / Uttam S. Purty*

अनुसंधान सहयोगी/रामानुजन् फैकल्टी / Research Associates/Ramanujan Faculty
केशव राम त्रिपाठी / Keshav Ram Tripathi
षिम्ना के. / Shimna K
श्रीबा श्रीकुमार / Sreeba Sreekumar
स्नेहा ए. गोकानी / Sneha A. Gokani@

अनुसंधान अध्येता / Research Fellows
ललिता जी. / Lalitha G.
श्रुती टी. वी. / Sruthi T. V.
रिचा नाजा जैन / Richa Naja Jain
मनु टी. / Manu T.
सौम्यनील बैनर्जी / Soumyaneal Banerjee
आर्या अशोक / Arya Ashok
रूबिन सैमसन याकुब / Reuben Samson Yaqub
विष्णुप्रिया के. एस. / Vishnupriya K S

** Relieved in December 2022*
@ Relieved in January 2023

Equatorial Thermosphere Ionosphere Processes

On the Behavior of Thermospheric O^1D 630.0 nm Dayglow Emission during Counter Electrojet Events

The thermospheric airglow emissions provide crucial information on the thermal and dynamical state of the upper atmospheric layers and their coupling with ionospheric electrodynamics. This study presents the response of thermospheric O^1D 630.0 nm dayglow emission to the variability associated with equatorial Counter Electrojet (CEJ) events. The analysis based on the data from a meridian scanning Dayglow Photometer, Digital Ionosonde and Proton Precession Magnetometer over Trivandrum (8.5 ^{o}N, 77 ^{o}E, 0.5 ^{o}dip lat.), indicates that the O^1D 630.0 nm emission behave distinctly different during the CEJ events compared to that on normal days. It has been observed that O^1D 630.0 nm emission shows enhancement during the negative excursion of the ΔH, followed by an unusual depletion during the peak CEJ time (Fig.1). The observed variability was found to be more pronounced in a latitudinal region of ±3^o centered at around the dip equator. In addition, the emission intensities also exhibit the presence of enhanced short period oscillations of periodicity 20-30 minutes during the CEJ events. Analysis of the data from the collocated ionosonde revealed that the F-region electron density showed enhancement during the early phase of the CEJ and a decrease during the peak CEJ (Fig. 2). Further, simulation studies using an in-house developed Quasi 2 dimensional ionospheric model showed

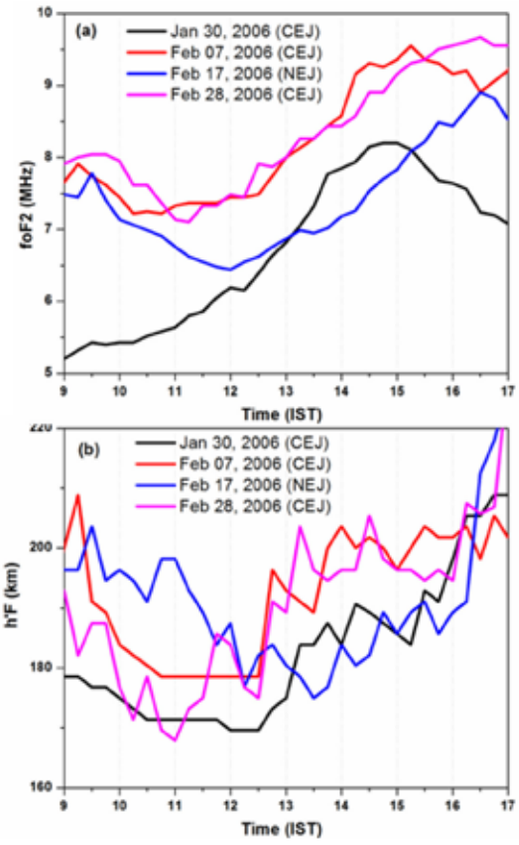

Figure 2: Time variation of the critical frequency of the (a) ionospheric F2- region (foF2) and (b) Base height of the F-region (h'F) over Trivandrum on January 30, 2006, February 07, 2006 and February 28, 2006 (CEJ days) along with the same on February 17, 2006 (NEJ day) [Vineeth et al., Adv. Space Res., 2023].

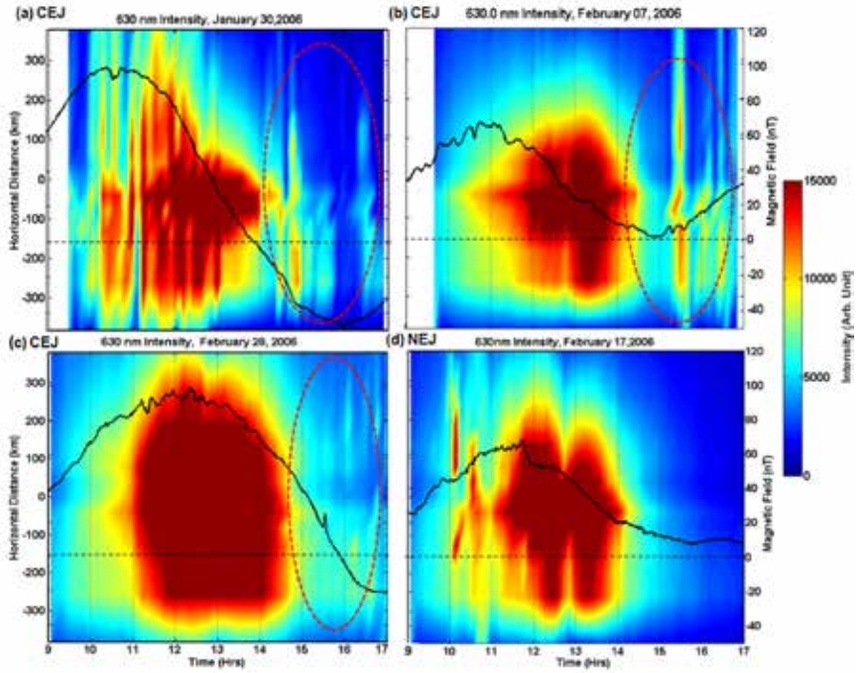

Figure 1: Time variation of EEJ Induced magnetic field and Spatio-temporal variation of thermospheric O^1D 630.0 nm emissions on January 30, 2006, February 07, 2006 and February 28, 2006 (CEJ days) along with the same on February 17, 2006 (NEJ day) [Vineeth et al., Adv. Space Res., 2023].

that the modified plasma fountain during the CEJ can alter the plasma density at the emission centroid. The study reveals a strong dynamical coupling between the E and F-region of the dip equatorial ionosphere.

Nocturnal thermospheric neutral wind and temperature measurement using a Fabry-Perot Interferometer

First systematic measurements of nocturnal thermospheric neutral winds and temperature using a Fabry-Perot Interferometer (FPI) are presented from Trivandrum (8.5 °N, 77 °E, 0.5° dip latitude), an Indian station close to the geomagnetic equator. The state-of-the-art solid etalon FPI system provides neutral wind and temperature based on the measurements of spectral line shape and the Doppler wavelength shift of the OI630 nm nightglow emission. The results presented here are based on the measurements made during the low solar activity period of June 2017 to April 2018. Nocturnal variability of the monthly mean temperature and winds have been obtained from these measurements. The mean temperature and winds are compared with the predictions of the neutral atmospheric models, Mass Spectrometer and Incoherent Scatter Radar 2000 (MSISE-00) and Horizontal Wind Model 2014 (HWM14).

The FPI observed mean thermospheric temperatures (Fig. 3) are found to be maximum post sunset during all seasons. One prominent feature in the temperature variability is a double peaked enhancement structure that is seen at the post evening and pre-dawn hours in the autumnal equinox and winter seasons. The double peak temperature structure is not represented by the model. Overall, MSIS model predictions show agreement with the FPI temperatures, although large deviations between them noticed in some months indicate limitation of the model in representing the equatorial thermosphere.

The observed monthly mean thermosperic meridional wind found to vary between 71 m/s (equatorward) in April 2018 and 67 m/s (poleward) in December 2017. The observed meridional wind during solsticial months clearly exhibits signatures of the inter-hemispheric flow (Fig. 4) and agree with the model predictions. Monthly mean observed zonal wind speeds during August, October and February, agree well with the model in the post-midnight hours. For remaining months, there are large differences between the two in the pre- and post-midnight hours, and in fact they are out of phase during most of the times. Overall, the HWM14 model poorly represents the zonal winds over the dip equatorial station Trivandrum. In this study, the behavior of nocturnal thermosphere has been studied in context of its coupling with ionosphere.

Generation of Post Sunset E Region Electron Density Stratifications at the Magnetic Equator: An Analysis Using In Situ Measurements and Theoretical Simulations

In-situ measurements of electron density/irregularities and ion drift velocity/neutral wind were undertaken with Electron Density and Neutral Wind (ENWi) payload on-board an RH300 flight on 6 April 2018 as part of the first Sounding Rocket Experiment (SOUREX-1). The presence of a clearly structured ENWi measured electron density

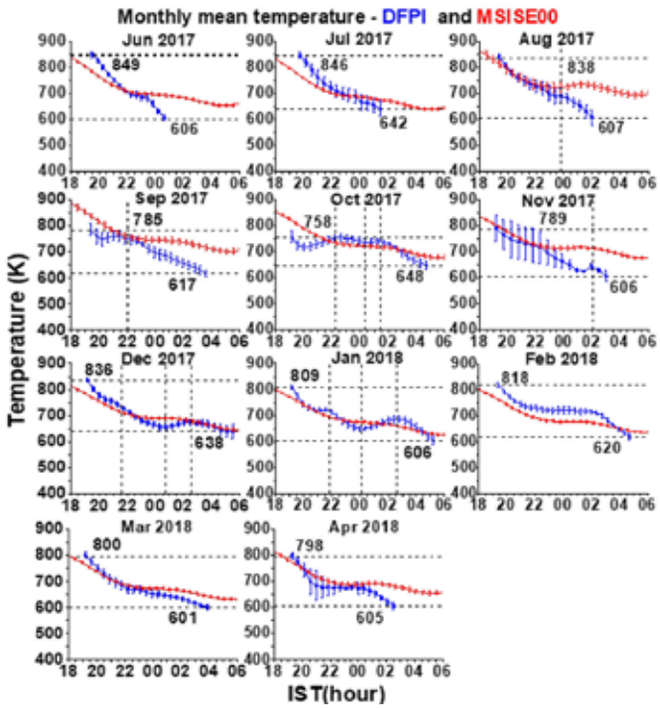

Figure 3: Seasonal variation of monthly mean nocturnal thermospheric neutral temperature (a) Measured using FPI (Blue curve) and (b) Predicted by MSISE-00 model (red curve) [Hossain et al., Adv. Space Res., 2023].

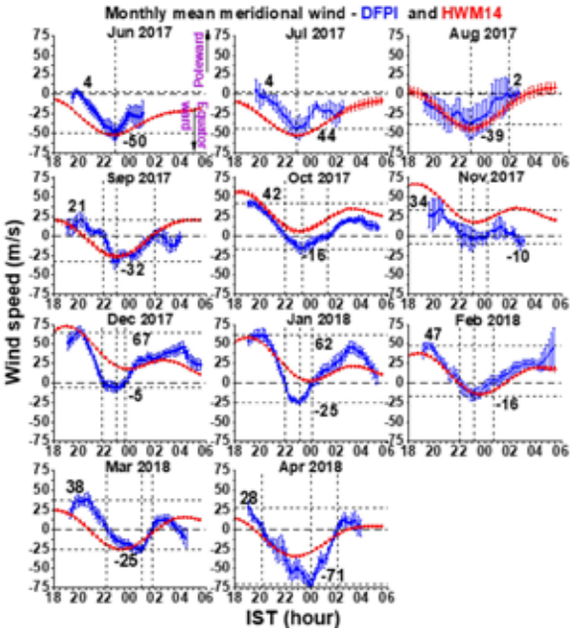

Figure 4: Seasonal variation of monthly mean nocturnal thermospheric neutral meridional wind (a) Measured using FPI (Blue curve) and (b) Predicted by HWM14model (red curve) [Hossain et al., Adv. Space Res., 2023].

(Fig.5a) profile is an interesting feature observed on this day. Concurrently electron density/ irregularities are measured by a Langmuir probe payload which confirmed the presence of stratifications in electron density (Fig.5a). The neutral wind measurements by ENWi also reveals a structured pattern. The hodograph analysis of the neutral wind components reveals an elliptical pattern and clockwise rotation indicating downward phase propagation characteristics associated with the gravity waves (Fig.5b). Theoretical simulations of the requisite ion convergence at the magnetic equator for occurrence of electron density stratifications using the observed electron density structures during the post sunset hours in relation to the estimated ion convergence due to gravity wave winds are performed. This analysis reveals that conditions favoring the formation of stratification related ion convergence are present in the ionosphere on 6 April 2018. Hence, the present study for first time, uses actual measurements of neutral winds and electron densities from same instrument to demonstrate the role of gravity wave induced winds in producing ion convergence at the magnetic equatorial region, Trivandrum in the postsunset hours.

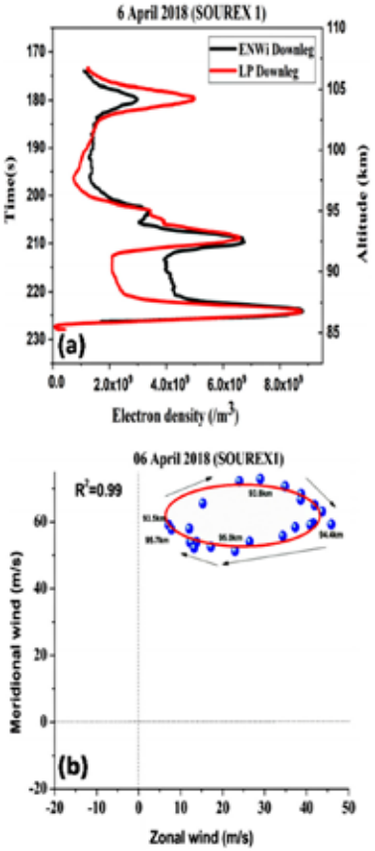

Figure 5: (a) Electron density profiles derived from ENWi and LP data. (b) The hodograph exhibiting the rotation of wind with altitude [Manju et al., J. Geophys. Res., 2023].

Space Weather

On the significant impact of the 17 March 2015 St. Patrick's Day geomagnetic storm on the ionosphere over Indian region

Understanding the Ionosphere Thermosphere (IT) system variability is very important to address the corrections to be accounted for in trans-ionospheric communication and navigation systems due to path delays caused by the ionosphere. This is very crucial during geomagnetically disturbed periods when the variability is very high. In this scenario, coordinated observations across the globe during St.Patrick's Day storm have provided a unique opportunity to address the IT system variability in response to a major geomagnetic disturbance. The response of the ionosphere in the Indian region to the

extreme space weather events of 17-19 March 2015 is studied using Global Positioning System (GPS) Total electron Content (TEC) measurements, Thermosphere Ionosphere Electrodynamics-General Circulation Model (TIE-GCM) simulations and High Frequency (HF) Radar observations. The data from Thiruvananthapuram (8.5 °N, 77 °E geographic, 0.3°N magnetic latitude) and northern hemispheric mid latitude station Hanle (32.80 °N, 79 °E geographic, 23.9°N magnetic latitude) have been analyzed for the above event. The TEC over Thiruvananthapuram, a dip equatorial location, exhibits a decrease during the post sunset hours on 17 March 2015 and is followed by the generation of F region irregularities at an altitude of 600 km, as observed by HF radar as well as TEC scintillations. The TEC over the mid latitude station of Hanle decreased during the storm recovery phase on 18March 2015 in response to negative storm effects. The extent of decrease in TEC as observed during the recovery phase could not be simulated by TIE-GCM over Hanle (Figure 6a,b). This difference is attributed to the enhanced Joule heating taking place in the polar region during St. Patrick's Day storm and the associated composition changes. An anomalous heating scenario was introduced and the simulated TIE-GCM results were found to match the observations. The present study clearly brings out the impact of 17 March 2015, St.Patrick's Day geomagnetic storm on the ionization distribution over equatorial as well as mid latitude stations over the Indian region using observations as well as TIE-GCM simulations and the evolutionary features of ionospheric irregularities over equatorial location using TEC and HF radar observations (Fig. 6c).

The role of the storm-time prompt penetrating electric field on the net distribution of plasma density over the low latitude ionospheric regions

A study was conducted to examine the relative influence of prompt penetration of electric fields and neutral winds on the distribution of ionospheric plasma during geomagnetic storms in the Indian ionosphere region. Four geomagnetic storms, characterized by similar onset times but varying strengths, were analyzed using data from ground-based magnetometers, as well as the ACE, GPS, and TIMED satellites. To determine the strength and magnitude of the prompt penetration electric field, we inferred variations in the horizontal component of the magnetic field (DH) at Tirunelveli, a dip-equatorial station, from the data obtained by ground-based magnetometers. The distribution of electron density across the Indian ionospheric region was quantified using vertical total electron content (VTEC) derived from GPS measurements. Signatures of prompt penetration electric fields were observed for all considered storms, primarily during the daytime. It was observed that as the strength of the penetration electric field increased, the latitudinal extent of electron density distribution also increased. During a severe geomagnetic storm, the gradient in electron density extended up to Shimla, a mid-latitude station (Fig.7). The gradient was less pronounced for moderate geomagnetic storms. To analyze the contribution of neutral winds, which affect electron density modulation during geomagnetic storms, we examined the thermospheric O/N2 ratio measured by NASA's TIMED satellite's global ultraviolet imager (GUVI) instrument.

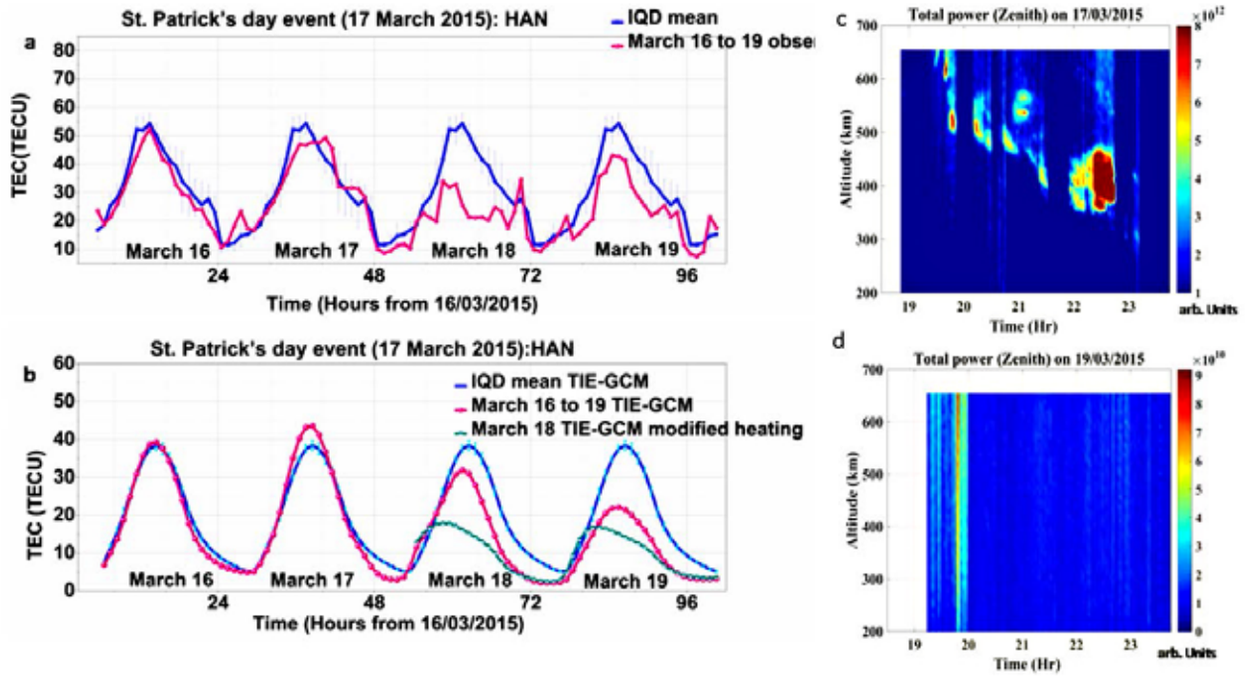

Figure 6: (a,b) GPS TEC variations during 16 March 2015 to 19 March 2015 over Hanle, and the TIE-GCM model derived TEC for the same period. (c,d) Total power observed using HF Radar during 17 March 2015 and 19 March 2015 in the F region over Trivandrum [Mridula et al., Adv. Space Res., 2022].

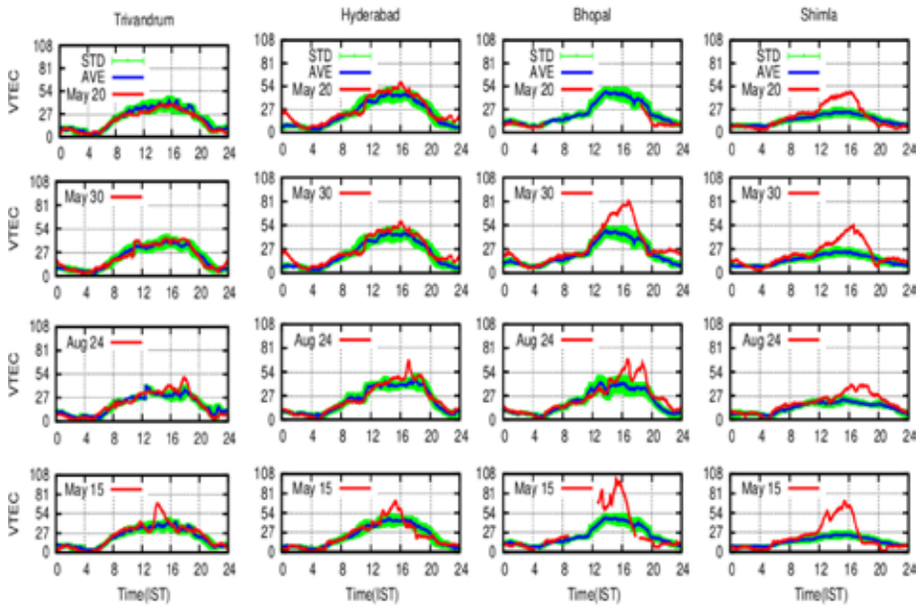

Figure 7: VTEC variation at Trivandrum, Hyderabad, Bhopal and Shimla on 15 May, 24 August, 30 May and 20 May 2005 storm events [Ambili K.M., and R.K. Choudhary, Adv. Space Res, 2023].

However, the observed increase in the O/N_2 ratio did not correspond to the increase in VTEC. Based on the evidence, it is inferred that during the first day of the storm, the penetrating electric field plays a crucial role in controlling electron density distribution in the low-latitude region. Subsequently, the plasma density distribution is primarily governed by thermospheric winds.

Response of the Indian sector to a strong but short lived geomagnetic storm

A comprehensive study was conducted on the response of the low latitude ionosphere to a powerful geomagnetic storm (Dst ~ 132 nT) in the Indian sector. This storm occurred on 30-31 May 2005 and had its onset near noon in the Indian sector. It resulted in intense and sustained activity at high latitudes for a duration of twelve hours. The magnetometer data collected near the geomagnetic equator provided clear evidence of a strong Prompt Penetration Electric Field (PPEF). Furthermore, the Total Electron Content (TEC) data, reaching as far north as Delhi, indicated a subsequent Storm Enhanced Density (SED) event. On the following day, 31 May, a notable observation in the morning was the presence of a robust counter-electrojet, accompanied by a threefold reduction in plasma density in the Equatorial Ionization Anomaly (EIA) region and beyond (Fig. 8). This reduction aligned with the concept of a disappearing eastward electric field at the equator and the direct influence of an upper thermospheric equatorward wind, caused by high latitude Joule heating from the auroral regions. An unexpected observation from the afternoon of 31 May was a fluctuation in the height of the peak F-region density at the magnetic equator at Trivandrum. A closer examination of the ionosonde data revealed the existence of an F3 layer until mid-afternoon, strongly suggesting the presence of equatorward winds in the upper thermosphere. However, by 16:00 IST, the F3 layer rapidly disappeared, leading to a 200 km decrease in the height of the peak F-region density within a two-hour timeframe. The most reasonable explanation for this phenomenon was the cessation of winds blowing toward the equator by 16:00 IST.

Radio Occultation and Venusian Ionosphere

On the estimation of frequency residuals in a radio occultation experiment

In radio occultation (RO) experiments, the difference between the observed and predicted Doppler, known as frequency residuals, serves as the fundamental input data for retrieving vertical profiles of atmospheric parameters. A comparison of various methods for estimating frequency residuals in a one-way downlink single frequency RO experiment has been done and a new method proposed that not only enhances residual estimates but is also easy to implement. Our findings demonstrate that the Doppler broadening in received radio signals, which introduces uncertainties in Doppler estimation, primarily stems from changes in line-of-sight velocity between the receiver and transmitter during the sampling period. When combined with random noise in the receiving system and plasma medium fluctuations along the propagation path, the resulting uncertainty in Doppler estimates can reach magnitudes as high as 60 Hz (Fig. 9). Conversely, the expected phase changes caused by ionospheric dispersion/refraction are typically in the range of 0.01-2 Hz only. To address this issue, we implemented a resampling technique by dividing the observed radio signals into smaller time packets. Following the removal of DC constant shift, a

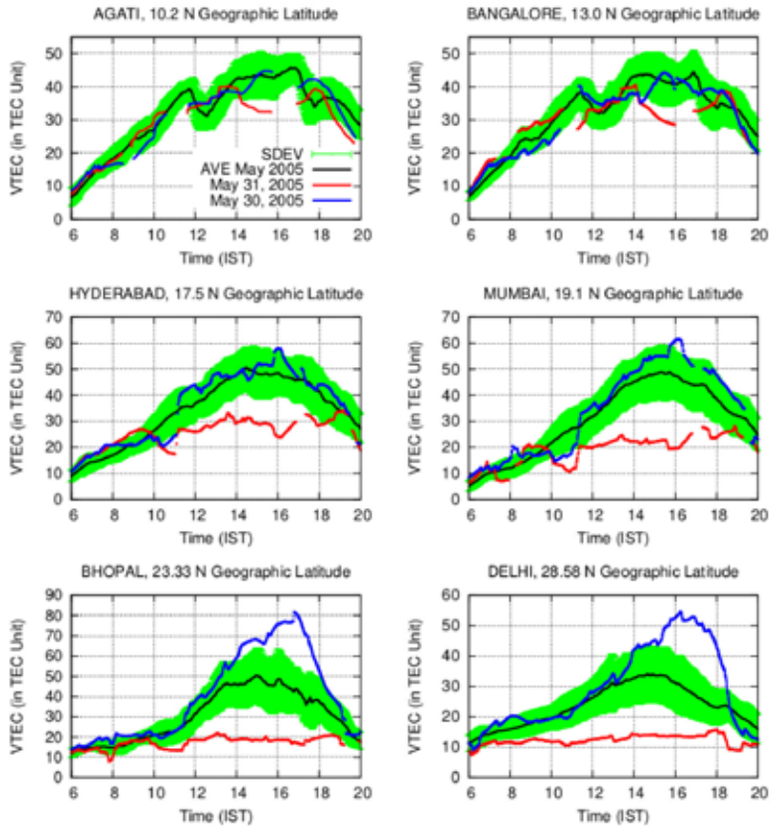

Figure 8: Time variation of TEC between 08:00 and 20:00 IST on May 30 and 31, 2005. Also shown are the monthly TEC average for May 2005 along with the standard deviations for the month. [Choudhary et al., Adv. Space Res, 2023].

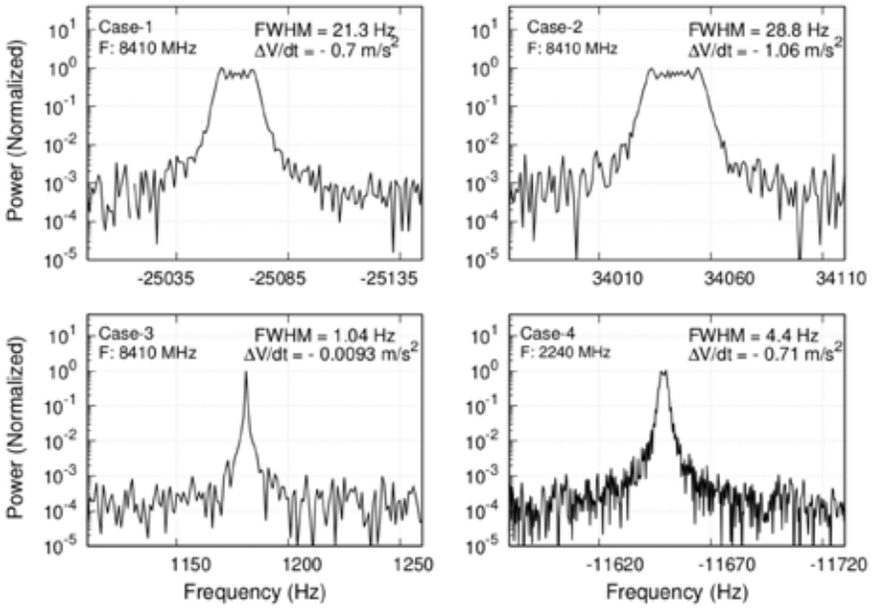

Figure 9: A few examples of the varying shapes of 1-s cadence Doppler spectra as observed during different phases of a radio occultation experiment. The 200 K pairs of I, and Q channel power data, sampled each second were taken for generating the spectrum. Case-1: Signal were passing through the Venusian ionosphere (about 140 km altitude) during an ingress occultation event on DOY 212, 2017. Case-2: Signals passed through the vacuum (~1500 km above the Venusian surface) during the egress occultation event on DOY 212, 2017. Case-3: Signal passing through the interplanetary medium only on DOY 73, 2021. Case-4: DFRS (CH2) radio signals passing through the Lunar atmosphere/ionosphere with closest approach of ~80 km above the Lunar surface during an ingress occultation event on DOY 230, 2021. FWHM stands for spectrum's full-width at half-maximum. $\Delta V / \Delta t$ is change in the line of sight velocity. In the y-axis, power is $I^2 + Q^2$ and normalized with maximum power value. I and Q stand for an in-phase and in-qua ature component of received voltage. The frequency resolution on the x-axis is 1 Hz. [Tripathi et al, MNRAS, 2023].

narrow bandpass filter was applied to suppress small-scale fluctuations, enabling estimation of Doppler and power in the received signals. To validate our method, we compared our results using Akatsuki radio signals, tracked at the Indian Deep Space Network, with the residuals provided by the Akatsuki team and the method used for analyzing Cassini RO data. The results indicate that our method yields superior estimates of frequency residuals with lower standard deviations.

On the origin and characteristic features of the V1 layer in Venus ionosphere using Akatsuki radio science experiment and the one-dimensional photochemical model

Utilizing the radio science experiment onboard the Akatsuki spacecraft, in combination with our in-house developed one-dimensional photochemical model (1D-PCM), we conducted a study on the V1 layer in the Venus ionosphere, which peaks around 125 km. The V1 layer exhibits highly variable characteristics, ranging from a mere slope change below the V2 layer to a distinct and prominent peak. To simulate the observations, we employed the 1D-PCM and noted that the model's solar X-ray flux at the 1.5-3 nm and 5-10 nm bands needed to be enhanced by a factor of 2-4 to accurately replicate the V1 layer. Our model simulations also indicated that the primary ions below 135 km are O_2^+, and NO^+, with O_2^+ showing a linear increase up to approximately 135 km, while NO^+ reaches its peak around 127 km. Our analysis revealed that when the V1 layer appears as a slope change below the V2 layer, O_2^+ ions dominate, whereas when a distinct V1 peak emerges, NO^+ ions become the major component. Additionally, when both ion densities are comparable, the layer manifests as a ledge (Fig. 10).

Gravity Wave Modulations at the Lower Altitudes of Venus Ionosphere

Venus is known to have a peak in the plasma density at ~140 km altitude (V2 layer), and a secondary permanent peak at ~127 km (V1 layer). A sporadic enhancement in the electron density below 120 km altitude (now known as V0 layer) has also been reported. Initially, it was believed that the V0 layer was limited to specific areas on Venus. However, using measurements from the Akatsuki spacecraft, we had shown that it was present across all latitudes, including equator during local noon hours. The origin of this density enhancement in the V0 layer, however, is still unknown. By analyzing data obtained from radio science experiments conducted by the Venus Express and Akatsuki orbiters, we investigated the factors that influence the presence and spatial characteristics of an electron density enhancement at lower altitudes in the Venus ionosphere, known as the V0 layer. Our findings indicate that Gravity Waves (GWs) play a vital role in shaping the V0 layer. When the solar zenith angle (SZA) is below 40° and the average gravity wave potential energy (AGPE) remains below 4.7 J/kg, the V0 layer exhibits a well-defined single peak. However, as the AGPE increases beyond this threshold, the height of the V0 peak becomes perturbed, displaying a wave-like structure. On the other hand, for SZA values exceeding 40° and AGPE surpassing 4.7 J/kg, a predominant wave-like feature emerges at the base of the V0 layer (Fig. 11). These results suggest that the enhancement in the AGPE above a certain threshold value perturbs the plasma of the V0 layer and plays a pivotal role in defining its shape, but it does not impact the formation of this layer. We also observe the local time effect on the frequency of high AGPE leading to varying V0 layer features.

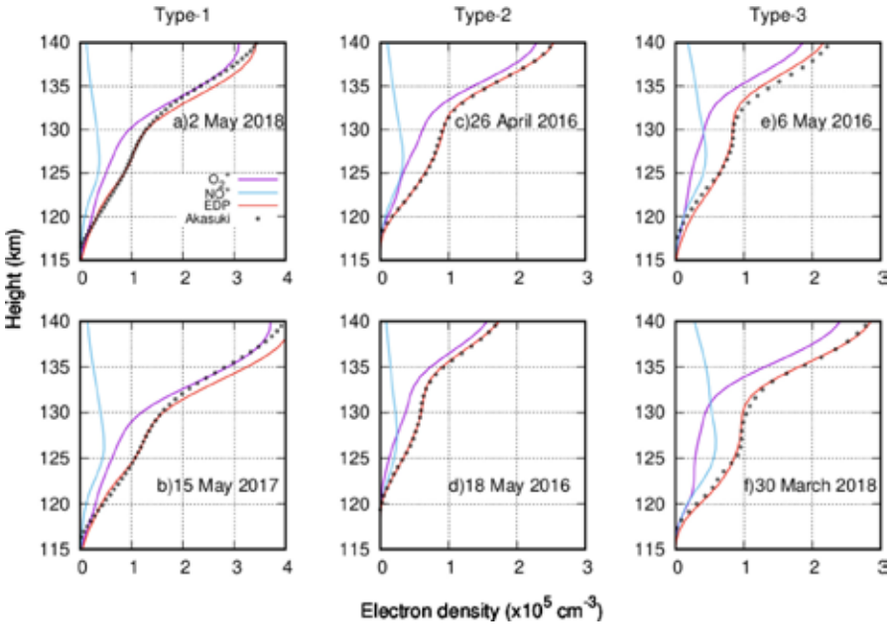

Figure 10: Comparison of NO^+ and O_2^+ density with modeled and observed electron density during: (a,b) Type 1 on 2 May 2018 and 15 May 2017, (c,d) Type 2 on 26 April 2016 and 18 may 2016 and (e,f) Type 3 on 6 May 2016 and 30 March 2018 [Ambili et al., MNRAS, 2023].

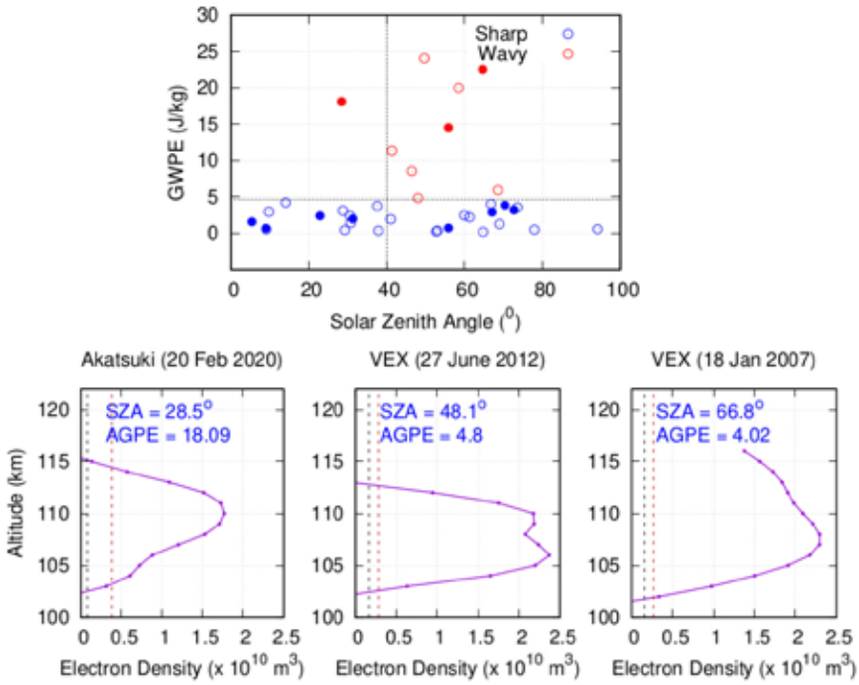

Figure 11: The top panel displays the distribution of the average gravity wave potential energy with solar zenith angles for the cases when the V0 layer is observed by Akatsuki (filled circle) and Venus Radio Science experiment (open circle) spacecraft. The red color circle represents the wavy structure of the V0 layer. The bottom panels show the cases when the AGPE is more than the threshold potential energy but still show varying V0 characteristics. Details are given in the text [Tripathi et al., Geophys. Res. Lett., 2023].

Venusian Ionosphere During Deep Solar Minima: Some New Insights Using Akatsuki Radio Science Experiment

A study was undertaken on the characteristic features of different layers in the Venus ionosphere during the deep solar minimum of solar cycle 24. This investigation utilized data from the radio science experiment conducted by the Akatsuki spacecraft, with radio signals tracked at various locations including the Indian Deep Space Network in Bangalore, the Usuda Deep Space Center in Japan, and the DLR Ground station in Weilheim, Germany. The unique orbital geometry of the spacecraft provided valuable opportunities to examine the Venusian ionosphere and atmosphere in the equatorial region at low solar zenith angles (SZAs) (Fig. 12). These observations revealed a distinct influence of the low solar activity period on the primary (V2) and secondary (V1) peak electron densities in the Venus ionosphere. These densities were found to be at their minimum levels ever reported. Interestingly, unlike

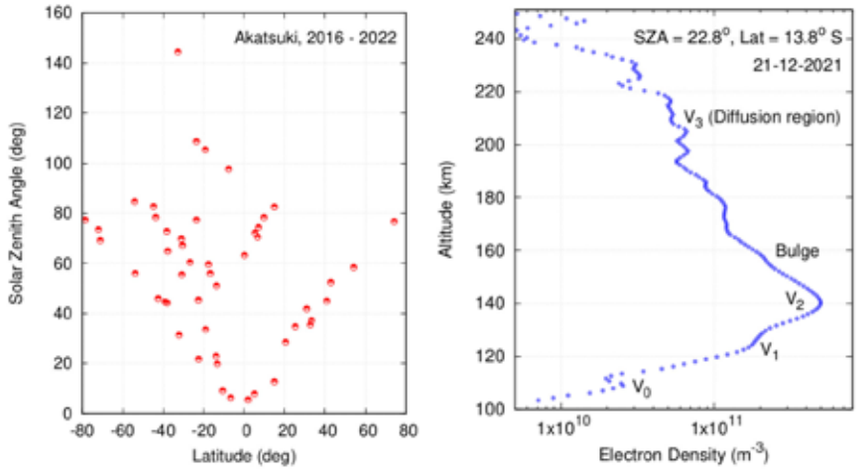

Figure 12: Left panel: distribution of observations conducted using Akatsuki Orbiter with respect to latitude and the solar zenith angle. Right panel: A sample altitude profile of electron density observed by Venus Akatsuki, radio science experiment on 21 November 2021. Apart from the V2 layer at ~140 km, and the V1 layer at ~125 km, the profile shows an enhancement in electron density below 120 km altitude and an additional enhancement in electron density above the V2 peak, bulge at 160 km altitude. A bulge in the electron density above the V2 peak and an additional layer (V3) above 180 km can also be noted which is a diffusion layer [Tripathi et al, J. Geophys. Res., 2023].

on Earth, the heights corresponding to these peaks did not vary significantly with respect to the solar zenith angle. A noteworthy finding from our observations is the presence of the V0 layer at an altitude of approximately 110 ± 4 km. Previously, this layer was observed sporadically, mostly during morning and evening hours. However, this study confirms its consistent presence during the observed period. Despite extensive coverage, the nightside ionosphere of Venus has rarely been observed. This observation leads us to conclude that there is no noticeable transport of electron density from the dayside to the nightside during the deep solar minimum. In summary, the present study sheds light on the distinctive characteristics of different layers in the Venus ionosphere during the deep solar minimum. The radio science experiment onboard the Akatsuki spacecraft, combined with tracking data from multiple locations, allowed us to gain valuable insights into the behavior of the Venusian ionosphere and its response to low solar activity.

Payload Development/ New Instrumentation

RAMBHA-LP payload on Chandrayaan-3

The basic operational parameters and the mechanical/ electrical system aspects related to RAMBHA-LP for Chandrayaan-3 Lander are similar to that of the Chandrayaan-2 version and have been discussed in previous years. The RAMBHA- LP payload consists of the mechanical module and the electronics module. Electronics system Proto FM of Ch-2 is the FM of Ch-3. The T & E and mechanical system of RAMBHA-LP, integrated test of electronics with mechanical system, payload delivery after pre shipment review and integrated test at URSC as well as Deployment test at URSC were completed and reported last year. This year the payload has undergone thermo vacuum tests successfully at URSC and the performance of the payload has been normal. The payload deployment and power on tests were carried out after TVAC. Post dynamic and post deployment tests for RAMBHA-LP have also been completed at URSC and payload performance is normal. Fig.13 shows the photograph of RAMBHA-LP system during spacecraft level deployment & functional test.

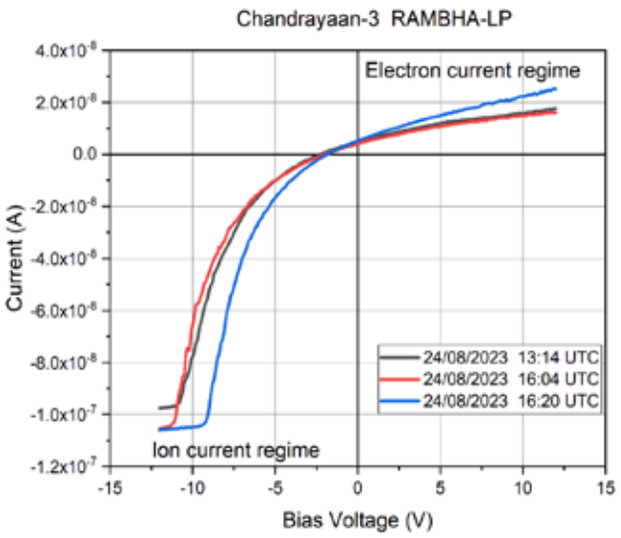

Figure 14: A sample V-I curve observed by RAMBHA-LP on 24 August 2023.

Subsequently, RAMBHA-LP has been successfully operated onboard Chandrayaan-3 Lander, Vikram, in the actual Lunar daytime conditions. RAMBHA-LP was deployed and the regular observations started on 24 August 2023 and continued till 02 September 2023 providing observations at 15 seconds interval. LP could be successfully operated in all modes envisaged and it provided the very first Lunar surface plasma density measurements from the Lunar south pole. Fig. 14 shows a typical plot of the variation of bias voltage versus current observed in RAMBHA-LP on 24 August 2023. The analysis is nearing completion to derive electron and ion densities and electron temperature from the individual observations made during the lunar day.

Development of Geomagnetically Induced Current Sensor

A Technology Development Project (TDP) on the development of a geomagnetically induced current (GIC) monitor has been completed and tested in the laboratory. This TDP involves the measurement of GICs which can potentially flow through power grids causing harmful effects like transformer saturation and failure in extreme

(a) (b)

Figure 13: (a) Photograph of RAMBHA-LP system during Spacecraft level Deployment & Functional Test. (b) The photograph the Chandrayaan-3 lander, showing the shadow of the deployed LP..

cases. The large fluctuations in overhead currents during geomagnetic disturbances result in corresponding variations in geomagnetic fields. These fluctuating fields will induce geo-electric fields on ground and cause GICs to flow with the magnitude of the GIC varying with ground resistivity.

A geomagnetically induced current sensor is developed with a GIC simulator, GIC acquisition system and the required software for filtering and down sampling the data to isolate the GIC component. In the GIC acquisition system, the acquisition is performed using an Arduino-UNO, with appropriate analog front-end. A LEM sensor (LA-55) acts as a current transducer, which is capable of measuring up to 50A of primary current. The Arduino-UNO operates in two modes, a standalone mode as well as a debug mode. The Arduino is configured to measure the temperature as well as the filtered LEM sensor output, using two analog channels. The GIC simulator is capable of generating a small quasi-DC current over high amplitude AC currents in the frequency range of 50~60Hz which is equivalent to actual GIC currents flowing in power grids. The photographs, of the GIC system and integrated GIC system test setup, are shown in Figs.15 and 16 respectively.

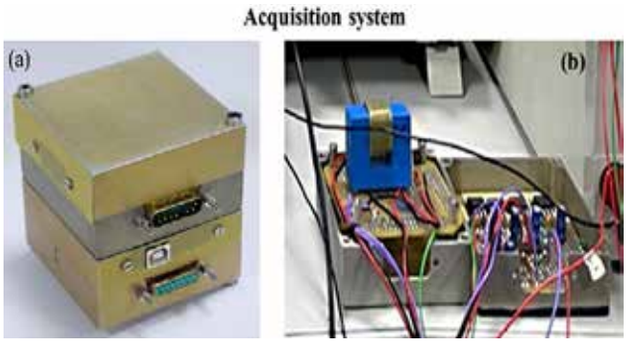

Figure 15: Photograph of enclosed GIC system (left panel) and in open condition (right panel).

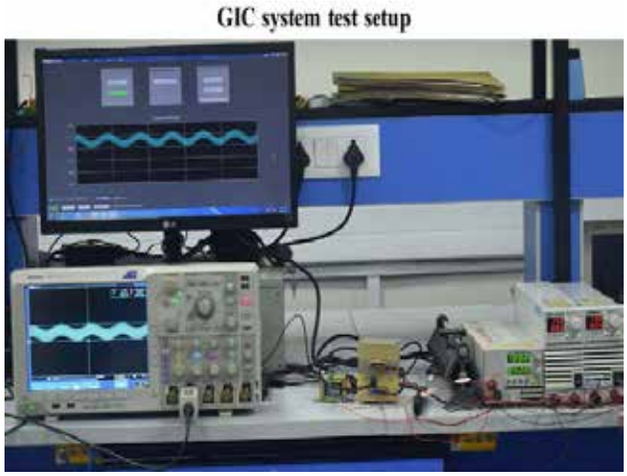

Figure 16: The GIC test setup for evaluating the performance of the sensor in laboratory

The GIC output current from acquisition system for a given input GIC current of 1.00196 A as well as the percentage deviation of the output at different times of the day are shown in Table 1. The ability of the system to delineate the low frequency GIC current from the high frequency noise signal is clear from the Table.

Table 1: GIC output current from acquisition system for a given input GIC current along with the percentage deviation at different times of the day.

GIC input (A)	GIC output (A)	% Deviation
1.00196	1.00195	-0.00100
1.00196	1.00684	0.48705
1.00196	1.00195	-0.00050
1.00196	0.99707	-0.48834
1.00196	1.00195	-0.00050
1.00196	1.00684	0.48734
1.00196	1.00195	-0.00050
1.00196	1.00684	0.48734
1.00196	1.00195	-0.00050
1.00196	1.00684	0.48715
1.00196	0.99707	-0.48834
1.00196	1.00195	-0.00050
1.00196	1.00195	-0.00050

Development of Atomic OXygen Sensor (ATOXS)

Atomic Oxygen (ATOX) is the predominant constituent in the Earth's thermosphere within altitudes ranging from 180 km to 700 km and is of significant consequences for both, spacecraft designers and space scientists. When a satellite moves through its orbit at typical velocities in Low Earth Orbit (LEO), impinging ATOX can lead to erosion of spacecraft materials. Being the dominant constituent at LEO altitudes, ATOX exerts a substantial drag force on spacecraft. In addition, ATOX plays a crucial role in the photochemistry of the upper atmosphere, acting as an important sink for solar energy. Given its long lifespan at LEO altitudes, ATOX can be employed as a tracer to study dynamic motion, vertical transport, atmospheric tides, and winds. Accurate knowledge of the distribution of ATOX, its diurnal and annual variations is essential to comprehend atmospheric photochemistry and energy balance. Atmospheric models like MSIS often have estimation errors of up to 25%, underscoring the necessity for in situ measurements of ATOX in the upcoming space missions.

To address this need, an ATomic OXygen Sensor (ATOXS) payload is proposed in the PS4 Orbital Platform, which operates based on the principle of change in conductance of a semiconductor thin film upon ATOX adsorption. Experimental studies have shown that when ATOX is absorbed by a semiconductor sample, pseudo surface states are created, leading to a decrease in the sample's intrinsic conductivity. This particular experiment employs a thin

film of Zinc Oxide, offering advantages such as compact size, low power consumption, and the ability to regenerate the sensor through heating.

Over the past year, the design of the ATOX sensor underwent multiple revisions and optimizations, considering various implementation constraints. A three-dimensional sensor layout has been worked out (Fig.17). Collaborative efforts with different entities of VSSC facilitated the coating of samples, with the alumina substrate manufactured by GEM/MME/MMG entity at VSSC. The masks for sensor deposition were fabricated at AMFF/CASG/ESAE entity. The material deposition was conducted using thermal evaporation technique at Indian Institute of Science & Technology (IIST). Several options, including gold and silver, were tested as track materials. However, due to the thinness of the tracks, soldering was not feasible as the solder tend to detach. Consequently, wire bonding technique using TECA-16 (thermally and electrically conducting adhesive) for sensor connections and ATCAP (a thermally conducting adhesive) for thermistor connections was employed during lab tests. These bonding processes were carried out at PSCD/PSCG/PCM, VSSC. A VSSC technical report was released (ISRO-VSSC_TR-0569-0-22) which provides detailed information on various aspects of the design and simulations performed. The development of an appropriate heating system for this ATOX Sensor is being carried out currently. The heating system is an important aspect for this experiment as it ensure sensor reusability in the orbit. The system developed is undergoing laboratory tests and is to be calibrated with standard atomic oxygen source.

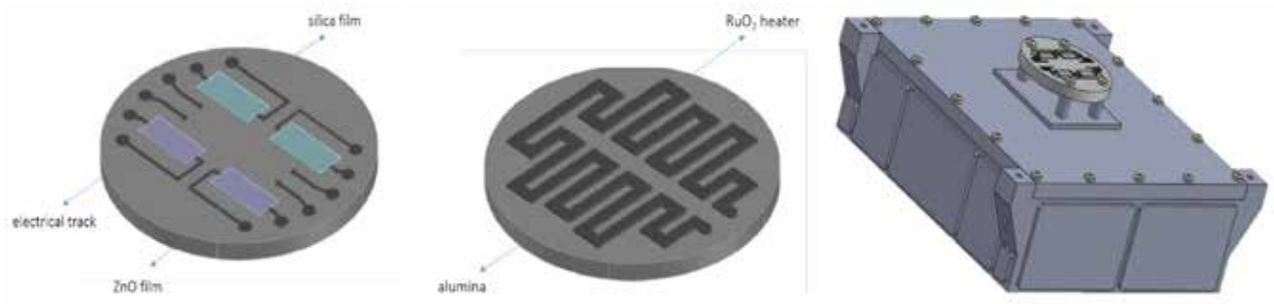

Figure 17: 3D CAD model of ATOXS.

Future Projections

- The very first set of near surface, direct plasma measurements from Lunar polar region using indigenously developed RAMBHA-LP payload aboard ISRO's Chandrayaan-3 mission have brought some new aspects of Lunar plasma dynamics and opened up a new area for detailed scientific investigation. These aspects will be explored.
- We continue to explore newer aspects of planetary atmosphere-ionosphere through in-house developed models in context of the radio occultation measurements of planetary environments.
- The Earth's magnetosphere, ionosphere, thermosphere is being studied as an integrated system. It's behaviour is being explored using ground and satellite based data/measurements, in-house developed models along with global model TIEGCM. These studies are envisaged to bring forth new results.
- The manifestations of the interactions of northward oriented interplanetary magnetic field with Earth's magnetosphere in the thermosphere-ionosphere system will be comprehended better on account of our ongoing studies.
- Studies concerning inner magnetospheric response to varying space weather conditions, especially in context of behaviour of energetic particles, are on and results awaited.
- The Equatorial Electrojet in terms of HF radar measured drifts, and inferred changes in the prevailing electric field are being systematically investigated for the current solar activity epoch of Solar cycle 25 which is approaching maximum.
- The problem of day-to-day variability in the Equatorial Spread-F onset, evolution and duration is being addressed with focus on the seeding perturbations and an effort will be made to address this problem end-to-end.
- As we continue to be actively participating in ISRO's forthcoming planetary missions through developing (a) experiments/payloads in-house, (b) ionospheric models, it is aimed to enhance the scope of our studies to planetary ionospheres involving both measurements and models. Further, some new experiments will be done from ISRO's PS-4 and sounding rockets platforms.

- In order to achieve the objective of monitoring, studying and eventually modeling the impact of space weather specifically over the Indian region, the INSWIM chain of stations will be strengthened through inclusion of more multi-constellation multi-frequency receivers multi-wavelength nightglow photometers and ionosondes. A 3-D ionospheric tomography framework based on INSWIM's multi-constellation multi-frequency receivers has been developed. This will be yielding new insight in to the ionosphere over low and equatorial latitudes.

Publications in Peer-Reviewed Journals

1. Mridula N, G. Manju, S. Sijikumar, Tarun Kumar Pant, Raj Kumar Choudhary, "On the significant impact of the 17 March 2015 St. Patrick's Day geomagnetic storm on the ionosphere over Indian region", Advances in Space Research, 70, 3674-3685, https://doi.org/10.1016/j.asr.2022.08.022, 2022.
2. Ambili, K. M. and R. K. Choudhary, On the impact of meridional wind circulation changes in the electron density distribution over the Indian equatorial and low latitude ionospheric region during a severe geomagnetic storm, Advances in Space Research, https://doi.org/10.1016/j.asr.2023.04.046, 2022.
3. Tripathi, K. R.,, R. K. Choudhary, Lakshmi Jayalal, On the estimation of frequency residuals in a radio occultation experiment, Monthly Notices of the Royal Astronomical Society, Volume 517, Issue 1, Pages 776-786, https://doi.org/10.1093/mnras/stac2653, 2022.
4. Gokani, S. A., D. S. Han, R. Selvakumaran, T. K. Pant, Dependence of radiation belt flux depletions at geostationary orbit on different solar drivers during intense geomagnetic storms, Frontiers in Astronomy and Space Sciences 9, 95248, doi: 10.3389/fspas.2022.952486, 2022.
5. Ambili, K. M., Tripathi, K. R., Choudhary, R. K., and Imamura, T., "On the origin and characteristic features of the V 1 layer in Venus ionosphere using Akatsuki radio science experiment and the one-dimensional photochemical model", Monthly Notices of the Royal Astronomical Society, 516(4), 5555-5562. https://doi.org/10.1093/mnras/stac2624, 2022.
6. Vineeth, C., K. M. Ambili and T. K. Pant, On the Behavior of Thermospheric O1D 630.0 nm Dayglow Emission during Counter Electrojet Events, Adv. Space Res., 71 115-128, https://doi.org/10.1016/j.asr.2022.08.048, 2023.
7. Hossain, M. M, T. K. Pant and C. Vineeth, Nocturnal thermospheric neutral wind and temperature measurement using a Fabry-Perot Interferometer: First results from an equatorial Indian station, Adaces in Space Research, https://doi.org/10.1016/j.asr.2023.03.040, 2023.
8. Choudhary, R. K., St.-Maurice, J.-P., and Ambili, K. M., The particularly clean response of the Indian sector to a strong but short lived geomagnetic storm; Advances in Space Research. https://doi.org/10.1016/j.asr.2023.05.048, 2023.
9. Ambili, K. M and R.K. Choudhary, The role of the storm-time prompt penetrating electric field on the net distribution of plasma density over the low latitude ionospheric regions; K Advances in Space Research, ISSN 0273-1177, https://doi.org/10.1016/j.asr.2023.04.046., 2023.
10. Tripathi, K.R., R.K. Choudhary,, K.M. Ambili and T.Imamura,, Venusian ionosphere during deep solar minima: Some new insights using Akatsuki radio science experiment. Journal of Geophysical Research: Planets, p.e2023JE007768, https://doi.org/10.1029/2023JE007768, 2023.
11. Tripathi, K. R., R. K. Choudhary,, J. S. Jose,., K. M. Ambili,, & T. Imamura., Gravity wave modulations at the lower altitudes of Venus ionosphere; Geophysical Research Letters, 50(4), e2022GL101793, https://doi.org/10.1029/2022GL101793, 2023.
12. Manju, G., N. Mridula,, T. V. Sruthi,., T. K. Pant,, R. P. Aswathy,., P. Sreelatha,, et al., Generation of post sunset E region electron density stratifications at the magnetic equator: An analysis using in situ measurements and theoretical estimations. Journal of Geophysical Research: Space Physics, 128, e2022JA030903. https://doi.org/10.1029/2022JA030903, 2023.
13 . Singh, P. R., A. K. Singh, T. K. Pant, Solar wind plasma variations with interplanetary magnetic field during solar cycles 22-24, Journal of Astrophysics and Astronomy 44 (1), 14, https://doi.org/10.1007/s12036-023-09916-0, 2023.

Scientific/Technical Reports

1. Ayisha M . Ashruf and Pramod P P, Design of an ATomic OXygen Sensor (ATOXS) for Low-Earth Orbit Applications, ISRO-VSSC-TR-0569-0-22.

Articles/Book Chapters

1. Ayisha M. Ashruf, Chapter 2 - Moon's Influence on Earth - The Story of a Long and Fruitful Partnership, On the Shores of Tranquility - A Preface to the Moon, Vikram Sarabhai Space Centre, July 2022.
2. Ayisha M. Ashruf, Chapter 11 - Lunar Colonization - Fiction and Reality, On the Shores of Tranquility - A Preface to the Moon, Vikram Sarabhai Space Centre, July 2022.
3. Joarder, R., Dai, B.K., Nagaraju, K., Roopa, M.V., Ramakrishna, B.N., Choudhary, R.K, Estimation of Mars Orbiter Orbit Based on Mars Color Camera Images. In: Kumar, S., Setia, R., Singh, K. (eds) Artificial Intelligence and Machine Learning in Satellite Data Processing and Services. Lecture Notes in Electrical Engineering, vol 970. Springer, Singapore. https://doi.org/10.1007/978-981-19-7698-8_2, 2023.

Presentations in Symposia/Workshops/Conferences

1. Sruthi, T.V., G. Manju., "Study of Ionospheric Irregularities Using Rocket Borne In-Situ Measurement Probes in Association With Ground Based HF Radar Observations During Different Geophysical Conditions", 16th International Symposium on Equatorial Aeronomy [ISEA-16] at Kyoto university Japan, September 12-16, 2022.
2. Sruthi, T. V., G. Manju, "Study on the role of gravity wave induced perturbations for the sustenance of night time ionospheric plasma irregularities using multi beam HF radar observation in association with ionosonde and GPS data at Thumba", URSI-Regional Conference on Radio Science (URSI-RCRS 2022), at IIT Indore, 1-4 December, 2022
3. Manju G., RAMBHA-LP payload on Chan ayaan 3 mission: An overview. Chandrayaan-3 Data analysis and training workshop, 28-29 March 2023.
4. Vineeth, C, K. M. Ambili and T. K. Pant, "Signature of the MTM Phenomenon in Thermospheric Oxygen Airglow Emissions: Results from the First Ship-Borne Airglow Measurements from the Indian Region", 44th COPSAR Assembly, Athens Greece, 16-24 July 2022.
5. Ambili K.M., and R. K. Choudhary,"Three-dimensional distribution of surface boundary exosphere and the resultant ionosphere of the Moon",, Commission B, 44th COPSAR Assembly, Athens Greece, 16-24 July 2022.
6. Keshav R. Tripathi, R.K. Choudhary, K. M. Ambili, R. Manikantan, and Umang Parikh "A study on the characteristic features of the lunar ionosphere using DFRS experiment onboard Chandrayaan-II" Commission B, 44th COPSAR Assembly, Athens Greece, 16-24 July 2022.
7. Richa Jain, "Frontier Symposium in Physics" (FP-PHY 2023) Indian Institute of Science Education and Research, Thiruvananthapuram, 25-26 February 2023.
8. Richa Jain, 'A study on the evolution of fast solar wind streams in the inner solar corona using results from solar radio sounding experiments conducted by Akatsuki Spacecraft' in the Akatsuki-SWT#23 (Science Working Team), JAXA, 30th May, 2023.
9. Richa N. Jain, R. K. Choudhary, Anil Bhardwaj, and T. Imamura, "Coronal Plasma Turbulence characteristics and flow speeds using Radio sounding experiment by Akatsuki spacecraft", by in URSI - RCRS 2022, IIT (Indore), India, 1 - 4 December, 2022
10. Keshav R. Tripathi, and R.K. Choudhary, "Quantitative assessments of errors in the planetary at atmospheric / ionospheric profiles derived from Radio Occultation measurements", at AGU Fall Meeting 2022, Chicago, USA during 12-16 December 2022.
11. Keshav R. Tripathi, R.K. Choudhary, K M Ambili, "Evidence for the enhanced electron density in the wake region of the Lunar ionosphere using dual-frequency radio science (DFRS) experiment onboard Chandrayaan-2 orbiter, AGU Fall Meeting 2022, Chicago, USA, 12-16 December 2022.
12. Ajay Potdar and R. K. Choudhary, "Simulating three-dimensional ionospheric electron density reconstruction using IRI model and SMART technique", International Reference Ionosphere Workshop held at the Korea Astronomy and Space Science Institute, Daejeon, South Korea, 8-19 May, 2023

13. Ajay Potdar and R.K. Choudhary, "Comparison of F2 layer characteristics over the dip-equator in the Indian Ionospheric sector using the IRI model and long term ionosonde observations.", International Reference Ionosphere Workshop held at the Korea Astronomy and Space Science Institute, in Daejeon, South Korea, 8-19 May, 2023
14. Ajay Potdar and R.K. Choudhary, " 3D tomography of ionosphere above the Indian region using InSWIM GNSS network receivers", International Symposium on Equatorial Aeronomy, Kyoto University, 12-16 September 2022.
15. Tarun Kumar Pant, Manju G., Vineeth C., Md. Mosarraf Hossain, Ankush T. Bhaskar, Satheesh Thampi, "Day-to-day changes in equatorial electrodynamics and response to Transient solar processes - Need for an aeronomy satellite at geostationary orbit", 5th COSPAR symposium on "Space science with small satellites", Nanyang Technical University, Singapore, 16-21April, 2023.
16. Ankush Bhaskar, Tarun Kumar Pant, Satheesh Thampi, Jayadev Pradeep, Vineeth C., Vipin Yadav, Smitha V. Thampi, "Twin CubeSat mission to study aurora and particle precipitation asymmetries in northern and southern auroral ovals" 5th COSPAR symposium on "Space science with small satellites", Nanyang Technical University, Singapore, 16-21 April, 2023

Conference/Workshop

1. Mridula N., Workshop and Hands on training on Chandrayaan-3 payload data utilization, 28-29 March 2023, ISSDC, Bangalore.
2. Ambili, K. M., Workshop on Space Situational Awareness & Space Traffic Management, Organised by ISRO and Astronautical Society of India in association with IN-Space and NSIL, 11-13 January 2023, Bengaluru.
3. Ambili, K. M., First Russian-Indian joint online workshop on Lunar Exploration, 25 January 2023.
4. Richa Jain, USO - PRL Solar Physics Workshop (USPW-2023) organized by Udaipur Solar Observatory, 3-5April, 2023
5. Richa Jain, Radio Astronomy School (RAS-2023) at NCRA (National Center for Radio Astrophysics) -TIFR, GMRT, Pune, 11-27 March, 2023.
6. Richa Jain, Science from In-situ Measurement from Aditya L1 (SIMA-01), Space Physics Laboratory, VSSC, Trivandrum, 11-13 April, 2023.
7. Ayisha Ashruf, Science from In-situ Measurements of Aditya-L1 (SIMA-01), Space Physics Laboratory, VSSC, Trivandrum, 11-13 April, 2023.
8. Ajay Potdar, Capacity building and the International Reference Ionosphere Workshops held at the Korea Astronomy and Space Science Institute, in Daejeon, South Korea, 8- 19 May, 2023.
9. Mridula N., Workshop on space situational awareness and space traffic management, organised by ISRO, 11-13 January 2023, Bangalore.

Deputations

Choudhary R. K.

- 44th COSPAR Scientific Assembly, 14-26 July 2022, Athens, Greece.

Ambili K. M.

- 44th COSPAR Scientific Assembly, 14-26 July 2022, Athens, Greece.

Tarun Kumar Pant

- 5th COSPAR symposium on "Space science with small satellites", Nanyang Technical University, Singapore, 16-21 April, 2023.

Ajay A. Potdar

- Capacity Building and International Reference Ionosphere Workshops held, Korea Astronomy and Space Science Institute, Daejeon, South Korea, 8-19 May, 2023.

Invited Talks

Tarun Kumar Pant

- "Study of the variability in the ionospheric zonal drift and electric field - an investigation of dynamo region using HF radar at 18 MHz over equator", URSI - RCRS 2022, IIT (Indore), India, 1 - 4 December, 2022.
- "Space weather and atmospheric environments", ISRO's Structured Training Programme, ISTRAC, Bangalore, 16-20 January 2023.
- "Space - Situational Awareness and Weather", IMPRESS Programme, Indian Institute of Geomagnetism, Navi Mumbai, 13-14 February 2023.
- "Solar-Terrestrial Interaction and Space Weather", Virtual Conference on the Frontiers in Space and Atmospheric Sciences, (COFSAS-2023), 15-16 March, 2023.
- "Exoplanets & Life Components", YUVIKA Programme, HRDD, Vikram Sarabhai Space Centre, 19 May, 2023

Manju G.

- "Solar terrestrial relations and implications for space weather: An overview", Sri Sathya Sai Arts and Science College, Saigramam, Thiruvananathpuram, 10 October, 2022
- "Ionospheric studies and Aditya L1 relevance", SIMA-01 workshop, Space Physics Laboratory, VSSC, 11-13 April, 2023.

C. Vineeth

- *"The Moon",* Moon Day Celebration, GGHSS, Cotton Hill, Thiruvanathapuram, 21 July, 2022.
- "Sun Earth Connections and Space Weather", Refresher Course Winter School in Physics and Chemistry, UGC-Human Resource Development Centre, Kannur University, 07 December 2022.
- "Space Weather and its Terrestrial Impacts", Sri Sathya Sai Arts and Science College, Saigramam, Thiruvananathpuram, National Science Day, 28 February 2023.
- "Venusian Upper Atmosphere and Solar Wind Interactions", Theme based discussions on Venusian Ionosphere and Solar wind interaction science, SPO, ISRO HQ, 26 April 2023.
- 'Celestial Bodies', YUVIKA Programme, HRDD, VSSC, 18 May 2023.

Mridula N.

- "Advances in Space Weather Monitoring and prediction: A global perspective", workshop on "Journey of Meteorological Instrumentation Systems", SAMEER, IIT Mumbai, 23- 24 February 2023.

Richa Naja

- "Dynamics in Inner-Middle Corona", USO-PRL Solar Physics Workshop (USPW-2023) Udaipur Solar Observatory, 3-5 April, 2023.

ग्रहीयविज्ञान शाखा
Planetary Science Branch

ग्रहीय विज्ञान शाखा (पीएसबी) सूर्य, ग्रहों, चंद्रमाओं तथा धूमकेतुओं के मॉडलिंग तथा प्रयोगात्मक अन्वेषण में प्रयासरत है। यह मुख्यतः तीन प्रमुख विषयों पर केंद्रित है। (क) सौर पवन तथा इसकी सौर मंडल के ग्रहों तथा अन्य ग्रहीय पिंडों के साथ परस्पर क्रिया (ख) सौर विकिरण की ग्रहीय वायुमंडल के साथ परस्पर क्रिया तथा इनकी परस्पर क्रिया से उत्पन्न प्रक्रम (ग) ग्रहीय पिंडों के वायुमंडल की संरचना तथा इनकी गतिकी। इन उद्देश्यों की पूर्ति हेतु यह शाखा, सौर पवन प्लाज़्मा, अंतरग्रहीय तथा ग्रहीय चुंबकीय क्षेत्रों, साथ ही प्लाज़्मा के अभिलक्षणों तथा ग्रहीय वायुमंडल के निरावेशी कणों के मापन हेतु अत्याधुनिक वैज्ञानिक प्रदायभारों की संकल्पना, अनुकरण, अभिकल्पना तथा विकास का कार्य करती है।

The Planetary Science Branch (PSB) carries out experimental and modeling investigations of the Sun, planets, moons and comets, mainly focusing on three major themes: (a) Solar wind and its interaction with solar system planets and planetary bodies, (b) Interaction of solar radiation with planetary atmospheres and the processes initiated through this interaction, and (c) Dynamics and composition of the atmospheres of planetary bodies. To realize these objectives, this group undertakes the conceptualization, simulations, design and development of state-of the- art scientific payloads for the measurement of solar wind plasma, interplanetary and planetary magnetic fields as well as the characteristics of plasma and neutrals in the planetary atmospheres.

वैज्ञानिक टीम / Science Team
सतीश तंपी आर. / Satheesh Thampi R.
स्मिता वी. तंपी / Smitha V. Thampi
विपिन कुमार यादव / Vipin Kumar Yadav
धन्या एम. बी. / Dhanya M. B.
वेन्कटरामन वी. / Venkataraman V.
अभिषेक जे. के. / Abhishek J. K.
अंकुश टी. भास्कर / Ankush T. Bhaskar
चेमुकुला मात्तिन यादव / Chemukula Mathin Yadav

तकनीकी टीम / Technical Team
दिनकर प्रसाद वज्जा / Dinakar Prasad Vajja
अनीष ए. एन. / Aneesh A. N.

अनुसंधान सहयोगी/एनपीडीएफ / Research Associates/NPDF
शीर्ष लता सोनी / Shirsh Lata Soni *
रूबिया आर. / Rubia R.
सेल्वाकुमारन आर. / Selvakumaran R.#

अनुसंधान अध्येता / Research Fellows
इंदु वेणुगोपाल / Indu Venugopal
शिबोतोष बिश्वास / Shibotosh Biswas

 # Relieved in January 2023
** Relieved in February 2023*

Modeling studies of Planetary and Lunar Plasma Environments

Electrostatic solitary waves in the Venusian ionosphere pervaded by the solar wind: A theoretical perspective

The electrostatic solitary waves (ESWs) in the Venusian ionosphere impinged by the solar wind is investigated using a homogeneous, collisionless and magnetized multi-component plasma consisting of Venusian H^+ and O^+ ions, Maxwellian Venusian electrons and streaming solar wind protons and suprathermal electrons following κ– distribution. The model supports the propagation of positive potential slow O+ and H+ ion-acoustic solitons. The evolution and properties of the solitons occurring in two sectors, viz., dawn-dusk (DD) and noon-midnight (NM) sector of the Venus ionosphere at an altitude of (200-2000) km is studied. The theoretical model predicts positive potential solitons with amplitude ~ (0.067-56) mV, width ~ (1.7-53.21) m and velocity ~ (1.48 -8.33) km s^{-1}. The bipolar soliton electric field has amplitude ~ (0.03-27.67) mV m^{-1} with time duration ~ (0.34-22) ms. These bipolar electric field pulses, when Fourier transformed to the frequency domain, occur as a broadband electrostatic noise with frequency varying in the range of ~ 9.78 Hz to 8.77 kHz. Fig. 1 shows the plot of (a) normalized potential φ vs. ξ, and (b) normalized electric field, E vs. ξ for slow O^+ ion-acoustic mode at an altitude of 1000 km for different parameters. The results can explain the observed electrostatic waves in the frequency range of 100 Hz to 5.4 kHz in the Venus ionosphere by the Pioneer Venus Orbiter (PVO) mission. The model can also be relevant in explaining the recent observation of ESWs in Venus magnetosheath by the Solar Orbiter during its first gravity assist maneuver of Venus.

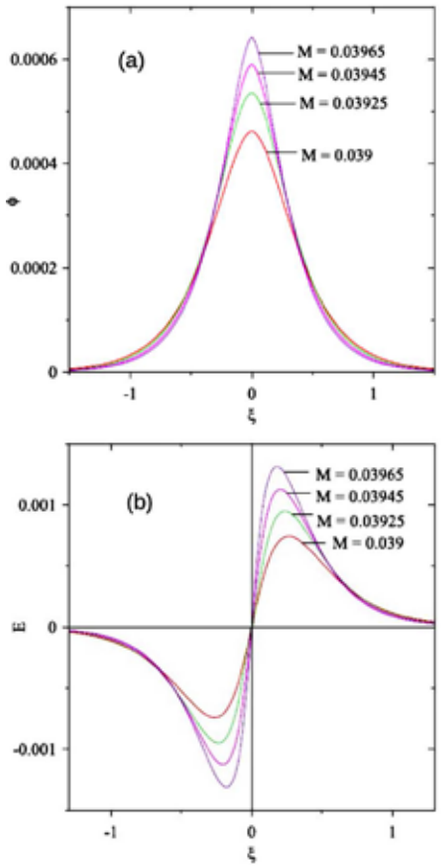

Figure 1: Plot of (a) normalized potential φ vs. ξ, and (b) normalized electric field, E vs. ξ for slow O^+ ion-acoustic mode at an altitude of 1000 km for the parameters: n_{vh0}=0.4, n_{vo0} = 0.5, n_{sp0}=0.1, v_0=4.92, $\sigma_{vh} = \sigma_{vo}$ = 0.005, σ_{sp}=0.5, σ_{be}=0.025, and k=2 [Rubia et al., 2023].

Investigations of Plasma Instability in Lunar Ionosphere

The two-stream instability (TSI) generation in the lunar ionosphere is analyzed by taking the TSI as a small perturbation in plasma number density which leads to the bunching of electrons and the resulting electric field grows with time. Eventually this growth facilitated by the plasma background itself. In the lunar ionosphere, this instability is generated when the electron plasma in the solar wind encounters the lunar electron plasma. In this analysis, the conditions which allow the instabilities to form and how they evolve with time (the growth factor) are obtained, which shows that not all modes, at a certain altitude, grow at the same rate. The TSI dispersion relation about the local plasma gives two solutions which are complex conjugates of each other. The solution corresponding to $+\omega_{im}$ correspond to the instability and the solution with $-\omega_{im}$ corresponds to a decaying mode as with time the amplitude will decrease with time. These growing and decaying modes show striking similarity in its properties with the instability. It is seen that a mode with the highest decay rate will decay early and with increasing n_e, the k value with the highest decay rate will also increase. The interaction of solar wind plasma with the lunar electron background is carried out with PIC simulations and is shown as the phase-space diagram in Fig. 2.

Planetary & Terrestrial Space Weather

Investigation of the energisation of Martian ionospheric plasma during the passage of a stealth CME

Solar eruptions like coronal mass ejections (CMEs) are usually associated with low-coronal signatures like flare, magnetic reconnection, jets or filaments that assist in understanding the magnetic flux rope configuration in the CME source region. However, classes of eruption called "stealth CMEs" lacks such low-coronal signatures and hence pose difficulty in connecting a specific source region on the Sun. During the declining phase of Solar cycle 24, a stealth CME impacted Mars (max v_{sw} = 580 km s^{-1} near 1.5 AU) and caused a major space weather event during 27-28 August 2018. The impact of the stealth CME on the topside of the Martian ionosphere was investigated using Solar

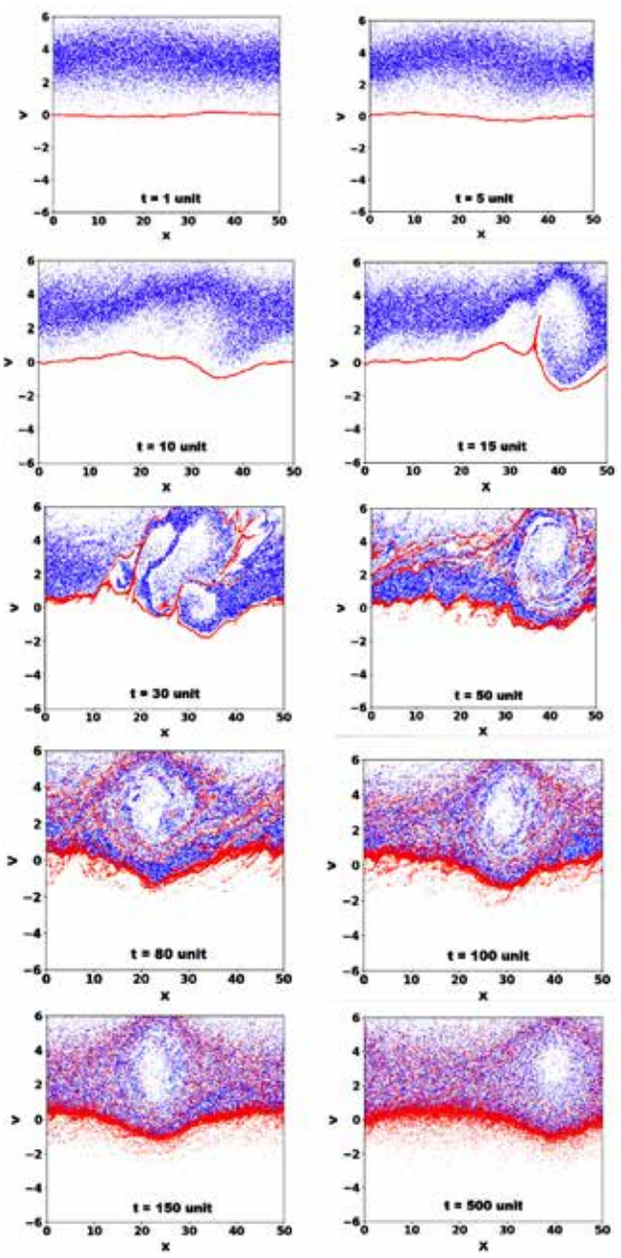

Figure 2. The phase space simulation plot outputs for various time steps starting from t = 1 unit to t = 500 units [Chakrabarty, Yadav and Kumar, 2023].

Wind Ion Analyser (SWIA), Solar Energetic Particle (SEP) and Suprathermal and Thermal Ion Composition (STATIC) onboard Mars Atmosphere and Volatile EvolutioN (MAVEN) mission. Variation in ion and electron fluxes within the plasma boundaries during the passage of stealth CME were observed using Electron Spectrometer (ELS) and the Ion Mass Analyser (IMA) sensors onboard Mars Express (MEX) mission. The plasma boundaries of the induced magnetosphere of Mars showed considerable enhancement in the observed fluxes during the event. SWIA observations during the interaction of the CME with the Martian plasma environment showed enhancement in the ion flux. STATIC observations showed energisation of planetary heavy ions like O^+ and O_2^+ to energies between 10 eV up to several hundreds of eV at altitudes near 300 km (Fig. 3). SEP measurements of energetic O+ pick-up ions at energies below 50 keV further support the claim on planetary ion energisation. Energisation of both heavy and lighter ions during the event at ionospheric altitudes of Mars suggest deeper penetration of solar wind causing considerable acceleration and heating of the ionospheric plasma leading to enhancement in atmospheric loss.

The global response of terrestrial ionosphere to the December 2015 space weather event

Tracing a space weather event from its origin at Sun to its impact at Earth is essential in view of several practical applications. This is also important in view of the upcoming Aditya L1 mission and the Aeronomy satellite mission being planned. In this context, the space weather event of December 19-21, 2015 was studied. It is seen that the event was initiated by two successive CME eruptions, and this caused a G3 space weather event on Earth. The event has been studied using the in situ electron density (N_e), electron temperature (T_e) and the Total Electron Content (TEC) measurements from SWARM-A satellite, as well as the O/N_2 observations from TIMED/GUVI. The observations reveal the longitudinal and hemispherical differences in the ionospheric response to the storm event. A positive ionospheric storm was observed over the American, African and Asian regions on 20 December, and the next day showed a negative storm. Both these exhibited hemispheric differences. A positive storm was observed over the East Pacific region on 21 December. It is seen that the net effect of both the disturbance dynamo electric field and composition differences become important in explaining the observed variability in topside ionospheric densities. The morning overshoot of T_e showed a clear enhancement over Southern mid-latitudes in contrast to the typical quiet time pattern. Fig. 4 shows the global map of in situ topside electron density observed by SWARM-A for (a) 18 December 2015 (quiet day) and (b) 20 December 2015 (event day) respectively.

The Possible Cause of the Most Intense Geomagnetic Superstorm of the 21st Century (20 November 2003 event)

All notable space weather events (superstorms) are caused by interplanetary coronal mass ejections (ICMEs). But not every ICME leads to an extreme storm. How an extreme storm forms, or which explicit characteristic of ICME actually is responsible for inducing a superstorm is still not well understood. In this context, the ICME characteristics that are mainly responsible for the most intense storm of the current century that occurred on 20 November 2003 are re-investigated. Interestingly, the studied ICME magnetic cloud shows characteristics of extremely flattened (pancaked) structure i.e. quasi-planar magnetic structure (PMS). The pancaked ICME shows less adiabatic expansion than usual in the compressed direction, which

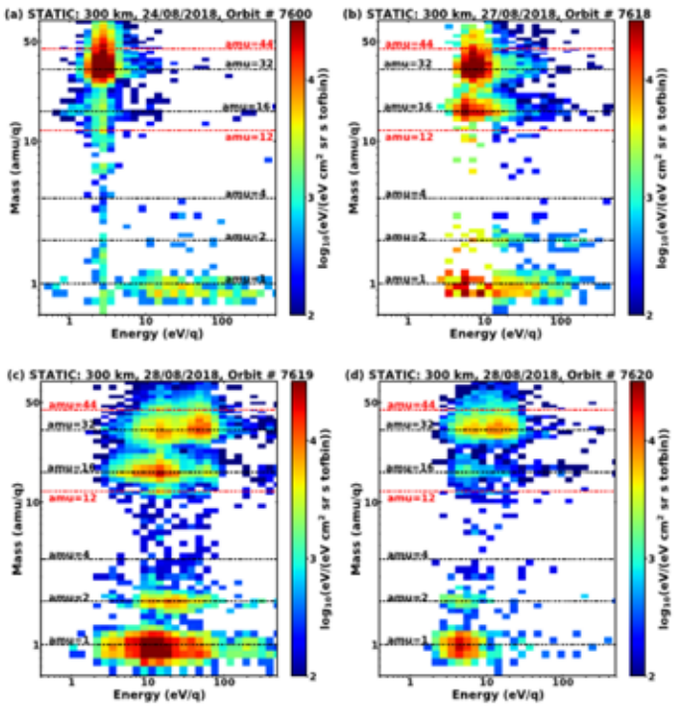

Figure 3: STATIC observations at an altitude of 300 km during the quiescent and in the course of interaction of the stealth CME and Martian upper atmosphere. The panels a & b show the observations during the quiescent and event orbits 7600, 7618 respectively on 24 and 27 August 2018. The panels c & d panel show the plasma energisation during the impact of the stealth CME on 28 August 2018 in the orbits 7619 and 7620 [Venkataraman and Thampi, 2023].

leads to enhanced magnetic field, high plasma density, high solar wind speed, high dynamic pressure, and high eastward interplanetary electric field. Further, the study indicates that the ICME transformed into a quasi-PMS had the aforementioned enhanced features with a strong southward magnetic field component that contributed to efficiently transferring plasma and energy into the Earth's magnetosphere to cause the observed superstorm.

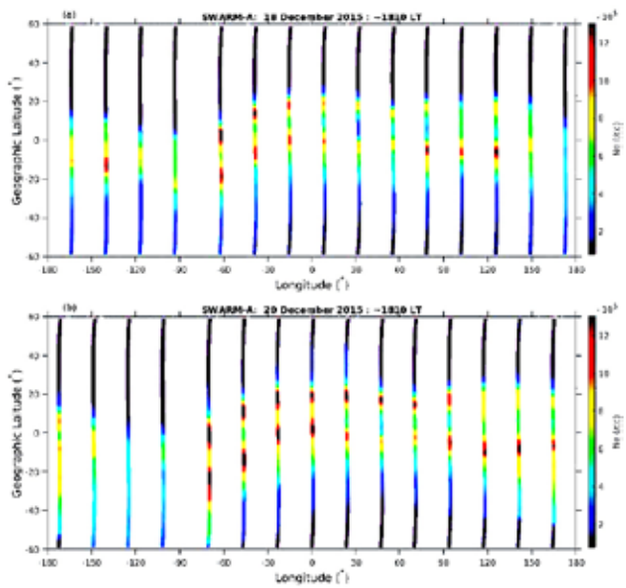

Figure 4: Global map of in situ topside electron density observed by SWARM-A for (a) 18 December 2015 (quiet day) and (b) 20 December 2015 (event day) [Thampi et al., 2022].

Experiments in Aditya-L1 Mission

Plasma Analyser Package for Aditya (PAPA)

Test and Calibration

Plasma Analyser Package for Aditya (PAPA) onboard Aditya-L1 mission was successfully realised and after completing the T&E and calibration, the payload was flagged off by Director, VSSC on 02nd November 2022 and was delivered to URSC on 04th November 2022. Subsequently, the payload was baked for more than 51 hrs and moved to clean room for integration. The payload was integrated with the Aditya-L1 spacecraft (Fig. 5) and all the disassembled and assembled mode tests using spacecraft checkout was performed successfully.

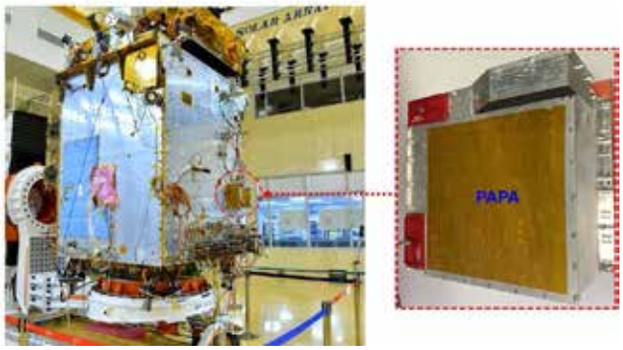

Figure 5: PAPA payload onboard Aditya-L1 spacecraft mounted on the EP-01 Panel.

Aditya-L1 spacecraft was subjected to Thermovac tests at CATVAC facility ISITE, and during the cold soak cycles

(long and short), PAPA payload high voltage was enabled and all the different modes of operations envisaged were tested including the mission scenario tests (MST) using MACROS. The complete data sets were analysed and presented to the thermovac committee for clearance. Since the payload was operated under no source condition, only dark counts are expected during these tests. It was found that the performance of both SWEEP and SWICAR sensors are as expected and satisfactory.

PAPA Calibration

PAPA Proto-Flight Model (PFM) and Flight Model (FM) were calibrated at High Vacuum Space Simulation Facility (HVSSF) at SPL using the electron and ions sources. Considering the time critical nature of the delivery of payload, a calibration strategy was adopted wherein the FM calibration was primarily targeted at key parameters verification, Lookup table (LUT) generation and Environmental Test & Evaluation, whereas the PFM underwent a broader calibration covering a wide swath of input scenarios. The calibration plan was also formulated keeping in mind the ultra-high vacuum requirement of 2 x 10^{-6} mbar required for safe operation of High Voltage Programmable Power Supply (HVPPS) subsystem in PAPA, and also that payload should not exceed the safe operating temperature limit of 50^{0}C. The key payload specifications that were tested includes: 1. Energy resolution, 2. Angular resolution, 3. Field of view, 4. Time of Flight bin positions. All these benchmark parameters were recorded at multiple energy and direction values for initial SRC tests. Subsequent to ISRC, PFM underwent EMI-EMC, Thermo-vacuum test and vibration. The set of benchmarks were evaluated after each environment stress test. The FM was subsequently subjected to T&E following the same sequence. The section below details the calibration results of PAPA.

Energy Resolution

The energy resolution of both SWEEP and SWICAR sensors were tested by positioning the sensors along the line of sight of the particle beam and varying the incident energy. The SWEEP sensor energy range of 10 eV to 3 keV is divided into 16 energy bins. The analyser plate voltage corresponding to each bin was determined first. The voltage determination involves enabling the default mode in the payload followed by loading a modified LUT which contains 512 values centred on a tentative voltage obtained from EM calibration, and scanning to find the exact analyser voltage corresponding the incident energy. This process was repeated for all energy bins. Following this step, the payload was switched to calibration mode, and the energy response of each analyser voltage was determined. In addition to the normal incidence condition, the analyser voltage-energy bin relations as well as the energy resolution were tested for the entire field of view of the payload. Individual energy response curves were generated first and then consolidated to obtain the energy resolution throughout the energy range. Fig. 6 shows the PAPA SWEEP sensor energy resolution for the entire energy range. It is clear from the figure that energy resolution is between 8-9% at low energies (< 100 eV) and above which is giving good energy resolution of < 8% and the results are matching well with the projected simulated values mentioned in the CDR document.

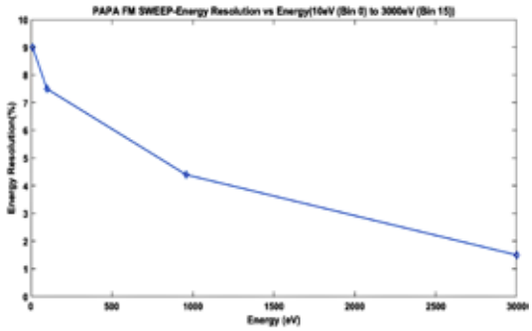

Figure 6: PAPA FM SWEEP energy resolution (%) vs. Energy (eV)

SWICAR sensor has two operating modes, one for electron detection and the other for ion detection. These modes were tested independently. The test procedure for SWICAR-electron mode was similar to that of SWEEP. The only extra step involved the determination of the attraction electrode voltage in addition to the analyser voltage. Fig. 7 shows the energy resolution as a function of incident energy for the entire energy range of SWICAR ion mode. It shows that the energy resolution for ion mode is less than 7.5% for all the specified energies.

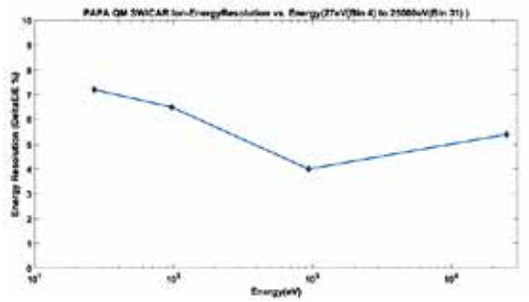

Figure 7: PAPA SWICAR ion energy resolution (%) vs. Energy for full range.

Angular Resolution

Determining the angular response of each sensor in PAPA involves two steps. In the first step, the angle-voltage relation has to be established. This was accomplished by enabling the default operation mode and loading an LUT with the guiding plate voltage steps in high resolution. The payload was rotated in the azimuth in single degree increments to determine the angle-voltage relation. Following this, the payload was switched to calibration mode, and the angular response of each bin was determined. The individual angular responses were combined to obtain the angular resolution as a function of incident angle. The process was repeated for selected energies throughout the energy range. Fig. 8 shows the angular response of SWEEP

sensor as a function of incident angle for multiple input energies. Fig. 9 shows the angular response of SWICAR ion mode across the entire energy range.

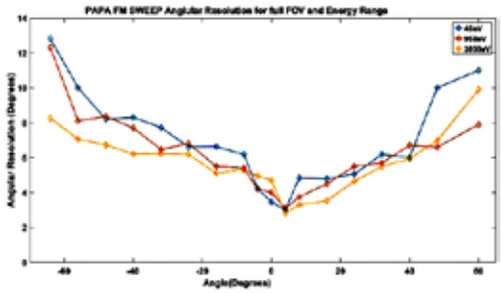

Figure 8: PAPA FM SWEEP angular resolution for full FOV and Energy Range.

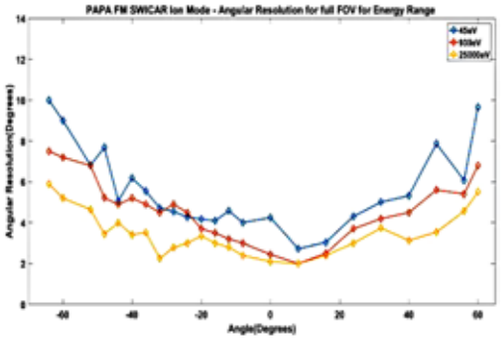

Figure 9: PAPA FM SWICAR ion angular resolution for full FOV and Energy Range

The angular resolution of electrons and Ions in PAPA sensors are < 5.6° within ±20° azimuth, within 8° (from ±20° to ±40°) and 12° (±40° to ±64°). For plasma analyzer (3DP instrument) onboard WIND spacecraft, the angular resolution (for both ions and electrons) is 5.6° in the ecliptic plane. The EVDF and pitch angle distribution based scientific discoveries were made with 5.6° uncertainty in WIND 3DP instrument. We are targeting similar scientific investigations using PAPA. There may be an added uncertainty of 2.4° from 20°- 40° and 6.4° beyond 40°. PAPA, however, has better energy resolution (8.5%) than 3DP instrument (20%) and this will help uncover more details of EVDF in the energy domain.

Time of Flight

The time-of-flight section of PAPA was tested first to establish the mass bin - time of flight value correlation using laboratory gases as certain energies. This relation was extrapolated to find the relation for the entire energy range. The validity of extrapolation was checked by selecting values randomly from the energy range and ensuring that the mass of the specie was obtained in the correct bin. The tests were carried out using the Electron Cyclotron Resonance (ECR) ion source for 1 keV to 25 keV range. A normal Electron impact ionisation source was used for the sub-100 eV range. Laboratory gases with 99.999% purity were used to test Hydrogen, Helium, Oxygen, Nitrogen and Argon. Fig. 10 shows the time-of-flight spectra from PAPA for 25 keV input. As the incident energy of the particle reduces the spread in the TOF curve increases. This is due to the energy straggling occurring due to the carbon foil. Fig. 11 shows the time-of-flight spectra for 3319 eV. The energy straggling effect is evident in the figure at higher masses.

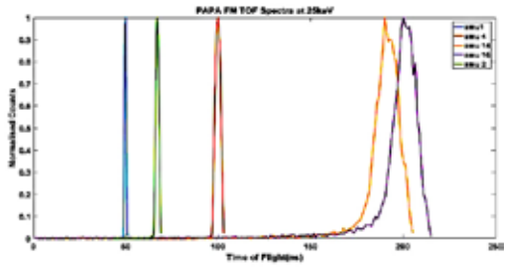

Figure 10: PAPA Time-of-flight spectra at 25keV for five ions (amu 1, 2, 4, 14 and 16).

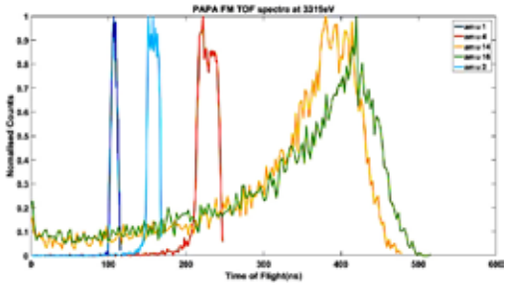

Figure 11: PAPA TOF Spectra at 3319 eV.

Mass resolution specification was projected based on the tests carried out in the Engineering model using 0.5 ug/cm^2 thick carbon foils. Oxygen and nitrogen ions were used as input to the foil at 25000 eV and we found that the masses are resolved. However, based QDPC recommendation thicker 1 µg/cm^2 foil for flight due to which energy straggling is more and accordingly TOF spread increases. Hence the resolution goes below 1 for masses above Helium. Since 99% of solar wind is composed of Hydrogen and Helium, PAPA will be able to resolve these with 1 amu resolution at all energies. The rest 1% composed of higher masses will be analysed on a case-by-case basis.

Geometric Factor

The geometric factor (GF) of an electrostatic plasma analyser (ESA) facilitates the conversion of the number of particles detected by the analyser during an integration time to the ambient plasma differential energy flux. The GF depends on several factors such as inlet aperture area, detector efficiencies, carbon foil efficiency, input energy and angle of incidence. The GF was characterised for various incident energies and fluxes. Figs. 12 and 13 show the variation of GF as a function of energy for both SWEEP and SWICAR respectively.

The geometric factor shows the sensitivity of the payload and it is matching with the simulated values. The detailed calibration of the PAPA-Proto FM is in progress at HVSSF. The cross-calibration of the PAPA and SWIS sensor of ASPEX payload is scheduled and the overlapping energy and mass ranges will be calibrated at HVSSF.

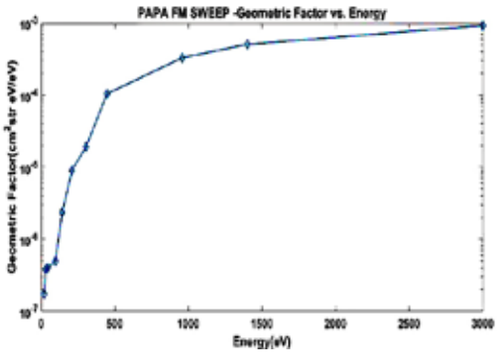

Figure 12: PAPA FM SWEEP Geometric factor vs. Energy

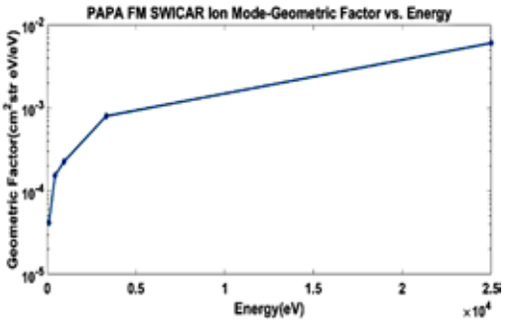

Figure 13: PAPA SWICAR Ion Mode Geometric factor as a function of Energy.

Ground Segment Activities of PAPA on Aditya-L1

QLD software

The detailed Test & Evaluation (T&E) of PAPA QLD software was completed. Based on the T&E committee suggestions, the GUI of the QLD has been modified. Fig. 14 shows the final GUI of QLD software. Development of data pipelines for the Level-1&2 data products are in progress.

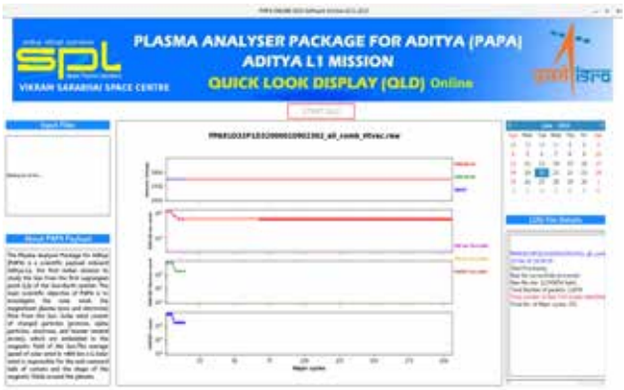

Figure 14: PAPA QLD GUI, where the observed counts for SWICAR ion mode, SWICAR electron mode and SWEEP with corresponding threshold counts, as well as the detector voltages are plotted as a function of the major cycle (representative of time series).

Magnetometer (MAG) onboard Aditya-L1 Spacecraft

FM Sensor calibration at MTF/ISITE

SPL is responsible for the scientific activities of MAG-Aditya-L1 payload developed by LEOS, and participated in the test & evaluation and technical reviews. The MAG payload was delivered to the Project on February 17, 2023 for integration with the spacecraft after calibration initially at the LEOS and later at Magnetic Test Facility (MTF), ISITE. The MAG FM sensitivity as observed at the MTF is shown in Fig. 15.

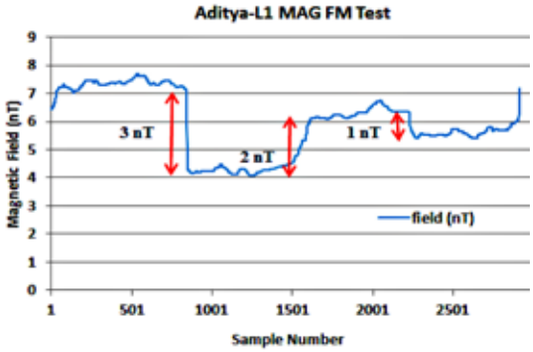

Figure 15: The MAG FM sensitivity as observed at the MTF

CHACE-2 Experiment in Chandrayaan-2 Mission

Peak Filter Algorithm for the Calibration of Mass Spectra from CHACE-2 aboard Chandrayaan-2 Orbiter

The data products from CHACE-2 observations provide the partial pressure for different masses that essentially constitute the mass spectra. CHACE-2 scans different masses using suitable voltages such that each mass is contributed by nine mass bins, known as samples. Each mass spectrum is constructed based on these 9 samples, where the fifth sample is expected to be at the center of the peaks. During the actual measurements in space, mass shifts have been observed such that the center of the peaks does not coincide with the expected mass bin, but rather shifted to either lower or higher mass bins. Also, the 9 samples that determine the peak shape need not follow the expected pattern. A criterion has been arrived at in order to verify the quality of each spectrum. In view of the large data sets, an algorithm has been developed to determine and calibrate the mass shift, verify the quality of the spectrum based on the criteria and generate suitable flags in the output file. The algorithm is referred to as 'Peak Filter Algorithm'. The output of the algorithm has been validated and the output has been found to be matching with that expected. The algorithm is significant for the scientific analysis of CHACE-2 data, and also useful for the analysis of data from instruments similar to that of CHACE-2 in future missions. Fig. 16 shows the mass spectra before and after applying the algorithm for the 18 amu group for the spectra acquired on 20 September 2019 (sweep number 163) in orbit around the Moon. It is clear from the figure that after correcting the mass shift using the algorithm, the center of the peaks for different masses (18 amu, 17 amu and 16 amu) appears at the expected mass position.

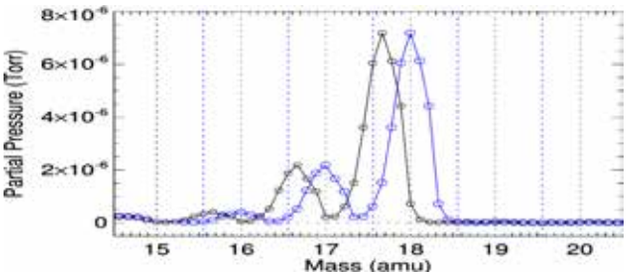

Figure 16: Comparison of the mass spectrum zoomed for 18 amu group, before and after the application of the peak filter algorithm for the mass spectra acquired on 20 September 2019 (sweep number 163) in orbit around the Moon. The black curve with the symbols shows the original spectrum with the mass shift. The blue curve with symbols shows the curve after correcting the spectrum using the output generated by the algorithm. The vertical black dotted grid lines are drawn at centre mass (from 15 amu to 20 amu) where the peak of the spectrum for each m/q is expected, and the vertical blue grid lines indicate the start mass bin of the 9 samples corresponding to each m/q. As an example, for 16 amu, the mass bin ranges from ~15.55 amu to 16.44 amu. So the blue dotted line can be found at 15.55 amu. The spectra have been acquired with CEM detector ON with bias voltage of 1800 V. The negative partial pressure values represent noise [Dhanya et al., 2023].

Payload Operation Centre (POC)

The payload Operation Centre (POC) serves the nodal point connecting the payload, mission, and ISSDC teams. CHACE-2 is being operated regularly (maximum two operations per day with each operation lasting for ~4 hours) and the data are received at POC. The data processing and logging is done on a daily basis and in a nearly automated manner. Total 633 data products covering the data acquired for the period of 24 Nov 2020 to 31 Jul 2022 were released in September 2022. In March 2023, 203 data products that cover the CHACE-2 data acquired for the period of 01 Aug 2022 to 31 Jan 2023 were released. The data products are available in the PRADAN portal.

POC is also ready to meet the requirements of the payloads on Chandrayaan-3 mission and gearing up for the PAPA and MAG payloads on Aditya-L1 mission. All the maintenance activities required for the smooth functioning of POC from time to time have been carried out.

Future Projections

- Commissioning of PAPA payload during PV phase, derivation of higher level products from PAPA and utilization for solar and space weather studies.
- Data processing and related activities at POC for PAPA and MAG onboard Aditya-L1
- To generate high quality dataset from PAPA and MAG payloads and dissemination to ISSDC for public release
- To study the solar wind characteristics, EVDF and IVDF for understanding the solar wind dynamics.
- Evaluating the impact of solar wind transients like shocks, ICMEs, and CIRs on the radiation belt: Observation and modeling.
- Development of space weather forecasting modules using machine learning and physics-based models.
- Development of Electron Temperature Analyser and its demonstration onboard POEM.
- Development of engineering model of a triaxial electric field sensor (EFS) for future space mission.
- Infrared investigation of polycyclic aromatic hydrocarbons (PAHs) on a sample of comets and asteroids
- Assessment of s/c outgassing aspects using CHACE-2 data (background estimation).
- To further extend the plasma instability studies and the plasma waves around planetary bodies such as the Moon, planets such as Mars and Venus and comets using theoretical techniques and also by analyzing the plasma and electric, magnetic field observations.
- To establish an advanced high vacuum space simulation laboratory (AHVSSL) in SPL.

Publications in Peer Reviewed Journals

1. Soni,S.L., R. Selvakumaran, R. Satheesh Thampi, “Assessment of the arrival signatures of the March 2012 CME- CME interaction event with respect to Mercury, Venus, Earth, STEREO-B and Mars locations’, Frontiers in Astronomy and Space Sciences, 9, 441, doi:10.3389/fspas.2022.1049906, 2022.
2. Gokani, S, De-Sheng Han, R Selvakumaran and Tarun K. Pant, “Dependence of Radiation Belt Flux Depletions at Geostationary Orbit on Different Solar Drivers During Intense Geomagnetic Storms”, Frontiers in Astronomy and Space Sciences-Space Physics, 9, 952486, doi:10.3389/fspas.2022.952486, 2022.
3. Mukundan, V., Withers, P., González-Galindo, F., Thampi, Smitha V., Bhardwaj, A., and Felici, M., “A typically intense and delayed response of the Martian ionosphere to the regional dust storm of 2016: A study using MAVEN observations and models”, Journal of Geophysical Research: Planets, 127 (12), e2022JE007645, doi:10.1029/2022JE007645, 2022.

4. Ledvina, V.E., Palmerio, E., McGranaghan, R.M., Halford, A.J., Thayer, A., Brandt, L., MacDonald, E.A., Bhaskar, A., Dong, C., Altintas, I. and Colliander, J., "How open data and interdisciplinary collaboration improve our understanding of space weather: A risk and resiliency perspective", Frontiers in Astronomy and Space Sciences, 9, 1067571. doi:10.3389/fspas.2022.1067571, 2022

5. Thampi, S.V., and Mukundan V., "The global response of Terrestrial ionosphere to the December 2015 space weather event", Advances in Space Research, 71 (1), 286-297, doi:10.1016/j.asr.2022.10.037, 2023.

6. Bhaskar, A., Sibeck, D.G., Carter, J.A., Zong, Q. and Daglis, I.A., Editorial: Magnetosphere and Ionosphere Response to the Solar Wind Transients", Frontiers in Astronomy and Space Sciences, 10, 1230248, doi:10.3389/fspas.2023.1230248, 2023.

7. Chakraborty, M., Vipin K. Yadav, and Rajneesh Kumar, "Two Stream Instability Generation in the Lunar Ionosphere", Advances in Space Research, 71 (6), 2954-2966, doi:10.1016/j.asr.2022.11.050, 2023.

8. Dhamane, O., Raghav, A., Shaikh, Z., Panchal, U., Ghag, K., Tari, P., Choraghe, K., Bhaskar, A., Telloni, D. and Mishra, W., "Observation of Alfvén Waves in an ICME-HSS Interaction Region", Solar Physics, 298(3), 34, doi:10.1007/s11207-023-02127-4, 2023.

9. Manju, G., N. Mridula, T.V. Sruthi, Tarun K. Pant, Aswathy R.P., P. Sreelatha, Rosmy John, R. Satheesh Thampi, A.N. Aneesh, and J.K. Abhishek, "Generation of Post Sunset E region Electron Density Stratifications at the Magnetic Equator: An Analysis Using In-Situ Measurements and Theoretical Estimations", Journal of Geophysical Research: Space physics, 128 (3), e2022JA030903, doi:10.1029/2022JA030903, 2023.

10. Raghav, A., Shaikh, Z., Vemareddy, P.,Bhaskar, A., Dhamane, O., Ghag, K., Tari, P., Dayanandan, B. and Mohammed Al Suti, B., "The Possible Cause of Most Intense Geomagnetic Superstorm of the 21st Century on 20 November 2003", Solar Physics, 298(5), 64, doi:10.1007/s11207-023-02157-y, 2023.

11. Rubia, R. S.V. Singh, G.S. Lakhina, S. Devanandhan, M.B. Dhanya, and T. Kamalam, "Electrostatic Solitary Waves in the Venusian Ionosphere Pervaded by the Solar Wind: A Theoretical Perspective", The Astrophysical Journal, 950(2), 111, doi:10.3847/1538-4347/acd2d7, 2023.

12. Lakhina, G. S., S.V. Singh, T. Sreeraj, S. Devanandhan, and R. Rubia, "A Mechanism for Large-Amplitude Parallel Electrostatic Waves Observed at the Magnetosphere", Plasma, 6 (2), 345-361, doi:10.3390/plasma6020024, 2023.

13. Venkataraman, V., Smitha V. Thampi, "Effects of stealth CME to ion energisation at ionospheric altitudes of Mars", Planetary and Space Science, 234, 105721, doi:10.1016/j.pss.2023.105721, 2023.

14. Dhanya, M. B. Chemukula MathinYadav, Smitha V Thampi, R Satheesh Thampi, TirthaPratim Das, "Peak Filter Algorithm for the Calibration of Mass Spectra from CHACE-2 aboard Chandrayaan-2 Orbiter", International Journal of Mass Spectrometry, 117098, doi:10.1016/j.ijms.2023.117098, 2023.

Publications in Proceedings

1. Durgesh Tripathi, D. Chakrabarty, A. Nandi, B. Raghvendra Prasad, A.N. Ramaprakash, Nigar Shaji, K. Sankarasubramanian, R. Satheesh Thampi, V. K. Yadav, "The Aditya-L1 mission of ISRO", The Era of Multi-Messenger Solar Physics, Proceedings IAU Symposium No. 372, Eds. G. Cauzzi & A. Tritschler, 2022.

Scientific / Technical Reports

1. PAPA Operational Proposals Format Document, Version 1.2, VSSC/DSG/AVID/PAPA/2022/13.

2. Plasma Analyzer Payload for Aditya, Operational Manual Ver1.0, VSSC/DSG/AVID/PAPA/2022/14.

3. Spacecraft level test plan document for Plasma Analyser Package for Aditya (PAPA) V1.0, VSSC/DSG/AVID/PAPA/2022/15.

4. Payload User Manual - Plasma Analyzer Package for Aditya (PAPA), VSSC/DSG/AVID/PAPA/2022/16.

5. Plasma Waves: Nature, Generation and Detection in Space, ISRO-VSSC-TR-0180-0-23, February 2023.

6. Ultrathin carbon foil for Time-Of-Flight (TOF) Measurements: Aspects of characterization for space Application, VSSC-MS-23-074.

Popular Article

1. Plasma Analyser Package for Aditya (PAPA) onboard Aditya-L1 Mission, Countdown, Pages: 3-7, February 2023.

Presentations in Conferences/Symposiums/Meetings/Workshops

1. Ankush Bhaskar, Tarun Pant, Satheesh Thampi, Jaydev Pradeep, C. Vineeth, Vipin Yadav, and Smitha Thampi, "Twin CubeSat Mission Concept to Study Aurora and Particle Precipitation in Northern and Southern Auroral Ovals", Session PSW.1 (Microsatellites for Space Weather and Radio Astronomy) in Panel on Space Weather (PSW), 5th COSPAR Symposium, Singapore, April 16-21, 2023.
2. Vipin K. Yadav, "Streaming Plasma Instability in Lunar Ionosphere", 4th Indian Planetary Science Conference (IPSC-2023), Physical Research Laboratory (PRL), Ahmedabad, Gujarat, March 22-24, 2023.
3. Abhishek J K., "Ultra-thin carbon foil behavior under vibration stress- structural and functional implications for space borne TOF systems", 4th Indian Planetary Science Conference (IPSC-2023), Physical Research Laboratory (PRL), Ahmedabad, Gujarat, March 22-24, 2023.
4. Ankush Bhaskar, "Magnetospheric Physics and Aditya-L1", First Meeting of Science from In-situ Measurements of Aditya-L1 (SIMA-01), Space Physics Laboratory (SPL), Vikram Sarabhai Space Centre (VSSC), Thiruvananthapuram, Kerala, April 11-13, 2023.
5. Mehul Chakraborty, Vipin K. Yadav and Rajneesh Kumar, "Streaming Instability Generation in Lunar Plasma Environment", URSI Regional Conference on Radio Science (RCRS-2022), Indian Institute of Technology (IITI), Indore, Madhya Pradesh, December 1-4, 2022.
6. Ashna V. M., Ankush Bhaskar, G. Manju, Sini R.,"Solar Cycle Dependence of the solar wind-magnetosphere coupling during geomagnetic storms of 23-34 solar cycles", URSI Regional Conference on Radio Science (RCRS-2022), Indian Institute of Technology (IITI), Indore, Madhya Pradesh, December 1-4, 2022.
7. Mehul Chakraborty, Vipin K. Yadav and Rajneesh Kumar, "Plasma Instability in Lunar Ionosphere", 37th National Symposium on Plasma Science & Technology (Plasma-2022), Indian Institute of Technology (IITJ), Jodhpur, Rajasthan, December 12-14, 2022.
8. Ashna V. M, Ankush Bhaskar, Tarun K. Pant, Manju G, Geeta Vichare, Sini R., "An Investigation on the Efficiency of Viscous Interaction during Intense Northward IMF Bz events of 23- 24 Solar Cycles", First Meeting of Science from In-situ Measurements of Aditya-L1 (SIMA-01), Space Physics Laboratory (SPL), Vikram Sarabhai Space Centre (VSSC), Thiruvananthapuram, Kerala, April 11-13, 2023.
9. Soni S., R. S. Thampi, "Influence of a CME on Mars and Earth constrained by Remote Sensing and In Situ Measurements", 44, 1396, 44th COSPAR Scientific Assembly, Athens, Greece (online), July 16-24, 2022.
10. Ravindran S., S. Gokani, T.K. Pant, S. Soni, R. S. Thampi, "Detailed understanding of reduced geo-effectiveness of solar cycle 24", 44, 1401, 44th COSPAR Scientific Assembly, Athens, Greece (online), July 16-24, 2022.
11. Vipin K. Yadav, "Magnetometer onboard Aditya-L1 Spacecraft", The ISRO-NOAA meeting for cross-calibration between the payloads onboard ISRO and NOAA spacecraftsonline via Webex (online), October 13, 2022.
12. Ankush Bhaskar, Amaravadi, K., Dayanandan, B. and Pant, T.K., "Forecasting relativistic electron fluxes of the Earth's radiation belt using machine learning", AGU Fall Meeting Abstracts (Vol. 2022, pp. NG43A-07) (online), December, 2022.
13. Soni S., W. Mishra, R. S. Thampi, "3D Reconstruction of Interacting CMEs Constrained by Remote and In-situ measurements", AGU Fall Meeting Abstracts (Vol. 2022, pp. SH25C-05) (online), December, 2022.

Scientific Organizing Committee (SOC) member/Session Chair/Convener

R. Satheesh Thampi

1. 4th Indian Planetary Science Conference (IPSC-2023), Physical Research Laboratory (PRL), Ahmedabad, Gujarat (SOC member), March 22-24, 2023.
2. "Aditya-L1 and Beyond", USO-PRL Solar Physics Workshop (USPW-2023) on Multi-scale Phenomena on the Sun: Present Capabilities and Future Challenges, Udaipur Solar Observatory (USO), Physical Research Laboratory (PRL), Udaipur, Rajasthan (SOC member), April 3-5, 2023.

3. 23rd National Conference on Atomic and Molecular Physics (NCAMP-2023), Space Physics Laboratory, Vikram Sarabhai Space Centre (VSSC), Thiruvananthapuram, Kerala (Convener), February 22, 2023.
4. 23rd National Conference on Atomic and Molecular Physics (NCAMP-2023), Space Physics Laboratory, Vikram Sarabhai Space Centre (VSSC), Thiruvananthapuram, Kerala (Co-Convener), February 22, 2023.
5. "Session 4: Space & Planetary Instrumentation", 4th Indian Planetary Science Conference (IPSC-2023), Physical Research Laboratory, Ahmedabad, Gujarat (Session Chair), March 22-24, 2023.
6. "Session 5: Solar Wind Physics", First Meeting of Science from In-situ Measurements of Aditya-L1 (SIMA-01), Space Physics Laboratory), Vikram Sarabhai Space Centre (VSSC), Thiruvananthapuram, Kerala (Session Chair), April 11-13, 2023.

Vipin K. Yadav

1. "H5 Theme: Waves in Plasmas", URSI-Regional Conference on Radio Science RCRS-2022), Indian Institute of Technology, Indore, Madhya Pradesh (Session Chair), December 1-4, 2022.
2. Observing Magnetospheric and ionospheric Impact-II", First Meeting of Science from In-situ Measurements of Aditya-L1 (SIMA-01), Space Physics Laboratory (SPL), Vikram Sarabhai Space Centre (VSSC), Thiruvananthapuram, Kerala (Session Chair), April 11-13, 2023.

Smitha V. Thampi

1. "Future Exploration of the Inner Solar System: Scope and the Focus Areas", National Meet on the completion of 8 Years of Mars Orbiter Mission, ISRO HQ, Bengaluru (Panel Member), September 27, 2022.
2. Session III-B: "Surfaces and Clusters", National Conference on Atomic and Molecular Physics (NCAMP-2023), Space Physics Laboratory (SPL), Vikram Sarabhai Space Centre (VSSC), Thiruvananthapuram, Kerala (Session Chair), February 22, 2023.

Deputation

R. Selvakumaran

1. 44th COSPAR Scientific Assembly, Athens Greece, July 14 - 22, 2022.

Invited Talks

R. Selvakumaran

1. "Detailed understanding of reduced geoeffectiveness of solar cycle 24", 44th COSPAR Scientific Assembly, Athens, Greece, July 14 - 22, 2022.
2. "Solar Eruptions and space weather", PG Physics Association, American College, Madurai, Tamil Nadu, August 29, 2022.

Ankush Bhaskar

1. "The Earth's Dynamic Magnetosphere", 'Space Physics and Astronomy' Seminar Series, All Saints' College, Thiruvananthapuram, Kerala, August 30, 2022.
2. "Basics of Earth's Magnetosphere Physics", 'Space Physics and Astronomy' Seminar Series, SatyaSai Arts and Science College, Saigramam, Kerala, September 03, 2022.
3. "Multi-spacecraft Investigation of Multiple Particle Injections Induced by isolated Interplanetary Shock", URSI Regional Conference on Radio Science (RCRS-2022), Indian Institute of Technology, Indore, Madhya Pradesh, December 02, 2022.

Vipin K. Yadav

1. "VIPER: A Plasma Wave Detection Instrument onboard Indian Venus Orbiter Spacecraft", URSI Regional Conference on Radio Science (RCRS-2022), Indian Institute of Technology, Indore, Madhya Pradesh, December 02, 2022.
2. "Fluxgate Magnetometer (MAG) onboard Aditya-L1 Solar Mission Spacecraft", Regional Workshop on Solar Science and Aditya-L1, St. Joseph University, Bengaluru, Karnataka, January 04, 2023.
3. Magnetic field measurements at L-1 point using Fluxgate Magnetometer (MAG) onboard Aditya-L1 Spacecraft", Indian Institute of Geomagnetism (IIG), Navi Mumbai, Maharashtra, December 05, 2022.

4. Magnetic Field Measurements onboard Aditya-L1 Solar Mission Spacecraft with a Fluxgate Magnetometer (MAG)", USO-PRL Solar Physics Workshop (USPW-2023) on Multi-scale Phenomena on the Sun: Present Capabilities and Future Challenges, Udaipur Solar Observatory (USO), Physical Research Laboratory (PRL), Udaipur, Rajasthan, April 3-5, 2023.
5. "MAG Onboard Aditya-L1 Spacecraft: Overview and Capabilities", First Meeting of Science from In-situ Measurements of Aditya-L1 (SIMA-01), Space Physics Laboratory (SPL), Vikram Sarabhai Space Centre (VSSC), Thiruvananthapuram, Kerala, April 11-13, 2023.
6. "Magnetic Field Measurements in Space", Conference on Frontiers of Space and Atmospheric Science (COFSAS-2023), (online), March 15, 2023.

R. SatheeshThampi

1. "Investigation of Solar wind using Plasma Analyser Package for Aditya (PAPA) onboard Aditya-L1 Mission", 23rdNational Conference on Atomic and Molecular Physics (NCAMP-2023), Space Physics Laboratory (SPL), Vikram Sarabhai Space Centre (VSSC), Thiruvananthapuram, Kerala, February 22, 2023.
2. "PAPA onboard Aditya-L1 Solar Mission", Regional Workshop on Solar Science and Aditya-L1, St. Joseph University, Bengaluru, Karnataka, January 04, 2023.
3. "PAPA onboard Aditya-L1 Spacecraft", USO-PRL Solar Physics Workshop (USPW-2023) on Multi-scale Phenomena on the Sun: Present Capabilities and Future Challenges, Udaipur Solar Observatory (USO), Physical Research Laboratory (PRL), Udaipur, Rajasthan, April 3-5, 2023.
4. "PAPA onboard Aditya-L1 Mission", First Meeting of Science from In-situ Measurements of Aditya-L1 (SIMA-01), Space Physics Laboratory (SPL), Vikram Sarabhai Space Centre (VSSC), Thiruvananthapuram, Kerala, April 11-13, 2023.

Dhanya M.B.

1. "Solar wind interaction with the moon - the neutral and plasma environment", 23rdNational Conference on Atomic and Molecular Physics (NCAMP-2023), Space Physics Laboratory (SPL), Vikram Sarabhai Space Centre (VSSC), Thiruvananthapuram, Kerala, February 22, 2023.
2. "Effect of Solar wind on the Moon - utilization of Aditya-L1 data", First Meeting of Science from In-situ Measurements of Aditya-L1 (SIMA-01), Space Physics Laboratory (SPL), Vikram Sarabhai Space Centre (VSSC), Thiruvananthapuram, Kerala, April 11-13, 2023.
3. "Lunar ion exosphere studies through Solar wind and energetic neutral measurements", ISRO-RAS Workshop on Lunar Exploration organized by ISRO HQ, (online), January 25, 2023.

SmithaV. Thampi

1. "Planetary Space Weather: Observational Perspective", First Meeting of Science from In-situ Measurements of Aditya-L1 (SIMA-01), Space Physics Laboratory (SPL), Vikram Sarabhai Space Centre (VSSC), Thiruvananthapuram, Kerala, April 11-13, 2023.

Public Outreach

1. Smitha V. Thampi, World Space Week (WSW-2022), Online Lecture for two schools, October 2022.
2. AnkushBhaskar, World Space Week (WSW-2022): "Space Exploration and Society", Saint Stephen's College, Thiruvananthapuram, Kerala, October 11, 2023.
3. AnkushBhaskar, World Space Week (WSW-2022): "Space Exploration and Society", SaraswatiCollege, Thiruvananthapuram, Kerala, October 13, 2023.

Training Programme

1. V. Venkataraman, The SPARC workshop on Machine Learning in Solar Physics and Space Weather, (Online) June 28 - July 02, 2022.
2. ChemukulaMathinYadav, ISRO Induction Training Programme (IITP-33) - Phase III, Vikram Sarabhai Space Centre (VSSC), Thiruvananthapuram, Kerala, September 19-23, 2022.
3. ChemukulaMathinYadav, ISRO Induction Training Programme (IITP-33) - Phase III, SatishDhawan Space Centre (SDSC), Sriharikota, Andhra Pradesh, September 26-27, 2022.
4. Smitha V. Thampi, AnkushBhaskar, Space Situational Awareness/Space Traffic ManagementWorkshop,, ISRO, Bengaluru, January 11-13, 2023.

वायुमंडल प्रौद्योगिकी प्रभाग
Atmosphere Technology Division

वायुमंडल प्रौद्योगिकी प्रभाग (एटीडी) गुब्बारे, रॉकेट तथा अंतरिक्ष उन्मुख प्रदायभारों की अवधारणा स्तर से लेकर अभिकल्पना, विकास तथा परीक्षण सहित वायुमंडलीय, अंतरिक्ष तथा ग्रहीय विज्ञान क्षेत्रों के लिए अभिकल्पित प्रयोगात्मक प्रणालियों के प्रौद्योगिकी पक्ष पर तथा स्वस्थाने अन्वेषण हेतु भू-आधारित प्रणालियों के विकास और वायुमंडल के सुदूर संवेदन पर ध्यान केंद्रित करता है।सक्रिय प्रयोगात्मक प्रणालियों के संवर्धन तथा रखरखाव, एसपीएल के वैज्ञानिक गतिविधियों को तकनीकी समर्थन देने तथा सामान्य तकनीकी सुविधाओं के अनुरक्षण के लिए भी एटीडी उत्तरदायी है। यह एसपीएल की वैज्ञानिक शाखाओं के साथ निकट समन्वय करते हुए कार्य करता है तथा वैज्ञानिक विचारों को मूर्तरूप देने हेतु तकनीकी विशेषज्ञता प्रदान करता है।

Atmosphere Technology Division (ATD) focuses on the technological aspects of experimental systems designed for atmospheric, space and planetary science areas, including the development and testing of balloon-, rocket-, and space-borne payloads from the proof-of-concept and development of ground-based systems for in-situ probing and remote sensing of the atmosphere. ATD is also responsible for the augmentation and maintenance of the ongoing experimental systems, providing technical support to the scientific activities of SPL and maintenance of the common technical facilities. It works in close coordination with the scientific branches of SPL and provides technical expertise for realization of scientific ideas.

वैज्ञानिक/इंजीनियर / Scientists/Engineers

दिनकर प्रसाद वज्जा / Dinakar Prasad Vajja
प्रमोद पी. पी. / Pramod P. P.
मणिकंठन नायर एन. / Manikantan Nair N.
मोहम्मद नज़ीर एम. / Mohammed Nazeer M.
लाली पी. टी. / Lali P. T.
अनीष ए. एन. / Aneesh A.N.

तकनीकी टीम / Technical Team

अनुमोद पी. जी. / Anumod P. G.
सतीश कुमार बी. / Satheesh Kumar B.
उत्तम एस. पूर्ती / Uttam S. Purty*

** Superannuated on 30 December, 2022*

Executive Summary

Atmosphere Technology Division (ATD) has made significant contributions to the scientific and technical activities of SPL during the reporting period. These include contributions to the following activities: (i) Integrated spacecraft testing of onboard electronics (flight model) for the ChaSTE payload onboard Chandrayaan-3 Lander, (ii) Test and evaluation of the PAPA payload on board the Aditya-L1 mission, (iii) Design and development of rocketsonde for profiling middle atmospheric temperature (TDP), (iv) Design and development of payload electronics for the Solar Occultation Experiment (TDP), (v) Design and development of sensor electronics for Atomic Oxygen sensor payload (TDP), (vi) Operation, maintenance and augmentation of HF radar and Digisonde Systems, and (vii) Fabrication of mechanical systems, fixtures, generation of CAD drawings and installation of various scientific instruments. ATD is also carrying out the operation, maintenance and upgradation of the common facilities and looking after the safety aspects of SPL.

Payloads for Space Missions

Onboard Electronics of ChaSTE Payload of the Chandrayaan-3 Lander

The Chandra's Surface Thermophysical Experiment (ChaSTE) payload onboard the Chandrayaan-3 lander has been developed by SPL/VSSC in collaboration with various entities of VSSC (ESAE, MVIT, PCM, STR, SR, SPRE, AERO) and PRL, Ahmedabad. The prime objective of the experiment is to make in-situ observations of the thermal behaviour of the outermost 100 mm layer of the lunar surface.

The processing electronics was designed at SPL/VSSC, which drives BLDC motors for the probe deployment and penetration, acquires digitized sensors data through the front-end card and interfaces to Lander for data transfer, telecommand reception and telemetry generation. Front-end electronics was designed and developed at PRL and does signal conditioning of RTD sensors and digitization of the signals.

Integrated Spacecraft Tests of the Onboard Electronics (Flight Model)

During the reporting period, the electronics package has successfully undergone integrated spacecraft tests (IST) at ISITE, Bangalore (Table 1). The tests conducted during the IST were dis-assembled mode performance test, assembled mode functional test (Fig.1), thermo-vacuum cycling performance test, EMI/EMC performance test, post thermo-vacuum functional test and post-dynamic functional test. During the performance tests, the electronics was tested for switch ON and switch OFF, data acquisition, motors drive operation and probe heater drive operation. During the functional tests, the electronics was tested for end to end operations including probe deployment and probe penetration operations as per the payload's mission operational plan.

Performance reviews, action closeouts and global audit assessment of the payload electronics have been completed. Mission operational plan of the payload has been finalized with contingency plans under various scenarios.

Table 1: Spacecraft level tests of the ChaSTE payload electronics

Dis-assembled mode	Assembled mode	Thermo-vacuum cycling				EMI/ EMC	Post Thermo-vacuum	Post Dynamic
		Short Cold Soak	Short Hot Soak	Long Cold Soak	Long Hot Soak			
✓	✓	✓	✓	✓	✓	✓	✓	✓

Figure 1: ChaSTE probe deployment and penetration operations as part of the IST

Operations after the Chandrayaan-3 Landing

The electronics package of the payload was successfully deployed and inserted thermal probe of the payload in to the lunar soil in a controlled manner by driving motorized mechanisms. The operations were carried out by using telecommands of multiple numbers and by monitoring the payload telemetry in near real-time. The probe deployment operation (Fig. 2) from stowed condition to vertical down position was executed by 9 telecommands and the probe penetration operation (Fig. 3) into the lunar regolith was executed by 116 telecommands. The electronics has precisely measured temperature profile of the topmost 100 mm layer of the lunar soil continuously during the lunar day by using 10 RTD temperature sensors. It has conducted lunar soil thermal conductivity experiment at the end of the lunar day by powering the probe heater for over 2 hours. This experiment was repeated twice at two levels. Retraction of the thermal probe was also done for the lander hop experiment and re-insertion of the thermal probe at a different location was carried out after the hop experiment. Performance of the electronics is found normal throughout the experiments. The measured temperature profile and thermal conductivity of the regolith are the first ever observations at the lunar South pole.

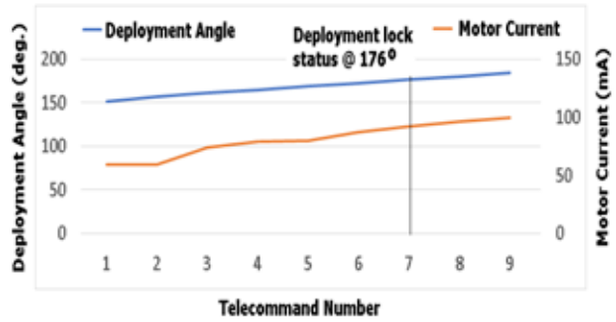

Figure 2: ChaSTE probe deployment angle and motor current versus telecommand

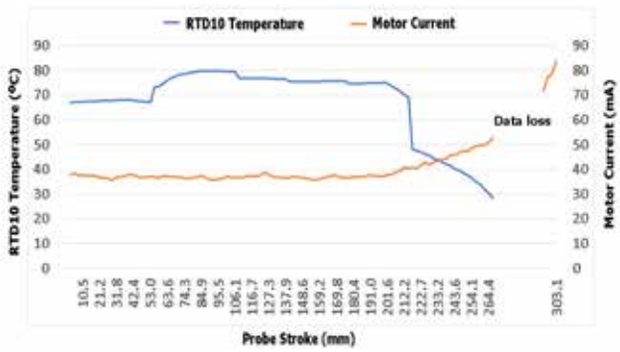

Figure 3: ChaSTE probe stroke versus RTD10 temperature and motor current during penetration operation

Qualification Activities of the PAPA Payload of the Aditya-L1 Mission

Plasma Analyser Package for Aditya-L1 (PAPA) is one of the scientific payloads of ISRO's Aditya-L1 mission, jointly developed by SPL, AVN and SR in association with the other entities of VSSC.

Test and Evaluation (T&E) of the Flight Model (FM)

The following T&E activities have been successfully completed for the FM as per the flight acceptance levels of the ETLS (Environmental Test Level Specifications) of the mission.

Initial SRC and Final SRC: Energy resolution, angular resolution and mass resolution tests have been carried out for the SWICAR (Solar Wind Ion Composition AnalyseR) sensor of the PAPA using high and low energy ion sources with different gases. The SWEEP (Solar Wind Electron Energy Probe) sensor of the PAPA has been tested for energy resolution and angular resolution for different energies by using an electron gun. MIL-STD-1553 protocol and power supply variation tests have been completed. All these tests were carried out at the High Vacuum Space Simulation Facility (HVSSF), SPL.

Vibration: The package has been subjected to both sine and random vibration tests. These tests have been carried out at the structural vibration facility, STR Entity. Test setup of the payload for the vibration test is shown in the Fig. 4. Pre and post vibration tests were conducted at the HVSSF, SPL.

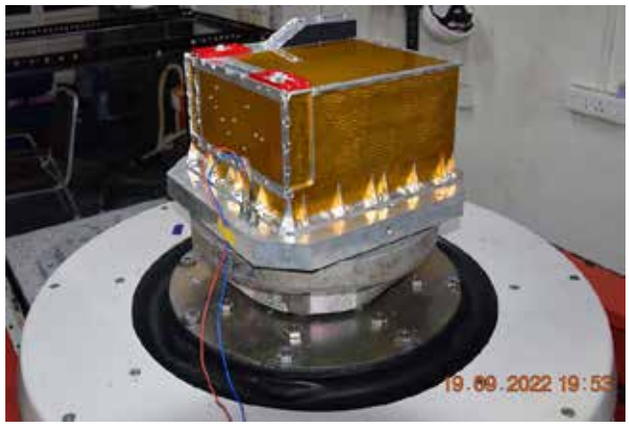

Figure 4: Vibration test setup of the PAPA FM.

Thermo-Vacuum Cycling: The package has been subjected to five short cycles of 2 hours each and a long cycle of 24 hours in the range from -15 °C to +55 °C. The thermo-vacuum cycling has been carried out at the QDVF facility, SR Entity. Pre and post thermo-vacuum cycling tests were conducted at the HVSSF, SPL.

Calibration

Extensive calibration of the FM has been carried out for both the SWICAR and the SWEEP sensors of the FM. These include (i) Energy calibration, (ii) Angular calibration and (iii) Calibration of time of flight measurements.

Magnetic Field Measurement: Magnetic field measurement has been carried out with the proto-FM package in passive mode. Three magnetic field sensors have been used in the test for the three axes magnetic field measurements. Multiple measurements have been carried for every 10° change in physical orientation. The measurements are within the acceptance limits of the mission. The test has been conducted at the at the magnetic field test facility, ISITE, Bangalore.

T&E of the Proto-FM

T&E of the proto-FM has been successfully completed in SRC, EMI/EMC, thermal soak, vibration and thermo-vacuum cycling as per the specified levels. Test setup of the proto-FM for the EMI/EMC test is shown in the Fig. 5.

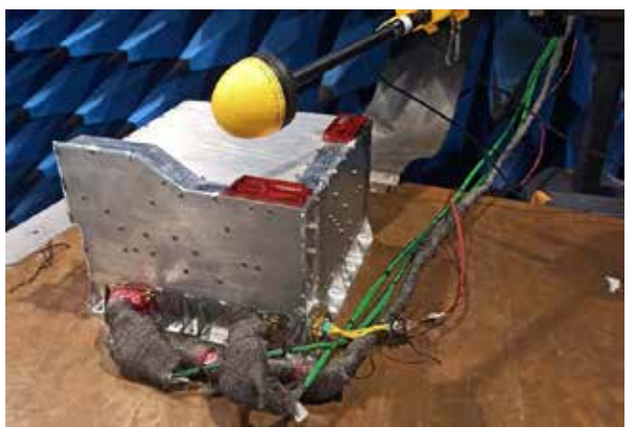

Figure 5: EMI/EMC test setup of the PAPA payload (proto-FM)

Ruggedization of Channel Electron Multiplier (CEM) detectors

The CEM detector (Fig. 6) consists of a dynode with ceramic body and an anode terminal connected to the body by M1.6 screws. To strengthen the bonding between the anode terminal and the body, an araldite material has been applied. In order to find out the effectiveness of the bonding at extreme temperatures, thermal soak tests have been carried out at -20 °C and +55 °C for a duration of 2 hours each. Electrical parameters (dark count and V-I characteristics) of the CEM detector have been recorded before and after applying the bonding material. Performance was found to be normal. Also, the detectors integrated with the payload have been successfully qualified after the vibration test.

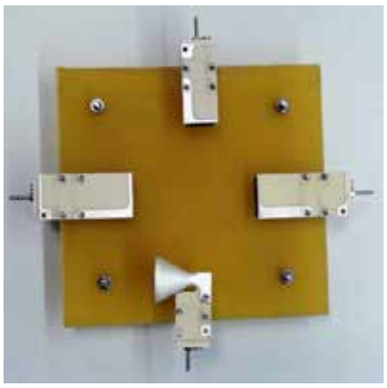

Figure 6: The CEM detectors reinforced with Araldite material

Ground-based Systems

Operation and Maintenance of HF Radar System

The in-house developed HF radar is a phase coherent, monostatic, pulsed radar operating at 18 MHz. The radar is a powerful tool to study the plasma instability processes responsible for the generation of Equatorial Electro Jet (EEJ) and Equatorial Spread-F (ESF) irregularities in the ionosphere. Transmitter of the radar generates 50 kW peak power. The antenna system used is an interlaced phased array, consisting of 72 wire dipoles arranged in a 12x6 rectangular array configuration spread over a physical area of 10,000 m^2. The radar employs Doppler beam swinging with beam orientations in vertical, 30° East and 30° West. The backscattered signal collected by the array antenna is processed by a digital receiver and a PC based data acquisition system.

The radar has been operated daily for fixed duration and also on 24x7 mode during experimental campaigns. Preventive breakdown maintenance for the radar was carried out periodically. Fig. 7 shows the equatorial electrojet echoes observed using the HF radar on 13 March, 2023.

Operation and Maintenance of Digisonde System

Digisonde is an ionospheric radar that uses high frequency radio waves (2 to 20 MHz) for monitoring electron density in the ionosphere. It generates 300 W peak transmission power. Signal transmission is performed with two (NE-SW and NW-SE) crossed delta antennas of 30 m in height. Signal reception is done with an array of four crossed magnetic dipole receive antennas in a triangular arrangement.

The system has been operated in 24×7 mode. Periodic maintenance was carried out on the system.

Augmentation of Nighttime Photometer

The Automatic Nighttime Photometer (ANP) is an in-house developed optical instrument capable of measuring five different airglow emissions (557.7 nm, 630.0 nm, 777.4 nm, 731.6 nm and 740.2 nm) from Earth's upper atmosphere simultaneously. The ANP has been augmented with sky scanning mirror unit for measuring the airglow emissions at different azimuth and elevation positions. The scanning unit consists of two stepper motors with gears for positioning the unit at different angles.

Control and data acquisition unit (CDAQ) has been developed for operation of the ANP. The CDAQ unit

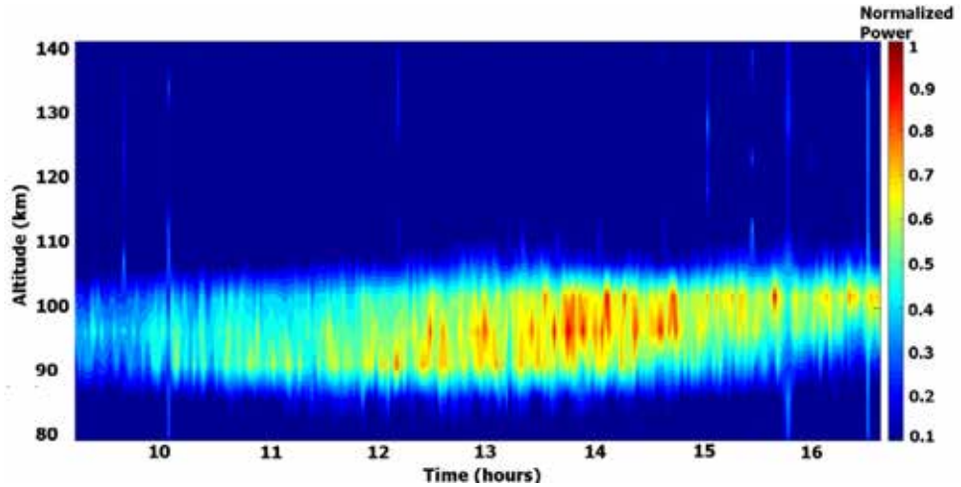

Figure 7: Equatorial electrojet echoes observed by the HF radaron 13 March, 2023

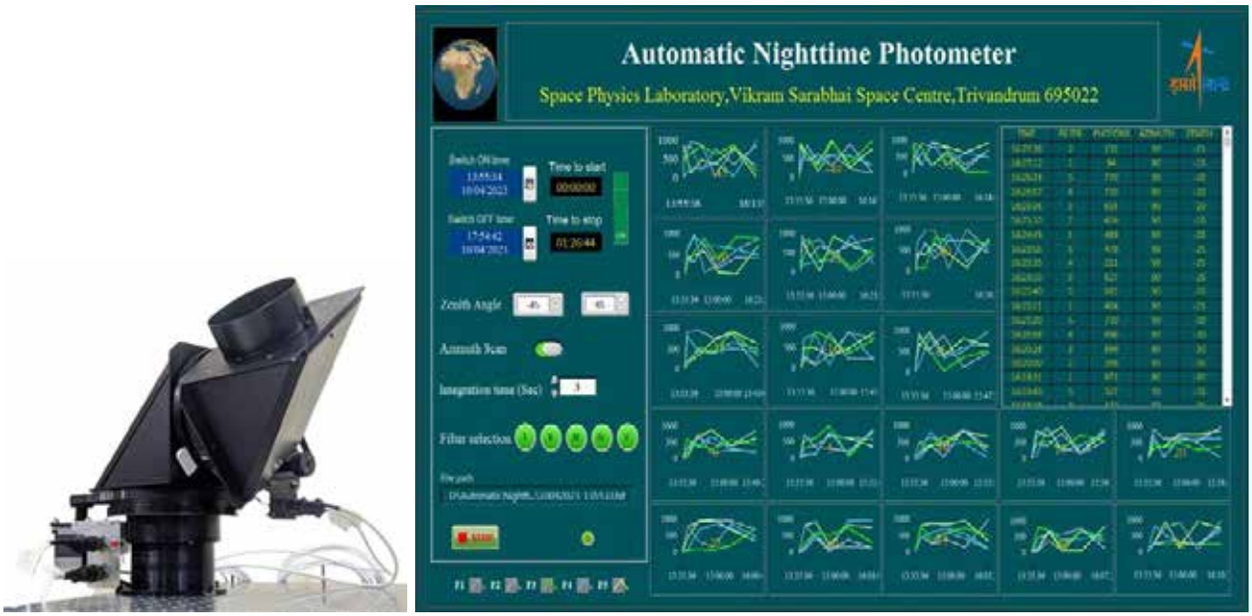

Figure 8: Sky scanning mirror unit of nighttime photometer and its control & data acquisition software.

consists of LabVIEW based software (Fig. 8), motors driver, temperature control and PMT driver. The unit measures airglow emissions at every 5° elevation from -45° to +45° for each 0° and 90° azimuth by scanning the sky. The software acquires the data by USB interface and archives it in PC for further processing. It has real time tabular as well as graphical display of the acquired data. The software has features to select signal integration time, filter number, scanning angle range and acquisition time.

Experimental and Common Facilities

Operation, Maintenance and Augmentation of HVSSF

The HVSSF (High Vacuum Space Simulation Facility) is operated, maintained and augmented with sub-systems for the development, testing and calibration of scientific payloads. The HVSSF facility has been extensively utilized for testing, calibration and characterization of the PAPA payload. Testing of the PAPA payload (FM) in the HVSSF is shown in the Fig. 9.

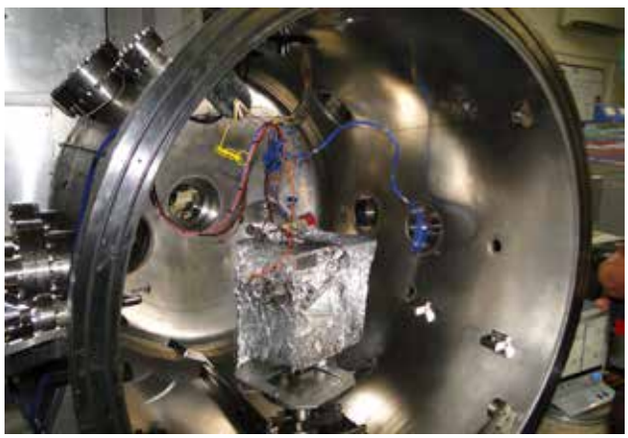

Figure 9: PAPA payload(FM) kept in the HVSSF for testing

Design and Development of User Interface (UI) for the HVSSF Automation Software

The following new features were incorporated in the UI application of the HVSSF automation software.

(i) A visual block based automation editor has been developed with the help of Google Blockly library for automation of test equipment for a particular experiment. It is a Java Script based library for creating a visual block based programming environment. The custom blocks for each instrument were defined and integrated with the Blockly GUI.

(ii) Implementation of interlock feature for the operation of high voltage power supplies based on vacuum level of the chamber has been completed. Range of vacuum levels can be entered through the UI and the values will be saved in a database. Vacuum level of the chamber will be acquired from a vacuum gauge controller and vacuum interlock will be activated by switching off the power supplies automatically if the level exceeds the specified vacuum range in real time.

(iii) Operational parameters of each equipment and its read out values are stored as a separate collection in a database. The necessary python code was developed at the server side for storing and retrieving the data. The client side UI is provided with a feature to select a particular equipment, view its data log and save the data in the client side computer.

Operation and Maintenance of Clean Room Facility

The clean room facility at SPL (with class 10000 and class 100000 clean rooms equipped with work benches of class 100 and class 1000 Laminar flow tables) has been utilized for development and testing activities for

scientific payloads of SPL and for the requirements from other entities of VSSC. Regular up-keep and maintenance of the facility have been carried out. The clean room has been extensively utilized for realization and testing of the ChaSTE payload onboard Chandrayaan-3 mission and the PAPA payload onboard the Aditya-L1 mission (Fig. 10) in addition to the usage of other Entities.

Figure 10: Assembled PAPA payload (FM) in the clean room

Technology Development Programmes (TDPs)

Electronics for Solar Occultation Experiment Payload

Development of payload for Solar Occultation Experiment (SOE) is an ongoing TDP of SPL/VSSC. The objective of the payload is to measure the altitude profiles of aerosols and thin clouds above the thick cloud layers in any planetary atmosphere, including Earth. The payload consists of three units, optics, gimbal and electronics.

The electronics of the SOE payload consists of three cards: front-end, processing and motor driver. All the three electronic cards have been designed and developed. Electrical and power interfaces of the payload are compatible for testing it onboard high altitude balloon from the National Balloon Facility/TIFR, Hyderabad. Ground testing of the electronics integrated with the payload has been successfully completed.

Front-end Electronics

The front-end electronics has been developed for pre-amplification of twenty analog signals from six aerosol measurement channels and two Sun sensors (coarse and fine). The measurement channels have four single-element photodiodes and two 128-element linear photodiode arrays as detectors. The electronics card also supplies bias voltage (+2.5 V) to the linear photodiode arrays. The bias voltage is derived from a precision voltage reference. The electronics operates with a +5 V power supply. The supply is derived from an input power supply (+7 V to +12 V) by using a low noise linear regulator. The developed front-end electronics card is shown in the Fig. 11.

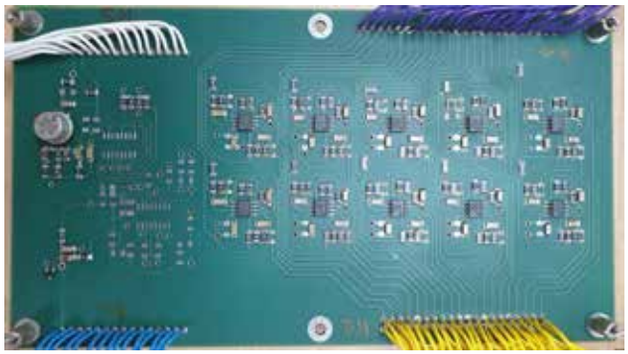

Figure 11: Front-end electronics card of the SOE payload

Processing Electronics

The processing electronics has been developed for data acquisition from the six measurement channels. It does signal conditioning of the six signals from the measurement channels and digitization of the analog signals by a 12-bit multi-channel ADC. The electronics also acquires the Sun tracking information from motor drive electronics. It packetizes the measurement channels data and the Sun tracking information with necessary information (header, packet number, checksum etc.) and transmits the data to the balloon telemetry by RS-232 interface. It also receives telecommands by 8-bit CMOS interface from the balloon telecommand module for different operations of the payload. The electronics operates with two +5 V power supplies for powering its analog and digital circuit sections. The supplies are derived from an input power supply by using two low noise linear regulators. The electronics is built around a Microchip microcontroller. The developed processing electronics card is shown in the Fig. 12.

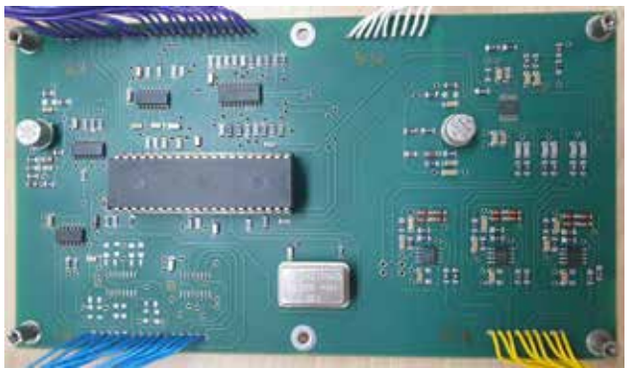

Figure 12: Processing electronics card of the SOE Payload.

Motor Drive Electronics

The motors drive electronics has been developed for driving azimuth and elevation motors of the payload's gimbal unit in closed-loop configuration for precision Sun tracking with Sun sensors as feedback. The drive electronics does signal conditioning of fourteen signals of the coarse and fine Sun tracking sensors and digitization of the signals by a high-resolution multi-channel ADC. The electronics consists of four H-bridge drives for driving two bipolar stepper motors of the gimbal unit. It transmits the Sun tracking status, the gimbal's azimuth and elevation angles and Sun

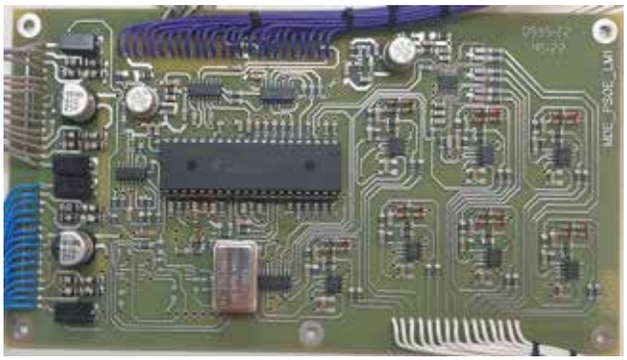

Figure 13: Motors drive electronics card of the SOE Payload.

sensors data to the processing electronics by I/O lines and RS-232 interface. The electronics operates with two +5 V power supplies for powering its analog and digital circuit sections. The supplies are derived from an input power supply by using two low noise linear regulators. The motors are operated from the input supply. The electronics is built around a Microchip microcontroller. The developed motor drive electronics card is shown in the Fig. 13.

Onboard Software for the SOE Payload

Onboard software for the payload electronics has two parts: (1) software for the motor drive electronics and (2) software for the processing electronics.

Functional requirements of the motor drive electronics software include (i) acquiring the Sun sensors (coarse and fine) data from a 12-bit multi-channel ADC, (ii) driving the azimuth and the elevation motors for precise Sun tracking and (iii) interfacing with the processing electronics by RS-232 interface for transmitting Sun tracking information.

Functional requirements of the processing electronics software include (i) generating required timing clock pulses for the two 128-element linear photodiodes, (ii) acquiring the measurement channels (two linear array and four single element photodiodes) data from the multi-channel ADC, (iii) forming payload data packet with the measurement channels data and the Sun tracking information with the necessary information, (iv) transmitting the payload data to the balloon telemetry by RS-232 interface, (v) receiving telecommands from the balloon by 8-bit parallel interface and processing the commands and (vi) interfacing with the motor drive electronics by RS-232 interface for transmitting the telecommands and receiving the Sun tracking information.

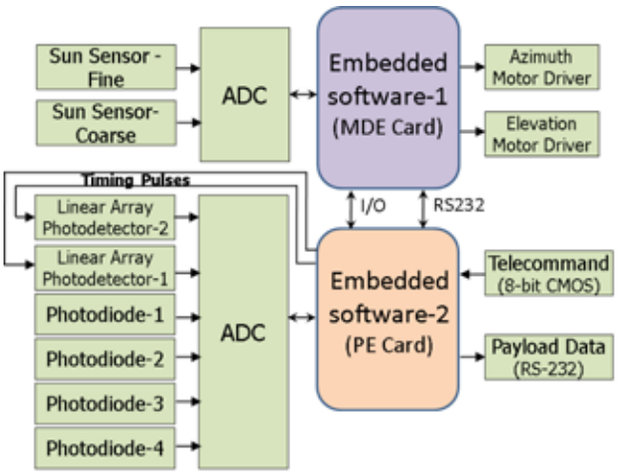

Figure 14: Context level diagram of the software of the SOE payload

Design of the software has been completed. Field testing of the SOE payload is in progress. Context level diagram of the software is shown in the Fig. 14.

Rocketsonde for Middle Atmospheric Temperature Measurement

Design and development of rocketsonde for middle atmospheric temperature measurement is a TDP of SPL/VSSC. Its objective is vertical profiling of the middle atmospheric temperature in the stratosphere and lower mesosphere regions up to ~ 60 km altitude onboard RH200 rocket on regular basis. The payload will be ejected from the rocket after reaching its peak altitude and decelerated to ground by using a parachute for making measurements.

The payload consists of a special type temperature sensor, a thin film based mount for the sensor, sensor electronics, a GPS receiver and battery power supply. The position information obtained from the GPS receiver will be used for deriving atmospheric wind parameters. Specifications of the developed rocketsonde payload (Fig. 15) are given in the Table 2. Development details of the payload are listed below.

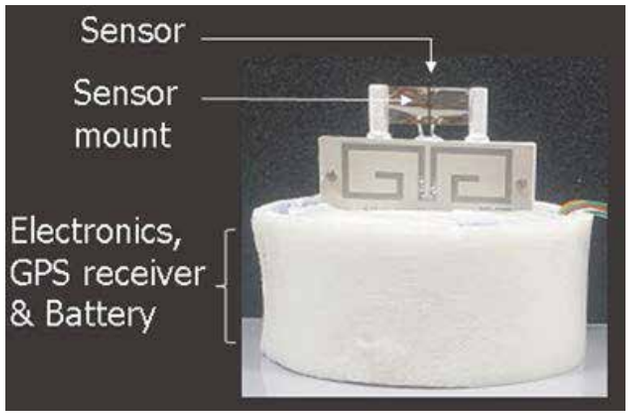

Figure 15: The developed Rocketsonde

***Table 2:** Specifications of the Rocketsonde*

Data rate	1 Hz
Telemetry frequency	866 MHz
Transmitting power	22 dBm
Dimensions	99 mm diameter, 85 mm height
Weight	~ 300 g

Temperature Sensor

The sensor has been designed for temperature measurement in a rarefied middle atmosphere. The challenge is to minimize various sources of contamination in the measurements, including conduction of heat from payload structures, short wave and long wave radiation, atmospheric drag, ohmic heating and measure in the rarefied atmosphere with fast response time. Design parameters of the sensor are sensor type and its size. Smaller dimension sensors have fast response time to make measurements in the upper atmosphere. Also, smaller dimension sensors with thin lead wires have smaller radiation error. Small bead thermistors (Fig. 16) of 0.3 mm diameter with lead wires of 0.03 mm diameter were finalized for the temperature measurement in the range from 190 K to 300 K. The sensors with prescribed specifications were fabricated by an Indian manufacturer. Lead wires of the sensor are made with Platinum alloy for sufficient strength during the rocket launch. Both the sensor and its lead wires were applied a very thin Aluminum coating to reduce their sensitivity to short wave radiation.

Figure 16: A pack of five thermistor sensors (small dots inside)

Sensor Mount

A proper mount for the thermistor sensor has been designed and developed to thermally isolate the sensor from the rocketsonde structures. A clear thin Polyester film of 10 µm thickness, one-inch length and half-inch width was chosen for fixing the temperature sensor. The thin film has low thermal conductivity and low absorption for solar radiation. The dimensions of the film were chosen to accommodate in the available space onboard the RH200 rocket and to give sufficient strength during launch and the payload expulsion. The film was also applied with thin Aluminum coating to minimize solar radiation heating. While applying the Aluminum coating, it was properly masked for producing insulating strips at the center and at the two edges of the film mount. The film was stretched between two plastic posts and secured by means of an adhesive with good bonding strength. The leads of the thermistor sensor were joined to the top edge of the film, one on each side of the center insulating strip. They were joined to the film by inserting the end of each thermistor lead into a tiny hole which was punched through the film and were then secured in place by a small amount of silver adhesive. The electrical connections to the electronics of the payload were secured to the lower edge of the film in a similar manner. The mount assembly was fabricated (Fig. 17) with the support of PSCD/PCM and GEM/MME of VSSC.

Figure 17:Fabricated sensor mount

Sensor Electronics

Sensor electronics (Fig. 18) has been designed and developed for data acquisition and telemetry. The electronics provides precision sensor excitation with low power dissipation in the thermistor sensor for its entire operating temperature range and does signal conditioning and digitization of the sensor signal with a high resolution ADC. It also measures payload internal temperature and battery voltage for monitoring payload health during operation. The electronics includes a wireless data transmitter with peak output power of 22 dBm and operates at license-free 866 MHz frequency. A G-shaped half wave dipole antenna is used for data transmission. It was designed and developed by ADD/AVN of VSSC. The antenna provides omni directional pattern with 1 dBi peak gain. Total operation of the electronics is controlled by a Microchip microcontroller. Two low noise and low drop-out voltage regulators derive required operating voltages for the electronics from battery power supply. The electronics card, two small size Lithium batteries and a compact GPS receiver were assembled to a plastic chassis. The chassis was covered with PU foam for thermal insulation and protected with vapor barrier coating (VBC). The chassis was designed and developed by AMFF/ESAE and the PU foam fixing with the VBC was done at APD/ PCM of VSSC.

Figure 18: Developed electronic card of the rocketsonde.

Onboard Software

The software has been designed and developed for the microcontroller in assembly language. Functionalities of the software include (i) initialization of the microcontroller for peripherals, (ii) initialization of the ADC for data rate, (iii) configuration of the GPS receiver for baudrate and required GPS data string, (iv) configuration of the wireless transmitter chip for modulation, frequency, bandwidth, packet structure and transmitting power, (v) acquisition of the payload position information, the sensor data, the payload temperature and the battery voltage periodically for every second and (vi) transmission of the payload data by the wireless chip periodically for every second. Operational flow-chart of the software is shown in Fig. 19.

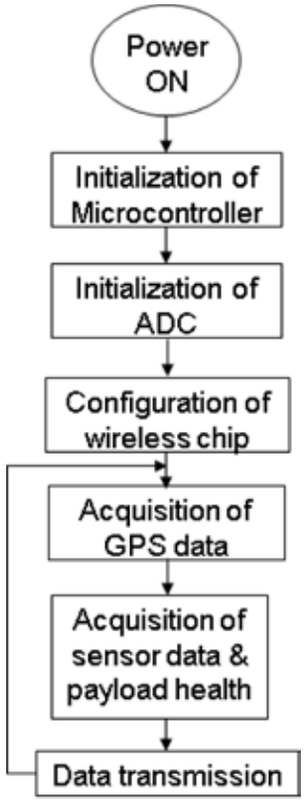

Figure 19:Flow-chart of the rocketsonde onboard software.

Checkout System

Checkout system of the payload consists of a wireless data receiver module (Fig. 20) and a PC based data acquisition software (Fig. 21). The data receiver includes a wireless data receiver with sensitivity of -130 dBm and a quadrifilar helical antenna with 3 dBi peak gain and 130° 3-dB beamwidth. The antenna was designed and developed by ADD/AVN of VSSC. The data receiver transmits the received data to PC by RS-232 interface.

The data acquisition software is a GUI developed in LabVIEW. Functionalities of the software include (i) data acquisition, (ii) data processing, (iii) tabular and graphical display of the processed data in real time and (iv) data archival in PC.

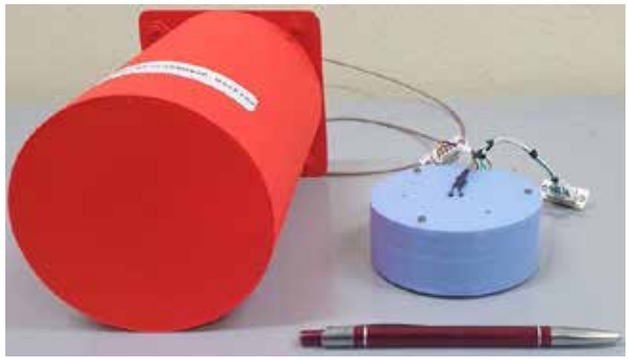

Figure 20: The developed wireless data receiver with antenna for the rocketsonde.

Corrections for the temperature measurements

Temperature of ambient low density air of the upper atmosphere as measured by the thermistor differs from actual temperature because of low efficiency of heat exchange among the thermistor, the film and the surrounding environment. This requires corrections for the measured temperatures. The correction factors include conduction of heat from the rocketsonde structures, solar radiation, long wave radiation, aerodynamic drag and ohmic heating of the sensor. All these factors were estimated theoretically. It was found that the major error sources at higher altitudes are solar radiation and aerodynamic drag. Heating due to

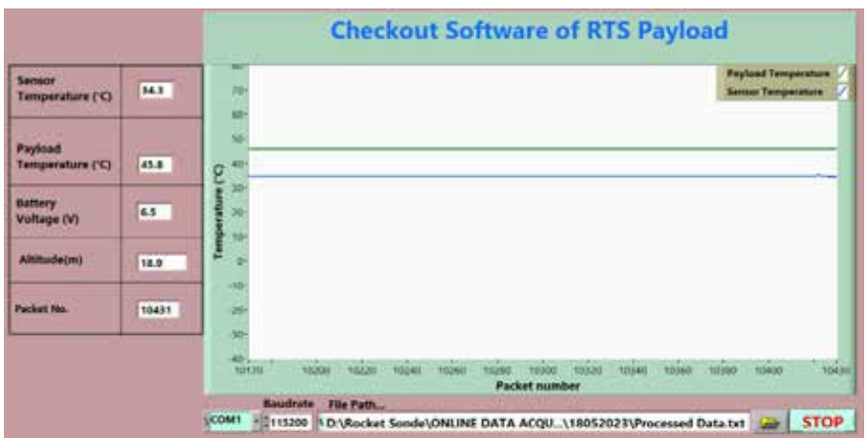

Figure 21:The developed checkout software for the rocketsonde.

the other factors has been minimized through optimized design.

Calibration of the Payload

To obtain an optimum temperature resolution in the range from 190 K to 300 K, non-linear temperature-resistance characteristic of the thermistor sensor was determined by calibrating the sensor with a standard reference temperature sensor in a high precision thermal well. During the calibration, temperature-resistance characteristics of the sensor (Fig. 22) were obtained.

To compare response time of the sensor, a low pressure test (Fig. 23) was conducted. During the test, the rocketsonde sensor (RTS), a radiosonde sensor (iMET) and a Pt-100 RTD sensor were kept in a vacuum chamber at room temperature. Chamber pressure was reduced from ambient condition to 0.1 mbar pressure. Initially, all the sensors showed decrease in temperature followed by increase in temperature as expected. The RTS sensor reached equilibrium with the chamber temperature at much faster rate than the other sensors.

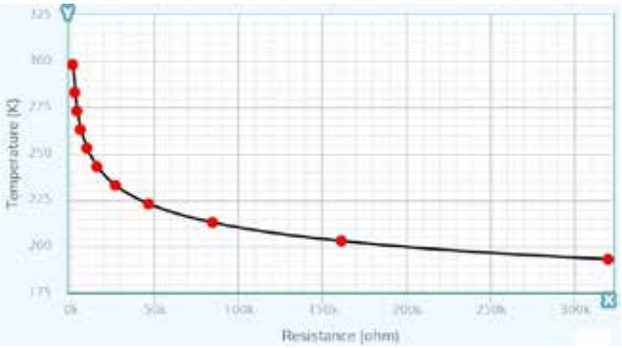

Figure 22:Calibrated temperature-resistance characteristics of the sensor

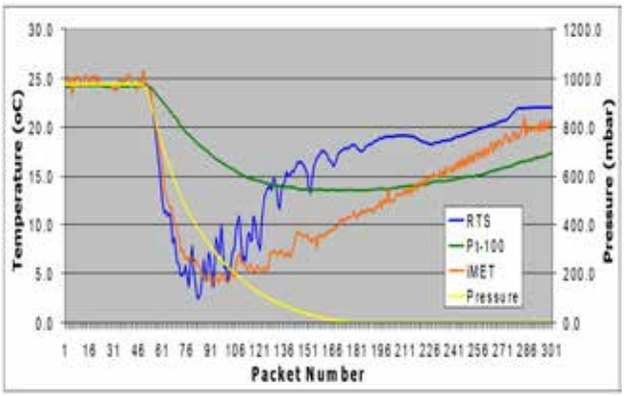

Figure 23:Low pressure test of the sensor

Electronics for Atomic Oxygen Sensor

Design and development of Atomic Oxygen Sensor (ATOXS) is one of the TDPs of SPL/VSSC. Its objective isto measure atomic oxygen density in the Earth's upper atmosphereand there by understanding the role of atomic oxygen in various processes in the upper atmosphere-ionosphere region.

Sensing element of the ATOXS is Zinc Oxide (ZnO) based thin film with Alumina as substrate. It contains four ZnO films (two bare and two coated with SiO_2). The films coated with SiO_2 will be used as a reference to nullify the effect of UV radiation. The sensor has also a heater for reusing the films and two thermistors for monitoring sensor temperature. Fabrication of the sensing element (proto model) has been completed at the IIST, Thiruvananthapuram.

Sensor electronics (proto model) has been designed and developed (Fig. 24). Integrated testing of the electronics with the sensor is in progress. Functionalities of the electronics include (i) maintaining the sensor temperature at ~40 °C with an accuracy of +/-0.5 °C by operating the sensor heater, (ii) excitation of the ZnO films with high precision current, (iii) conditioning of the sensor signals, (iv) digitization of the signals by using a high resolution ADC, (v) transmitting the sensor data by RS-232 interface and (vi) heating of the sensor up to 100 °C for its reuse.

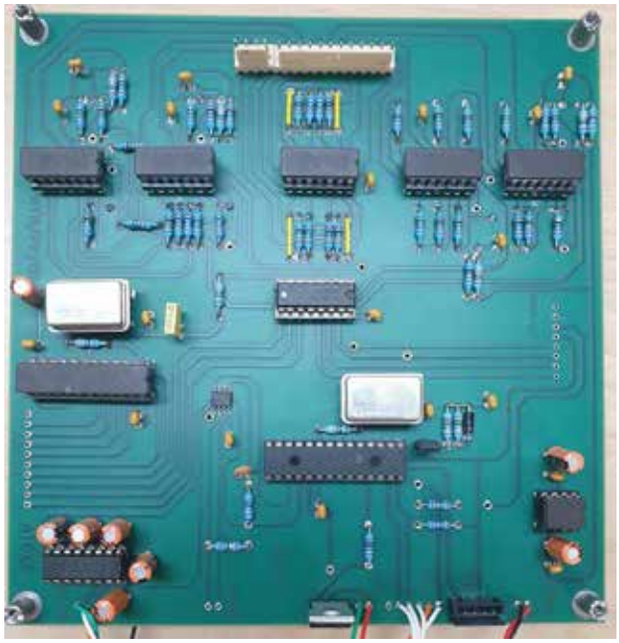

Figure 24: The developed electronics for the atomic oxygen sensor

Solid-state RF Power Amplifier for HF Radar

Design and development of solid-state 50 kW RF power amplifier for HF Radar is one of the TDPs of SPL/VSSC. Existing power amplifier of the radar is based on vacuum tubes. The system is over 25 years old and the parts are obsolete. The solid-state power amplifier is modular based design. Each module is a 2.4 kW power amplifier consisting of two LDMOS transistors. Multiple such modules are to be cascaded by Wilkinson type power combiner with matching section to achieve the required output power. Specifications of the solid-state power amplifier are provided in Table 3.

The amplifier with 16.8 kW power output (Fig. 25) has

been developed and tested. Three such modules will be combined to achieve the required peak output power of 50 kW. A 200 W driver amplifier has also been developed for the 16.8 kW amplifier.

Table 3: Specifications of the solid-state power amplifier

Parameter	Specification
Peak output power	50 kW
Frequency	18 MHz
Bandwidth	500 kHz
Output impedance	50 Ω
Pulse width	20 µs to 100 µs
Repetition rate	250 Hz to 100 Hz

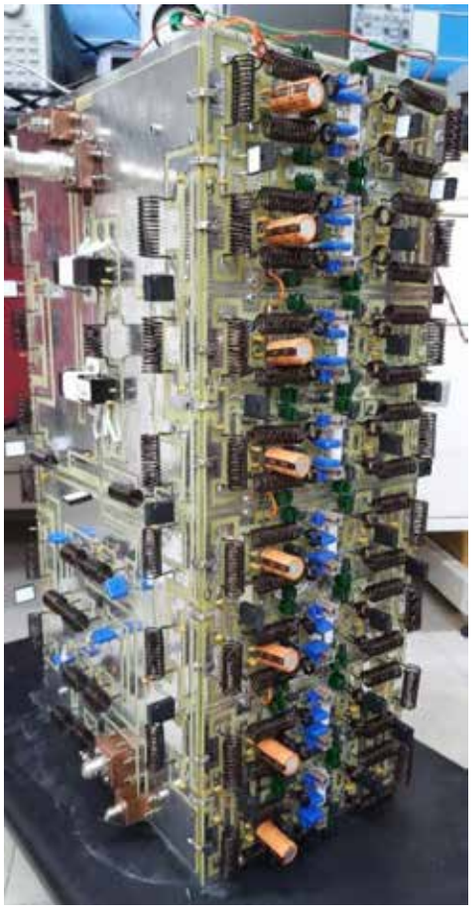

Figure 25: The developed 16.8 kW RF power amplifier module

Mechanical Engineering Activities

The following mechanical engineering activities were carried out at SPL workshop and CAD design unit: (1) realization of mechanical housing for nighttime photometer sky scanning mirror unit (Fig. 26), (2) realization of mount for Electron Temperature Analyzer (ETA) probe (Fig. 27), (3) realization of heat sink for the solid-state power amplifier of HF radar, (4) fabrication of mounts for photodetectors of the SOE payload, (5) generation of CAD drawings for fabrication of chassis of the rocketsonde data receiver and CAD drawings for fabrication of chassis of high altitude aerosol sampling system and (6) generation of location sketches of Ionosonde antenna field for fencing.

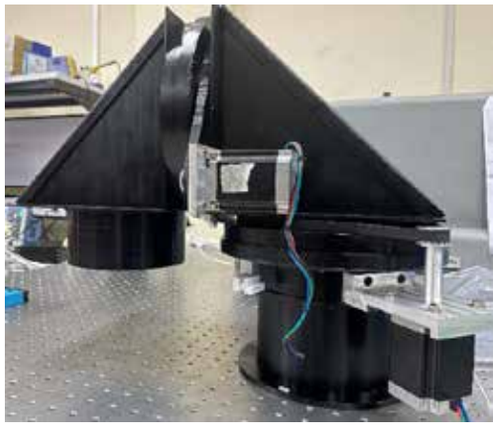

Figure 26: Housing for mirror unit of photometer

Figure 27: Mount for ETA probe

Future Projections

- Qualification of payload for middle atmospheric temperature measurement onboard RH200
- Development of the remaining electronics module for SOE payload onboard satellite
- Electronics for Atomic Oxygen sensor onboard PS4
- Solid-state 50 kW power amplifier and digital receiver for HF radar
- Control and data acquisition system for Rayleigh-Mie LIDAR system

Technical Reports

- Mission Operational Plan for ChaSTE Payload, Chandrayaan-3 Lander, July, 2023, Doc. No.: SPL-TR-01-2023

Conferences/Symposium

Dinakar Prasad Vajja, Mohammed Nazeer M and Manikantan Nair N

- Attended “FAST -2023 (LaRA)” organized by VSSC on 30 June and 01 July, 2023.

Dinakar Prasad Vajja

- Attended “Engineers Conclave - 2022” jointly organized by ISRO and INAE during 13-15 October, 2022.

Training Programmes

Pramod PP and Mohamed Nazeer M

- Attended training on “Design of Avionics package based on thermal consideration” conducted by HRDD/VSSC during 13-14 October, 2022.

योजना और समन्वय प्रकोष्ठ
Planning and Coordination Cell

The Planning and Coordination Cell of SPL (SPL - PCC) is responsible for the overall planning of the activities at SPL, annual budget preparation and presentations for approval, coordination of need aspect review of scientific and technical items required for SPL activities, monitoring of procurement status and budget utilisation, coordination with other entities of VSSC and ISRO HQ and the periodic progress report preparation of the laboratory for submission to higher management.

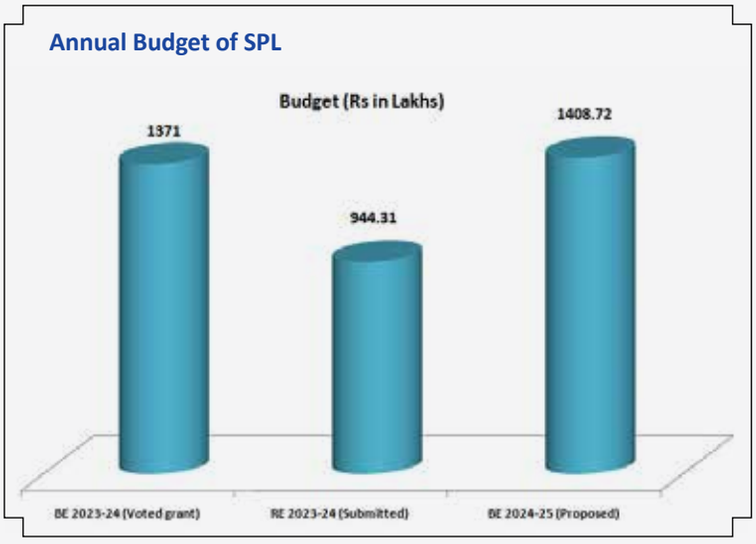

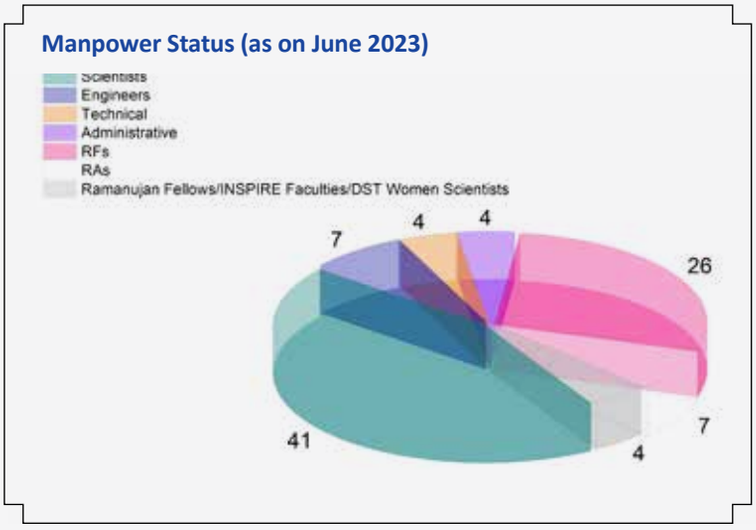

एसपीएल-पीसीसी टीम/SPL-PCC Team

सुरेश बाबू एस., प्रधान पीसीसी / Suresh Babu S., Head PCC
विजयकुमार एस. नायर / Vijayakumar S. Nair
अजीषकुमार पी. एस. / Ajeeshkumar P. S.
षिजी एन. डी. / Shiji N. D.

कार्यालय और प्रशासनिक सहायता
Office and Administrative Support

एसपीएल कार्यालय टीम / SPL Office Team

गीता सी. / Geetha C.*
शालिनी एम.एस. / Salini M.S.
षिजी एन.डी. / Shiji N.D.
सिमी इस्माइल / Simi Ismail
यूसफ एन. / Yoosaf N.

SPL administration facilitates the administrative and secretarial requirements for a smooth and effective functioning of SPL by providing co-ordination, communication and logistics. Besides the general administration, office management and housekeeping of SPL, it caters to the necessary official assistance to different ISRO projects such as ARFI, ICARB, RAWEX and NOBLE. It co-ordinates and provides logistic support for different national observation campigns of SPL. Also SPL administration is responsible for coordinating activities within SPL, involving other Divisions, Facilities of VSSC and/or other ISRO centers and different Institutions/Universities. It meets the administrative requirements of different payload such as ChaSTE, RAMBHA and PAPA development for ISRO's space missions.

Research programme facilitated by ISRO fellowship program including research fellowship program and research associate program is a major activity of SPL. SPL administration provides the required assistance in terms of documentation and organizing Ph.D. Synopsis/Defence, Doctoral Committee meetings, student reviews, regular student/faculty seminars and Central Level Monitoring Committee meeting of VSSC. It also supports for arranging Seminar Talks/Invited Talks in SPL by leading scientists from India and abroad and arranges necessary logistics required during their visit and stay.

** Relieved in March 2023*

अकादमिक परियोजनाएं / ACADEMIC PROJECTS

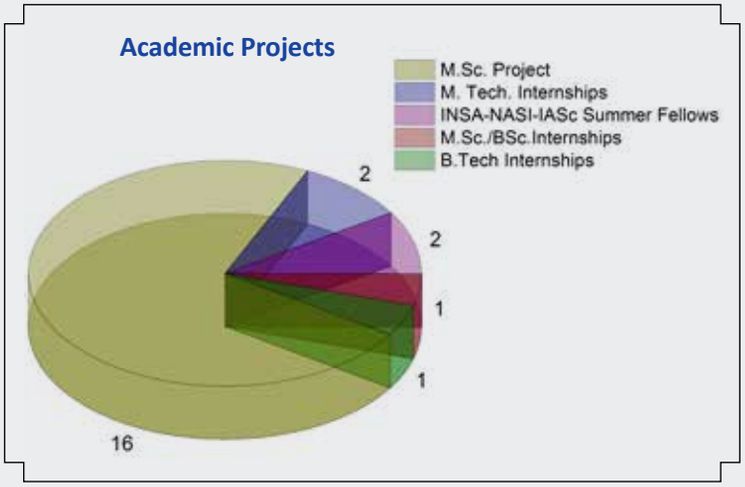

M.Sc.

1. Junaida, S., All Saints' College, University of Kerala, "Study on the long-term trend in the stratospheric water vapour over the Asian Summer monsoon region", August 2022 [Supervisor: Siddarth Shankar Das].
2. Arunkumar, L., NIT Rourkela under the IASc-INSA-NASI Summer Research Fellowship Programme, "Effect of aerosols on surface temperature over South Asia", April-July, 2022 [Supervisor: Vijayakumar S. Nair].
3. Aiswarya, S.M., University of Kerala, Thiruvananthapuram,"Study of temperature trend over the Indian region during 1901-2020 using CRU-TS v4.05 Temperature Dataset", May-July, 2022 [Supervisor: Vijayakumar S. Nair].
4. Swathy G Krishna, University College, Thiruvananthapuram, "Investigation of long-term trend in columnar aerosols over Port-Blair in the Bay-of-Bengal based on ground-based measurements and satellite remote sensing", April-June, 2023 [Supervisor: Mukunda M.Gogoi].
5. Akshaya P., University of Kerala, Thiruvananthapuram, "Response of ionosphere over Trivandrum to space weather event of 22-24 April 2023", May-June, 2023 [Supervisor: Manju G.].
6. Anjali V., University of Kerala, Thiruvananthapuram,"The calculation of Total Electron Content using the Indian Regional Navigation Satellite System (IRNSS) data and comparison with the GPS observations.", May-June, 2023 [Supervisor: K. M. Ambili].
7. Likhith Gopinath, Government College, Madappally, "Atmospheric boundary layer variability over urban environment (New Delhi) during the winter of 2022-23", March-June 2023 [Supervisor: M. Santosh].
8. Adya, C. R.,Department of Physics, Sri SathyaSai Arts and Science College, Thiruvananthapuram, "Inter-annual variations of rainfall over the southwest coast of peninsular India", August-October 2022, [Supervisor: S. Sijikumar].
9. Ardra Ajith, CMS College, Kottayam, "Assessment of the Indian monsoon rainfall patterns using CMIP6 models under different Shared Socioeconomic Pathways (SSPs)", March-May 2023 [Supervisor: K. N. Uma].
10. Krishnanjali. S., Department of Physics, Indira Gandhi College of Arts and Science, Nellikuzhi, Kotha-mangalam, Kerala, "Study of Lunar Exosphere Using LADEE Mission observations", August-September 2022 [Supervisor: Dhanya M.B.]

11. Aisha S., Department of Physics, University of Kerala, Thiruvananthapuram, “Study of solar wind for the solar cycles 23 and 24”, May-September, 2022 [Supervisor: Dhanya M.B.].

12. Pavithra P., University of Kerala, “The evolution of solar wind and geomagnetic activity during solar cycle 23, 24, and 25”, June-October, 2022 [Supervisors: Tarun Kumar Pant and Ankush Bhaskar].

13. Sandra Surendran,Mahatma Gandhi University, Kottayam, “Radiation belt response to Geomagnetic storm”, April-June, 2023 [Supervisor: Ankush Bhaskar].

14. Keerthana, A., University of Kerala, Thiruvananthapuram, Kerala, “Development of a methodology to integrate the data obtained to decipher the plasma wave information by a plasma wave detector onboard a spacecraft”, April-June, 2023 [Supervisor: Vipin K. Yadav].

15. Akash, N., University of Kannur, Kannur, Kerala, “Electrical characterization of Channel electron multiplier detector”, April-June, 2023 [Supervisor: Abhishek J.K.].

16. Sinju Sajin, P., University of Calicut, “Investigation on the Impact of Space Weather Events on Thermospheric Airglow Emissions over the Magnetic Equator", May-July 2023 [Supervisor: C. Vineeth].

M. Tech.

1. Thejas, K.V., Indian Institute of Space Science and Technology (IIST), Thiruvananthapuram, “Study on aerosol-warm cloud interaction over eastern Indo-Gangetic Plain during winter season”, April 2022-May 2023 [Supervisor: Vijayakumar S. Nair].

2. Ushas A. K., College of Engineering, Trivandrum, Artificial Intelligence (Branch), “Signature Identification of Atoms/Molecules in the mass spectra data using a Machine Learning Algorithm”; May-June 2023 [Supervisor: Dhanya M.B.].

INSA-NASI-IASc Summer Projects

1. Benerjee, S., National Institute of Technology, Rourkela, “Diurnal variation of metallic and carbonaceous components in urban aerosols from Eastern Central India”, May-June, 2023 [Supervisor: Suresh Babu S].

2. Jagdish Jena, National Institute of Technology, Rourkela, “Characteristics of Mesoscale Convective Systems during the Onset of Monsoon over Thumba using Weather Radar” May-June, 2023 [Supervisor: Uma K.N.].

Internships (B.Sc./B.Tech./M.Sc.)

1. Abhinav B Roy, Indian Institute of Science Education and Research, Thiruvananthapuram, “A Study on the Impact of Dust Storms on Aerosol Optical Properties over Indian Region“, May-June, 2023 [Supervisor: Prijith S. S.].

2. Mr. Anubhav Panda, BITS Pilani, Rajasthan, ‘Development of firmware for a high-altitude pump system controller’, June-July 2023 [Supervisor: Ajeeshkumar P S].

हिंदी गतिविधियां / Hindi Activities

डी. बाला सुब्रहमण्यम

- Best Paper Award (First Prize) in Inter-Technical Hindi Seminar, IIST: "वृहत भंवर सतत अनुकरण के माध्यम से तिरुवनन्तपुरम के वायुमंडलीय सीमा परत की ऊंचाई में होने वाले दैनिक परिवर्तनों का अन्वेषण", भारतीय अंतरिक्ष विज्ञान एवं प्रौद्योगिकी संस्थान, वलियमला, २५ नवंबर २०२२।

वीएसएससी की हिन्दी में गृह-पत्रिका "गगन" में लेख

विपिन कुमार यादव

- "अँग्रेजी जासूसी-कथा लेखन व उनके लेखक" गगन-55; अप्रैल – सितंबर, 2022, पृष्ठ: 16-19

हिन्दी में तकनीकी लेख एवं मौखिक प्रस्तुतियाँ

विपिन कुमार यादव

- "अन्तरिक्ष में प्लाज़्मा तरंगों का मापन"; तकनीकी सत्र; हिन्दी तकनीकी संगोष्ठी: "अन्तरिक्ष अनुसंधान में हाल की प्रगति: नवाचार और उद्भवन के अवसर"; नवंबर 25, 2022; भारतीय अन्तरिक्ष विज्ञान एवं प्रौद्योगिकी संस्थान (IIST), वलियामाला, केरल।
- "अन्तरिक्ष रोबोटिकी: अन्तरिक्ष कार्यक्रमों का एक अभिन्न अवयव"; तकनीकी सत्र; तकनीकी हिन्दी संगोष्ठी: "अन्तरिक्ष रोबोटिकी: भविष्य अन्तरिक्ष कार्यक्रमों में सही मायने में खेल परिवर्तन"; जून 02, 2023; इसरो जड़त्व प्रणाली यूनिट (IISU), तिरुवनन्तपुरम, केरल।

हिन्दी संगोष्ठियों/ कार्यक्रमों के आयोजन में भागीदारी

विपिन कुमार यादव

- सदस्य, आयोजन समिति; हिन्दी तकनीकी संगोष्ठी: "अन्तरिक्ष अनुसंधान में हाल की प्रगति – नवाचार और उद्भवन के अवसर"; नवंबर 25, 2022; भारतीय अन्तरिक्ष विज्ञान एवं प्रौद्योगिकी संस्थान (IIST), वालियमाला, केरल।
- सदस्य, संपादकीय समिति; अंतर-केंद्र तकनीकी हिन्दी संगोष्ठी: "अन्तरिक्ष रोबोटिकी: भविष्य अन्तरिक्ष कार्यक्रमों में सही मायने में खेल परिवर्तन"; जून 02, 2023; इसरो जड़त्व प्रणाली यूनिट (IISU), तिरुवनन्तपुरम, केरल।

हिन्दी कार्यशाला में भागीदारी

चेमुकुला मात्तिन यादव

- वैज्ञानिक/अभियन्ता एस सी एवं एस डी के लिए राजभाषा नीति पर हिन्दी कार्यशाला; जनवरी 25, 2023; वीएसएससी, तिरुवनन्तपुरम, केरल।

आगंतुक / Visitors

1. Dr. Pravata K Mohanty, Reader, TIFR, Mumbai, 12 August 2022.
2. Prof. Rajmal Jain, Outstanding Professor, IPS Academy, Indore/Hon. Scientist, PRL, Ahmedabad, 27 July 2022.
3. Dr. Olle Norberg, Director General, Swedish Institute of Space Physics (IRF), 09-10 November 2022.
4. Prof. Stas Barabash, Deputy Director General, IRF, Lead Co-I of VISWAS/VNA sensor, 09-10 November 2022.
5. Dr. Yoshifumi Futaana, Co-PI of VISWAS instrument, IRF, 09-10 November 2022.
6. Mr. Herman Andersson, VNA Experiment Manager, IRF, 09-10 November 2022.
7. Mr. Rikard Ottemark, VNA Deputy Experiment Manager, IRF, 09-10 November 2022.
8. Prof. H. B. Menon, Vice Chancellor, Goa University, 01 May 2023.

PAPA - Aditya-L1 Flag Off by Dr. S. Unnikrishnan Nair, Director, VSSC (02 November 2022)

Science from In-situ Measurements of Aditya-L1 (SIMA-01; 11-13 April, 2023 at SPL)

The workshop was inaugurated by Dr. S. Unnikrishnan Nair, Director, VSSC. 155 students and scientists from universities and national institutions attended the meeting. The meeting had 5 plenary talks given by distinguished scientists in the field of solar physics and space weather. A total of 47 invited talks covered the complete spectrum of the Sun and space weather starting from Aditya-L1 mission overview, technical and science capabilities of the Aditya-L1 payloads, solar transients: flares and coronal mass ejections, solar winds, magnetospheric and Ionospheric Impact, Space Weather Modeling, Monitoring, and Forecasting, and Planetary Space Weather. Two panel discussion sessions were conducted during the meeting, the first on "Aditya-L1 data and Science collaboration at national and international level" and the second on "Beyond Aditya -L1".

39th Meeting of the Scientific Advisory Committee - SPL in hybrid mode (18-19 October 2022)

Release of the compendium of SPL research publications during SSC meeting at VSSC (1 November 2022)

Prof. H. B. Menon, Vice Chancellor, Goa University, visited SPL and delivered the invited lecture on "Climate change adaptation and mitigation efforts on coastal and estuarine waters: An optical remote sensing perspective." (01 May 2023)

Delegation from the Swedish Institute of Space Physics (IRF), Sweden for discussion on science payload development and scientific collaboration (09-10 November 2022)

Chandrayaan-3: ISRO Shares 'First Observations' Made By ChaSTE Onboard Vikram Lander on Moon

THE TIMES OF INDIA

Chandrayaan-3: Vikram's RAMBHA completes first in-situ measurements of plasma in polar region

Chethan Kumar / TNN / Updated: Aug 31, 2023, 17:04 IST

You're Reading: "The measurements have been carried out by the Radio Anatomy of Moon Bound Hypersensitive Ionosphere and Atmosphere-Langmuir Probe (RAMBHA-LP) payload onboard the lander ... These quantitative measurements potentially assist in

RAMBHA-LP on-board Chandrayaan-3 measures near-surface plasma content: ISRO

ANI | Updated: Aug 31, 2023 17:01 IST

New Delhi [India], August 31 (ANI): The Indian Space Research Organisation (ISRO) on Thursday said that the RAMBHA-LP, a payload attached to the lander module Vikram, which is on the lunar surface, of the Chandrayaan-3 mission, has made the first-ever measurements of the near-surface Lunar plasma environment over the south polar region.

Taking to social media platform X, ISRO said, "Radio Anatomy of Moon Bound Hypersensitive Ionosphere and Atmosphere - Langmuir Probe (RAMBHA-LP) payload onboard Chandrayaan-3 Lander has made first-ever measurements of the near-surface Lunar plasma environment over the south polar region."

india.com

Chandrayaan-3: ChaSTE Payload Aboard Vikram Lander Measures Lunar Surface Temperature, How It Works

ISRO said ChaSTE payload aboard Vikram lander of the Chandrayaan-3 measured the temperature profile of the lunar topsoil around the pole to understand the thermal behaviour of the Moon's surface.

abp LIVE

Chandrayaan-3's Vikram Lander Payload Makes First-Ever Measurements Of Plasma Environment Over Lunar South Pole

Chandrayaan-3: The RAMBHA-LP payload onboard the Vikram lander has discovered that the plasma (ionised gas) above the lunar surface on the Moon's south pole is sparse compared to other regions.

Chandrayaan-3 | ISRO's Space Physics Laboratory gears up for big moment

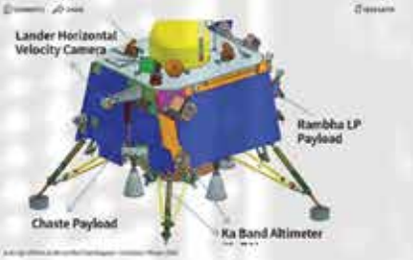

Chandrayaan-3's Vikram lander drills into Moon

The spacecraft, which landed on the Moon's surface on August 23, has begun conducting experiments and relaying valuable data back to ture headquarters.

INDIA TODAY

ISRO shares first data observed by Chandrayaan-3 from Moon

Chandrayaan-3 ChaSTE has measured the temperature profile of the lunar topsoil around the Moon's south pole. ISRO said in its latest statement.

Chandrayaan-3 probe shows 50°C difference between moon's surface and 10 cm below

ChaSTE is a temperature probe that can be driven into the moon's surface using a motor to a depth of up to 10 cm.

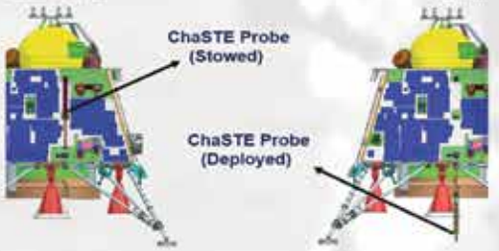

आज तक

रंभा, चास्टे, इल्सा और एरे... चंद्रयान-3 के वे पेलोड्स जो लैंडिंग के बाद खोलेंगे चांद के राज

भारत के मून मिशन चंद्रयान 3 (Chandrayaan 3) की लैंडी यानी अब अपने अंतिम पड़ाव पर है. इसकी सबसे अहम एक्टिविटी लैंडिंग की है. जो बहुत जटिल और जोखिम है. इसमें सबसे अहम अंतिम 17 मिनट होंगे, जिन्हें इसरो के वैज्ञानिक 17 मिनट्स ऑफ टेरर यानी 17 मिनट का आतंक बता रहे हैं. चंद्रयान के साथ जो पेलोड्स गए हैं, उनमें रंभा, चास्टे, इल्सा और एरे चांद के अहम राज खोलेंगे.

india.com

Chandrayaan-3: ChaSTE Payload Aboard Vikram Lander Measures Lunar Surface Temperature, How It Works

ISRO said ChaSTE payload aboard Vikram lander of the Chandrayaan-3 measured the temperature profile of the lunar topsoil around the pole to understand the thermal behaviour of the Moon's surface.

INDIA TODAY

In a first, Chandrayaan-3 shares observations of soil temperature on lunar south pole

Chandrayaan-3: रंभा ने बताया- चांद पर प्लाज्मा कम, यात्रियों को मिलेगी मदद; पढ़ें पूरी खबर

खबर

इसरो ने बताया कि उपकरण 'रेडियो एनाटॉमी ऑफ मून बाउंड हाइपरसेंसिटिव आयनोस्फीयर एंड एटमोस्फीयर-लैंगमुइर प्रोब' (रंभा-एलपी) ने दक्षिणी ध्रुव की चंद्र सतह पर पहली बार कोई परिमाण लिया।

First output from Chandrayaan-3 experiments: Temperature profile of lunar soil

The Chandra's Surface Thermophysical Experiment, or ChaSTE, an instrument onboard the lander module, has measured a sharp drop in temperature in the lunar topsoil.

Vikram lander observes temperature variation on lunar surface, records high of 70 degree Celsius

The payload has a temperature probe equipped with a controlled penetration mechanism capable of reaching a depth of 10 cm beneath the surface.

ANI

THE ECONOMIC TIMES News

Chandrayaan-3: RAMBHA, ILSA to help ISRO understand moon better

Chandrayaan-3 | RAMBHA aboard Vikram completes first in-situ measurements of lunar plasma over the moon

Days after the rover's LIBS detected sulphur in the moon's south polar region, the APXS instrument has confirmed the discovery

bt Business Today

Chandrayaan-3 update: ISRO shares first observations from the Vikram lander's ChaSTE payload

The graph shared by ISRO shows the temperature variations of the lunar surface/near-surface at various depths.

RAMBHA-LP on-board Chandrayaan-3 measures near-surface plasma content: ISRO

ANI | Updated: Aug 31, 2023 17:01 IST

New Delhi [India], August 31 (ANI): The Indian Space Research Organisation (ISRO) on Thursday said that the RAMBHA-LP, a payload attached to the lander module Vikram, which is on the lunar surface, of the Chandrayaan-3 mission, has made the first-ever measurements of the near-surface Lunar plasma environment over the south polar region.

ISRO @isro · Aug 31

Chandrayaan-3 Mission:
In-situ Scientific Experiments

Radio Anatomy of Moon Bound Hypersensitive Ionosphere and Atmosphere - Langmuir Probe (RAMBHA-LP) payload onboard Chandrayaan-3 Lander has made first-ever measurements of the near-surface Lunar plasma environment over the...
Show more

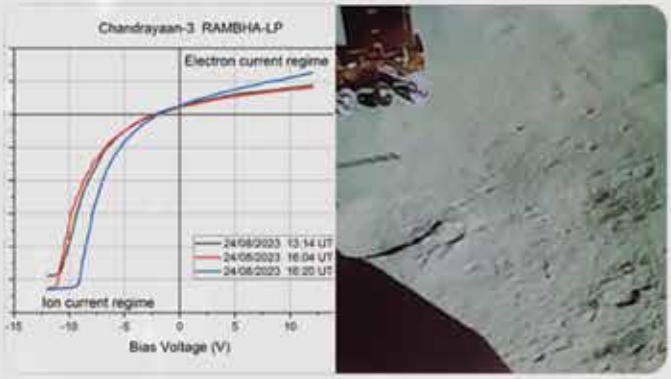

223 2.2K 17K 1.2M

ISRO @isro · Aug 27

Chandrayaan-3 Mission:
Here are the first observations from the ChaSTE payload onboard Vikram Lander.

ChaSTE (Chandra's Surface Thermophysical Experiment) measures the temperature profile of the lunar topsoil around the pole, to understand the thermal behaviour of the moon's...
Show more

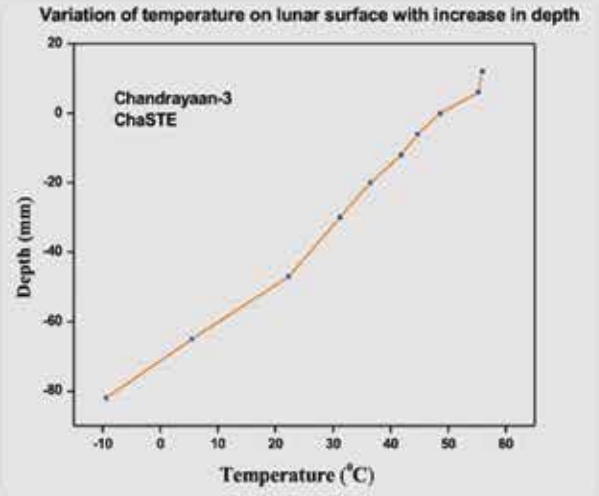

2.2K 11K 86K 5.5M

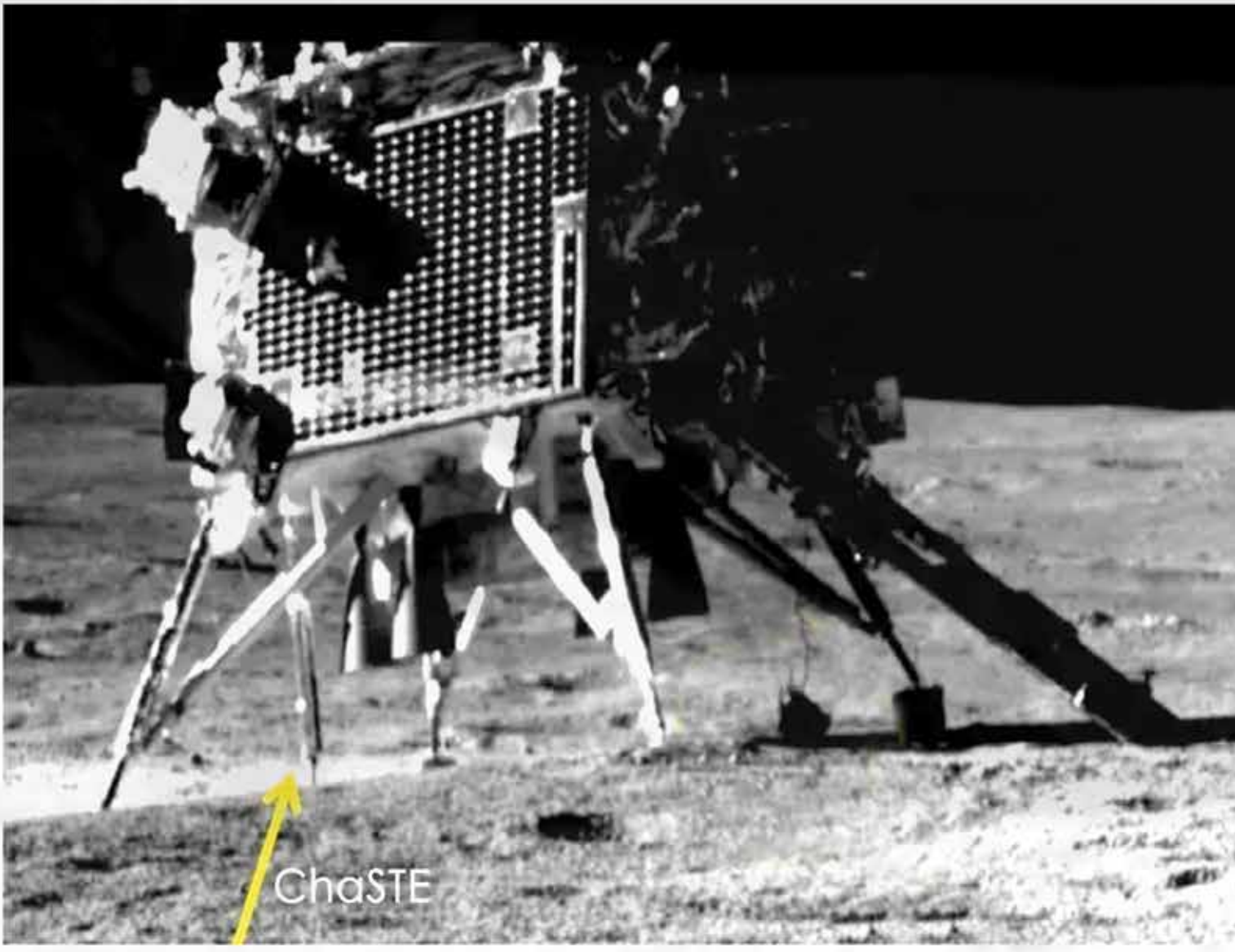

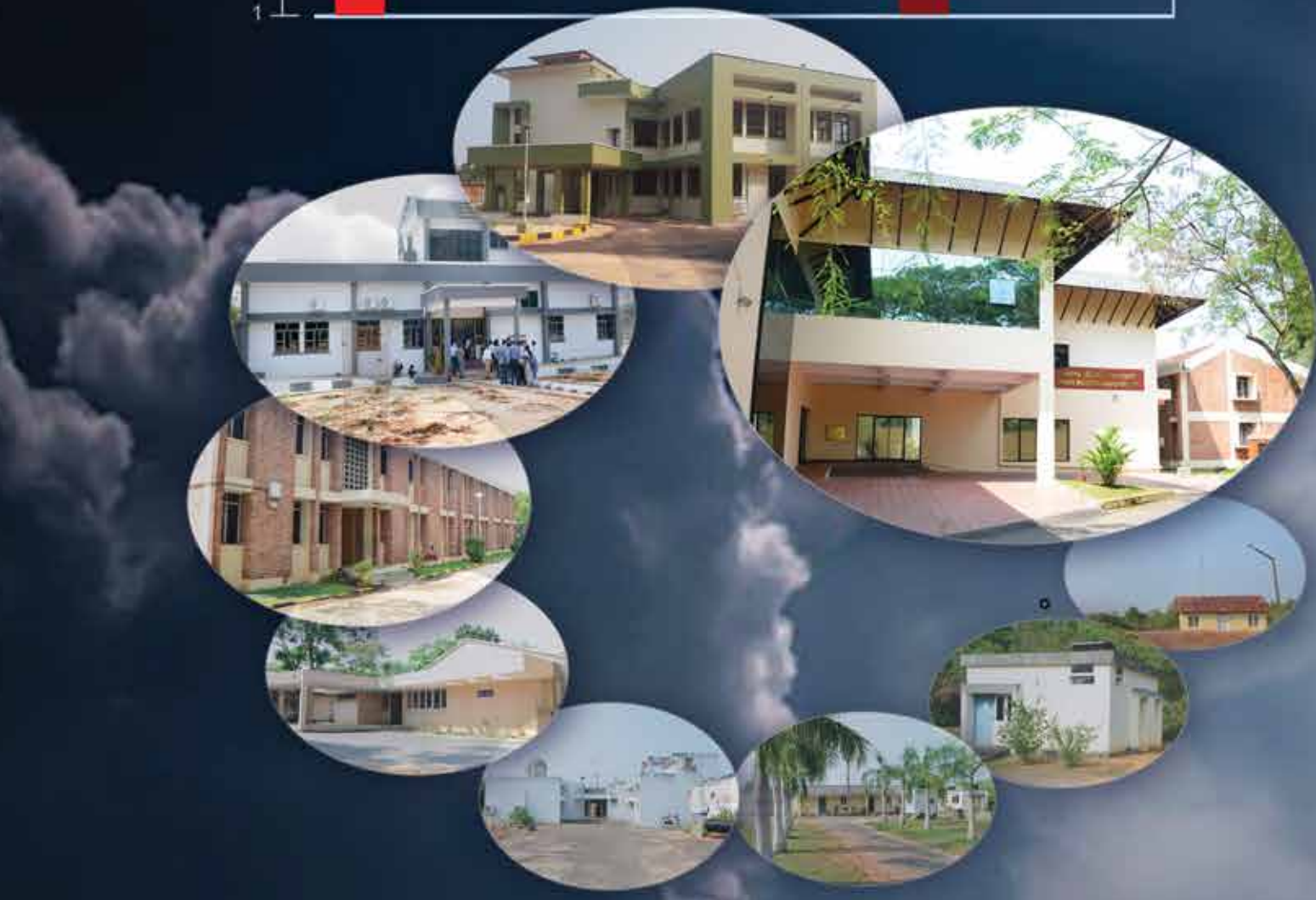

SPACE PHYSICS LABORATORY

Vikram Sarabhai Space Centre, Thiruvananthapuram - 695 022, INDIA

Email: directorspl@vssc.gov.in, Ph: +91 471 256 3663, Fax: +91 471 270 6535

https://spl.gov.in